Tratamiento electroquímico de fármacos y colorantes en medio acuoso mediante procesos de oxidación avanzada

Sergio Garcia Segura

Programa de Doctorado: Electroquímica. Ciencia y Tecnología

Tratamiento electroquímico de fármacos y colorantes en medio acuoso mediante procesos de oxidación avanzada

Tesis que presenta **Sergio Garcia Segura**
para optar al título de Doctor por la Universidad de Barcelona

Director de tesis:

Dr. Enric Brillas Coso
Departament de Química Física
Universitat de Barcelona

Agradecimientos

Todas las personas que nos rodean día a día tienen cierta influencia en nuestro desarrollo y crecimiento en mayor o menor medida, por lo que todas ellas son participes del trabajo de todos estos años.

Primero me gustaría agradecer a mi familia y muy en especial a mis padres, **Sergio** y **Joana**. Siempre he recibido de vuestra parte un apoyo incondicional en todos los retos de mi vida independientemente de la envergadura o dificultad de los mismos. Vuestro amor fraternal siempre ha ayudado a allanar el camino por arduo que fuese. De vosotros he aprendido a conseguir mis metas desde el esfuerzo y el sacrificio diarios, sin desfallecer nunca por difícil que parezca. **Óscar**, que decirle a la persona con la que he crecido toda mi vida. Pese que como todos los hermanos hemos tenido nuestros más y nuestros menos, siempre he podido contar contigo en cualquier momento. Eres una de las personas más queridas y admiradas por mí.

Una persona para la que no tengo suficientes palabras es para ti **Abi**, me has acompañado hasta los confines de la tierra, infatigable durante siete años (y los que quedan). No has dudado en ningún momento en sacrificarlo todo por estar conmigo sin importar tiempo ni distancia. Has sido siempre mi complemento y un pilar en mi vida.

Creo que también debo dedicarles unas palabras a mis amigos:

Un verdadero amigo es capaz de tocar tu corazón desde el otro lado del mundo, y pese que Sevilla no queda muy lejos de Barcelona, **Antonio**, tú has sido capaz de hacerlo. De todos, tú eres quien mejor ha sido capaz de entender los altibajos emocionales que conlleva una tesis doctoral. No solo eso, cuantas horas hemos dedicado a hablar de banalidades, salvar el mundo, o apoyarnos en diferentes dificultades. Me has apoyado mucho.

Mucha gente entra y sale de tu vida, pero solo algunas personas son capaces de dejar huella. **Albert**, tu risa, humor y esa aura de "buen-rollismo" han sido capaces de levantar el ánimo en incontables ocasiones.

Alejandro, amigo tenaz donde los haya. Siempre has estado disponible para cualquier cosa (aunque te diese un poco de *mandra*), los sarcasmos e ironías de los que sin duda eres un maestro hacen reír incluso en los momentos más difíciles.

También debo agradecer a mis amigos de un grupo cuyo nombre no pienso mentar, vosotros sabéis porqué **Alejandro, Anna, Josan** y **Pastu**. Cuantas cenas, risas y grandes

momentos (además de sus rememoraciones) hemos compartido desde hace ya muchos años. No puedo decir nada que no sepáis ya.

Sin duda alguna todo el *Laboratori d'Electroquímica de Materials i del Medi Ambient*, (LEMMA) del que he tenido el placer de formar parte durante todos estos años, merece mi especial agradecimiento. Los investigadores que forman parte de él me han hecho sentir en familia:

El **Dr. José Antonio Garrido** que fue uno de los mejores profesores de la carrera y el primero en abrirme la puerta del grupo. La **Dra. Rosa María Rodríguez** siempre enérgica y llena de alegría. Los dos sois una inseparable pareja sin igual.

Nuestro querido decano, el **Dr. Pere Lluís Cabot,** siempre ocupado resolviendo todos los problemas de la facultad, pero sin nunca olvidar del grupo y sus miembros.

Del **Dr. Francesc Centellas** he aprendido muchísimo a nivel personal y a nivel docente, gracias por todas las oportunidades que me has brindado tanto en el grupo de innovación docente *Química a la Interfase Secundaria Universitat* (QuISU) o como profesor de problemas. Tus opiniones, puntos de vista y las múltiples charlas que hemos podido mantener me han enriquecido como persona.

La **Dra. Conchita Arias** siempre infatigable y maternal ha llenado siempre el laboratorio de alegría. Siempre has procurado que no nos falte de nada material o emocional. Tus indicaciones, consejos y directas indirectas han sido una parte muy notoria del "alma" del laboratorio durante todos estos años y muy importantes para mí.

Por último y el más destacado de forma indiscutible, el *boss*, el **Dr. Enric Brillas**. Sin lugar a dudas eres la persona de la que más he aprendido profesionalmente. Debo agradecerte el que siempre hayas tenido a bien darme rienda suelta durante la tesis para desarrollar ideas y trabajos que en alguna ocasión no tenían tu aprobación absoluta o que no tenían relación directa con la tesis. Tus observaciones, indicaciones, consejos y explicaciones en lo referido al ámbito personal y profesional basadas en tu experiencia me acompañaran indelebles en el futuro. Contigo he comido prácticamente cada día y mantenido conversaciones de lo más diversas (química, docencia, historia, viajes, política y un largo etcétera) de las que he aprendido a nivel personal. También aprovecho para hacer el agradecimiento extensible a la **Dra. Rosa Mari Bastida** (la jefa del jefe), cuya simpatía y sinceridad deslumbran y de bien seguro algo ha tenido que ver.

El LEMMA es un grupo con mucho movimiento de gente que va y viene. No puedo olvidarme de toda la gente con la que he compartido laboratorio en algún momento, muchos de ellos ya doctores: **Birame, Paco, Marcel, Isaac, Nacho, Cristina, Elena, Anna, Isaraín, Amado, Núria, Abdo, Edgar, Lucio, Laye, Ricardo, Griselda, Serena, Alexa, Francisca, Brenda, Eliane, Claudio, Orlando, Alejandro, Angelo, Aline, Benji, Jennifer, Nelly, Fabio, Gabriel** y **Xavi**. En especial **Amado**, **Abdo** y **Laye**. Con vosotros tres he compartido días innumerables y horas que ya resultan incontables, tanto en el laboratorio como fuera de él. Creo que hemos tenido siempre un ambiente genial en el laboratorio y un apoyo mutuo que ha hecho que para mí fuera muy fácil trabajar día a día.

También quisiera destacar al **Dr. Lucio C. Almeida**, al **Dr. Ricardo Salazar**, **Francisca C. Moreria**, la **Dra. Eliane Bezerra Cavalcanti** y **Aline Sales Solano** con los que he trabajado codo con codo y a los que me une una gran amistad.

Fuera del laboratorio también hay vida en la universidad.

Me gustaría agradecer a la **Dra. Elvira Gómez** su ayuda en muchas gestiones que he realizado además de sus consejos impagables.

Ramón y **Lidia,** creo que habéis ayudado con vuestro trabajo al desarrollo de todas las tesis del departamento, pero sin lugar a dudas habéis ayudado en la mía. Especialmente quiero agradecer a **Ramón** su buena disposición y toda la ayuda que me ha brindado en más de una ocasión sin ser su obligación y sin ni siquiera tener que solicitarla.

No puedo dejar de agradecer a los miembros del *QuISU*, de los que he aprendido muchas cosas y sigo aprendiendo. En especial al **Dr. Jaume Granell**, la **Dra. Montserrat Cruells** y **la Dra. Mónica Martínez** con los que he compartido muchas horas de trabajo y que tantas cosas me han aportado.

Al **Dr. Sergi Dosta** le agradezco su buena disposición durante la colaboración que hemos establecido los dos entre el LEMMA y el CPT, que ha resultado en algunos trabajos que seguimos desarrollando.

A la **Dra. Jelena Radjenovic** y al **Dr. Jürg Keller** les agradezco la atención dedicada y la oportunidad de trabajar en el *Advanced Water Management Centre* de la Universidad de Queensland en la otra punta del mundo, Australia.

ÍNDICE

Acrónimos

A	Absorbancia (Absorbance)
ADE	Electrodo de difusión de aire (Air-diffusion electrode)
AO	Oxidación anódica (Anodic Oxidation)
AO7	Naranja ácido 7 (Acid Orange 7)
AOPs	Procesos de oxidación avanzada (Advanced Oxidation Processes)
AOX	Haluros orgánicos adsorbibles (Adsorbable organohalogens)
APS	Proyección térmica de plasma atmosférico (Atmospheric plasma spray)
AR151	Rojo ácido 151 (Acid Red 151)
AWMC	Advanced Water Management Centre
BDD	Diamante dopado con boro (Boron doped diamond)
BOD	Demanda bioquímica de oxígeno (Biochemical oxygen demand)
C-PTFE	Carbón-politetrafluoroetileno (Carbon-politetrafluoroethylene)
CHL	Cloranfenicol (Chloramphenicol)
CL	Quimioluminiscencia (Chemiluminescence)
COD	Demanda química de oxígeno (Chemical oxygen demand)
CPC	Colector parabólico compuesto (Compound parabolic collector)
CPT	Centro de Proyección Térmica
CR	Eliminación de color (Color removal)
δ_0	Velocidad de decoloración inicial (Initial decoloration rate)
DB71	Azul Directo 71 (Direct blue 71)
DMA	Directiva del Marco del Agua
DOC	Carbono orgánico disuelto (Dissolved organic carbon)
DPD	N,N-Dietil *p*-fenilendiamina
DSAs	Ánodos dimensionalmente estables (Dimensional stable anodes)
DY4	Amarillo Directo 4 (Direct Yellow 4)
e_{cb}^-	Electrón de la banda de conducción (Electron of conduction band)
EAOPs	Procesos electroquímicos de oxidación avanzada

	(Electrochemical advanced oxidation processes)
EC	Consumo energético (Energetic consume)
ECL	Electroquimioluminiscencia (Electrochemiluminescence)
EDS	Espectrometría dispersión de energía de rayos X
	(Energy dispersive X-ray spectroscopy)
EF	Electro-Fenton
FQL	Fem Química al Laboratori
FLU	Flumequina (Flumequine)
h_{vb}^{+}	Hueco en la banda de valencia (Hole of valence band)
HFCVD	Deposición química de vapor de filamento caliente
	(Hot filament chemical vapour deposition)
HPLC	Cromatografía líquida de alta presión (High pressure liquid chromatography)
IC	Carbono inorgánico (Inorganic carbon)
ITO	Óxidos de iridio y estaño (Iridium tin oxides)
LC-MS	Cromatografía de líquidos acoplada a espectrometría de masas
	(Liquid chromatography- mass spectroscopy)
LC-MS/MS	Cromatografía de líquidos acoplada a espectrometría de masas/masas
	(Liquid chromatography- mass spectroscopy/mass spectroscopy)
LEMMA	Laboratori d'Electroquímica dels Materials i del Medi Ambient
MCE	Eficiencia de corriente de mineralización (Mineralization current efficiency)
MS	Espectrometría de masas (Mass spectroscopy)
NDIR	Detector de infrarrojos no dispersivo (Non-dispersive infrared detector)
NOM	Materia orgánica natural (Natural organic matter)
NPOC	Carbono orgánico no purgable (Non-purgable organic carbon)
PA-EF	Electro-Fenton fotoasistido (photoassisted electro-Fenton)
PC	Fotocatálisis (Photocatalysis)
PEC	Fotoelectrocatálisis (Photoelectrocatalysis)
PEF	Fotoelectro-Fenton (Photoelectro-Fenton)

POPs	Contaminantes orgánicos persistentes
QuISU	Química a la Interfase Secundaria-Universitat
RIR	Ratio de intensidad de referencia (Reference Intensity Ratio)
ROS	Especies reactivas de oxígeno (Reactive oxygen species)
SEM	Microscopio electrónico de barrido (Scanning electron microscopy)
SHE	Electrodo Normal de Hidrógeno (Standard hydrogen electrode)
SIM	Selección de iones concretos (Selected-ion acquisition)
SPC	Solar fotocatálisis (Solar photocatalysis)
SPE	Extracción en Fase Sólida (Solid phase extraction)
SPEC	Solar fotoelectrocatálisis (Solar photoelectrocatalyisis)
SPEF	Solar fotoelectro-Fenton (Solar photoelectro-Fenton)
TC	Carbono total (Total carbon)
TIC	Corriente total de iones (Total ion current)
TN	Nitrógeno total (Total nitrogen)
TOC	Carbono orgánico total (Total organic carbon)
UB	Universitat de Barcelona
UFLC	Cromatografía de líquidos ultra-rápida (Ultra fast liquid chromatography)
UQ	University of Queensland
USEPA	United States Environmental Protection Agency
UVA	Ultravioleta de onda larga (Ultraviolet A)
XRD	Difracción de Rayos X (X-ray difraction)

1.INTRODUCCIÓN

1.1. El agua

El agua es una molécula inorgánica formada por dos átomos de hidrogeno y uno de oxígeno; pero el agua es mucho más, el agua es vida. La vida tal y como la conocemos sólo es posible gracias a este bien natural considerado inagotable.

La consideración de que es un recurso inagotable parte de la base de que el agua en sus tres estados (gas, líquido y sólido) se ha mantenido invariable a lo largo de la historia del planeta desde su aparición. La circulación de agua cambiando entre los diferentes estados purifica y redistribuye el agua en el planeta. Todo el proceso se recoge en el llamado ciclo hidrológico.

Si bien podemos considerar dicho ciclo factible, no podemos decir lo mismo para el agua potable o de consumo. Si analizamos detenidamente la distribución del agua en el planeta sorprenderá apreciar que tan solo el 2,5 % del agua es dulce y tan solo un 1,3 % potencialmente aprovechable por el hombre (USGS). El gran consumo de agua, en ocasiones desmesurado, por parte de la población y la constante emisión de contaminantes está generando un problema adicional a la limitación del recurso; puesto que el porcentaje de agua aprovechable se reduce alarmantemente cada año debido a la contaminación, tal y como se recoge en el informe anual del desarrollo mundial del agua de acceso abierto (UNESCO- World Water Development Report).

El agua es un bien común cuya calidad se ha visto enormemente disminuida por el rápido desarrollo del ser humano en el ámbito tecnológico, científico e industrial que ha dado lugar a una continuada contaminación y su consiguiente impacto ambiental . La preocupación sobre el medio ambiente ha ido en aumento durante las dos pasadas décadas ya que el continuo desarrollo genera nuevos contaminantes y además, se evidencia el fuerte impacto ambiental de algunos compuestos que se consideraban prácticamente inocuos debido a sus bajas concentraciones en el medio acuático, como es el caso de los contaminantes orgánicos persistentes (POPs).

1.2. Contaminantes orgánicos persistentes

El objetivo principal de esta tesis ha sido el desarrollo de metodologías para afrontar la problemática que suponen los contaminantes orgánicos persistentes. Estos contaminantes reciben el calificativo de persistentes debido a que no son eliminados o tan solo son parcialmente degradados en las plantas de tratamiento de aguas residuales mediante tratamientos convencionales generando otros contaminantes (Andreozzi y col., 2003; Karthikeyan y Meyer, 2006; Homem y Santos, 2011).

Los contaminantes orgánicos persistentes más habituales son fármacos, herbicidas, pesticidas y colorantes. Es evidente que los fármacos, herbicidas y pesticidas se han concebido para que ejerzan una determinada actividad farmacológica o biológica, por lo que resultan potencialmente peligrosos para el medioambiente al ser capaces de causar respuestas metabólicas a muy bajas concentraciones.

Pese a que en el medio ambiente existe un gran número de fármacos que se encuentran en bajas concentraciones entre ng L^{-1} y µg L^{-1} (Tamtam y col., 2008; Kümmerer, 2009), ya se han constado algunos efectos perjudiciales como el desarrollo de cepas bacterianas multiresistentes (Naviner y col., 2011), cambio de sexo en peces (Yeh y col., 2003) y efectos en su diferenciación sexual (Devlin y Nagahama, 2002), influencias en los sistemas endocrinos de peces e invertebrados (Migliore y col., 1997), fallos renales (Triebskorn y col., 2004) o toxicidad en algas y pequeños vertebrados (Crane y col., 2006; Pomati y col., 2008). Todos estos efectos pueden ser considerados potencialmente adversos para la salud de los seres vivos.

Los colorantes orgánicos, de los cuales los colorantes azoicos suponen el 70 % de la producción mundial (Forgacs y col., 2004), son descargados en grandes concentraciones en los efluentes industriales. El problema medioambiental más fácilmente identificable está relacionado con la tinción de las aguas, incluso a muy bajas concentraciones de colorantes. La coloración del agua no tiene solamente un impacto visual considerable (ríos de color rojo, verde, amarillo, etc), sino que tienen un efecto directo en los ecosistemas acuíferos. La coloración del agua reduce al paso de radiación afectando a la fotosíntesis de plantas y algas, así como a la vida animal. Pero normalmente el problema de visibilidad no es el peor, ya que los colorantes azoicos son en muchos casos tóxicos, carcinogénicos y mutagénicos para los seres vivos incluido el ser humano (Umbuzeiro y col., 2005; Ulson de Souza y col., 2007; Sharma y col., 2007). Los colorantes azoicos

además son muy estables en el medio ambiente al ser muy resistentes a la oxidación y reducción naturales, la biodegradación y la fotodescomposición (Robinson y col., 2001; Martínez-Huitle y Brillas, 2009).

Todos estos problemas y riesgos medioambientales no son los únicos que suponen una creciente preocupación. Una degradación incompleta en las plantas de tratamiento puede en muchos casos generar intermedios todavía más nocivos y recalcitrantes que los productos iniciales agravando los problemas medioambientales (Oh y Tuovinen, 1991).

Todo lo expuesto anteriormente evidencia la necesidad de desarrollar e implantar técnicas de tratamientos de aguas mucho más potentes que sean capaces de eliminar completamente los contaminantes orgánicos persistentes y los intermedios generados durante su degradación.

1.3. Legislación

Los países de la Unión Europea se rigen por la Directiva del Marco del Agua (DMA) que es una norma del Parlamento Europeo y del Consejo de la Unión Europea en la que se establece un marco de actuación común para todos los países miembros de la U.E. en lo que se refiere a política y legislación sobre aguas. El principal objetivo de la DMA es promover un uso sostenible del recurso natural hídrico y su protección para garantizar la disponibilidad de agua de calidad a largo plazo.

En la legislación española se recogen las directrices europeas de la DMA en la directiva 2000/60/CEE estableciendo el marco comunitario para la protección de las aguas superficiales, costeras, subterráneas y de transición. Hay otras directrices más relacionadas con la contaminación del agua y su calidad. Así, la directiva 98/83/CEE tiene como objeto la protección de la salud de las personas estableciendo unos marcos de salubridad y limpieza del agua para consumo humano; la directiva 91/676/CEE trata sobre la contaminación producida por nitratos utilizados en la Agricultura; y la directiva 91/271/CEE modificada por la directiva 98/15/CEE relacionada con el tratamiento de las aguas residuales urbanas, considera su tratamiento y la gestión de vertidos de aguas residuales de determinados sectores industriales.

Estas leyes establecen unos parámetros límites de demanda bioquímica de oxígeno (BOD), demanda química de oxígeno (COD), sólidos en suspensión, fósforo y nitrógeno.

Desgraciadamente no hacen referencia directa a los contaminantes que contengan, pero teniendo en cuenta la preocupación que se desprende de los informes anuales del desarrollo mundial del agua (UNESCO- World Water Development Report) sobre ciertos contaminantes específicos entre ellos los POPs y de forma destacada sobre aguas residuales procedentes de las industrias de tinción (colorantes azoicos) y del cuero (taninos) y de otros contaminantes con efectos directos en los ecosistemas acuáticos (fenoles, organoclorados aromáticos, fármacos, herbicidas, etc.) no cabe duda de que en los próximos años la Unión Europea tomará la iniciativa en legislación ambiental sobre este tipo de contaminantes tan perjudiciales y difíciles de tratar.

1.4. Tratamientos convencionales

Los tratamientos convencionales se clasifican en tres grandes grupos: físicos, químicos y biológicos.

Los métodos físicos consisten en separar los contaminantes, sin degradarlos, del medio acuoso bien por precipitación, floculación (Julien y col., 1994), coagulación (Boye y col., 2003), sedimentación (O'Melia, 1998), adsorción sobre carbón activo (Newcombe y col., 2002) o filtración por membranas (Ersahin y col., 2012). Si bien son métodos efectivos para eliminar contaminantes a altas concentraciones, no son especialmente buenos para los contaminantes orgánicos persistentes ya que éstos presentan bajas concentraciones. Además, estos métodos conllevan un gran coste energético, generan un residuo sólido que requiere un tratamiento posterior y, en algunos casos, precisan costosos mantenimientos como son la recuperación de los adsorbentes (Shende y Mahajani, 2002) o de las membranas (Ebrahim, 1994; Donose y col., 2013).

Los métodos químicos se basan en tratamientos oxidantes para tratar de eliminar los contaminantes o modificar su estructura. Se utilizan agentes oxidantes fuertes (ver **Tabla 1**) como el cloro (Vaid y col., 2010), el permanganato de potasio (Zhang y col., 2009), el peróxido de hidrógeno (Dionysiou y col. 2004) o el ozono (Freese y col., 1999; Skoumal y col., 2006). Los problemas que presentan estas metodologías dependen del oxidante empleado. El uso de cloro o hipoclorito puede generar intermedios organoclorados (Ivancev-Tumbas y col., 1999) que son carcinogénicos e incluso peores que los contaminantes de partida. El $KMnO_4$ es mucho más caro que el cloro y genera residuos

sólidos de dióxido de manganeso (Zhang y col., 2009). Los problemas del ozono residen en que es poco soluble en agua, tóxico, inestable y de difícil manejo.

Los métodos biológicos son los más utilizados debido a su bajo coste, sin embargo presentan serias limitaciones. Los tratamientos requieren mucho tiempo (hasta meses) y requieren grandes superficies (Chan y col., 2009). Además, desgraciadamente los compuestos no biodegradables y los tóxicos para los microorganismos no pueden ser tratados.

1.5. Procesos de oxidación avanzada

Los procesos de oxidación avanzada (AOPs) aparecen como una interesante alternativa a los métodos anteriores al ser capaces de oxidar completamente los contaminantes orgánicos a CO_2, H_2O e iones inorgánicos (Klavarioti y col., 2009). Estos procesos se basan en la generación *in situ* del radical hidroxilo ($^{\bullet}OH$) con un E^o = 2,80 V vs SHE. El $^{\bullet}OH$ es el segundo agente oxidante más fuerte conocido después del flúor (ver **Tabla 1**) (Brillas y col., 2009). El ataque no selectivo a los contaminantes orgánicos, su alta reactividad, la no generación de residuos adicionales y su corto tiempo de vida (menos de 70 ns) hacen del radical $^{\bullet}OH$ el oxidante perfecto.

Dependiendo de la naturaleza de las especies orgánicas en disolución, se describen tres tipos de ataques del radical hidroxilo con constantes cinéticas de segundo orden en el rango de 10^6 a 10^{10} M^{-1} s^{-1} (Brillas y col., 2009):

(I) Abstracción de un átomo de hidrogeno para formar agua mediante la reacción (1), principalmente con alcanos y alcoholes.

$$RH + {}^{\bullet}OH \rightarrow R^{\bullet} + H_2O \qquad (1)$$

(II) Hidroxilación del compuesto orgánico según la reacción global (2), como es común con alquenos y compuestos aromáticos.

$$R + {}^{\bullet}OH \rightarrow ROH \qquad (2)$$

(III) Reacciones de transferencia de carga (reacción (3)):

$$^{\bullet}OH + H^+ + e^- \rightarrow H_2O \qquad (3)$$

Tabla 1. *Potenciales de reducción de agentes oxidantes*.

Oxidante	**Reacción de reducción**	**Potencial estándar de reducción, E^o/ V vs SHE**
Flúor	$F_2(g) + 2H^+ + 2e^- \rightarrow 2HF$ $F_2(g) + 2e^- \rightarrow 2\ F^-$	3,05 2,87
Radical hidroxilo	$^{\bullet}OH + H^+ + e^- \rightarrow H_2O$	2,80
Anión sulfato radical	$SO_4^{\bullet -} + e^- \rightarrow SO_4^{2-}$	2,60
Ion ferrato	$FeO_4^{2-} + 8H^+ + 3e^- \rightarrow Fe^{3+} + 4H_2O$	2,20
Ozono	$O_3(g) + 2H^+ + 2e^- \rightarrow O_2(g) + H_2O$	2,07
Ion peroxodisulfato	$S_2O_8^{2-} + 2e^- \rightarrow 2SO_4^{2-}$	2,01
Peróxido de hidrogeno	$H_2O_2 + 2H^+ + 2e^- \rightarrow 2H_2O$	1,76
Ion permanganato (I)	$MnO_4^- + 4H^+ + 3e^- \rightarrow MnO_2(s) + 2H_2O$	1,67
Radical hidroperoxilo (I)	$HO_2^{\bullet} + 3H^+ + 3e^- \rightarrow 2H_2O$	1,65
Ion permanganato (II)	$MnO_4^- + 8H^+ + 5e^- \rightarrow Mn^{2+} + 4H_2O$	1,51
Radical hidroperoxilo (II)	$HO_2^{\bullet} + H^+ + e^- \rightarrow H_2O_2$	1,44
Ion dicromato	$Cr_2O_7^{2-} + 14H^+ + 6e^- \rightarrow 2Cr^{3+} + 7H_2O$	1,36
Cloro	$Cl_2(g) + 2e^- \rightarrow 2Cl^-$	1,36
Dióxido de manganeso	$MnO_2 + 4H^+ + 2e^- \rightarrow Mn^{2+} + 2H_2O$	1,23
Oxígeno	$O_2(g) + 4H^+ + 4e^- \rightarrow 2H_2O$	1,23

1.6. Procesos electroquímicos de oxidación avanzada

Los procesos electroquímicos de oxidación avanzada (EAOPs) permiten la generación continua de $^{\bullet}OH$ mediante métodos electroquímicos (Martínez-Huitle y Brillas, 2009; Panizza y Cerisola, 2009) y su estudio es el principal objetivo de esta tesis. Las principales ventajas de estos sistemas residen en que no requiere la adición de productos químicos peligrosos por lo que eliminan los riesgos de manipulación, transporte y almacenamiento de los mismos ($KMnO_4$, H_2O_2, Cl_2, etc). No generan residuos que se deban retirar posteriormente (métodos físicos o MnO_2), ni precisan costosos mantenimientos como membranas de filtración o la recuperación de adsorbentes (Brillas y col., 2009; Feng y col., 2013). Además, el electrón, el principal reactivo, es barato y limpio siempre y cuando la corriente eléctrica provenga de una fuente de energía renovable, por lo que consecuentemente es amigable con el medio ambiente y con un potencial interés industrial.

1.6.1. Fotoelectrocatálisis con TiO_2

La fotocatálisis con TiO_2 (PC) se basa en la irradiación de nanopartículas de TiO_2 (principalmente en fase anatasa) con radiación UV de suficiente energía para promover que un electrón de la banda de valencia llena se desplace a la banda de conducción vacía (e_{cb}^-) generando a su vez una vacante o hueco (h_{vb}^+) tal y como se recoge en la reacción (4) (Fujishima y col., 2008; Akpan y Hameed, 2009). Si la fuente de radiación es la luz solar el proceso se conoce como fotocatálisis solar (SPC).

$$TiO_2 + h\nu \rightarrow e_{cb}^- + h_{vb}^+ \qquad (4)$$

En consecuencia, los compuestos orgánicos pueden reducirse por el electrón generado u oxidarse por el hueco. Adicionalmente el hueco es capaz de generar $^{\bullet}OH$ con el agua adsorbida en la superficie o con los iones OH^- :

$$h_{vb}^+ + H_2O \rightarrow {}^{\bullet}OH + H^+ \qquad (5)$$

$$h_{vb}^+ + OH^- \rightarrow {}^{\bullet}OH \qquad (6)$$

Dado que el oxidante es el $^{\bullet}OH$, este proceso quedaría englobado dentro de los AOPs. El problema de este procedimiento está relacionado con la perdida de eficiencia debida a la recombinación de los electrones promocionados con los huecos por la reacción (7) o los

radicales hidroxilos generados por la reacción (8) (Andreozzi y col., 1999; Martínez-Huitle y Brillas, 2009).

$$e_{cb}^- + h_{vb}^+ \rightarrow \text{calor} \quad (7)$$

$$e_{cb}^- + {}^{\bullet}OH \rightarrow OH^- \quad (8)$$

Cuando se trabaja con nanopartículas en suspensión se requiere de un costoso post-tratamiento, bien para eliminar estas nanopartículas de la disolución o para recuperarlas para su reutilización. Una alternativa que elimina la necesidad del post-tratamiento es recurrir a la fotocatálisis heterogénea, inmovilizando los fotocatalizadores de TiO_2 sobre una superficie sólida mediante diferentes metodologías. El principal inconveniente de la fotocatálisis heterogénea está asociado con el problema de la recombinación que se ve incrementada por la gran pérdida de área específica disponible para la fotorreacción (Shan y col., 2010).

Es justo en este punto donde aparece la electroquímica. Si se emplea como sustrato del depósito un material conductor, se puede utilizar el depósito de TiO_2 como ánodo. La aplicación de una densidad de corriente anódica al fotoánodo de TiO_2 sometido a radiación UV permite la extracción de forma contínua de los electrones fotogenerados mediante un circuito externo (Daghrir y col., 2012). Esto permite inhibir las reacciones (7) y (8) de recombinación favoreciendo la generación de radical $^{\bullet}OH$ y aumentando así la ratio de reacciones de oxidación de los compuestos orgánicos favoreciendo la destrucción de los contaminantes, por lo que se mejora la eficiencia oxidativa del proceso de fotocatálisis. Si en PC se aplica corriente eléctrica el proceso se denomina fotocatálisis electroasistida o fotoelectrocatálisis (PEC); y en el caso de utilizar radiación solar natural, fotoelectrocatálisis solar (SPEC).

1.6.2. Oxidación anódica

La oxidación anódica (AO) es el EAOPs más utilizado y estudiado. Se basa en la utilización de ánodos de elevado sobrepotencial de evolución de O_2. Estos ánodos favorecen la generación de radicales $^{\bullet}OH$ adsorbidos en la superficie anódica (Marselli y col., 2003; Panizza y Cerisola, 2009; Sales y col., 2013) como resultado de la oxidación de agua por la reacción (9):

$$M + H_2O \rightarrow M(^{\bullet}OH) + H^+ + e^- \quad (9)$$

donde M es el ánodo y M(•OH) el radical adsorbido sobre la superficie anódica. Los ánodos más utilizados son de Pt (Sirés y col., 2006; Rocha y col., 2012), PbO_2 (Iniesta y col., 2001; Flox y col., 2009; Aquino y col., 2011), ánodos dimensionalmente estables (DSA) formados por óxidos metálicos (IrO_2, SnO_2, Ta_2O_5, etc) y mezclas de los mismos óxidos (Martínez-Huitle y col., 2004a; 2004b; Scialdone y col., 2009; Bagastyo y col., 2013) y capas delgadas de diamante dopado con boro (BDD) (Panniza y col., 2001; Boye y col., 2006; Borràs y col., 2013).

Cabe destacar que además de la oxidación indirecta debida a la electrogeneración de radicales •OH en las superficies anódicas, también pueden ocurrir reacciones de transferencia de carga directa en el ánodo.

El grupo del Prof. Comninellis, principal impulsor del BDD en sus inicios (Panizza y col., 2001; Bellagamba y col., 2002; Duo y col., 2003), propuso clasificar los materiales anódicos en dos grandes grupos, activos y no activos, según que eliminaran a los contaminantes (Comninellis, 1994) de la siguiente manera:

I) Los ánodos activos conducen a la **conversión electroquímica**, en la que los compuestos orgánicos recalcitrantes son convertidos en compuestos biodegradables.

II) Los ánodos no activos dan lugar a la **combustión o incineración electroquímica**, en la que los compuestos orgánicos son completamente mineralizados y convertidos en CO_2, agua e iones inorgánicos.

Evidentemente los ánodos pueden describir simultáneamente ambos comportamientos aun cuando puede predominar uno de los dos. El grupo del Prof. Comninellis (Kapalka y col., 2008) también ha relacionado el poder oxidante de diferentes ánodos en función de la entalpía de adsorción del radical •OH, estableciendo que cuanto menor es la adsorción mayor es la reactividad del radical hidroxilo favoreciendo la mineralización de los compuestos orgánicos (ver **Tabla 2**).

Las evidencias experimentales recogidas durante los últimos años señalan al BDD como el material anódico de mayor interés para el tratamiento de contaminantes orgánicos persistentes mediante AO (Cañizares y col., 2004; Hammami y col., 2008; Sirés y col. 2008; Brillas y col., 2010), llegando incluso a mineralizar los recalcitrantes ácidos carboxílicos alifáticos (Cañizares y col., 2003; Martínez-Huitle y col., 2004a; Scialdone y col., 2008).

Tabla 2. *Relación del poder oxidante de distintos materiales electródicos en función de la entalpía de adsorción del radical •OH sobre la superficie anódica y relación de sobrepotenciales de evolución de oxígeno (Kapalka y col. (2008).*

Electrodo	Eº / V	Sobrepotencial de evolución de O_2 / V	Entalpia de adsorción M-OH	Poder oxidante
RuO_2-TiO_2	1,4 – 1,7	0,18	Quimisorción	Menor
IrO_2-Ta_2O_5	1,5 – 1,8	0,25	⇑	⇓
Ti-Pt	1,7 – 1,9	0,3		
Ti-PbO_2	1,8 – 2,0	0,5		
Ti/SnO_2-Sb_2O_5	1,9 – 2,2	0,7		
p-Si/BDD	2,2 – 2,6	1,3	Fisisorción	Mayor

1.6.3. Electro-Fenton

El proceso electro-Fenton (EF) se basa en la reacción de Fenton. En el año 1894 se describió que el peróxido de hidrogeno en medio ácido y en presencia de un catalizador metálico (principalmente el catión hierro (II)) genera grandes cantidades de radical hidroxilo en el seno de la disolución (Fenton, 1894), reacción que se conoce como la clásica reacción de Fenton (10):

$$H_2O_2 + Fe^{2+} \rightarrow Fe^{3+} + OH^- + {}^{\bullet}OH \qquad (10)$$

El proceso Fenton es uno de los AOPs que goza actualmente de gran popularidad y ha sido profundamente estudiado por diferentes grupos como posible proceso aplicable al tratamiento de POPs (Rodríguez y col., 2002; Gernjak y col., 2003; Tokumura y col., 2008).

En la reacción de Fenton el Fe^{2+} es un reactivo puesto que es someramente regenerado por la reacción Fenton-like (11) que consume peróxido de hidrogeno generando radical hidroperoxilo ($HO_2^{\bullet}$) de un poder oxidante considerablemente menor. Además, los radicales hidroxilo pueden ser simultáneamente consumidos en las reacciones parásitas (12) y (13) que consumen ambos reactivos.

$$H_2O_2 + Fe^{3+} \rightarrow Fe^{2+} + HO_2^{\bullet} + H^+ \qquad (11)$$

$$H_2O_2 + {}^{\bullet}OH \rightarrow HO_2{}^{\bullet} + H_2O \quad (12)$$

$$Fe^{2+} + {}^{\bullet}OH \rightarrow Fe^{3+} + OH^- \quad (13)$$

El pH óptimo para el desarrollo de la reacción de Fenton es cercano a 3,0 (Sun y Pignatello, 1993; Sirés y Brillas, 2012). A pH inferiores el protón actúa de *scavenger* del $^{\bullet}OH$ (Pignatello, 1992) disminuyendo su disponibilidad para reacciones orgánicas, mientras que a pH superiores la precipitación de hidróxidos de hierro decrecen considerablemente la concentración del Fe^{2+} de la disolución.

Las ventajas que ofrece el proceso EF residen en la contínua electrogeneración de peróxido de hidrogeno mediante la reducción catódica bielectrónica de oxígeno en el cátodo por la reacción (14) y la regeneración de Fe^{2+} por la reacción (15) de reducción del Fe^{3+} (Brillas y col., 2009). El oxígeno se reduce eficientemente a H_2O_2 en cátodos carbonáceos como el fieltro de carbón (Özcan y col., 2008; Oturan y col., 2010; El-Ghenymy y col., 2013b), fieltro de grafito (Panizza y Oturan, 2011), fibra de carbón activada (Wang y col., 2008a), electrodos de gas de carbón-politetrafluoroetileno (C-PTFE) (Boye y col., 2003; Flox y col., 2006, Serra y col., 2009; Cavalcanti y col., 2013), nanotubos de C-PTFE (Khataee y col., 2010; Zarei y col., 2010) o sobre BDD (Cruz-González y col., 2010).

$$O_2 + 2\,H^+ + 2\,e^- \rightarrow H_2O_2 \quad (14)$$

$$Fe^{3+} + e^- \rightarrow Fe^{2+} \quad (15)$$

En resumen, el proceso de EF electrogenera de forma continua el H_2O_2 necesario para la reacción por lo que no se requiere transporte de una sustancia química peligrosa y el Fe^{2+} actúa como catalizador de la reacción al ser continuamente regenerado y no únicamente consumido. Ambos efectos benefician notablemente el proceso de mineralización de compuestos orgánicos al favorecer notablemente la electrogeneración del radical hidroxilo en el seno de la disolución. El hecho de que el Fe^{2+} actúe de catalizador en el proceso EF hace que tan solo se requieran bajas concentraciones de catión cercanas al límite de 200 $\mu g\ L^{-1}$ establecido por ley (real decreto 140/2003) en las aguas para consumo humano, por lo que muchas aguas ya contienen el Fe^{2+} necesario y no es necesaria su adición para llevar a cabo el tratamiento. Cabe destacar que el H_2O_2 sobrante no supone ningún problema adicional al desproporcionarse rápidamente generando agua y oxígeno mediante la reacción (16).

$$2\ H_2O_2 \rightarrow 2\ H_2O + O_2 \qquad (16)$$

La principal limitación del proceso EF está relacionada con la generación de los intermedios finales previos a la mineralización completa, los ácidos carboxílicos de cadena corta. Los ácidos carboxílicos de bajo peso molecular como los ácidos oxálico, oxámico o fórmico son recalcitrantes de *per se*, pero al formar complejos con el Fe(III) son incluso más recalcitrantes (Pera-Titus y col., 2004; Garcia-Segura y Brillas, 2011). Adicionalmente, la formación de estos complejos estables de Fe(III) tiene otro efecto negativo: la captura y disminución del catalizador disponible en disolución, hecho que frena o incluso inhibe irremediablemente la reacción de Fenton (10). Debido a todo lo comentado anteriormente, mediante este proceso no se alcanza la mineralización completa, pese a que la materia orgánica remanente se torna biodegradable.

1.6.4. Fotoelectro-Fenton y fotoelectro-Fenton solar

En el proceso fotoelectro-Fenton (PEF) la solución tratada por EF es simultáneamente irradiada con luz ultravioleta de onda larga (UVA) de $\lambda_{máx}$ = 360 nm. La luz UVA tiene genera radical $^{\bullet}OH$ adicional como resultado de la fotoreducción de las especies de Fe^{3+} que regeneran simultáneamente el catalizador por la reacción (17) propagando la reacción de Fenton (10). Si se usa luz UVC de $\lambda_{máx}$ = 254 nm se produce adicionalmente la fotodescomposición de H_2O_2 por la reacción (18).

$$[Fe(OH)]^{2+} + h\nu \rightarrow Fe^{2+} + {}^{\bullet}OH \qquad (17)$$

$$H_2O_2 + h\nu \rightarrow 2\ {}^{\bullet}OH \qquad (18)$$

Otro efecto relacionado con la irradiación UVA es quizás el más relevante en lo que a la mineralización se refiere y está relacionado con la eliminación de los complejos de Fe(III)-carboxilato. Estas especies son en muchos casos fotodescarboxiladas (Guinea y col., 2009; Garcia-Segura y Brillas, 2011) favoreciendo la completa mineralización y la liberación del ion Fe^{3+} complejado, fotorreduciéndolo simultáneamente a ion Fe^{2+} mediante una reacción de transferencia de carga del ligando al centro metálico (Šima y Makáňová, 1997), cuya expresión global se muestra en la reacción (19) (Faust y Zepp, 1993).

$$[Fe(OOCR)]^{2+} + h\nu \rightarrow Fe^{2+} + CO_2 + R^{\bullet} \qquad (19)$$

Pese a que los trabajos realizados por otros grupos y el nuestro han demostrado sobradamente su eficiencia (Brillas y col., 2003; Wang y col., 2008a; Zarei y col., 2010; Almeida y col., 2012; Anotai y col., 2011), el problema que plantea el proceso PEF está relacionado con el alto consumo energético de las lámparas comerciales de UVA. Sin embargo, es un problema fácilmente solventable mediante el uso de radiación solar. La luz solar es una fuente inagotable, gratuita y de mayor intensidad de radiación que las lámparas, por lo que reduce drásticamente el consumo energético y permite plantear un nuevo proceso más eficiente y amigable con el medio ambiente que se denomina fotoelectro-Fenton solar (SPEF) (Skoumal y col., 2009; Ruiz y col., 2011; Moreira y col., 2013).

1.7. Reacciones parásitas del radical $^{\bullet}OH$

El radical hidroxilo es tan reactivo que no solo se consume en reacciones orgánicas dando lugar a la mineralización de los contaminantes, sino que también se consume en reacciones parásitas no oxidantes como las indicadas en las reacciones (10) y (12). Muchas de estas reacciones involucran diferentes especies reactivas de oxígeno (ROS) en el medio reaccional, como las reacciones (20) y (21):

$$2\ {}^{\bullet}OH \rightarrow H_2O_2 \qquad (20)$$

$${}^{\bullet}OH + HO_2{}^{\bullet} \rightarrow O_2 + 2\ H^+ \qquad (21)$$

Las reacciones parásitas también las puede producir el radical M($^{\bullet}$OH) adsorbido en las superficies anódicas, destacando por ejemplo:

$$2\ M({}^{\bullet}OH) \rightarrow 2\ M + O_2 + 2\ H^+ + 2\ e^- \qquad (22)$$

$$2\ M({}^{\bullet}OH) \rightarrow 2\ M + H_2O_2 \qquad (23)$$

$$H_2O_2 + M({}^{\bullet}OH) \rightarrow H_2O + M(HO_2{}^{\bullet}) \qquad (24)$$

$$M({}^{\bullet}OH) + M(HO_2{}^{\bullet}) \rightarrow 2\ M + O_2 + 2\ H^+ \qquad (25)$$

Pero en un medio altamente oxidante no sólo se favorece la generación de ROS, sino que debido a las condiciones de trabajo es factible la generación de otras especies menos oxidantes que el radical $^{\bullet}$OH a partir de reacciones de transferencia de carga sobre algunos ánodos, especialmente del BDD (Velazquez-Peña y col., 2013). Estos agentes se pueden formar a partir de otras especies en disolución como el ion peroxodisulfato a partir de los iones sulfato por la reacción (26) (Serrano y col., 2002), el ion peroxodifosfato a

partir del ion fosfato por la reacción (27) (Sánchez y col. 2013), el ozono a partir de la propia agua por la reacción (28) o incluso el ion ferrato por la reacción (29) (Cañizares y col., 2007):

$$2\ SO_4^{2-} \rightarrow S_2O_8^{2-} + 2e^- \quad (26)$$

$$2\ PO_4^{3-} \rightarrow P_2O_8^{4-} + 2e^- \quad (27)$$

$$3\ H_2O \rightarrow O_{3\ (g)} + 6\ H^+ + 6\ e^- \quad (28)$$

$$Fe^{3+} + 4\ H_2O \rightarrow FeO_4^{2-} + 8\ H^+ + 3\ e^- \quad (29)$$

Aunque estas reacciones dan lugar a productos de interés industrial, son consideradas reacciones parásitas en cuanto a la oxidación de contaminantes porque generan especies con menor capacidad reactiva que el radical $^{\bullet}OH$ por lo que reducen el poder oxidante del sistema, pese a que también puedan ser capaces en algunos casos de oxidar algunos contaminantes de forma eficiente.

1.8. Electroquimioluminiscencia

La quimioluminiscencia (CL) es el fenómeno en que la energía de las reacciones químicas no sólo se emite en forma de calor o energía química, sino también en forma de luz. La emisión lumínica se debe a que la reacción química genera una molécula en estado excitado que durante el proceso de relajación a su estado fundamental produce la emisión de luz (Dodeigne y col., 2000).

Recientemente, la CL electrogenerada o electroquimioluminiscencia (ECL) ha recibido un considerable y creciente interés en química analítica debido a su alta sensibilidad, amplio rango de aplicación y simple operatividad (Knight, 1999; Wang y col., 2008b). El proceso de ECL se suele explicar por mecanismos similares a los convencionales de CL, aunque se involucran procesos de oxidación anódica directos junto a reacciones con ROS electrogeneradas que permiten generar el emisor de radiación lumínica.

1.9. Antecedentes bibliográficos

Es indudable el grave problema ambiental que suponen los POPs tal y como se ha puesto de manifiesto en los anteriores apartados. El principal inconveniente en el tratamiento de estos contaminantes está relacionado con la escasez de procesos adecuados para su completa eliminación y que sean asequibles económicamente.

Dentro de este contexto se enmarca el trabajo desarrollado en la presente tesis, cuyo principal objetivo ha sido el estudio de diferentes procesos electroquímicos de oxidación avanzada aplicados al tratamiento de aguas sintéticas y aguas reales contaminadas con POPs tanto en reactor de tanque perfectamente agitado como en una planta pre-piloto de recirculación de 10 L.

La viabilidad de estas metodologías también se ha estudiado cosiderando contaminantes emergentes en aguas reales. Los compuestos estudiados durante el desarrollo de esta tesis se presentan a continuación.

Fármacos

Flumequina

La flumequina (FLU) es un agente antimicrobiano perteneciente a la familia de las fluoroquinolonas (ver su fórmula estructural en la **Fig. 1**). Este fármaco es muy utilizado en veterinaria para el control de infecciones bacterianas principalmente en piscifactorías, donde se administra en grandes concentraciones debido a la baja biodisponibilidad en peces (Burridge y col., 2010).

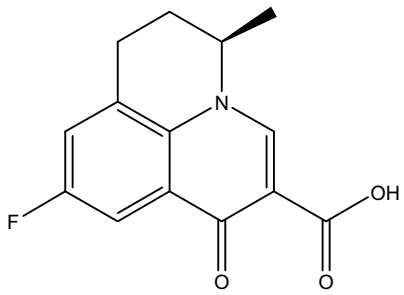

Figura 1.- *Estructura molecular de la flumequina.*

La FLU ha sido detectada en ríos en concentraciones de hasta 50 ng L^{-1} (Tamtam y col., 2008; Muñoz y col., 2010), lo que puede favorecer la aparición de cepas bacterianas multiresistentes (Naviner y col., 2011).

Estudios medioambientales demuestran que este contaminante presenta una alta resistencia a la fotodegradación, requiriéndose más de 121 dias para degradar un 50% generando otros contaminantes (Pouliquen y col., 2007), además de presentar una completa inactividad fotoquímica durante los primeros 14 días de exposición a radiación solar. Asimismo también se ha señalado que posee una alta resistencia a la degradación por oxidación química con ClO_2 (Wang y col., 2010), a diferencia de otras fluoroquinolonas. En la bibliografía se ha descrito el tratamiento de FLU por diferentes AOPs como la fotocatálisis con TiO_2 o procesos de tipo Fenton. En el caso de la fotocatálisis con TiO_2, se han tratado bajas concentraciones (de 100 μg L^{-1} a 20 mg L^{-1}) de FLU (Nieto y col., 2008; Miranda-García y col., 2011) degradándose el 90 % en 40 min, pero no se discute la mineralización del compuesto ni la generación de intermedios de degradación. En los procesos Fenton y foto-Fenton (Klamerth y col., 2011; Rodrigues-Silva y col., 2013), se alcanza la completa eliminación de la FLU de partida sin analizar el proceso de mineralización con profundidad. El trabajo de Rodrigues-Silva y col. (2013) describe algunos intermedios de degradación y la pérdida del efecto antibacteriano de las disoluciones tratadas al destruirse la FLU.

Cloranfenicol

El cloranfenicol (CHL) es un antibiótico de amplio espectro, efectivo contra una gran variedad de bacterias Gram-positivas, Gram-negativas e incluso organismos anaeróbicos. Es ampliamente utilizado en los países en vías de desarrollo para el tratamiento de infecciones bacterianas en diferentes formas farmacéuticas. En cambio, en los países desarrollados esta indicado principalmente para el tratamiento de conjuntivitis en forma de colirio. Su propiedad antibacteriana característica hace que el tratamiento biológico no sea aplicable al tratamiento de este contaminante. Debido a todo lo anteriormente expuesto y a su alta fotoestabilidad en condiciones ambientales,

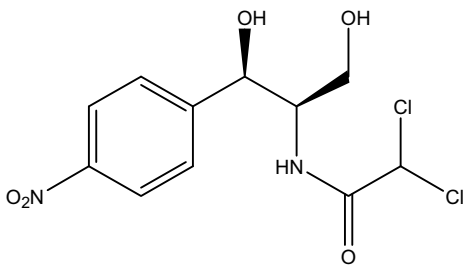

Figura 2. *Estructura molecular del cloranfenicol.*

este compuesto se detecta como contaminante por todo el mundo en lagos, ríos y efluentes de estaciones depuradoras (Xu y col., 2011; Zhou y col., 2013).

La imposibilidad de aplicar tratamientos biológicos a efluentes contaminados con CHL y su efecto directo sobre microorganismos genera un indiscutible impacto ambiental. Cabe señalar algunas publicaciones donde se ha estudiado la eliminación de este fármaco por varios métodos descritos anteriormente. La destrucción bajo irradiación UVC y el tratamiento con aire ionizado de 10 mg L^{-1} de compuesto redujeron la toxicidad sobre bacterias aunque con grandes costes asociados (Suling y col., 2002). Los tratamientos fotocatáliticos con TiO_2 y ZnO_2 eliminaron el 90% de una concentración inicial de 50 mg L^{-1} de CHL en 90 min y destruyeron casi completamente los correspondientes 15 mg L^{-1} de DOC después de 4 h (Chatzitakis y col., 2008). La ozonización también permitió una drástica reducción de la toxicidad de varias disoluciones de CHL después de 120 min de tratamiento, dando lugar a una mineralización parcial (Wang y col., 2012).

Colorantes

Tal y como se describió anteriormente en el apartado sobre los POPs, los colorantes son unos contaminantes que generan una gran preocupación debido a la alarma social que produce la contaminación visual de las aguas. Diversas fotografías que denuncian la contaminación muestran ríos de coloraciones diversas, desde rojo sangre a verde fosforescente, ya que es más fácil concienciar a la gente sobre aquello que puede ver a simple vista. El problema de la coloración de cuerpos acuosos va más allá de un problema estético; la coloración tiene un efecto directo sobre los ecosistemas acuáticos ya que reduce el paso de radiación afectando a plantas, algas y vida animal.

Además, los colorantes azoicos estudiados en la presente tesis presentan en muchos casos toxicidad, carcinogénesis y efectos mutagénicos (Umbuzeiro y col., 2005; Sharma y col., 2007).

Debido a los problemas ambientales que generan y su alto carácter biorefractario que los hace altamente resistentes a los tratamientos convencionales (Robinson y col., 2001; Martínez-Huitle y Brillas, 2009) se han aplicado algunos AOPs y EAOPs como posibles vías de remediación. La fotocatálisis con TiO_2 (Essawy y col., 2008; Juang y col., 2010) ha demostrado ser efectiva para decolorar aguas con contenidos muy bajos de colorantes (del orden del μM), siendo ineficientes para la mineralización de las mismas.

Tabla 3. *Colorantes tratados por EAOPs en la presente tesis.*

Nombre del Color Índex	Número del Color Índex	Estructura	$\lambda_{máx.}$ (nm)
Acid Orange 7	15510	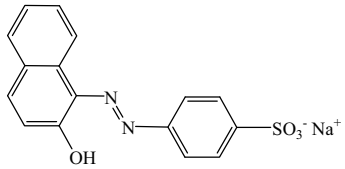	484
Acid Red 151	26900	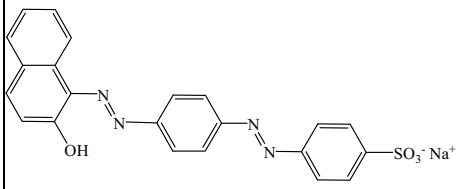	500
Direct Blue 71	34140	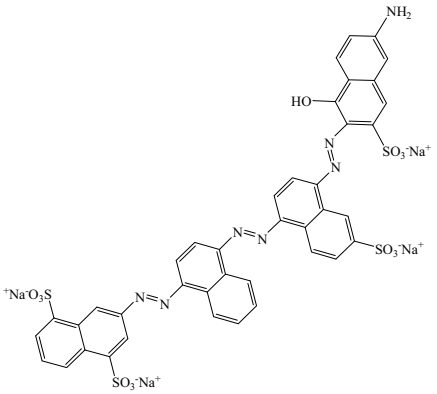	584
Direct Yellow 4	24890	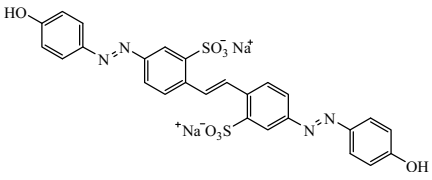	400

Los procesos de ozonización (Martins y col., 2006; Turhan y Turgut, 2009) al igual que los procesos Fenton y foto-Fenton (Elmorsi y col., 2010; Soon y Hameed, 2011) han sido ampliamente ensayados ya que han demostrado ser tecnologias prometedoras al conducir a mineralizaciones superiores al 80% con decoloraciones completas en tiempos muy cortos (20-30 min) para disoluciones con contenidos de mg L^{-1} de colorante. En los últimos años, EAOPs como la AO con BDD (Migliorini y col., 2011; Aquino y col., 2012) y el EF (Özcan y col., 2009; Ruiz y col., 2011) también han demostrado que son capaces de decolorar totalmente disoluciones de colorantes. Sin embargo, al aplicar el proceso de

EF sólo se precisan tiempos cortos de 20-30 min, mientras que en el caso de la AO los tiempos son mucho más largos, casi similares a los requeridos para alcanzar la mineralización completa. Con estas metodologías se han descrito mineralizaciones prácticamente completas para tiempos de electrólisis < 8 h

En el presente trabajo se han tratado colorantes azoicos de la industria textil y del papel al considerarse más perjudiciales que los alimentarios, puesto que éstos son compuestos inocuos tal y como se requiere para su aplicación como aditivo alimentario. Además, los colorantes utilizados en la industria textil y del papel son utilizados en mayores cantidades, por lo que son de mayor interés. Los colorantes utilizados se encuentran resumidos en la **Tabla 3**.

Productos de oxidación

Los productos que se recogen en este grupo aparecen usualmente como intermedios del proceso degradativo de algunos o de todos los contaminantes recogidos en los grupos I y II, por lo que han sido considerados de gran interés para completar los estudios realizados.

Ácidos oxálico y oxámico

Los ácidos oxálico y oxámico (ver estructura en **Fig. 3**) son contaminantes biodegradables, pero se ha estudiado su degradación al jugar un papel fundamental en la eficiencia de los EAOPs. Ambos ácidos son los productos finales de la degradación de POPs (el ácido oxámico sólo en el caso de compuestos nitrogenados) previo a la mineralización total a CO_2. Dado su alto carácter recalcitrante y el de los complejos que forman con iones metálicos (Fe^{2+}, Fe^{3+}, Cu^{2+}, etc), influyen directamente en la eficiencia de los procesos electroquímicos.

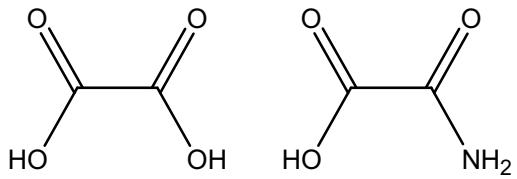

Figura 3. *Estructuras de los ácidos oxálico y oxámico.*

Pese a que la AO del ácido oxálico había sido estudiada previamente evidenciando su completa mineralización para tiempos superiores a 5 h de tratamiento a densidades de

corriente de 30 mA cm^{-2} (Martinez-Huitle y col., 2004b; Scialdone y col., 2008), la degradación de sus complejos de hierro y de los procesos fotoquímicos asociados sólo había sido considerado parcialmente por nuestro grupo (Guinea y col., 2009). En dicho trabajo se puso de manifiesto el carácter fotoactivo de los complejos de Fe(III)-oxalato y su alto carácter recalcitrante, motivo por el cual eran difícilmente mineralizados en el proceso EF. Sin embargo, no se ensayó el efecto del Fe(III) sobre el ácido oxálico en otros EAOPs ni se consideró la influencia de otro agente complejante del Fe(III) como puede ser el ácido oxámico durante su eliminación. Cabe señalar que no se ha descrito previamente la acción del Fe(III) sobre el ácido oxámico.

Ácido ftálico

El ácido ftálico (ver estructura molecular en la **Fig. 4**) se detecta como intermedio en la degradación de compuestos con anillos naftalénicos. Además, el ácido ftálico y los ftalato-derivados son muy utilizados industrialmente como plastificantes en la manufactura de productos de plástico.

El ácido ftálico es considerado un contaminante prioritario por la United States Environmental Protection Agency (USEPA) (United States Environmental Protection Agency 7407, 1994) debido a sus efectos perjudicioales sobre ratas que afectan al sistema reproductor masculino produciendo atrofia (Oishi y Hiraga, 1980) y al desarrollo de fetos (Makoto y col., 1997). Estudios medioambientales han constatado su presencia en aguas (Bauer y Herrman, 1997; Fromme y col., 2002; Zhang y col., 2012).

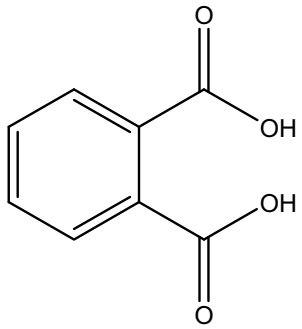

Figura 4. *Estructura del ácido ftálico.*

El gran riesgo ambiental que genera el acido ftálico y sus derivados ha incentivado el estudio del tratamiento de este contaminante por diferentes métodos. En el caso de la

fotocatálisis con TiO_2 (Taborda y col., 2001) se obtuvieron degradaciones prácticamente totales del ácido ftálico en una concentración milimolar, aunque se evidenció su conversión en derivados hidroxilados más perjudiciales, sin mineralizarlo. Los métodos convencionales de adsorción (Ayranci y Bayram, 2005) y de coagulación (Zheng y col., 2009) permitieron retirar parcialmente del medio el ácido ftálico generando un residuo sólido que requiere un post-tratamiento que encarece el proceso. Mediante la biodegradación aeróbica-anaeróbica (Fang y col., 2009) se encontró que podía eliminarse 2000 mg L^{-1} de ftalatos en 300 dias de tratamiento. Sin embargo, no se conoce nada sobre el mecanismo de degradación del ácido ftálico mediante EAOPs.

Tratamiento de aguas reales

Los buenos resultados obtenidos por los métodos de AO en el tratamiento de aguas contaminadas sintéticas llevan a considerar los EAOPs como tecnologías prometedoras para la remediación de POPs. El trabajo en aguas sintéticas facilita la aplicación de estos métodos al eliminar serios problemas que pueden acompañar las matrices de agua real como son altos contenidos en NOM e iones inorgánicos que pueden afectar la eficiencia del sistema. Por ejemplo, la presencia de altas concentraciones de cloruro puede favorecer la generación de productos organoclorados en algunos casos más perjudiciales que el propio contaminante. El estudio de aguas reales permitirá establecer en qué contextos podrían aplicarse estas tecnologías. Trabajos previos realizados por diferentes grupos en efluentes industriales (Aquino y col., 2011; Martínez-Huitle y col., 2012; Sales y col., 2013) y los trabajos realizados principalmente en el grupo del Advanced Water Managemente Centre (AWMC) (Radjenovic y col., 2011; Bagastyo y col., 2012, 2013) sobre tratamiento de efluentes de estaciones depuradoras han demostrado las posibilidades de estas metodologías, pero un estudio más profundo sobre matrices de aguas reales resulta necesario antes de decidir sobre la viabilidad y el uso definitivo de estas técnicas en plantas de tratamiento de aguas residuales. En este contexto, se trabajó con un efluente secundario contaminado con una mezcla compleja de 29 POPs para estudiar la posible implantación de la AO como tratamiento terciario. La mezcla de 29 POPs está formada por los herbicidas y plaguicidas recogidos en la **Tabla 4** y los fármacos resumidos en la **Tabla 5**.

Tabla 4. *Herbicidas y plaguicidas presentes en la matriz de 29 contaminantes*.

Herbicida o plaguicida	Estructura
Atrazina	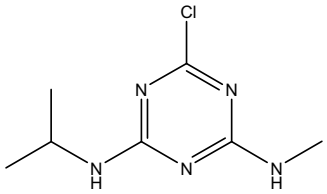
2,4-D	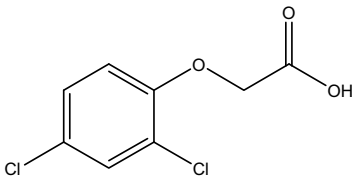
DEET	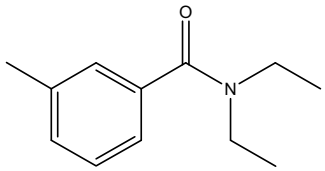
Diazonina	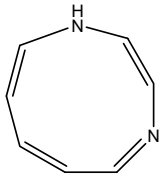
Diuron	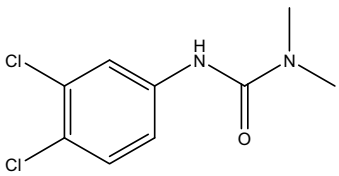
Metalocloro	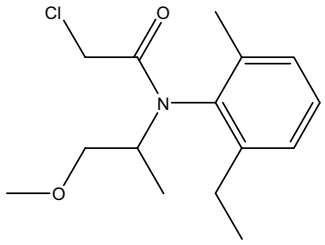
Triclopir	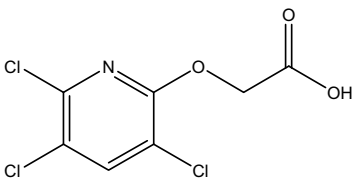

Tabla 5. *Fármacos presentes en la matriz de 29 contaminantes.*

Fármaco	Estructura
Acetaminofén (Paracetamol)	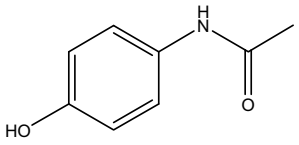
Cafeína	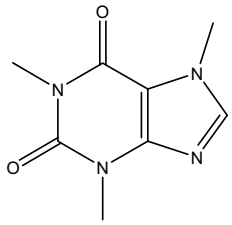
Carbamazepina	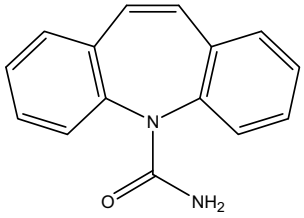
Citalopram	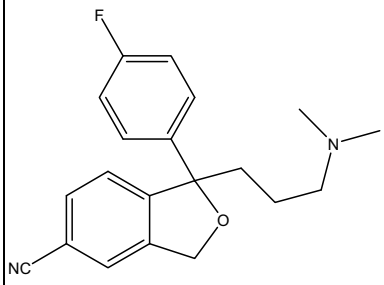
Diclofenaco	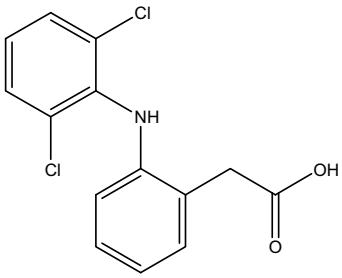

Tabla 5 – Continuación

Fármaco	Estructura
Ditriazoato	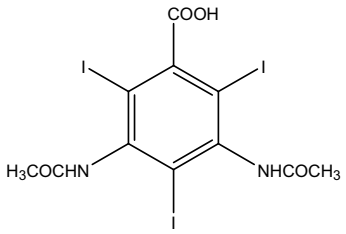
Enrofloxacina	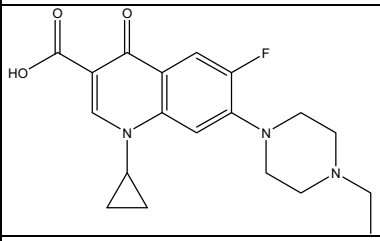
Fenitoína	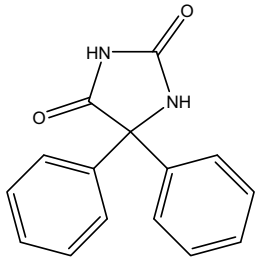
Gemfibrozil	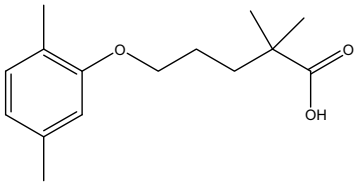
Hidroclorotiazida	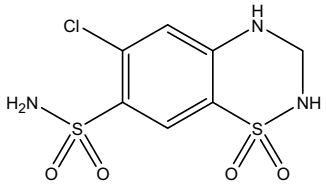
Ibuprofeno	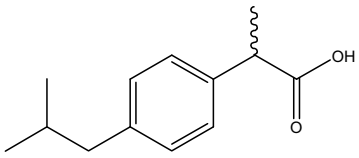
Iopromida	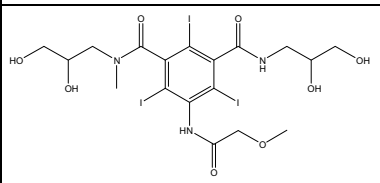

Tabla 5. Continuación

Fármaco	Estructura
Lincomicina	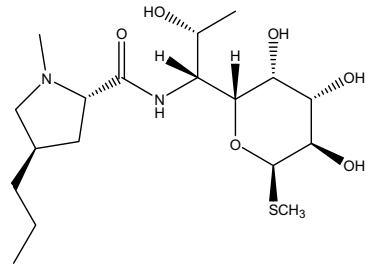
Metroprolol	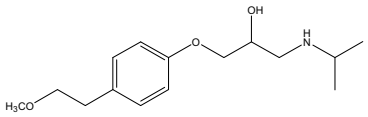
Norfloxacino	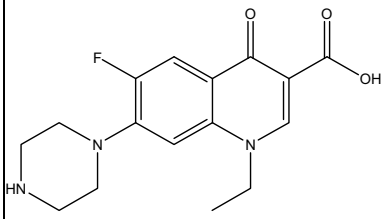
Ranitidina	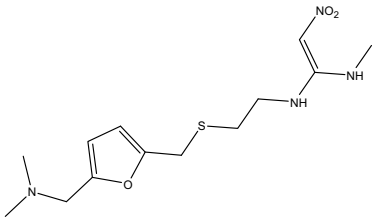
Roxitromicina	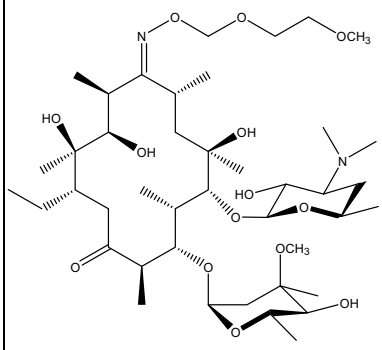
Sertralina	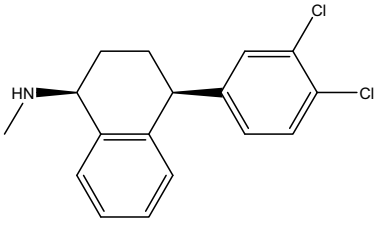

Tabla 5. Continuación

Fármaco	Estructura
Sulfadiazina	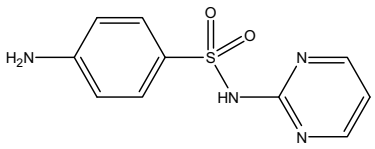
Tramadol	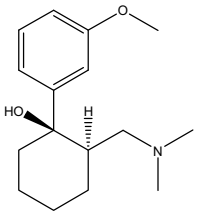
Trimetoprima	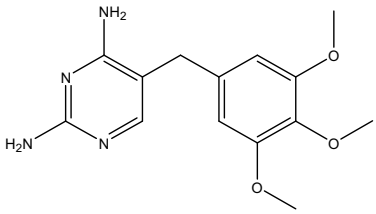
Venlafaxina	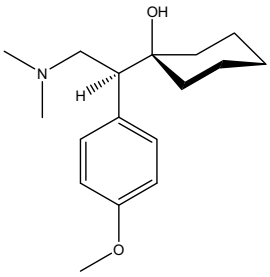

Luminol

El estudio de la ECL no es una aplicación directa de los EAOPs, pero ha permitido profundizar en una propiedad estrechamente relacionada con ellos que es la electrogeneración de radicales sobre ánodos de BDD.

El luminol (5-amino-2,3-dihidro-1,4-ftalazinadiona) (ver estructura en la **Fig. 5**) es el reactivo más popular empleado en CL. El luminol emite una luz fluorescente azulada característica con una $\lambda_{máx}$= 425 nm tras reaccionar químicamente. Por ejemplo, cuando una disolución de luminol en medio alcalino y en presencia de peróxido de hidrógeno se pone en contacto con restos de sangre, la emisión de luz característica aparece. De hecho, durante más de 40 años se ha utilizado esta propiedad en ciencia e ingeniería forenses para determinar la presencia de sangre en la escena del crimen (Barni y col., 2007).

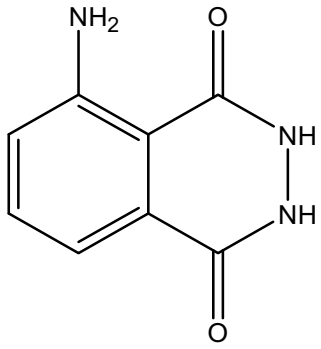

Figura 5. *Estructura del luminol.*

Este fenómeno se explica porque a pH 8-12 en presencia de un oxidante como el H_2O_2 y de un catalizador adecuado como un ion metálico, el luminol se oxida. La reacción de oxidación se debe a la transferencia de carga entre especies reactivas de oxígeno (ROS). En este proceso se forma como intermedio el dianión 3-aminoftalato en su estado excitado que es el causante de la emisión de luminiscencia al relajarse a su estado fundamental. En este trabajo se ha estudiado la ECL inducida por la electrogeneración de radicales sobre el ánodo de BDD y por transferencia de carga directa.

Varios autores han reportado diferentes trabajos de ECL con luminol en medio alcalino con ánodos de Au (Cui y col., 2004; Wang y col., 2008b), Pt (Wróblewska y col., 2005), materiales carbonáceos (Lin y col., 2008) y óxidos de iridio y estaño (ITO) (Guo y col., 2010). Estos trabajos habían sido realizados siempre en ausencia de H_2O_2 y no se había considerado, hasta el momento, el uso de un ánodo de BDD.

2. OBJETIVOS

Los objetivos de la presente tesis se encuentran focalizados en el estudio de la degradación y eliminación de POPs de origen farmacéutico y de la industria de los colorantes azoicos mediante la aplicación de EAOPs. La mayor parte de este trabajo fue realizado en el *Laboratori d'Electroquímica de Materials i del Medi Ambient* (LEMMA) de la Universitat de Barcelona (UB) bajo la dirección del **Prof. Dr. E. Brillas**. Con el fin de completar la formación adquirida en este campo, se realizó una estancia pre-doctoral en el *Advanced Water Management Centre* (AWMC) de la Universidad de Queensland (UQ) de Australia bajo la supervisión del **Prof. Dr. J. Keller** y la **Dra. J. Radjenovic**, donde se trabajó en el tratamiento mediante AO de un efluente secundario real contaminado con una mezcla compleja de POPs a concentración real (100 $\mu g\ L^{-1}$).

Los EAOPs ensayados en la presente tesis doctoral incluyen procesos de SPEC con nuevos fotoánodos de TiO_2, AO con ánodos de Pt y de BDD y métodos electroquímicos basados en la reacción de Fenton (EF; PEF y SPEF). Estas tecnologías emergentes se están desarrollando actualmente para el tratamiento de aguas contaminadas con POPs para que sean viables tecnológica, económica e industrialmente.

Adicionalmente se estudió la generación de radicales en ánodos de BDD mediante reacciones de electroquimioluminiscencia.

El estudio de los EAOPs aplicados se planificó con el fin de cumplir con los siguientes objetivos:

(1) Degradación de contaminantes orgánicos evaluando su mineralización e intermedios generados a partir de medidas de carbón orgánico disuelto (DOC) y cromatografía líquida de alta presión (HPLC), respectivamente. En el caso de los colorantes también se evaluó el proceso de decoloración a partir del descenso de la absorbancia UV-Vis en los sistemas:

- Escala de laboratorio: Estudio en celdas de 100 mL por los métodos SPEC, SPC, AO, EF, PEF y SPEF.
- Planta piloto de 10 L acoplada o no a un fotorreactor solar para escalar los EAOPS.

(2) Evaluación de la influencia de diferentes variables en los procesos como son la densidad de corriente aplicada, la concentración de contaminante, la concentración de catalizador metálico, etc.

(3) Cálculo de la eficiencia de corriente de mineralización y efecto de las diferentes variable experimentales sobre este parámetro.
(4) Identificación de intermedios aromáticos, ácidos carboxílicos e iones inorgánicos generados en el tratamiento de cada POP estudiado para cada método.
(5) Monitorización de la evolución de los intermedios generados durante los tratamientos EAOPs.
(6) Propuesta de mecanismos de reacción de los POPs estudiados para los diferentes EAOPs.

Objetivos específicos para los experimentos realizados en planta piloto.

(7) Cálculo de la energía consumida en el funcionamiento de la planta piloto en las diferentes condiciones ensayadas.
(8) Implementación de un sistema de alimentación energética autónoma mediante la utilización de placas fotovoltaicas.

El estudio de electroquimioluminiscencia se llevó a cabo con el fin de evidenciar la generación de radicales adsorbidos sobre la superficie anódicas. Los objetivos de este estudio fueron:

(1) Determinación del tipo de radicales generados en la condiciones de trabajo mediante análisis voltamperométricos y el uso de *quenchers* y *scavengers* específicos.
(2) Evaluación de la influencia de la concentración de H_2O_2 y del potencial aplicado en la generación de radicales.

3. EXPERIMENTAL

3.1. Reactivos

Las disoluciones de trabajo contenían Na_2SO_4 como electrolito soporte y en el caso de los procesos basados en la reacción de Fenton se añadía $FeSO_4 \cdot H_2O_2$, siendo ambos productos suministrados por las casas Fluka y Sigma-Aldrich, respectivamente. La **Tabla 6** recoge las características de los principales productos estudiados en la presente tesis. Los ácidos carboxílicos de grado analítico utilizados como patrones para la identificación y cuantificación en cromatografía HPLC de exclusión iónica se adquirieron en las casas Avocado, Fluka y Panreac. Las casas Acros y Panreac proveyeron los ácidos y bases utilizados de grado reactivo y de grado analítico. El H_2O_2 (33% w/v) de la casa Panreac se utilizó para realizar las rectas de calibrado para determinar el H_2O_2 electrogenerado y en los ensayos de electroquimioluminiscencia. Los disolventes orgánicos y demás reactivos de grado HPLC y para uso en cromatografía de líquidos acoplada a espectrometría de masas (LC-MS) para la preparación de fases móviles fueron suministrados por las casas Panreac, Merck y Teknochroma. Las disoluciones de trabajo sintéticas en celda pequeña así como las fases móviles de HPLC y LC-MS se prepararon con agua Millipore Milli-Q, con una resistividad > 18 MΩ cm a 25ºC. En los ensayos realizados con agua real las muestras de agua se obtuvieron de la planta municipal de tratamiento de aguas residuales de Manresa (Barcelona) y en Australia de la planta de tratamiento de Brisbane (Queensland). Las disoluciones tratadas en la planta piloto se prepararon con agua desionizada con un contenido de DOC inferior a 0,3 mg L^{-1}.

Tabla 6. *Características de los principales compuestos estudiados en la presente tesis.*

Compuesto	**Estructura**	**Proveedor**	**Pureza**
Amarillo Directo 4	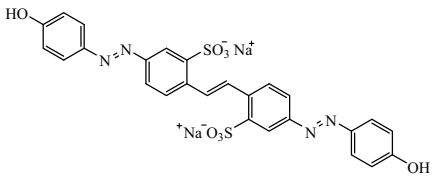	Sigma-Aldrich	Grado analítico
Azul Directo 71	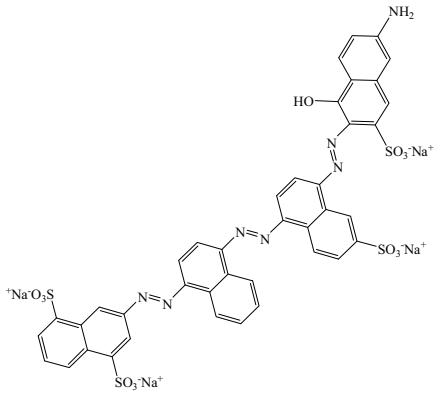	Acros Organics	Grado analítico
Cloranfenicol	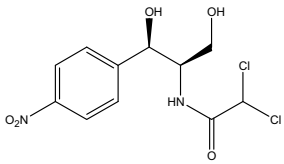	Sigma-Aldrich	98 %
Flumequina	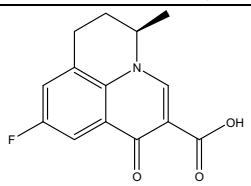	Laboratorios SYVA S.A.V.	99 %
Luminol	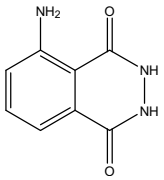	Applichem	Grado HPLC
Naranja Acido 7	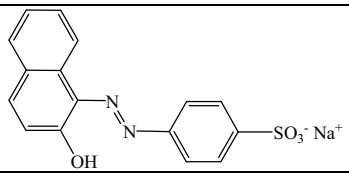	Acros Organics	Grado analítico
Rojo Ácido 151	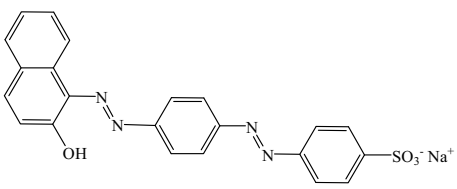	TCI Europe	Grado analítico

3.2. Reactor de tanque agitado

En los tratamientos a escala laboratorio de AO, EF, PEF, SPEF y con fotoánodos de TiO_2 se utilizó una celda cilíndrica monocompartimental de vidrio de 150 mL con doble camisa para termostatizar la disolución, mientras que las experiencias de EQL se realizaron en una celda de paredes planas.

La intensidad constante a los electrodos se suministró con un potenciostato-galvanostato Amel modelo 2053. Normalmente se determinó el voltaje de la celda cuando se trabajó galvanostaticamente y, en algunos casos la intensidad al operar potenciostaticamente, usando un multímetro Demestres DM 605. Las disoluciones de trabajo se mantuvieron termostatizadas a 35 ºC y agitadas vigorosamente a 700 rpm mediante un agitador magnético. En los experimentos de PEF las disoluciones se irradiaron simultáneamente con luz UVA utilizando para ello un fluorescente Philips de 6 W (λ= 300 – 420 nm, $\lambda_{máx}$= 360 nm) colocado a 7 cm sobre la disolución. Para los experimentos de SPEF la disolución de trabajo se irradió directamente con luz solar natural.

3.2.1 Electrodos

Los electrodos empleados en los experimentos aparecen recogidos en la **Tabla 7**. Dadas las características especiales del electrodo de diamante dopado con boro (BDD), del fotoánodo de TiO_2 y del electrodo de difusión de aire (ADE), se explica su preparación más detalladamente a continuación.

La síntesis del BDD se efectúa mediante la técnica de deposición química de vapor en la variante de filamento caliente (HFCVD) sobre obleas de silicio monocristalino puro tipo-*p* cortado en el plano de índices de Miller (100) como sustrato conductor que presentan una resistividad de 0.1 Ω cm. Mediante esta técnica se obtienen depósitos delgados de BDD de 1 μm de espesor y diferentes contenidos del dopante boro que hace al diamante conductor. Los electrodos de BDD utilizados en este trabajo contienen un dopaje de 1300 ppm de boro.

Tabla 7. *Electrodos utilizados en escala laboratorio.*

Electrodos		**Proveedor, morfología y área electroactiva**
Ánodo	Diamante dopado con boro	Adamant Technologies, placa 3 cm^2 y 0,5 cm^2
	Fotoánodo de TiO_2	CPT, Placa 5 cm^2
	Platino	SEMPSA, placa 3 cm^2 99,99 % pureza
Cátodo	Acero Inoxidable AISI 304	Placa 3 cm^2
	Electrodo de difusión de aire	E-TEK, carbón-PTFE tela de 3 cm^{-2}
	Grafito	Sofacel, barra 3 cm^2
	Platino	SEMPSA, placa 3 cm^2 99,99 % pureza
Referencia	Ag | AgCl, KCl (sat.)	Metrohm

Los fotoánodos de TiO_2 se obtuvieron por proyección térmica de plasma atmosférico (APS) sobre un sustrato conductor de acero inoxidable 316L en el Centro de Proyección Térmica (CPT). El recubrimiento se obtuvo utilizando micropolvo de TiO_2 que se calienta, mezcla y homogeniza durante el tiempo de residencia en la zona del jet de plasma donde las partículas funden parcialmente (Gardon y col., 2013). Las partículas fundidas en el plasma son aceleradas hacia el sustrato del recubrimiento sobre el que quedan adheridas capa por capa (Dosta y col., 2008).

El ADE consiste en un tubo de PVC hueco y cerrado con una entrada de aire tal y como se muestra en la **Fig. 6**. Se bombea aire al interior del cátodo para que pase a través de la tela de C-PTFE en la parte inferior del sistema, la cuál es la parte electroactiva del electrodo. La tela está en contacto con una malla de níquel que actúa de colector de corriente y distribuidor eléctrico, además de mejorar la resistencia mecánica del sistema. La malla de níquel está en contacto con un hilo de Ni-Cr cuya función es de conector o contacto eléctrico. Cabe destacar que la tela es permeable y con el fin de evitar una indeseada percolación del cátodo conviene que la presión que ejerce el aire sea ligeramente superior a la del líquido, sin generar burbujas que aíslen la tela del contacto con el líquido.

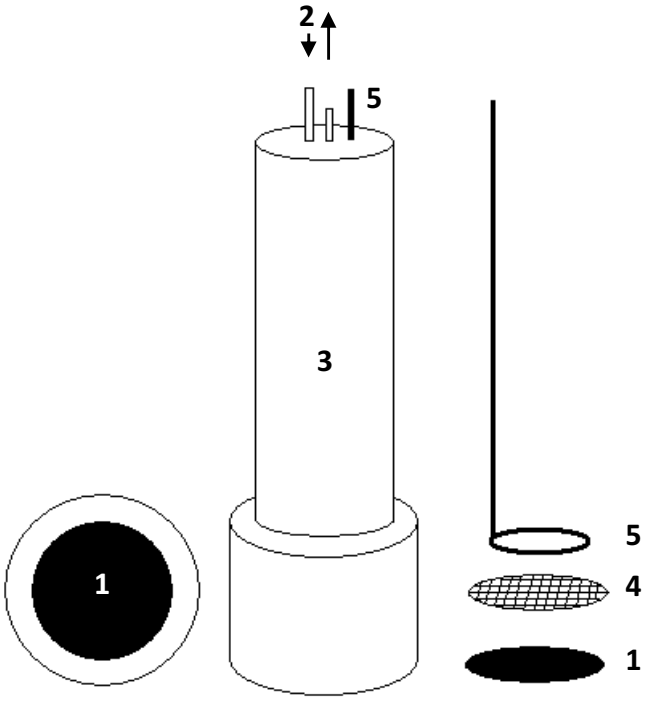

Figura 6. *Esquema del electrodo de difusión de aire (ADE): (1) Tela de carbón-politetrafluoroetileno, (2) tubos de vidrio para la entrada y salida de aire, (3) soporte de PVC, (4) malla de níquel y (5) conector de Ni-Cr.*

3.3. Escala pre-piloto

3.3.1. Planta pre-piloto de 10 L utilizada en tratamientos basados en la reacción de Fenton

En la **Fig. 7** se muestra una foto de la planta piloto de 10 L utilizada en los tratamientos de EF y SPEF. El agua contaminada tratada recirculaba en el sistema mediante una bomba de membranas hasta el final del tratamiento. La temperatura se mantuvo constante a 35 ºC utilizando dos intercambiadores de calor y el flujo se controló mediante un rotámetro. Se aplicaron densidades de corriente constantes durante el trabajo galvanostático con una fuente de alimentación Grelco GDL3020.

Figura 7. *Planta pre-piloto de tratamiento electroquímico de aguas de 10 L: (1) Bomba de aire, (2) fuente de alimentación, (3) celda electroquímica tipo filtro prensa, (4) fotorreactor tipo colector parabólico compuesto (CPC), (5) termostato, (6) intercambiadores de calor, (7) bomba de membranas, (8) rotámetro y (9) depósito*.

Se utilizó una celda electroquímica tipo filtro prensa de un compartimento. El esquema de la celda se muestra en la **Fig. 8**, donde aparecen los diferentes componentes de dimensiones 12 cm x 18 cm separados entre ellos por vitón. El vitón favorece el sellado entre los componentes evitando así fugas en la celda. En todos los trabajos realizados el ánodo fue una placa de platino de 99,99 % de pureza y como cátodo un ADE de C-PTFE con una separación entre electrodos de 1,2 cm. Ambos electrodos utilizados son de 100 cm^2 de area geométrica y 90,25 cm^2 de área electroactiva, puesto que la celda que tiene una ventana central de 9,5 cm x 9,5 cm. La cara interior del cátodo es presionada contra una malla de Ni que actúa de colector y refuerzo mecánico (como en el caso del ADE de escala laboratorio), con una cámara de gas interna de PVC donde circula aire a un flujo de 4,5 L min^{-1} regulado con una válvula de salida.

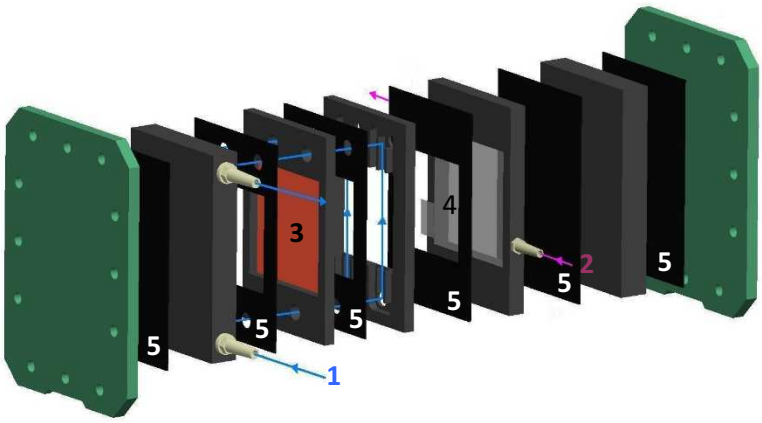

Figura 8. *Esquema de la celda electroquímica tipo filtro prensa: (1) Circulación del líquido en la celda, (2) circulación de aire en la cámara de gas del electrodo de difusión de gas (ADE), (3) ánodo, (4) cátodo de C-PTFE sobre malla de Ni y (5) junta de vitón.*

El fotorreactor consiste en un CPC con un área de 0,4 m^2. Está compuesto por 12 tubos de borosilicato de 50,5 cm de largo x 1,82 cm de diámetro interno (1,57 L de volumen irradiado) ensamblados sobre una superficie de aluminio inclinada 41º para recoger mejor la radiación en nuestro laboratorio (latitud 41º 21' N, longitud 2º 10' E), tal y como se muestra en la **Fig. 7**. Los tubos están dispuestos sobre unos espejos cóncavos cuya función es concentrar la radiación dispersa en el centro del tubo por lo que el CPC tiene un factor de concentración 1.

La utilización de un panel fotovoltaico (**Fig. 9**) permite la generación de la energía suficiente para que la planta trabaje de forma autónoma y eficiente reduciendo el coste energético a cero (Valero y col., 2008).

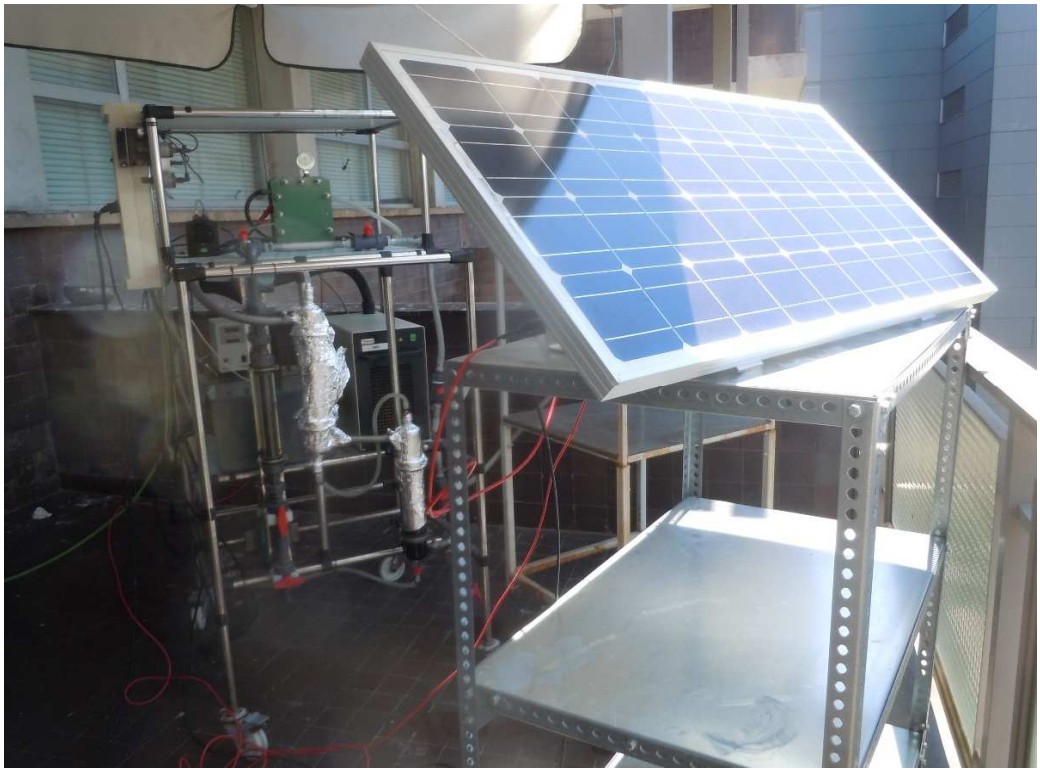

Figura 9. *Planta pre-piloto autosuficiente en funcionamiento gracias a la aplicación directa de energía solar fotovoltaica.*

3.3.2. Planta pre-piloto de 10 L utilizada en tratamientos basados en oxidación anódica

La planta pre-piloto que se utilizó en el AWMC de Australia en el estudio de viabilidad del proceso de AO para el tratamiento de una matriz compleja de contaminantes en un efluente secundario real consistió en un sistema similar al presentado en el apartado anterior. A diferencia de la celda filtro prensa descrita en el apartado anterior, en el AWMC se utilizó una celda de dos compartimentos (**Fig. 10**) para aislar el agua tratada en el compartimento anódico de procesos de reducción indeseados en el cátodo. Consecuentemente se utilizaron dos depósitos de 10 L, uno para el agua contaminada tratada o anolito y el otro para el catolito. Los diferentes componentes de policarbonato de la celda se mantenían sellados entre ellos por juntas de goma y los dos componentes centrales correspondientes al volumen de anolito o catolito presentaban dimensiones internas de 20 cm x 5 cm x 1,2 cm y estaban separados entre ellos por la membrana de intercambio catiónico Ultrex CMI-7000. Durante todo el estudio realizado se utilizó un ánodo de BDD y como cátodo una placa de acero inoxidable con un área de 40,8 cm^2.

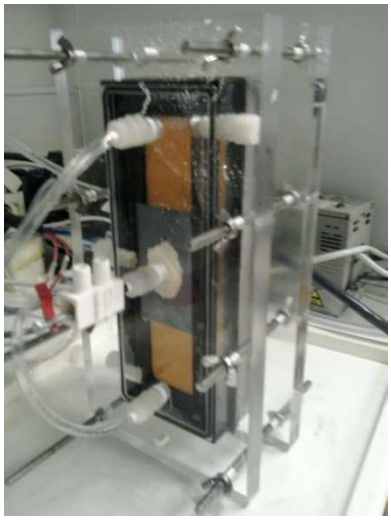

Figura 10. *Celda filtro-prensa dividida.*

3.4 Procedimientos analíticos

3.4.1. Análisis voltamperométricos

Se realizaron voltamperometrías de barrido lineal y cíclicas con una celda cilíndrica estándar de tres electrodos utilizando un potenciostato-galvanostato Ecochemie Autolab PGSTAT100, controlado mediante el software Autolab Nova 1.5. El electrodo de trabajo era un electrodo de BDD de 0,50 cm^2, el contraelectrodo un alambre de Pt y el electrodo de referencia un electrodo de Ag|AgCl, KCl (sat.) ($E°$ = 0,197 V vs Electrodo Normal de Hidrógeno (SHE)). Todos los voltamperogramas se registraron a velocidades de barrido de 5 a 100 mV s^{-1}, a temperatura ambiente (25 ºC) y con la disolución en reposo, aunque algunas veces bajo agitación constante con un núcleo magnético a 700 rpm. Los voltamperogramas se registraron bajo atmosfera de argón tras previo burbujeo de la disolución con este gas durante 30 min.

3.4.2. Carbono orgánico total

La técnica de análisis del carbono orgánico total (TOC) o carbono orgánico en disolución (DOC) se basa en la conversión completa de los átomos de carbono de una disolución a CO_2 cuya concentración es posteriormente determinada por infrarrojos. Estos análisis se realizaron utilizando un equipo TOC-VCSN de Shimadzu. Este equipo inyecta un pequeño volumen de disolución en un horno a 680 ºC, donde en presencia de un

catalizador de Pt soportado sobre esferas de alúmina el agua se vaporiza y todo el carbono contenido en la disolución se incinera a CO_2. El CO_2 generado se analiza en un detector de infrarrojos no dispersivo (NDIR) que proporciona una señal directamente proporcional a la concentración de carbono en disolución o el carbono total (TC).

El TC corresponde a la suma del carbono orgánico e inorgánico en disolución. Con el fin de discernir la correspondiente concentración orgánica se pueden realizar dos tipos de análisis:

1) El primero consiste en analizar el carbono inorgánico (IC). Para ello, la muestra es acidificada con ácido clorhídrico para que el carbono inorgánico (en forma de carbonatos) se descomponga en CO_2 y se dirige directamente al analizador NDIR sin pasar por el horno. Consecuentemente, el TOC corresponde a la diferencia entre el TC y el IC.
2) El segundo consiste en acidificar las muestras y gasificar para purgar el CO_2 generado a partir del carbono inorgánico. Posteriormente, la disolución remanente se incinera en el horno y analiza dando directamente la medida del Carbono Orgánico no Purgable (NPOC). Esta medida puede llevar asociada algunos errores por la pérdida de compuestos orgánicos volátiles.

Cabe señalar que en el sistema electro-Fenton el contínuo burbujeo de aire y el desprendimiento de O_2 en el ánodo, sumado al pH ácido de la disolución, favorece la constante eliminación del carbono inorgánico de la disolución dando como resultado medidas prácticamente idénticas de TC y de TOC (o DOC).

3.4.3. Nitrógeno total

La medida del nitrógeno total permite evaluar la concentración total de nitrógeno orgánico e inorgánico (TN) en disolución. La medida se realizó con el módulo TNM-1 acoplado al analizador TOC-VCSN descrito en el apartado anterior. El análisis se basa en la combustión de todas las especies de nitrógeno a monóxido de nitrógeno que tiene lugar en el mismo tubo de combustión con el mismo catalizador que el TOC. El NO generado es posteriormente analizado en el módulo TNM-1 mediante un método basado en quimioluminiscencia que permite la cuantificación de nitrógeno en un rango muy amplio

de 0,1 a 4000 mg L^{-1}. Sin embargo, este procedimiento no es útil para muchos colorantes que dan una conversión parcial de su N inicial en monóxido de nitrógeno.

3.4.4. Análisis de haluros orgánicos adsorbibles

La concentración de compuestos orgánicos halogenados se determinó mediante el método estándar de determinación de haluros orgánicos adsorbibles (AOX) basado en la adsorción de compuestos halogenados en carbón activo. Previamente al análisis, la muestra se ajustó a pH 2,0 utilizando ácido nítrico al 70 %. Luego se pasó a través de cartuchos de carbón activo utilizando el módulo de adsorción Mitsubishi TX-3AA. El carbón activo con los compuestos adsorbidos es después incinerado en presencia de oxígeno a 1000 ºC en un Horno Rápido Automático Mitsubishi AQF-2100H. En este proceso se generan gases de halógenos que son absorbidos en agua Milli-Q con un 0,003 % de H_2O_2 y finalmente son analizados por cromatografía iónica en un HPLC iónico Dionex ICS-2100 para cuantificar las concentraciones de cloruro, bromuro e ioduro que están relacionadas con la concentración de organoclorados en el medio.

3.4.5. Decoloración

El proceso de decoloración de las disoluciones tratadas de colorantes se monitorizó siguiendo el decaimiento de la absorbancia (A) a la longitud de onda máxima característica de cada colorante (Martínez-Huitle y Brillas, 2009; Garcia-Segura y col., 2011) con el tiempo. El porcentaje de eliminación de color (% CR) fue determinado mediante la ecuación (30):

$$\% \text{ CR} = \frac{A_0\text{-}A}{A_0} \times 100 \qquad (30)$$

donde A_0 y A son la absorbancia al tiempo inicial y al tiempo t, respectivamente. La obtención de las medidas de absorbancia y el registro de los espectros se llevó a cabo con un espectrofotómetro Shimadzu 1800 UV-vis de doble haz termostatizado a 35 ºC.

3.4.6. Cuantificación de la demanda química de oxígeno

La COD es un parámetro que permite evaluar el oxígeno (en mg O_2 L^{-1}) requerido para oxidar todos los compuestos oxidables presentes en medio acuoso, tanto orgánicos como inorgánicos, mediante agentes fuertemente oxidantes en medio ácido.

Para realizar estos análisis se utilizó un kit comercial de determinación de COD Spectroquant® de Merck Millipore, que consiste en una mezcla oxidante preparada en medio ácido compuesta por dicromato de potasio como agente oxidante, sulfato de mercurio (II) como catalizador de la oxidación y sulfato de plata como inhibidor de las interferencias producidas por la oxidación de halógenos. Tras añadir el volumen de muestra a la mezcla, esta es introducida en un digestor a 150 ºC durante 2 h para favorecer y asegurar la máxima oxidación. Tras la digestión de la muestra, se enfrió a temperatura ambiente y se analizó el valor de la COD a partir de la absorbancia de la mezcla que proporciona el valor de la concentración de oxígeno requerida.

3.4.7. Cuantificación de ClO^-

El hipoclorito se determinó mediante el método colorimétrico con *N*,*N*-dietil-*p*-fenilendiamina (DPD), un método ampliamente utilizado en Plantas Potabilizadoras (Radjenovic y col., 2011). Para los análisis se utiliza una mezcla comercial que contiene DPD. Esta sal es la que reacciona con el ClO^- del medio acuoso, formando un complejo de color rosado a fucsia y consecuentemente dando una señal colorimétrica característica. El resto de componentes de la mezcla, tienen la función de crear un medio favorable para la reacción. La medida directa de la absorbancia permite determinar la concentración de cloro libre expresada como mg L^{-1} de Cl_2.

3.4.8. Cuantificación de H_2O_2

La cuantificación de H_2O_2 se realizó por el método colorimétrico basado en la medición de la absorbancia del complejo peroxo-titanato de color amarillento-anaranjado con una $\lambda_{máx}$=408 nm (Welcher, 1975). La ecuación (31) describe la formación del complejo de titanato a partir de una disolución de Ti^{4+}.

$$Ti^{4+} + H_2O_2 + 2\ SO4^{2-} \rightarrow [TiO_2(SO_4)]^{2-} + 2H^+ \qquad (31)$$

3.4.9. Técnicas cromatográficas

La cromatografía es un método analítico que permite la separación e identificación de substancias de una mezcla compleja. La técnica se basa en el desplazamiento de la muestra con una fase móvil (gas, líquido o fluido supercrítico) a través de una fase estacionaria con la que es inmiscible fijada en una superficie sólida (columna). La selección de ambas fases se realiza de forma que los diferentes componentes de la muestra se distribuyan de forma diferente entre las dos fases en función de su afinidad debida a diferentes propiedades (polaridad, tamaño molecular, etc). Los compuestos que son retenidos por la fase estacionaria se desplazan más lentamente con la fase móvil, contrariamente a los que tienen poca afinidad con la fase estacionaria que se desplazan con rapidez. La distinta movilidad de los componentes de la mezcla compuesta permite por lo tanto su separación y análisis cualitativo y/o cuantitativo.

3.4.9.1. Cromatografía de líquidos

En la cromatografía líquida de alta presión (HPLC) la fase móvil que se utiliza es líquida. En la **Tabla 8** se recogen los diferentes tipos de columna y fase móvil utilizados en los análisis de los compuestos principales, sus intermedios aromáticos y otros intermedios comunes como son los ácidos carboxílicos o los iones inorgánicos generados durante los tratamientos. En el caso de los ácidos carboxílicos se utilizó la técnica de HPLC de exclusión iónica, en el de los iones inorgánicos HPLC de intercambio iónico y en el de los compuestos aromáticos HPLC de fase inversa. Los análisis de compuestos aromáticos y ácidos carboxílicos se realizaron en un cromatografo HPLC Waters 600 LC acoplado a un detector de arreglo de fotodiodos Waters 996. El equipo utilizado para la cuantificación de iones inorgánicos fue un HPLC Shimadzu CDD 10 Avp acoplado a un detector de conductividad Shimadzu CDD 10 Avp.

Tabla 8. *Columnas y fases móviles utilizadas en la determinación de los compuestos.*

Compuesto	Columna	Fase Móvil
Ácidos carboxílicos	Bio-Rad Aminex HPC 87H 300 mm x 7,8 mm	4 mM H_2SO_4 0,6 mL min^{-1}, 35 ºC
Cationes (NH_4^+)	Shodex IC YK-421 125 mm X 4,6 mm	5,0 mM ácido tartárico, 1,0 mM ácido dipicolinico, 24,2 mM ácido bórico y 1,5 mM éter corona 1,0 mL min^{-1}, 40 ºC
Aniones (Cl^-, NO_3^-, SO_4^{2-}, etc)	Shim-Pack IC-A1S 100 mm x 4,6 mm	2,4 mM tris(hidroximetil)aminometano y 2,5 mM ácido ftálico Tampón de fosfatos pH=3,5 1,5 mL min^{-1}, 40 ºC
Flumequina	Thermo Hypersil BDS C18 5µm 250 mm x 4,6 mm	40:60 (v/v) acetonitrilo:agua Tampón de fosfatos pH=3,5 0,6 mL min^{-1}, 35 ºC
Cloranfenicol	Spherisorb ODS2 5µm 150 mm x 4,6 mm	20:80 (v/v) acetonitrilo:agua Tampón de fosfatos pH=3,5 0,4 mL min^{-1}, 35 ºC
Naranja Acido 7	Spherisorb ODS2 5µm 150 mm x 4,6 mm	30:70 (v/v) acetonitrilo:agua 2,4 mM n-butilamina Tampón de fosfatos pH=3,5 0,6 mL min^{-1}, 35 ºC
Rojo Ácido 151	Spherisorb ODS2 5µm 150 mm x 4,6 mm	30:70 (v/v) acetonitrilo:agua 2,4 mM n-butilamina Tampón de fosfatos pH=3,5 0,6 mL min^{-1}, 35 ºC
Azul Directo 71	Spherisorb ODS2 5µm 150 mm x 4,6 mm	50:50 (v/v) acetonitrilo:agua 2,4 mM n-butilamina Tampón de fosfatos pH=3,5 0,6 mL min^{-1}, 35 ºC
Amarillo Directo 4	Spherisorb ODS2 5µm 150 mm x 4,6 mm	50:50 (v/v) acetonitrilo:agua 2,4 mM n-butilamina Tampón de fosfatos pH=3,5 0,3 mL min^{-1}, 35 ºC

3.4.9.2. Cromatografía de líquidos acoplada a espectrometría de masas

La cromatografía de líquidos acoplada a espectrometría de masas (LC-MS) tiene esencialmente el mismo funcionamiento que la de HPLC con la diferencia de que, tras la separación en la columna (y/o el paso tras un detector), fase móvil y compuestos separados son nebulizados e ionizados. El proceso de ionización se produce mediante una corriente eléctrica, generando un compuesto cargado positiva o negativamente (ganancia o pérdida de un H^+). Posteriormente el compuesto pasa a través de un cuadrupolo hasta el detector donde se determina la masa exacta del compuesto. No todos los compuestos son susceptibles de ser detectados por esta técnica, sólo podremos identificar aquellos susceptibles a sufrir procesos de ionización por lo que compuestos quinónicos o compuestos con grupos funcionales no ionizables serán completamente indetectables por MS, pese que el cromatograma de líquidos muestre el pico correspondiente.

El equipo de LC-MS permite discriminar los valores exactos de la masa molecular. La **Fig. 11** muestra, por ejemplo, el cromatograma del cloranfenicol (Garcia-Segura y col., 2014). Como se puede observar en la estructura se trata de un compuesto diclorado. El cloro tiene una particularidad bien conocida y está relacionada con su distribución isotópica 3:1 de los isótopos 35 y 37. La técnica de LC-MS permite identificar los picos correspondientes a los compuestos de cloranfenicol con 2 ^{35}Cl, 2 ^{37}Cl y un Cl de cada isótopo mostrando intensidades de pico correspondientes a la distribución isotópica del Cl; por lo que podemos aseverar que no solo identificamos el compuesto sino que somos capaces de discernir las diferencias de masa de dos unidades debidas a los isótopos de Cl.

Para la realización de los análisis de LC-MS se utilizó un cromatógrafo Shimadzu SIL-20AC LC equipado con una columna Teknockroma Mediterranean Sea C-18 3 µm (15 mm x 0,46 mm) a 30 ºC y acoplado a un espectrómetro de masas Shimadzu LCMS-2020 MS. El equipo de MS operó en modo negativo y positivo utilizando una fuente de ionización de electroespray (ESI) aplicando un voltaje interfacial de -4,5 y 4,5 kV, respectivamente, además de un voltaje de 60 V en el Q-array RF. La temperatura del tubo DL era de 250 ºC y se usó N_2 puro como gas de nebulización y de secado. Los valores de m/z se recogieron en rangos mediante el modo de análisis de la corriente total de iones (TIC) o seleccionando valores concretos de iones (SIM).

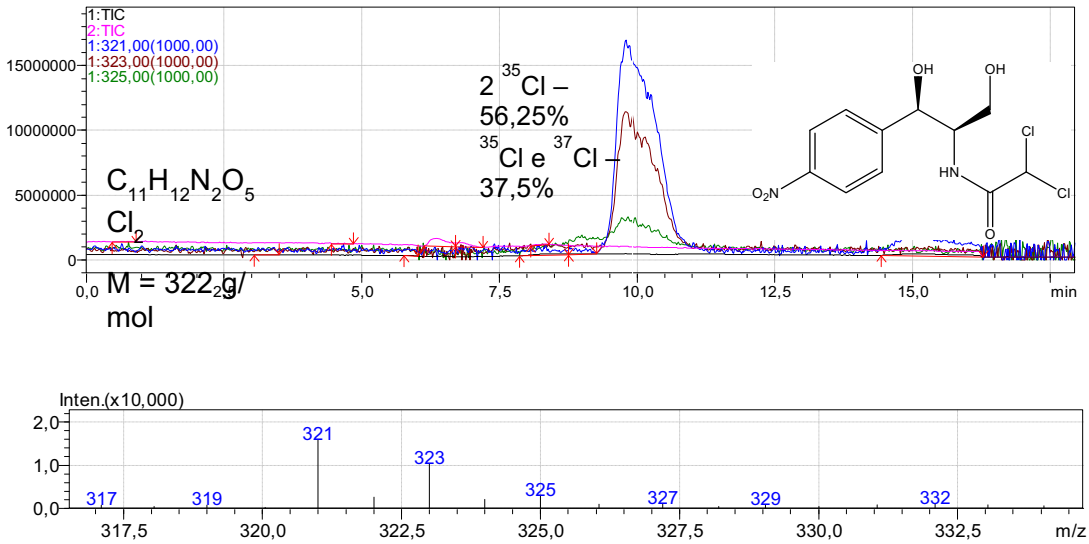

Figura 11. *Cromatograma de LC-MS del cloranfenicol y espectro de masas correspondiente al tiempo de retención del compuesto.*

3.4.9.3. Cromatografía de líquidos acoplada a espectrometría de masas/masas

La cromatografía de LC-MS/MS a diferencia del análisis de LC-MS permite la posterior fragmentación de los compuestos inicialmente ionizados aumentando así la sensibilidad de la medida, facilitando la identificación de compuestos y la discriminación de picos solapados.

La utilización de esta técnica permitió la cuantificación de concentraciones del orden de µg L^{-1} en una matriz compleja de 29 contaminantes orgánicos persistentes. Con el fin de realizar estos análisis, las muestras fueron preconcentradas tras ajustarlas a pH 7,0 mediante su extracción con cartuchos Oasis HLB (200 mg, 6 mL) de Waters previamente acondicionados con 10 mL de metanol y 10 mL de agua milliQ. Los análisis de estas muestras se llevaron a cabo utilizando un cromatógrafo de líquidos ultra-rápido (UFLC) acoplado a un espectrómetro de masas 4000 QTRAP de triple cuadrupolo lineal híbrido con trampa de iones (qQlit-MS) equipado con un electroespray ionizador. Se utilizó una columna Alltima C18 5µm (250 mm x 4,6 mm) para las separaciones cromatográficas termostatizada a 40 ºC.

3.4.10. Medidas de electroquimioluminiscencia

La intensidad relativa de ECL emitida en la superficie del ánodo de BDD se determinó con un sensor lumínico de 1 cm^2 de la casa Thorlabs, modelo S120A, acoplado al equipo Thorlabs S110 Optical Power Meter Console System. Con el fin de poder determinar la radiación emitida, la cara electroactiva del ánodo de BDD se situó de forma paralela a la pared plana de la celda a una distancia de 0,5 cm y el sensor se colocó en la pared externa frente el centro del electrodo de BDD. El cátodo de Pt se dispuso tras el ánodo de BDD a una distancia de unos 2 cm. La posición de ambos electrodos y del sensor se mantuvo invariable durante todos los ensayos comparativos

3.4.11. Caracterización de los ánodos de TiO_2 sintetizados

Las imágenes del recubrimiento y del corte transversal del electrodo se obtuvieron utilizando un microscopio de barrido electrónico (SEM) Jeol 5510 acoplado a un analizador de espectrometría dispersión de energía de rayos X (EDS) Röntec para analizar las fases.

Se realizó también un análisis de fases más exacto mediante difractometría de rayos X (XRD) utilizando un difractómetro Siemens D-500 tipo Bragg-Brentano $\theta/2\theta$ aplicando una radiación de Cu $K_{\alpha 1+2}$ ($\lambda(\alpha_1)$=0,154060 nm y $\lambda(\alpha_2)$= 0,154443 nm) a 40 kV y 30 mA de corriente. La ratio entre las fases cristalinas determinadas se calculó a partir de su ratio de intensidad de referencia (RIR) mediante el método de Chung (Chung, 1974) utilizando el software X'pert Highscore Plus.

La porosidad se calculó con el software analizador de imágenes Matrox Inspector. La microrugosidad se determinó con un equipo analizador de superficies Mitutoyo Surftest 301 y la adhesión según la normativa ASTM C633 estándar con un sistema Servosis modelo MCH-102ME. Las mediciones de la microdureza seccional se realizaron mediante el ensayo Vickers de microdureza con una carga de 300 g según la norma estándar UNE 7-423/2 con un equipo Matsuzawa modelo MXT-a. Las microindentaciones fueron analizadas con un microscopio óptico Leica modelo DMI 5000M.

3.4.12. Otras medidas

El pH de las disoluciones se determinó utilizando un pH-metro Crisom GLP 22. La intensidad de la radiación UV (300-400 nm), emitida tanto por las lámparas como por el sol, se midió con un radiómetro Kipp & Zonen modelo CUV 5.

3.5. Parámetros asociados al proceso

La eficiencia de corriente de mineralización (MCE) es un parámetro que proporciona información sobre cuanta corriente aplicada es realmente empleada en las reacciones orgánicas de interés que conducen a la completa mineralización de la materia orgánica en disolución (Hammami y col., 2008; Isarain-Chávez y col., 2010; Almeida y col., 2011). El parámetro queda definido y puede ser calculado a partir de la siguiente expresión:

$$\text{MCE (\%)} = \frac{nFV_s\Delta(TOC)_{exp}}{4.32 \text{ x } 10^7\, mIt} \times 100 \qquad (32)$$

donde n es el número de electrones consumido para mineralizar completamente el contaminante, F es la constante de Faraday (96487 C mol^{-1}), V_s es el volumen de disolución tratada, $\Delta(TOC)_{exp}$ es el decaimiento experimental del TOC (mg L^{-1}), 4,32 × 10^7 es un factor de homogeneización de unidades (3600 s h^{-1} x 12000 mg mol^{-1}), m es el número de carbonos por molécula de contaminante, I es la corriente aplicada (A) y t es el tiempo de electrolisis (h).

Por otro lado, también se determinó la energía consumida (EC) en los trabajos realizados en planta piloto (Salazar y col., 2011; El-Ghenymy y col., 2012b), en kWh kg^{-1} TOC, a partir de la siguiente ecuación:

$$\text{EC} = \frac{1000\, E_{cell}\, It}{V_s\Delta(TOC)_{exp}} \qquad (33)$$

donde E_{cell} es la diferencia de potencial media entre electrodos (V), 1000 es un factor de conversión (mg g^{-1}) y el resto de parámetros tal y como fueron definidos para el cálculo de la MCE según la Eq. (32).

4. RESULTS AND DISCUSSION

Electrochemical Advanced Oxidation Processes applied to the treatment of wastewaters polluted with pharmaceuticals

Our research group LEMMA has investigated the efficient degradation of several widely used pharmaceuticals such as paracetamol (Sirés et al., 2004), ibuprofen (Skoumal et al., 2009), diclofenac (Brillas et al., 2010), atenolol (Isarain-Chávez et al., 2010) and some antibacterial drugs such as enrofloxacin (Guinea et al., 2010) and sulfanilamida (El-Ghenymy et al., 2013b) by different EAOPs in synthetic polluted waters. Nevertheless, more efforts are needed to clarify the degradation behaviour of more complex molecular structures with EAOPs, their scale-up and the viability of treating real wastewater.

In this section the treatment of two antimicrobial agents extensively used in medicine and veterinary such as flumequine (FLU) and chloramphenicol (CHL) is reported. This kind of pollutants suppose an environmental risk as stated for other drugs due to their toxicity, but they have an additional undesired effect that is the possibility to promote the emergence of multi-resistant bacterial strains. Then, it is obvious that the removal of that POPs by efficient technologies is a relevant objective in order to protect human health and the environment.

The degradations studied in these works cover a wide range of EAOPs such as AO with electrochemical conversion or combustion activity and the electrochemical processes based on Fenton's reaction such as EF, PEF and SPEF, where different control variables were evaluated. The SPEF process was scaled-up to a 10 L pre-pilot flow plant for CHL polluted solutions and the viability of EAOPs for treating real wastewaters were assessed by the effective treatment of sewage plant effluents contaminated with FLU.

Finally, the relevance of the final carboxylic acids generated in the removal of aromatics conducted to a deeper study about oxalic and oxamic acids. Both acids are the ultimate and more persistent by-products of the degradation of aromatic compounds (oxamic only in the case of *N*-aromatics) and their degradation study was carried on in order to better understand their behaviour during the EAOPs.

Table 9 summarizes relevant results obtained for the FLU and CHL treatment. It is clear that the oxidation ability of the processes increases in the order AO -Pt < AO -BDD < EF < PEF < SPEF. Besides, the effect of the anode used is easily appreciable and BDD compared to Pt produces an enhancement on the mineralization process, as can be seen for the AO processes of CHL. These results demonstrate the greatest

Table 9. *Percentage of DOC removal, maximum mineralization current efficiency and pseudo-first order constant obtained for the treatment of 245 mg L^{-1} of chloramphenicol and 62 mg L^{-1} of flumequine solutions by different EAOPs in stirred tank reactors equipped with 3 cm^2 electrode area at 33 mA cm^{-2}.*

	Flumequine			Chloramphenicol		
Methods	**% DOC removal**	**Máx. MCE / %**	**k_1 / s^{-1}**	**% DOC removal**	**Máx. MCE / %**	**k_1 / s^{-1}**
AO-Pt	---	---	---	0	0	3.0×10^{-5}
AO-BDD	---	---	---	78 (360 min)	17	1.4×10^{-4}
EF-BDD	77 (360 min)	21	1.0×10^{-2}	81 (360 min)	55	2.9×10^{-3}
PEF-BDD	96 (360 min)	19		100 (270 min)	56	
SPEF-BDD	---	---	---	10 (90 min)	101	

oxidizing power of physisorbed BDD(•OH) than Pt(•OH), since the weaker adsorption of •OH on BDD allows a greater reactivity of this radical.

The aforementioned findings agree with the classification of the anodes given by Comninellis (1994), where the active Pt anode leads to electrochemical conversion while the non-active BDD favors the electrochemical combustion. As can also be seen in **Table 9**, the Pt anode removes CHL very slowly in AO, without mineralization, and the corresponding pseudo-first-order rate constant (k_1) is one order of magnitude lower than that found for BDD.

When the EAOPs based on Fenton's reaction were applied, the use of a BDD anode instead of Pt improved and enhanced the oxidative process due to the combined action of the •OH generated in the bulk by Fenton's reaction (10) and BDD(•OH) radicals, which are more powerful oxidizing agents than Pt(•OH) ones.

In both compounds, the faster DOC removal was found in the EAOPs under UV irradiation. This light favours the mineralization due to the photodecarboxylation of iron(III) complexes with carboxylic acids like oxalic and oxamic acids achieving higher DOC removal percentages and significantly improving the MCE, even doubling it in the case of CHL. However, the use of MCE is not completely correct when the solution is irradiated because, as it is defined, the experimental DOC removal is expected to be only related to the electrochemical process, without considering the mineralization corresponding to photodegradation.

The effect of the intensity of the UV light can be assessed by comparing the PEF and SPEF processes for CHL solutions. While in PEF 360 min are needed to completely mineralize this drug, only 90 min are required for SPEF. This trend is explained on the basis that the UVA lamp intensity is 5 W m^{-2}, significantly lower than about 30 W m^{-2} determined in average for the solar UV radiation. This highlights the radiation intensity as a controlling parameter of the photodecomposition kinetics. However, **Table 9** evidences that the same k_1 was obtained for EF, PEF and SPEF, a value one magnitude order higher than in AO. This behaviour is explained by the fact that the initial pollutant is not photodegradable and its removal is only due to its reaction with $^{\bullet}$OH mainly formed from Fenton's reaction (10) and in much lesser extent with BDD($^{\bullet}$OH).

When the decay and mineralization of both antibiotics were compared, some differences could be noticed. Despite FLU is degraded more quickly than CHL, comparison of the mineralization and MCE allow conclude that CHL is the more easily electrochemically incinerated (see **Table 9**). The differences of one magnitude order observed for k_1 and the differences for MCE when compared could be justified by two main reasons:

1- The different recalcitrant character and oxidability of each pollutant.

2- Their different DOC and compound initial concentration.

Let us discuss then the influence of the compound initial concentration, which is an important control variable.

The study of the SPEF process of CHL included the effect of this parameter by treating solutions with contents from 10 to 100 mg L^{-1} of DOC. It was found that the DOC abatement required similar times to achieve full mineralization. It is therefore apparent that a higher concentration of organic matter in solution accelerated the mineralization

process and consequently, higher MCE values were obtained, rising from 12% to 100%. This enhancement can be ascribed to the inhibition of parasitic reactions (12), (13) and (20)-(29), favouring the organic events that mineralize these drugs or leading to the rapid accumulation of photolyzable species.

However, as can be seen in **Table 10**, the drop in concentration causes an unexpected increase of k_1 value, since from a theoretical point of view a first-order rate constant is independent of the initial concentration. This trend in k_1 may be related with the short live of $^{\bullet}$OH and BDD($^{\bullet}$OH) radicals of about 4×10^{-9} s (Root and Okada, 1975), which are continuously generated in the system. The higher amount of organic matter in the media seems to limit the generation of these radicals, giving a different stationary concentration depending on the experimental variables tested. This could explain that the pollutant decay follows a pseudo-first order kinetics with changing k_1 values. On the other hand, **Table 10** show similar k_1 values for CHL and FLU at analogous concentrations. The little difference between them is due to the different recalcitrant character and oxidability of each pollutant, FLU being the more degradable.

Table 10. *Pseudo-first-order rate constant at different initial concentrations of flumequine and chloramphenicol determined by EAOPs based on Fenton's reaction chemistry in 0.05 M Na_2SO_4 solutions at pH 3.0 and 33.3 mA cm^{-2}.*

Compound	**Concentration / mg L^{-1}**				
	24.5	**61.2-62.0**	**122.5**	**183.7**	**245.0**
CHL	1.5×10^{-2} s^{-1}	8.0×10^{-3} s^{-1}	7.6×10^{-3} s^{-1}	3.7×10^{-3} s^{-1}	2.9×10^{-3} s^{-1}
FLU	---	1.0×10^{-2} s^{-1}	---	---	---

The applied current density (j) is the main key factor governing the effectiveness of EAOPs and its influence was checked. It was found that greater j gave higher removal rate and mineralization degree at lower times. That enhancement can be ascribed to the concomitant acceleration of reactions (9) and (14), thereby enhancing Fenton's reaction (10) and producing more amounts of $^{\bullet}$OH radicals. However, the MCE is simultaneously reduced because the increase in j enhances the parasitic reactions (12), (13) and (20)-(29). Besides, the rise in j is the responsible of a higher cell voltage, as can be deduced from the Ohm's law, and hence, it causes an increase of energy consumption at any scale.

The evolution of oxidation by-products showed a similar behaviour in both antimicrobials. Ion chromatography evidenced the conversion of nitrogen and halogen atoms of the molecule into inorganic ions. The general tendency for F and Cl was their rapid release and accumulation as F^- and Cl^- ions, respectively, although Cl^- ion was further oxidized on BDD and released as Cl_2. In regard to N species, quantification by HPLC and TN determinations corroborated the main conversion into NO_3^- and oxamic, although some NH_4^+ was also accumulated in lesser extent. The sum of these *N*-derivatives in both cases corresponded to the expected theoretical N in solution because the initial TN remained almost completely unchanged in solution.

The analysis of intermediates by LC-MS and HPLC allowed the identification of nine aromatic by-products and thirteen hydroxylated derivatives for CHL. Ion-exclusion HPLC analyses demonstrated that short-chain carboxylic acids were formed from the cleavage of aromatic rings of FLU and CHL and they were the main remaining organic matter at the end of treatments. Some of these acids such as oxalic, oxamic and formic were found for both drugs, whereas malonic acid was only found for FLU and tartaric, maleic, acetic and dichloracetic acids were identified for CHL. The differences between the detected acids lie in the structures of the treated compounds that promote or not the formation and accumulation of certain acids over others. What it is really important to stand out is that in both cases oxalic and oxamic acids were accumulated in large contents up to 60 mg L^{-1}, as can be seen in **Fig. 12**. These compounds are the main components of the remaining DOC at the end of the electrolyses due to their high recalcitrant character and this effect is reflected in the MCE behaviour. When the change in MCE was analyzed, the maximum efficiency was depicted at short times followed by its progressive loss with prolonging electrolysis times. This decay in MCE can be ascribed to the gradual less organic matter in solution as well as along with the formation of more difficultly oxidizable products like short-chain carboxylic acids. Because of its relevance in the DOC removal efficiency and different behaviour depending on the EAOP tested, the oxamic and oxalic acid removal was studied deeply.

As pointed out above, oxalic and oxamic acids are the ultimate and more persistent by-products of the degradation of aromatic compounds (oxamic only in the case of *N*-aromatics). Their decay kinetics and oxidative paths were then studied for several EAOPs using a BDD anode and a stainless steel or ADE cathode.

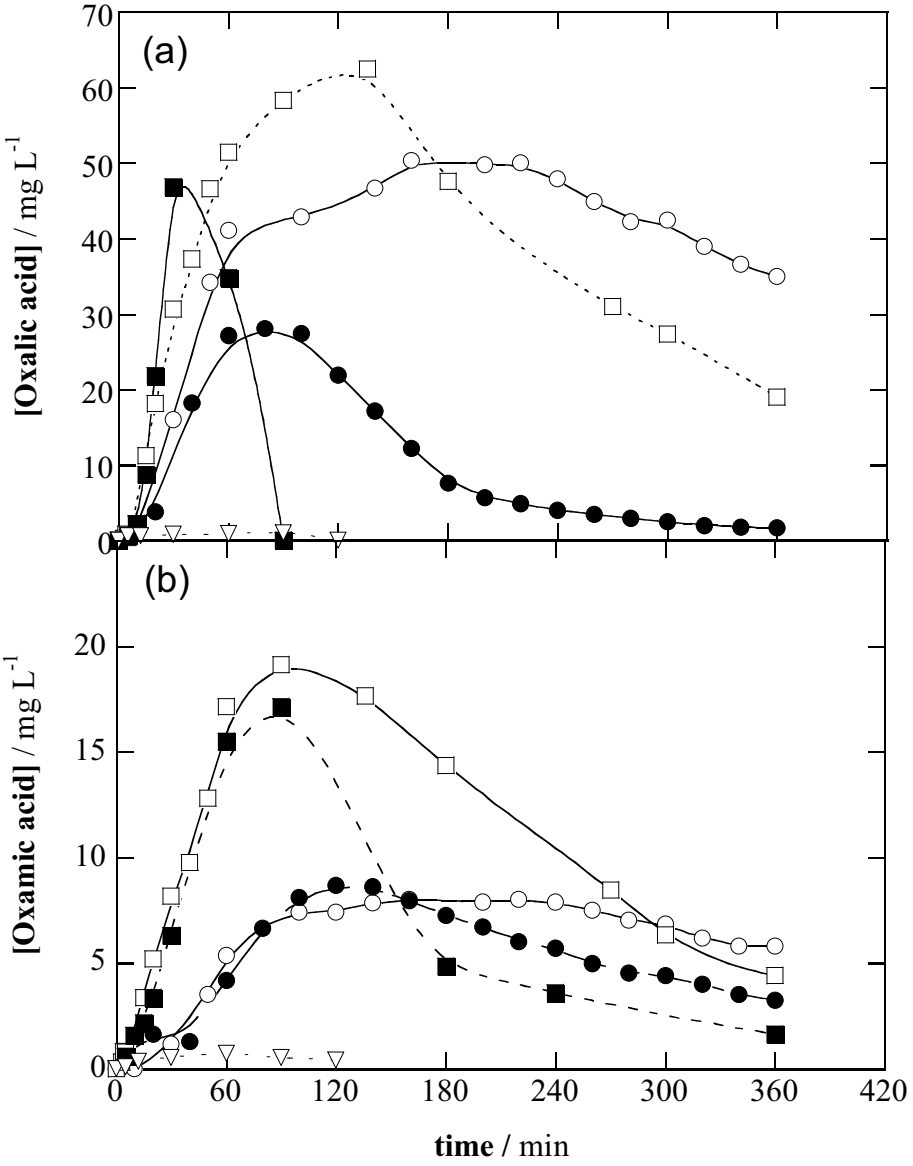

Figure 12. *Evolution of the concentration of (a) oxalic and (b) oxamic acids detected during the treatments of flumequine (○,●) and chloramphenicol (□,■,◊) by EF (○,□), PEF (●,■) and SPEF (◊).*

Voltamperometric analyses for the oxidation of oxalic, oxamic and their Fe^{2+} and Fe^{3+} complexes on BDD revealed important information. Thus, the complexes of oxalic with Fe^{2+} and Fe^{3+} are more recalcitrant than the free acid, whereas the oxamic iron complexes are more easily oxidized than the free acid. However, both acids are oxidized in the water discharge zone indicating that they react predominantly with BDD($^{\bullet}$OH) at the anode surface and not by direct charge transfer.

The degradative experiences showed similar behaviour for oxalic and oxamic acids. Both compounds were not directly photolyzed by UVA light, although they were removed by UVA light in the presence of Fe^{2+} and much quickly removed in presence of Fe^{3+}. These results highlighted that the most photoactive species were the Fe(III)-carboxylate complexes and their photodegradative process can be explained by a ligand to metal charge transfer that allows the photoreduction of the metallic centre and the oxidation of the oxalate or oxamate complex up to their total mineralization to CO_2.

As observed in voltammetric experiments, oxalic acid was mineralized faster than its iron-complexes by AO with BDD, whereas iron-oxamato complexes were mineralized faster than the free acid. In both cases, the EF treatment exhibited the same degradative behaviour than AO in presence of Fe^{2+}. That result indicated that the iron-carboxylate complexes were mineralized only by the action of the BDD($^{\bullet}OH$) radicals while the $^{\bullet}OH$ radicals generated in the bulk have no effect on their mineralization.

Also a study over the simultaneous treatment of oxalic and oxamic acids was performed. The aim of this study was to understand their competitive reactions and their influences on the pseudo-first-order rate constants. Solutions containing 8, 25 and 43% of oxamic acid from the total acid concentration (oxalic + oxamic) were treated by AO, AO in the presence of Fe^{2+} and AO in the presence of Fe^{2+} simultaneously irradiated by UVA light. No appreciable differences were found in AO because the oxidation process is only controlled by mass transfer. Nevertheless, that was not the case of the other two treatments. For AO with Fe^{2+} greater oxamic acid concentration gradually upgraded the k_1 value. This was explained by the formation of more iron-oxamate complexes instead of competitive oxalate ones, which are more rapidly mineralized than the free oxamic acid. When UVA light was applied, the k_1 value for oxalic acid decreased with the increase of oxamic acid in solution as a result of the lower concentration of photoactive iron-oxalato species available for the photodegradation process.

The increase in current density led to quicker acids removal and the loss of MCE as well discussed above for FLU and CHL. Besides, it showed an effect on the inorganic N released during oxamic acid treatment. As current density rose, it was found a drop in NH_4^+ concentration and an increase in NO_3^- concentration and NOx evolution.

The initial concentration of Fe^{2+}, the catalyst of Fenton's reaction (10), is also a key parameter of the degradation process. Usually, it is found an optimum content for this ion

of 0.5 mM for almost all compounds. However, FLU is one exception and an optimum catalyst concentration of 2.0 mM was found, that is, 4 times higher. This was explained by the dual role played by Fe^{2+} during the FLU treatment, where acts as complexing agent of FLU and as Fenton's reaction catalyst to generate $^{\bullet}OH$.

The iron concentration effect was also studied for the treatment of oxamic acid, where interestingly the [oxamic acid]/[Fe^{2+}] ratio gave differences in the evolution of N species. The main effect of the rise in Fe^{2+} concentration was the inhibition of oxamic acid removal. This evidence was related to the competitive oxidation of free Fe^{2+} to Fe^{3+} at the anode from reaction (34) instead of the mineralization of the iron-oxamate complexes. The reduction of Fe^{3+} at the stainless steel cathode from reaction (15) regenerated Fe^{2+} ion and maintained the equilibrium between both ions in solution, decreasing the oxidation ability. That fall is also reflected in the gradual drop in NO_3^- content ascribed to the loss of the oxidative power of the system.

$$Fe^{2+} \rightarrow Fe^{3+} + e^- \qquad (34)$$

After the promising results obtained for CHL degradation, the SPEF process was scaled-up from the stirred tank reactor to a pre-pilot flow plant of 10 L with an electrochemical filter-press reactor of Pt/ADE coupled to a CPC photoreactor. During the SPEF treatment at 100 mA cm^{-2}, an 89 % of DOC removal was attained with a 49% of MCE and 0.347 kWh g^{-1} DOC of EC, related to 30.8 kWh m^{-3}, yielding an estimated cost of 4.35 € m^{-3}. This low cost and the excellent DOC removal confirms the viability of SPEF for possible application to industrial scale. Even more, the consideration of use of solar panels could allow the drastic reduction of EC.

To end with the work about the application of EAOPs to the remediation of wastewaters polluted with pharmaceuticals, the EF and PEF processes were applied to a real wastewater matrix provided gently by the Manresa's Sewage Treatment Plant, which was polluted with FLU. During these assays, a complete removal of the natural organic matter (NOM) from the real wastewater matrix was obtained. FLU was also removed at the same rate, reaching the same degradation degree as the synthetic wastewater treated previously. This promising result suggests the effectiveness of EAOPs in real water conditions to remove other POPs and even achieve the complete NOM degradation by the action of hydroxyl radicals in the electrolytic systems.

PAPER 1

Mineralization of flumequine in acidic medium by electro-Fenton and photoelectro-Fenton processes

Available online at www.sciencedirect.com

SciVerse ScienceDirect

journal homepage: www.elsevier.com/locate/watres

Mineralization of flumequine in acidic medium by electro-Fenton and photoelectro-Fenton processes

*Sergi Garcia-Segura, José A. Garrido, Rosa M. Rodríguez, Pere L. Cabot, Francesc Centellas, Conchita Arias, Enric Brillas**

Laboratori d'Electroquímica dels Materials i del Medi Ambient, Departament de Química Física, Facultat de Química, Universitat de Barcelona, Martí i Franquès 1-11, 08028 Barcelona, Spain

ARTICLE INFO

Article history:
Received 21 November 2011
Received in revised form
16 January 2012
Accepted 18 January 2012
Available online 3 February 2012

Keywords:
Flumequine
Electro-Fenton
Mineralization
Photoelectro-Fenton
Oxidation products
Water treatment

ABSTRACT

The mineralization of flumequine, an antimicrobial agent belonging to the first generation of synthetic fluoroquinolones which is detected in natural waters, has been studied by electrochemical advanced oxidation processes (EAOPs) like electro-Fenton (EF) and photoelectro-Fenton (PEF) with UVA light. The experiments were performed in a cell containing a boron-doped diamond (BDD) anode and an air-diffusion cathode to generate H_2O_2 at constant current. The Fe^{2+} ion added to the medium increased the solubility of the drug by the formation of a complex of intense orange colour and also reacted with electrogenerated H_2O_2 to form hydroxyl radical from Fenton reaction. Oxidant hydroxyl radicals at the BDD surface were produced from water oxidation. A partial mineralization of flumequine in a solution near to saturation with optimum 2.0 mM Fe^{2+} at pH 3.0 was achieved by EF. The PEF process was more powerful, giving an almost total mineralization with 94–96% total organic carbon removal. Increasing current accelerated both treatments, but with decreasing mineralization current efficiency. Comparative treatments using a real wastewater matrix led to similar degradation degrees. The kinetics for flumequine decay always followed a pseudo-first-order reaction and its rate constant, similar for both EAOPs, raised with increasing current. Generated carboxylic acids like malonic, formic, oxalic and oxamic acids were quantified by ion-exclusion HPLC. Fe(III)–oxalate and Fe(III)–oxamate complexes were the most persistent by-products under EF conditions and their quicker photolysis by UVA light explains the higher oxidation power of PEF. The release of inorganic ions such as F^-, NO_3^- and in lesser extent NH_4^+ was followed by ionic chromatography.

1. Introduction

Over the last two decades, a large variety of pharmaceutical drugs including analgesics, anti-inflammatory, beta-blockers, antimicrobials, blood lipid regulators and so on, has been detected at low contents of micrograms per litre in soils, surface waters, ground waters and even drinking waters (Tamtam et al., 2008; Kümmerer, 2009; Postigo et al., 2009; Li et al., 2010; McClellan and Halden, 2010). This pollution proceeds from production sites, excretion after drug administration to humans and animals, direct disposal of excess of drugs in households and treatments in fish and other animal farms (Bound and Voulvoulis, 2005). The accumulation of drugs in the aquatic environment is mainly due to their inefficient destruction in the processes currently used in sewage treatment plants (STPs) (Andreozzi et al., 2003; Karthikeyan

* *Corresponding author*. Tel.: +34 93 4021223; fax: +34 93 4021231.
E-mail address: brillas@ub.edu (E. Brillas).
0043-1354/$ – see front matter © 2012 Elsevier Ltd. All rights reserved.
doi:10.1016/j.watres.2012.01.019

and Meyer, 2006; Vieno et al., 2007; Homem and Santos, 2011). Despite their low content in natural waters, it has been documented the development of multi-resistant strains of microorganism by some drugs (Jarnheimer et al., 2004; Naviner et al., 2011), the effects of pharmaceuticals on the endocrine systems of fishes and invertebrates (Migliore et al., 1997) and their toxicity on algae and small invertebrates (Halling-Sørensen, 2000; Crane et al., 2006; Pomati et al., 2008). To avoid the possible adverse health problems on living beings, research efforts are needed for the development of powerful methods for the removal of these pollutants from the environment.

Several treatments involving ozonation and a large variety of advanced oxidation processes (AOPs) have been recently applied to the remediation of waters contaminated with drugs (Skoumal et al., 2006; Rosal et al., 2008; Brillas et al., 2009; Kim et al., 2009; Song et al., 2009; Rozas et al., 2010; Homem and Santos, 2011). AOPs are chemical, photocatalytic and electrochemical methods based on the in situ generation of hydroxyl radical ($^{\bullet}OH$). This species is the second strongest oxidant known after fluorine and has so high standard reduction potential ($E^{\circ}(^{\bullet}OH/H_2O) = 2.80$ V vs SHE) that can react non-selectively with most organic pollutants up to their total mineralization (conversion into CO_2, water and inorganic ions). Recently, electrochemical AOPs (EAOPs) based on Fenton's reaction chemistry such as electro-Fenton (EF) and photoelectro-Fenton (PEF) have received great attention for the degradation of organics in waters due to their simplicity, great efficiency and relative low cost (Skoumal et al., 2008; Balci et al., 2009; Brillas et al., 2009; Zarei et al., 2010; Almeida et al., 2011). In the EF process, H_2O_2 is continuously supplied to an acidic medium from the two-electron reduction of added O_2 at the cathode by reaction (1). The addition of a small Fe^{2+} concentration to the solution enhances the oxidation power of electrogenerated H_2O_2 giving $^{\bullet}OH$ and Fe^{3+} from Fenton reaction (2), which is promoted by the catalytic action of the Fe^{3+}/Fe^{2+} system, mainly from the regeneration of Fe^{2+} by the cathodic reduction of Fe^{3+} from reaction (3).

$$O_2 + 2H^+ + 2e^- \rightarrow H_2O_2 \quad (1)$$

$$Fe^{2+} + H_2O_2 \rightarrow Fe^{3+} + {}^{\bullet}OH + OH^- \quad (2)$$

$$Fe^{3+} + e^- \rightarrow Fe^{2+} \quad (3)$$

Good efficiencies for H_2O_2 generation from reaction (1) have been found using cathodes such as carbon nanotubes-polytetrafluoroethylene (PTFE) (Khataee et al., 2010; Zarei et al., 2010), carbon nanotubes on graphite (Khataee et al., 2011), carbon felt (Oturan et al., 2008, 2010; Balci et al., 2009; Özcan et al., 2010; Sirés et al., 2010) and carbon-PTFE gas (O_2 or air) diffusion (Sirés et al., 2007; Skoumal et al., 2008, 2009; Garcia-Segura and Brillas, 2011).

When an undivided cell is used in EF, it is possible the combined oxidation action of $^{\bullet}OH$ generated both in the bulk by Fenton reaction (2) and at the anode surface from water discharge (Brillas et al., 2009). For a boron-doped diamond (BDD) thin-film anode, the formation of the physisorbed BDD($^{\bullet}OH$) is given by reaction (4) (Marselli et al., 2003; Panizza and Cerisola, 2009):

$$BDD + H_2O \rightarrow BDD(^{\bullet}OH) + H^+ + e^- \quad (4)$$

The BDD electrode is currently considered the most potent anode because it interacts very weakly with generated $^{\bullet}OH$ resulting in a much greater O_2-overpotential than other materials like Pt (Sirés et al., 2006; Hamza et al., 2009; Brillas et al., 2010) and in an enhancement of organic removal with reactive BDD($^{\bullet}OH$) that makes it potent enough to mineralize aromatics and their generated carboxylic acids (Cañizares et al., 2008; Panizza and Cerisola, 2009; Garcia-Segura and Brillas, 2011).

Because of their different experimental conditions, the direct comparison between the mineralization efficiencies attained from the classical chemical Fenton and EF processes is difficult to be established (Serra et al., 2009). Nevertheless, the additional production of hydroxyl radicals from Fe^{2+} regeneration by reaction (3) and water oxidation by reaction (4) allows predicting that EF is more potent than classical chemical Fenton (Brillas et al., 2009).

The PEF process involves the simultaneous UV irradiation of the solution under EF treatment. This light causes the photolysis of $[Fe(OH)]^{2+}$, the more stable species of Fe^{3+} at pH ca. 3, regenerating more catalytic Fe^{2+} and producing more $^{\bullet}OH$ by reaction (5) (Brillas et al., 2009). Furthermore, UV light can induce the photodegradation of some intermediates, as the case of Fe(III)–carboxylate complexes by reaction (6) (Garcia-Segura and Brillas, 2011).

$$[Fe(OH)]^{2+} + h\nu \rightarrow Fe^{2+} + {}^{\bullet}OH \quad (5)$$

$$Fe(OOCR)^{2+} + h\nu \rightarrow Fe^{2+} + CO_2 + R^{\bullet} \quad (6)$$

In previous work, our group has investigated the efficient degradation of several drugs such as paracetamol (Sirés et al., 2007; Almeida et al., 2011), chloroxylenol (Skoumal et al., 2008), ibuprofen (Skoumal et al., 2009) and enrofloxacin (Guinea et al., 2010) by EF and PEF using electrochemical reactors with either a BDD or Pt anode and a carbon-PTFE gas diffusion cathode. To gain a better knowledge about the possible viability of these EAOPs for the treatment of wastewaters containing drugs, more research efforts are needed to clarify the degradation behaviour of more complex molecular structures. In this way, we have undertaken a study on the mineralization of flumequine ($C_{14}H_{12}FNO_3$, see formula in Fig. 1). It is an antimicrobial agent belonging to the first generation of synthetic fluoroquinolones, which has been widely used in veterinary medicine (poultry, livestock and aquaculture) to control bacterial infections, even in large quantities owing its low bioavailability in fish (Burridge et al., 2010). Flumequine has been detected in rivers at concentrations up to 50 ng L^{-1} (Tamtam et al., 2008; Muñoz et al., 2010) and its antimicrobial resistance in bacteria (Naviner et al., 2011) and algal toxicity have been well proven (Halling-Sørensen, 2000; Crane et al., 2006). Flumequine is poorly photolyzed in waters (Pouliquen et al., 2007) and is not oxidized with chlorine dioxide (Wang et al., 2010). It has also

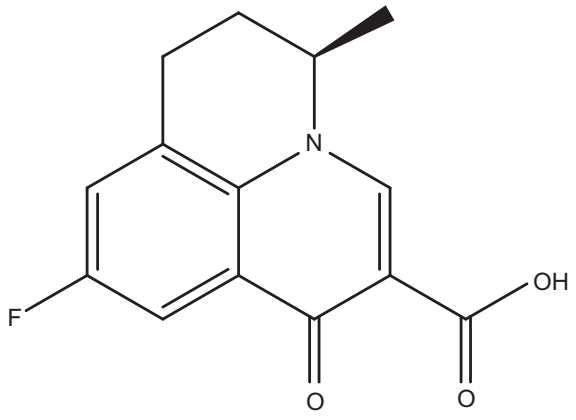

Fig. 1 – Chemical formula of flumequine.

been reported that flumequine can be degraded by means of AOPs like TiO_2 photocatalysis (Nieto et al., 2008; Miranda-García et al., 2011) and photo-Fenton (Klamerth et al., 2011).

This paper presents the results obtained for the mineralization of flumequine by EF and PEF processes using a BDD/air-diffusion cell. The influence of Fe^{2+} concentration and applied current on the degradation rate and mineralization degree was examined. The decay kinetics for the drug and the evolution of generated carboxylic acids and inorganic ions released were determined by chromatographic techniques to clarify the oxidative ability of both EAOPs. Comparative treatments of flumequine in a real wastewater matrix were also made to study the possible influence of natural organic matter (NOM) on their oxidation power, which has not been previously considered for other drugs.

2. Experimental

2.1. Chemicals

Flumequine (99% purity) was supplied by the Laboratories SYVA S.A.U. (León, Spain). Anhydrous sodium sulphate and iron (II) sulphate heptahydrate were of analytical grade from Panreac and Fluka, respectively. Oxalic, oxamic, malonic and formic acids were of analytical grade purchased from Avocado. All the other chemicals employed were either of HPLC or analytical grade from Merck, Panreac and Avocado. Solutions were prepared with high-purity water obtained from a Millipore Milli-Q system with resistivity >18 MΩ cm at 25 °C. All solutions were adjusted to pH 3.0 with analytical grade sulphuric acid from Merck.

2.2. Electrochemical system

All the electrolytic trials were conducted in an open, undivided and cylindrical glass cell of 150 mL capacity, with a double jacket in which external water circulated to maintain the solution temperature at 35 °C. This is the optimal temperature found for the degradation of other aromatics in the cell, without significant water evaporation from solution (Sirés et al., 2007). The anode was a BDD thin film from Adamant Technologies (La Chaux-de-Fonds, Switzerland) and the cathode was a carbon-PTFE air-diffusion electrode from E-TEK (Somerset, NJ, USA). The preparation of this cathode was described elsewhere (Brillas et al., 2004) and it was fed with air pumped at 300 mL min^{-1} to generate H_2O_2 from reaction (1). The geometric area of each electrode was 3 cm^2 and the interelectrode gap was 1 cm. To remove the impurities of the BDD surface and activate the air-diffusion cathode, they were previously polarized in 0.05 M Na_2SO_4 at 300 mA for 60 min. All experiments were carried out under vigorous stirring with a magnetic bar at 800 rpm to ensure homogenization and the transport of reactants towards/from the electrodes.

Comparative EF degradations of 100 mL of 62 mg L^{-1} flumequine solutions (40 mg L^{-1} of total organic carbon (TOC)) in 0.05 M Na_2SO_4 with concentrations of Fe^{2+} from 0.5 to 6.0 mM at pH 3.0 were performed. This solution pH was chosen since it was found optimal for the similar treatment of other organics (Oturan et al., 2008; Brillas et al., 2009). The influence of applied current between 50 and 300 mA on the EF and PEF treatments of the drug solution with 2.0 mM Fe^{2+} was also examined. For the trials with real wastewaters, effluents of the secondary biological treatment of the Municipal Wastewater Treatment Plant of Manresa (Barcelona, Spain) with TOC ca. 27 mg L^{-1} were taken and used the next day. In the PEF assays, a Philips TL/6W/08 fluorescent black light blue tube of $\lambda_{max} = 360$ nm was placed at the top of the cell at 7 cm above the solution, giving a photoionization energy input of 5 W m^{-2}, as detected with a Kipp&Zonen CUV5 radiometer.

2.3. Apparatus and analytical procedures

The solution pH was determined with a Crison 2000 pH metre. Galvanostatic electrolyses were performed with an Amel 2051 potentiostat–galvanostat. Before analysis, the aliquots were alkalinized to stop the mineralization process and filtered with 0.45 μm PTFE filters from Whatman. The solution TOC was determined with a Shimadzu VCSN TOC analyzer and reproducible values with an accuracy of ±1% were obtained by injecting 50 μL aliquots into it. From these data, the mineralization current efficiency (MCE, in %) for the electrolyzed solutions was then calculated by Eq. (7):

$$\mathrm{MCE}\ (\%) = \frac{nFV_s\Delta(\mathrm{TOC})_{exp}}{4.32\times10^7 mIt}\times 100 \qquad (7)$$

where F is the Faraday constant (96,487 C mol^{-1}), V_s is the solution volume (L), $\Delta(TOC)_{exp}$ is the experimental TOC removal (mg L^{-1}), 4.32×10^7 is a conversion factor (3600 s h^{-1} × 12,000 mg mol^{-1}), m is the number of carbon atoms of the compound (14 carbons), I is the applied current (A) and t is the electrolysis time (h). The number of electrons (n) consumed for the total mineralization of flumequine was taken as 66 considering that it is transformed into CO_2 and NO_3^- and F^- ions as the final products following Eq. (8):

$$C_{14}H_{12}FNO_3 + 28H_2O \rightarrow 14CO_2 + NO_3^- + F^- + 68H^+ + 66e^- \qquad (8)$$

The evolution of total nitrogen (TN) of the solution was determined with a TNM-1 module coupled to the above TOC analyzer.

The flumequine decay was followed by reversed-phase HPLC of electrolyzed solutions using a Waters 600 LC fitted with a Thermo Electron Corporation Hypersil BDS C18 5 μm (250 mm × 4.6 mm (i.d.)) column at 35 °C, coupled with a Waters 996 photodiode array detector selected at $\lambda = 233$ nm. Generated carboxylic acids were detected and quantified by ion-exclusion HPLC using the above LC fitted with a Bio-Rad Aminex HPX 87H (300 mm × 7.8 mm (i.d.)) column at 35 °C and the photodiode array detector selected at $\lambda = 210$ nm. For these measurements, 20 μL aliquots were injected into the chromatograph and the mobile phase was a 40:60 (v/v) acetonitrile/water (phosphate buffer, pH 3.5) mixture at 0.6 mL min^{-1} for reversed-phase HPLC and 4 mM H_2SO_4 at 0.6 mL min^{-1} for ion-exclusion HPLC.

The inorganic ions released during the mineralization process were quantified by ionic chromatography using a Shimadzu 10 Avp HPLC coupled with a Shimadzu CDD 10 Avp conductivity detector. These analyses were performed by injecting 25 μL aliquots. The NH_4^+ concentration was determined with a Shodex cationic column IC YK-421 (125 mm × 4.6 mm (i.d.)) at 40 °C and circulating a mobile phase composed of 5.0 mM tartaric acid, 1.0 mM dipicolinic acid, 24.2 mM boric acid and 1.5 mM crown ether at 1.0 mL min^{-1}. The F^- and NO_3^- concentrations were obtained with a Shim-Pack anionic column IC-A1S (100 mm × 4.6 mm (i.d.)) at 40 °C using a solution with 2.4 mM tris(hydroxymethyl)aminomethane and 2.5 mM phthalic acid of pH 4.0 at 1.5 mL min^{-1} as mobile phase.

3. Results and discussion

3.1. *Effect of Fe^{2+} concentration on EF degradation*

Fig. 1 shows the complex aromatic structure of flumequine containing a carboxylic group, with $pK_a = 6.35$ (Lin et al., 2004), which explains its different solubility in acidic and alkaline media. Thus, it possesses a high solubility in alkaline medium because the anionic form predominates, but it is quite insoluble in acidic medium where its neutral form is the major species. Nevertheless, when flumequine solutions were prepared to operate under EF conditions, it was found that the addition of Fe^{2+} to a saturated solution of pH 3.0 increased strongly the solubility of the drug. The initial colourless solution then changed to an intense orange colour, which can be ascribed with the formation of a stable complex between Fe(II) and flumequine. In the presence of 0.5 mM Fe^{2+}, the saturated solution contained 62 mg L^{-1} of the drug, as confirmed from TOC analysis, and this flumequine content at pH 3.0 was used to assess the influence of Fe^{2+} concentration up to 6.0 mM on the EF process operating with the BDD/air-diffusion cell at 50 mA for 360 min. In all these trials, the initial orange solutions became colourless after less than 90 min of treatment, when all coloured intermediates and/or iron (Fe(II) and/or Fe(III)) complexes with aromatics were destroyed. Moreover, the solution pH decreased slightly up to a final value close to 2.8, probably due to the generation of short-linear aliphatic carboxylic acids (Oturan et al., 2008; Brillas et al., 2009).

Fig. 2a depicts the slow, but gradual TOC decrease with electrolysis time found for the above EF experiments. As can be seen, the higher degradation rate for the flumequine solution was attained for 2.0 and 4.0 mM Fe^{2+} at least up to 240 min of electrolysis, although from 0.5 to 4.0 mM Fe^{2+} about 75% of mineralization was always achieved at 360 min. For the higher 6.0 mM Fe^{2+}, however, the EF process was strongly inhibited after 240 min, only reaching 58% of TOC removal at the end of electrolysis. This behaviour suggests that flumequine and its primary oxidation by-products are mainly destroyed by $^{\bullet}OH$ formed by Fenton reaction (2) up to yield species, like Fe(III) complexes of short carboxylic acids, that only react much more slowly at the anode surface with BDD($^{\bullet}OH$) produced by reaction (4) (Garcia-Segura and Brillas, 2011). The larger formation of the latter kind of products for the higher Fe^{2+} concentration of 6.0 mM can account for by the large inhibition of TOC removal observed at long electrolysis time under these conditions (see Fig. 2a).

To clarify the behaviour of generated hydroxyl radicals, the kinetics for the drug decay in the above assays was followed by reversed-phase HPLC, where it displayed a well-defined

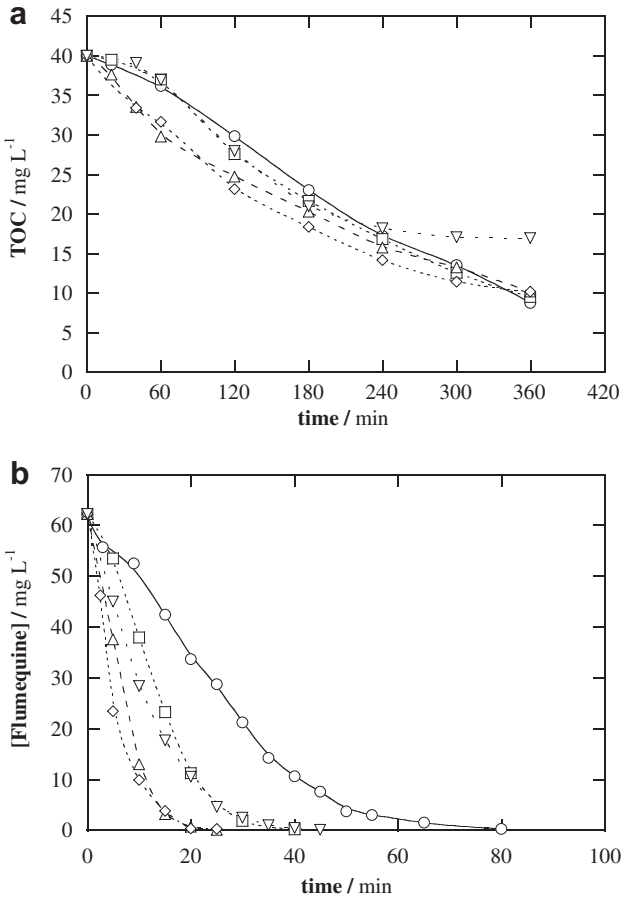

Fig. 2 – Abatement of (a) TOC and (b) flumequine concentration with electrolysis time for the electro-Fenton (EF) degradation of 100 mL of 62 mg L^{-1} of the drug (near to saturation) in 0.05 M Na_2SO_4 at pH 3.0 and 35 °C using a BDD/air-diffusion cell with 3.0 cm^2 area of each electrode at 50 mA. Fe^{2+} concentration: (○) 0.5 mM, (□) 1.0 mM, (△) 2.0 mM, (◇) 4.0 mM and (▽) 6.0 mM.

peak with retention time (t_r) of 13.5 min. Fig. 2b evidences a very rapid removal of the drug in all cases, disappearing from the medium in decreasing time from 80 min for 0.5 mM Fe^{2+} to 25 min for 2.0 and 4.0 mM Fe^{2+}. However, a longer time of 45 min was needed to achieve its total disappearance for 6.0 mM Fe^{2+}. The increase in flumequine decay rate when Fe^{2+} content rises from 0.5 to 4.0 mM can be related to the gradual acceleration of Fenton reaction (2). The smaller destruction rate found for 6.0 mM Fe^{2+} can then be explained by the loss of $^{\bullet}OH$ with the excess of Fe^{2+} added from the parasitic reaction (9) (Brillas et al., 2009):

$$Fe^{2+} + {}^{\bullet}OH \rightarrow Fe^{3+} + OH^{-} \quad (9)$$

The above considerations highlight the dual role of Fe^{2+} ion in the EF process, as complexing agent of flumequine and as reactant of Fenton reaction (2) to generate $^{\bullet}OH$ in the bulk to mainly oxidize the complex formed with the drug. From these findings, 2.0 mM Fe^{2+} was chosen as the optimum concentration to study the characteristics of both, the EF and PEF processes on flumequine mineralization.

3.2. *Comparative degradation by EF and PEF processes*

The applied current is the main key factor governing the effectiveness of EAOPs. To check the influence of this parameter, currents ranging between 50 and 300 mA were applied to the EF and PEF treatments of a 62 mg L^{-1} flumequine solution with the optimum 2.0 mM Fe^{2+} at pH 3.0. The corresponding TOC abatements are presented in Fig. 3a and b, respectively. These trials were performed without pH regulation since it only decayed up to 2.6–2.7 as maximum after 360 min of electrolysis, as expected if final short-aliphatic carboxylic acids are always produced (Brillas et al., 2009).

For EF, Fig. 3a shows an increasing TOC decay with rising current, reaching 75%, 77%, 78% and 89% mineralization at the end of the treatment at 50, 75, 100 and 300 mA respectively. The greater degradation rate and mineralization degree achieved at higher current can then be ascribed to the concomitant acceleration of reaction (1) producing more H_2O_2 to enhance the generation of $^{\bullet}OH$ via Fenton reaction (2), as well as of reaction (4) giving more amount of reactive BDD($^{\bullet}OH$). The same behaviour can be observed in Fig. 3b for the PEF process, although in this case a higher 94–96% TOC removal was attained after 360 min of all electrolyses. This means that the PEF treatment allows reaching an almost total mineralization of flumequine, having a much greater oxidation power than the EF one. The enhancement of mineralization in PEF can be related to the rapid photodegradation by UVA light of Fe(III) complexes with some final carboxylic acids, which are very slowly degraded by hydroxyl radicals in EF, as will be discussed below. Note that for the higher current of 300 mA, a 95% mineralization was already achieved at about 240 min of PEF (see Fig. 3b), indicating the formation of very recalcitrant by-products that remain in the final solution because they cannot be removed by the action of hydroxyl radicals and/or UVA light.

The MCE values calculated from Eq. (7) for the experiments given in Fig. 3a and b are depicted in their inset panels as

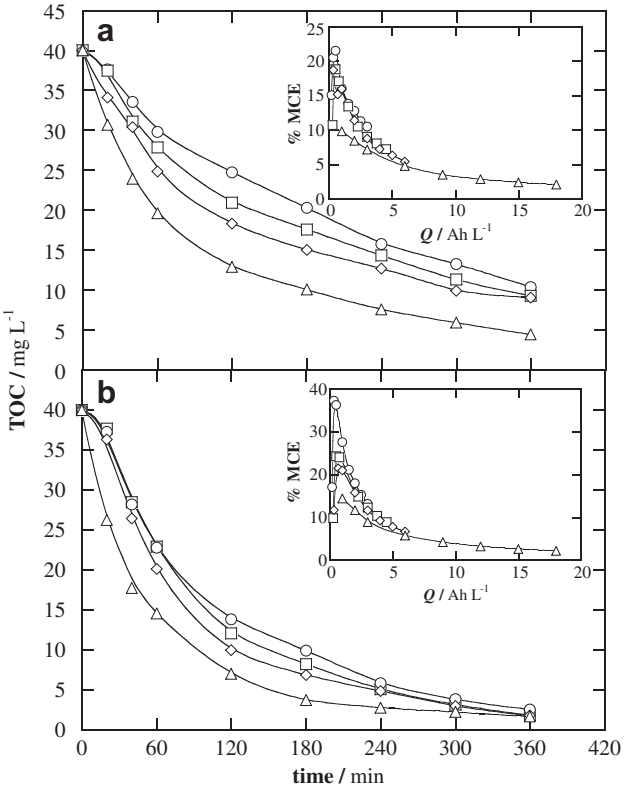

Fig. 3 – TOC removal vs electrolysis time for the (a) EF and (b) photoelectro-Fenton (PEF) processes of 100 mL of 62 mg L^{-1} flumequine in 0.05 M Na_2SO_4 with 2.0 mM Fe^{2+} at pH 3.0 and 35 °C using a BDD/air-diffusion cell operating at: (○) 50 mA, (□) 75 mA, (◇) 100 mA and (△) 300 mA. The PEF treatment was carried out with a 6 W UVA irradiation of λ_{max} = 360 nm. The inset panels present the corresponding mineralization current efficiency calculated from Eq. (7).

a function of the consumed specific charge (Q, in Ah L^{-1}). At the same current a higher efficiency can be observed for the PEF treatment, as a result of the greater mineralization achieved for the flumequine solution. The maximum MCE values obtained were 21% for EF and 37% for PEF at 50 mA after the consumption of 0.5 Ah L^{-1}. At higher Q values, the efficiency always decreased dramatically owing to the gradual formation of more recalcitrant by-products and the presence of less organic matter in solution (Panizza and Cerisola, 2009). Moreover, in both processes the efficiency dropped as current increased, being this effect more significant when passing from 100 to 300 mA. For example, the MCE values decayed in 13%, 12%, 11% and 8.5% for EF and 18%, 17%, 16% and 12% after consuming 2.0 Ah L^{-1} at 50, 75, 100 and 300 mA, respectively. This loss in efficiency in both treatments with rising current can be accounted for by the production of less relative oxidizing hydroxyl radicals due to the larger acceleration of their parasitic reactions, thereby decreasing the organic events. These waste reactions involve, for example, the oxidation of BDD($^{\bullet}OH$) to O_2 at the anode by reaction (10), the dimerization of $^{\bullet}OH$ to H_2O_2 by reaction (11) and the reaction

of this radical with H_2O_2 generating the hydroperoxyl radical ($HO_2^{\bullet}$) of lower oxidizing power by reaction (12) (Brillas et al., 2009; Panizza and Cerisola, 2009; Guinea et al., 2010):

$$2BDD(^{\bullet}OH) \rightarrow 2BDD + O_2 + 2H^+ + 2e^- \quad (10)$$

$$2^{\bullet}OH \rightarrow H_2O_2 \quad (11)$$

$$H_2O_2 + {}^{\bullet}OH \rightarrow HO_2^{\bullet} + H_2O \quad (12)$$

The kinetic decay for flumequine under the EF conditions of Fig. 3a is presented in Fig. 4. As expected, the drug was completely removed and disappeared much more rapidly with rising current due to its faster reaction with the greater amounts of $^{\bullet}OH$ generated from Fenton reaction (2) and BDD($^{\bullet}OH$) formed from reaction (4). Similar drug abatement for each current tested was found operating with the PEF process, as exemplified in Fig. 4 for the case of 100 mA. This evidences that the complex of Fe(II) with flumequine is not directly photolyzed by UVA irradiation and that the photolytic reaction (5) participates very poorly to generate $^{\bullet}OH$. The above concentration decays were further analyzed using kinetic equations related to simple reaction orders and good fits were only found for a pseudo-first-order reaction, as can be seen in the inset panel of Fig. 4. From this analysis, increasing pseudo-first-order rate constants (k_1) of $3.2 \times 10^{-3}\ s^{-1}$ ($R^2 = 0.997$) for 50 mA, $6.3 \times 10^{-3}\ s^{-1}$ ($R^2 = 0.982$) for 75 mA, $1.0 \times 10^{-2}\ s^{-1}$ ($R^2 = 0.978$) for 100 mA and $2.6 \times 10^{-2}\ s^{-1}$ ($R^2 = 0.976$) for 300 mA were obtained for EF. This behaviour is indicative of a constant production of oxidizing hydroxyl radicals ($^{\bullet}OH$ and BDD($^{\bullet}OH$)) during the EF and PEF treatments at each current, at least during the time required to destroy the initial complex of Fe(II) with flumequine.

The possible effect of NOM on the EF and PEF degradations of 62 mg L^{-1} flumequine in a real wastewater matrix was also studied under the above optimized conditions at 300 mA. Fig. 5 shows that TOC was reduced by 91% for EF and 97% for PEF in 360 min, thereby reaching similar mineralization degrees to those found in the synthetic solution (see Fig. 3). In contrast, the real wastewater alone was degraded at quite similar rate for both EAOPs, attaining ca. 93% mineralization at the end of electrolysis (see Fig. 5). These findings evidence the little influence of NOM on flumequine removal because PEF yields an almost total mineralization and is more powerful than EF by the synergistic action of UVA light. The fact that both EAOPs are able to degrade the real wastewater at similar rate, suggests that NOM is primordially destroyed by the hydroxyl radicals generated in the electrolytic system.

3.3. *Time course of generated carboxylic acids*

It is well-known that the degradation of aromatics and heteroaromatics with hydroxyl radicals involves the generation of short-linear aliphatic carboxylic acids coming from the cleavage of their aromatic moieties and lateral groups (Oturan et al., 2008; Balci et al., 2009; Brillas et al., 2009; Skoumal et al., 2009; Almeida et al., 2011). This behaviour was confirmed for the EF and PEF treatments of 62 mg L^{-1} flumequine with 2 mM Fe^{2+} of pH 3.0 by analyzing the solutions electrolyzed at 50 mA by ion-exclusion HPLC. These chromatograms exhibited well-defined peaks corresponding to carboxylic acids like oxalic ($t_r = 7.0$ min), oxamic ($t_r = 9.4$ min), malonic ($t_r = 9.8$ min) and formic ($t_r = 13.7$ min). Under the EF and PEF conditions tested, all these acids form complexes with Fe(III), which is formed in Fenton reaction (2) and is the predominant iron species at long electrolysis time (Brillas et al., 2009). Note that oxalic, oxamic and formic acids are ultimate carboxylic acids because they are directly converted into CO_2 (Oturan et al., 2008; Garcia-Segura and Brillas, 2011).

Fig. 6a shows that malonic and formic acids were accumulated to near 12 and 17 mg L^{-1} at 30 min, respectively, and further rapidly removed in 60–90 min of EF treatment, as expected if their Fe(III) complexes rapidly react with hydroxyl

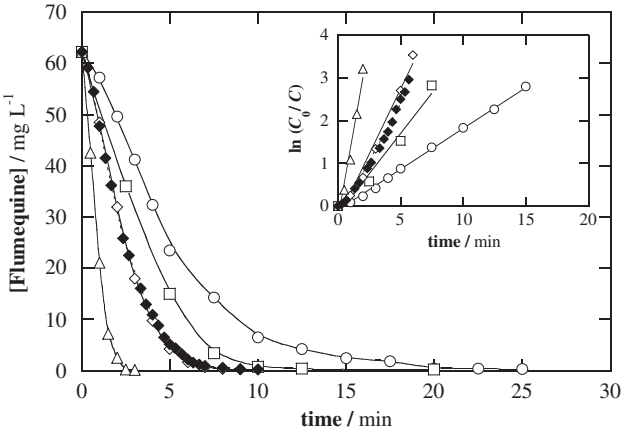

Fig. 4 – Flumequine concentration decay under the same conditions of Fig. 3. EF process at: (○) 50 mA, (□) 75 mA, (◇) 100 mA and (△) 300 mA. PEF process at (◆) 100 mA. The corresponding kinetic analysis assuming a pseudo-first-order reaction for flumequine is given in the inset panel.

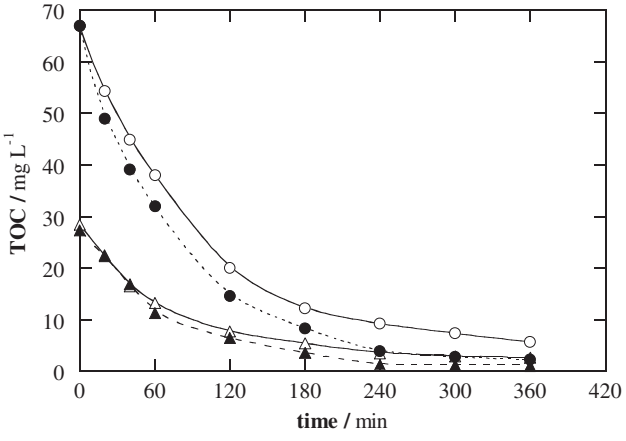

Fig. 5 – TOC decay with electrolysis time for the (○) EF and (●) PEF degradations of 100 mL of 62 mg L^{-1} flumequine in a real wastewater matrix of 27 mg L^{-1} TOC with 0.05 M Na_2SO_4 and 2.0 mM Fe^{2+} at pH 3.0, 300 mA and 35 °C. (△) EF and (▲) PEF treatments of the real wastewater matrix under the same conditions.

radicals. In contrast, oxalic and oxamic acids were much more recalcitrant and persisted largely up to the end of electrolysis. This evidences the stability of Fe(III)–oxalate and Fe(III)–oxamate complexes under EF conditions, because they react very slowly with BDD(•OH) at the anode surface while are not destroyed by •OH in the bulk (Brillas et al., 2009; Garcia-Segura and Brillas, 2011). Fig. 6a also shows that after 360 min of treatment, the resulting solution still contained 35.0 and 5.7 mg L^{-1} of oxalic and oxamic acids, respectively, corresponding to 9.3 and 1.5 mg L^{-1} of TOC. The addition of these values agrees with 10.4 mg L^{-1} of TOC determined for the final electrolyzed solution at 50 mA (see Fig. 3a), indicating that it is mainly composed of such mixture of both acids.

A similar evolution for malonic and formic acids to that found in EF can be seen in Fig. 6b when the PEF process was applied to mineralize flumequine. This means that Fe(III)–malonate and Fe(III)–formate are destroyed by hydroxyl radicals in PEF as in the case of EF. In contrast, Fig. 6b evidences a very different behaviour for oxalic acid, which was less accumulated up to 28 mg L^{-1} as maximal at 90 min to further decrease progressively to practically disappear in 360 min due to the quick photodecarboxylation of Fe(III)–oxalate complexes via reaction (6). The same trend can be observed in Fig. 6b for oxamic acid, although in this case it became more persistent by the lower photolytic rate of Fe(III)–oxamate complexes (Garcia-Segura and Brillas, 2011). At the end of electrolysis, the remaining solution contained 1.8 mg L^{-1} of oxalic acid and 3.2 mg L^{-1} oxamic acid, giving 1.3 mg L^{-1} TOC, which only corresponds to about 50% of its organic charge of 2.5 mg L^{-1} TOC (see Fig. 3b). This indicates that in PEF the action of UVA light favours the generation of a small proportion of some unidentified recalcitrant organics that are neither attacked by hydroxyl radicals nor photodecomposed. Results of Fig. 3b suggest that the relative proportion of such by-products becomes more significant as the current rises up to 300 mA.

The higher oxidation power of PEF than EF to mineralize flumequine can then be primordially related to the photolytic ability of UVA irradiation to remove the complexes of Fe(III) with final carboxylic acids like oxalic and oxamic. However, the PEF process enhances the production of small amounts of other recalcitrant by-products that avoid that flumequine can be completely mineralized.

3.4. *Evolution of inorganic ions released*

The mineralization of flumequine by the EAOPs tested is accompanied by the formation of F^-, NO_3^- and NH_4^+ ions, which were quantified by ionic chromatography. Fig. 7a and b shows the complete release of the initial F contained in the drug (4.54 mg L^{-1}) as F^- ion in only 20–25 min of the EF and PEF treatments at 50 mA, respectively. Comparison with the kinetic results found for flumequine decay (see Fig. 4) allows concluding that the C–F bond of the drug is broken in the attack of hydroxyl radicals. On the other hand, Fig. 7a and b also evidences that in both processes, the initial N of

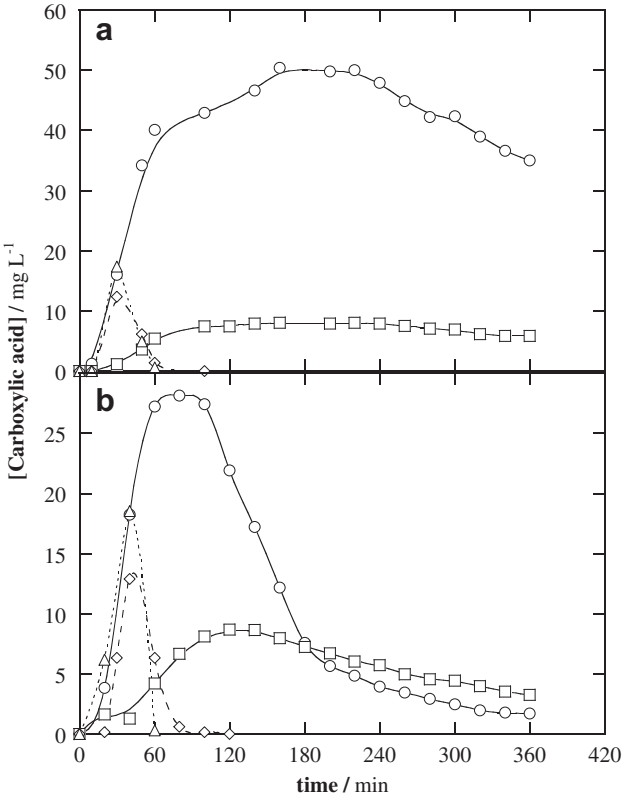

Fig. 6 – Evolution of the concentration of carboxylic acids generated during the (a) EF and (b) PEF degradations of 100 mL of 62 mg L^{-1} flumequine in 0.05 M Na_2SO_4 and 2.0 mM Fe^{2+} at pH 3.0, 50 mA and 35 °C. Acid: (○) oxalic, (□) oxamic, (◇) malonic and (△) formic.

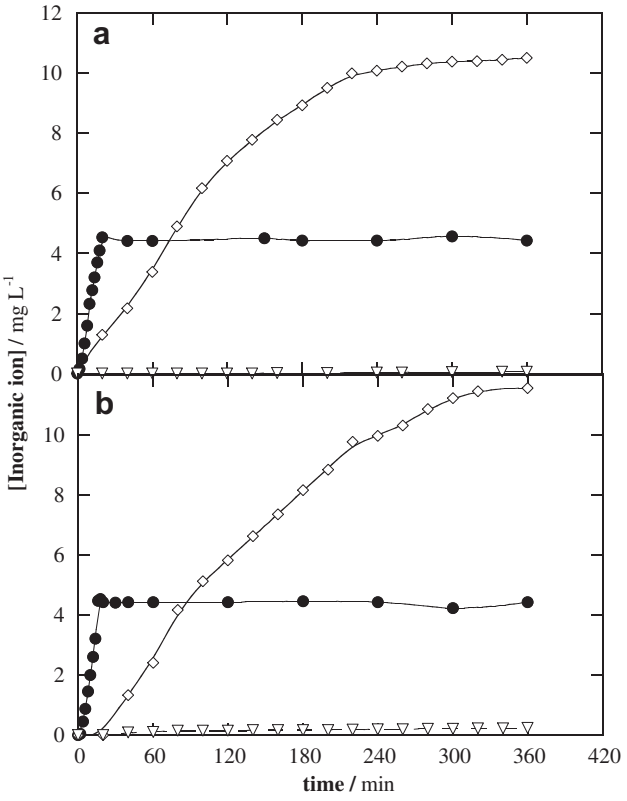

Fig. 7 – Time course of the concentration of inorganic ions released during the (a) EF and (b) PEF treatments of the solutions of Fig. 6. Ion: (●) F^-, (◇) NO_3^- and (▽) NH_4^+.

flumequine (3.35 mg L^{-1}) is converted into NO_3^- ion and in much lesser extent into NH_4^+ ion. A higher concentration of NO_3^- ion was accumulated in the final solution for PEF (11.55 mg L^{-1}) than for EF (10.50 mg L^{-1}) owing to the higher mineralization degree attained in the former process. This phenomenon was relatively more significant for the NH_4^+ ion, since it was more largely released in PEF (0.24 mg L^{-1}) than in EF (0.06 mg L^{-1}), suggesting that UVA light promotes the deamination process of intermediates during the degradation process.

To better analyze the evolution of N during the EF and PEF treatments of the drug, the TN of electrolyzed solutions was determined. As can be seen in Fig. 8a and b, no change in TN (3.35 mg L^{-1}) was found during both treatments indicating that all N is always present in the solution without losing of volatile *N*-compounds. A mass balance of this heteroatom was then made considering that the drug yields unidentified *N*-derivatives, oxamic acid and NO_3^- and NH_4^+ ions. At the end of EF (see Fig. 8a), the solution contained 0.91, 2.37 and 0.04 mg L^{-1} of N coming from the three latter species, respectively, whose addition of 3.32 mg L^{-1} matches with the initial N value of the drug. The same behaviour can be observed in Fig. 8b for the final solution of PEF with a contribution of 0.51, 2.61 and 0.18 mg L^{-1} of N from oxamic acid and NO_3^- and NH_4^+ ions, respectively. Taking this into account, a similar evolution of unidentified *N*-derivatives was found for both treatments, disappearing in about 210 min of electrolysis, as shown in Fig. 8a and b. This suggests that these by-products are mainly removed under the action of generated hydroxyl radicals, although the low participation of UVA light promotes slightly the deamination reactions, as stated above.

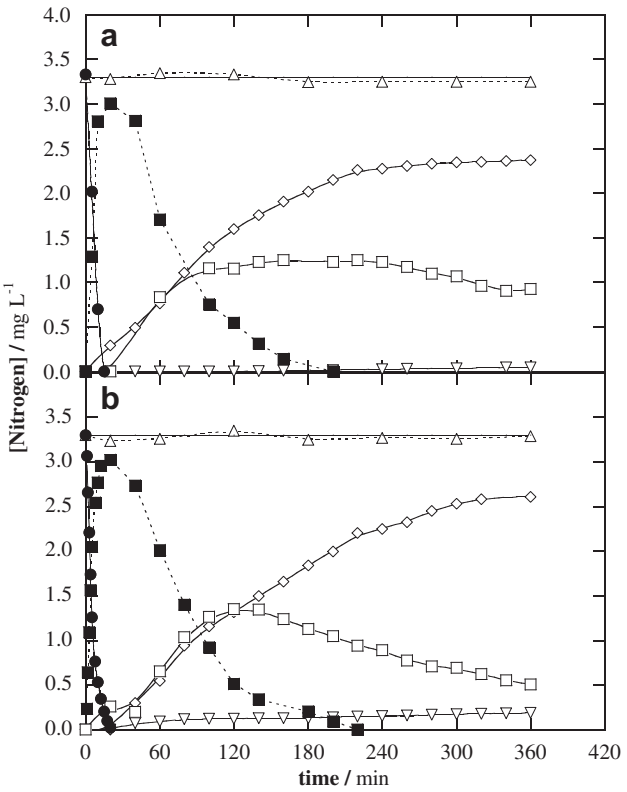

Fig. 8 – Evolution of nitrogen in solution during the (a) EF and (b) PEF experiments of Fig. 6. (—) Theoretical total nitrogen, (△) experimental TN and nitrogen present in: (●) flumequine, (◇) NO_3^- ion, (▽) NH_4^+ ion, (□) oxamic acid and (■) unidentified *N*-derivatives.

4. Conclusions

It has been demonstrated that the PEF process allowed an almost total mineralization with 94–96% TOC removal of a flumequine solution near to saturation at pH 3.0, whereas the EF process yielded a partial mineralization under comparable conditions. The Fe^{2+} ion added played a double role, since it formed an orange complex with the drug enhancing its solubility and it also reacted with electrogenerated H_2O_2 to form $^{\bullet}OH$ from Fenton reaction (2). A Fe^{2+} concentration of 2.0 mM was found optimal for the removal and mineralization of flumequine. An increase in current accelerated both EF and PEF degradations, but leading to lower efficiency due to the enhancement of the parasitic reactions of generated hydroxyl radicals. Comparative treatments using a real wastewater led to similar degradation degrees with a little influence of NOM, which was mainly oxidized by generated hydroxyl radicals. The kinetics for flumequine decay always followed a pseudo-first-order reaction with increasing rate constant as the current raised. The degradation process involved the formation of short-aliphatic carboxylic acids like malonic, formic, oxalic and oxamic acids. The complexes of Fe(III) with the two former acids were rapidly destroyed with hydroxyl radicals in both treatments. In contrast, Fe(III)–oxalate and Fe(III)–oxamate complexes were very persistent under EF conditions, being the main remaining species in the final treated solution. Their quicker photodecomposition in PEF explains its higher oxidation power, although a small proportion of very recalcitrant unidentified by-products promoted by UVA irradiation was formed, thus avoiding the total mineralization of flumequine. The initial F of the drug was rapidly and completely converted into F^- ion. Its N content was finally split into oxamic acid, NO_3^- ion and in a much lesser extent NH_4^+ ion, without release of volatile *N*-compounds, as confirmed from TN measurements.

Acknowledgements

The authors acknowledge the financial support from MICINN (Ministerio de Ciencia e Innovación, Spain) under the project CTQ2010-16164/BQU, co-financed with FEDER funds. S. Garcia-Segura thanks the grant awarded from MEC (Ministerio de Educación y Ciencia, Spain) to do this work.

REFERENCES

Almeida, L.C., Garcia-Segura, S., Bocchi, N., Brillas, E., 2011. Solar photoelectro-Fenton degradation of paracetamol using a flow plant with a Pt/air-diffusion cell coupled with a compound

parabolic collector: process optimization by response surface methodology. Applied Catalysis B: Environmental 103, 21–30.
Andreozzi, R., Marotta, R., Nicklas, P., 2003. Pharmaceuticals in STP effluents and their solar photodegradation in aquatic environment. Chemosphere 50 (10), 1319–1330.
Balci, B., Oturan, N., Cherrier, R., Oturan, M.A., 2009. Degradation of atrazine in aqueous medium by electrocatalytically generated hydroxyl radicals. A kinetic and mechanistic study. Water Research 43 (7), 1924–1934.
Bound, J.P., Voulvoulis, N., 2005. Household disposal of pharmaceuticals as a pathway for aquatic contamination in the United Kingdom. Environmental Health Perspectives 113 (12), 1705–1711.
Brillas, E., Baños, M.A., Camps, S., Arias, C., Cabot, P.L., Garrido, J.A., Rodríguez, R.M., 2004. Catalytic effect of Fe^{2+}, Cu^{2+} and UVA light on the electrochemical degradation of nitrobenzene using an oxygen-diffusion cathode. New Journal of Chemistry 28 (2), 314–322.
Brillas, E., Sirés, I., Oturan, M.A., 2009. Electro-Fenton process and related electrochemical technologies based on Fenton's reaction chemistry. Chemical Reviews 109 (12), 6570–6631.
Brillas, E., Garcia-Segura, S., Skoumal, M., Arias, C., 2010. Electrochemical incineration of diclofenac in neutral aqueous medium by anodic oxidation using Pt and boron-doped diamond anodes. Chemosphere 79 (6), 605–612.
Burridge, L., Weis, J.S., Cabello, F., Pizarro, J., Bostick, K., 2010. Chemical use in salmon aquaculture: a review of current practices and possible environmental effects. Aquaculture 306 (1–4), 7–23.
Cañizares, P., Beteta, A., Sáez, C., Rodríguez, L., Rodrigo, M.A., 2008. Use of electrochemical technology to increase the quality of the effluents of bio-oxidation processes. A case studied. Chemosphere 72 (7), 1080–1085.
Crane, M., Watts, C., Boucard, T., 2006. Chronic aquatic environmental risks from exposure to human pharmaceuticals. Science of the Total Environment 367 (1), 23–41.
Garcia-Segura, S., Brillas, E., 2011. Mineralization of the recalcitrant oxalic and oxamic acids by electrochemical advanced oxidation processes using a boron-doped diamond anode. Water Research 45 (9), 2975–2984.
Guinea, E., Garrido, J.A., Rodríguez, R.M., Cabot, P.L., Arias, C., Centellas, F., Brillas, E., 2010. Degradation of the fluoroquinolone enrofloxacin by electrochemical advanced oxidation processes based on hydrogen peroxide electrogeneration. Electrochimica Acta 55 (6), 2101–2105.
Halling-Sørensen, B., 2000. Algal toxicity of antibacterial agents used in intensive farming. Chemosphere 40 (7), 731–739.
Hamza, M., Abdelhedi, R., Brillas, E., Sirés, I., 2009. Comparative electrochemical degradation of the triphenylmethane dye methyl violet with boron-doped diamond and Pt anodes. Journal of Electroanalytical Chemistry 627 (1–2), 41–50.
Homem, V., Santos, L., 2011. Degradation and removal methods of antibiotics from aqueous matrices – a review. Journal of Environmental Management 92 (10), 2304–2347.
Jarnheimer, P., Ottoson, J., Lindberg, R., Stenström, T., Johansson, M., Tysklind, M., Winner, M., Olsen, B., 2004. Fluoroquinolone antibiotics in a hospital sewage line; occurrence, distribution and impact on bacterial resistance. Scandinavian Journal of Infectious Diseases 36 (10), 725–755.
Karthikeyan, K.G., Meyer, M.T., 2006. Occurrence of antibiotics in wastewater treatment facilities in Wisconsin, USA. Science of the Total Environment 361 (1–3), 196–207.
Khataee, A.R., Zarei, M., Asl, S.K., 2010. Photocatalytic treatment of a dye solution using immobilized TiO_2 nanoparticles combined with photoelectro-Fenton process: optimization of operational parameters. Journal of Electroanalytical Chemistry 648 (2), 143–150.
Khataee, A.R., Safarpour, M., Zarei, M., Aber, S., 2011. Electrochemical generation of H_2O_2 using immobilized carbon nanotubes on graphite electrode fed with air: investigation of operational parameters. Journal of Electroanalytical Chemistry 659 (1), 63–68.
Kim, I., Yamashita, N., Tanaka, H., 2009. Photodegradation of pharmaceuticals and personal care products during UV and UV/H_2O_2 treatments. Chemosphere 77 (4), 518–525.
Klamerth, N., Malato, S., Maldonado, M.I., Agüera, A., Fernández-Alba, A., 2011. Modified photo-Fenton for degradation of emerging contaminants in municipal wastewater effluents. Catalysis Today 161 (1), 241–246.
Kümmerer, K., 2009. Antibiotics in the aquatic environment – a review – Part I. Chemosphere 75 (4), 417–434.
Li, H., Helm, P.A., Metcalfe, C.D., 2010. Sampling in the Great Lakes for pharmaceuticals, personal care products and endocrine-disrupting substances using the passive polar organic chemical integrative sampler. Environmental Toxicology & Chemistry 29 (4), 751–762.
Lin, C.E., Deng, Y.J., Liao, W.S., Sun, S.W., Lin, W.Y., Chen, C.C., 2004. Electrophoretic behavior and pK_a determination of quinolones with a piperazinyl substituent by capillary zone electrophoresis. Journal of Chromatography A 1051 (1–2), 283–290.
Marselli, B., García-Gómez, J., Michaud, P.A., Rodrigo, M.A., Comninellis, Ch, 2003. Electrogeneration of hydroxyl radicals on boron-doped diamond electrodes. Journal of the Electrochemical Society 150 (3), D79–D83.
McClellan, K., Halden, R.U., 2010. Occurrence and loss over three years of 72 pharmaceuticals and personal care products from biosolids–soil mixtures in outdoor mesocosms. Water Research 44 (20), 6011–6020.
Migliore, L., Civitareale, C., Brambilla, G., Di Delupis, G.D., 1997. Toxicity of several important agricultural antibiotics to Artemia. Water Research 37 (7), 1801–1806.
Miranda-García, N., Suárez, S., Sánchez, B., Coronado, J.M., Malato, S., Maldonado, M.I., 2011. Photocatalytic degradation of emerging contaminants in municipal wastewater treatment plant effluents using immobilized TiO_2 in a solar pilot plant. Applied Catalysis B: Environmental 103 (3–4), 294–301.
Muñoz, I., Martínez-Bueno, M.J., Agüera, A., Fernández-Alba, A.R., 2010. Environmental and human health risk assessment of organic micro-pollutants occurring in a Spanish marine fish farm. Environmental Pollution 158 (5), 1809–1816.
Naviner, M., Gordon, L., Giraud, E., Denis, M., Mangion, C., Le Bris, H., Ganière, J.P., 2011. Antimicrobial resistance of *Aeromonas* spp. isolated from the growth pond to the commercial product in a rainbow trout farm following a flumequine treatment. Aquaculture 315 (3–4), 236–241.
Nieto, J., Freer, J., Contreras, D., Candal, R.J., Sileo, E.E., Mansilla, H.D., 2008. Photocatalyzed degradation of flumequine by doped TiO_2 and simulated solar light. Journal of Hazardous Materials 155 (1–2), 45–50.
Oturan, M.A., Pimentel, M., Oturan, N., Sirés, I., 2008. Reaction sequence for the mineralization of the short-chain carboxylic acids usually formed upon cleavage of aromatics during electrochemical Fenton treatment. Electrochimica Acta 54 (2), 173–182.
Oturan, N., Zhou, M., Oturan, M.A., 2010. Metomyl degradation by electro-Fenton and electro-Fenton-like processes: a kinetics study of the effect of the nature and concentration of some transition metal ions as catalyst. Journal of Physical Chemistry A 114 (39), 10605–10611.
Özcan, A., Oturan, N., Sahin, Y., Oturan, M.A., 2010. Electro-Fenton treatment of aqueous clopyralid solutions. International Journal of Environmental Analytical Chemistry 90 (3–6), 478–486.

Panizza, M., Cerisola, G., 2009. Direct and mediated anodic oxidation of organic pollutants. Chemical Reviews 109 (12), 6541–6569.

Pomati, F., Orlandi, C., Clerici, M., Luciani, F., Zuccato, E., 2008. Effects and interactions in an environmentally relevant mixture of pharmaceuticals. Toxicological Sciences 102 (1), 129–137.

Postigo, C., López de Alda, M.J., Barceló, D., 2009. Drugs of abuse and their metabolites in the Ebro River basin: occurrence in sewage and surface water, sewage treatment plants removal efficiency, and collective drug usage estimation. Environment International 36 (1), 75–84.

Pouliquen, H., Delépée, R., Larhantec-Verdier, M., Morvan, M.L., Le Bris, H., 2007. Comparative hydrolysis and photolysis of four antibacterial agents (oxytetracycline oxolinic acid, flumequine and florfenicol) in deionised water, freshwater and seawater under abiotic conditions. Aquaculture 262 (1), 23–28.

Rosal, R., Rodríguez, A., Perdigón-Melón, J.A., Mezcua, M., Hernando, M.D., León, P., García-Calvo, E., Agüera, A., Fernández-Alba, A.R., 2008. Removal of pharmaceuticals and kinetics of mineralization by O_3/H_2O_2 in a biotreated municipal wastewater. Water Research 42 (14), 3719–3728.

Rozas, O., Contreras, D., Mondaca, A., Perez-Moya, M., Mansilla, H.D., 2010. Experimental design of Fenton and photo-Fenton reactions for the treatment of ampicillin solutions. Journal of Hazardous Materials 177 (1–3), 1025–1030.

Serra, A., Domènech, X., Arias, C., Brillas, E., Peral, J., 2009. Oxidation of α-methylphenylglycine under Fenton and electro-Fenton conditions in the dark and in the presence of solar light. Applied Catalysis B: Environmental 89 (1–2), 12–21.

Sirés, I., Cabot, P.L., Centellas, F., Garrido, J.A., Rodríguez, R.M., Arias, C., Brillas, E., 2006. Electrochemical degradation of clofibric acid in water by anodic oxidation. Comparative study with platinum and boron-doped diamond electrodes. Electrochimica Acta 52 (1), 75–85.

Sirés, I., Centellas, F., Garrido, J.A., Rodríguez, R.M., Arias, C., Cabot, P.L., Brillas, E., 2007. Mineralization of clofibric acid by electrochemical advanced oxidation processes using a boron-doped diamond anode and Fe^{2+} and UVA light as catalysts. Applied Catalysis B: Environmental 72 (3–4), 373–381.

Sirés, I., Oturan, N., Oturan, M.A., 2010. Electrochemical degradation of β-blockers. Studies on single and multicomponent synthetic aqueous solutions. Water Research 44 (10), 3109–3120.

Skoumal, M., Cabot, P.L., Centellas, F., Arias, C., Rodríguez, R.M., Garrido, J.A., Brillas, E., 2006. Mineralization of paracetamol by ozonation catalyzed with Fe^{2+}, Cu^{2+} and UVA light. Applied Catalysis B: Environmental 66 (3–4), 228–240.

Skoumal, M., Arias, C., Cabot, P.L., Centellas, F., Garrido, J.A., Rodríguez, R.M., Brillas, E., 2008. Mineralization of the biocide chloroxylenol by electrochemical advanced oxidation processes. Chemosphere 71 (9), 1718–1729.

Skoumal, M., Rodríguez, R.M., Cabot, P.L., Centellas, F., Garrido, J.A., Arias, C., Brillas, E., 2009. Electro-Fenton, UVA photoelectro-Fenton and solar photoelectro-Fenton degradation of the drug ibuprofen in acid aqueous medium using platinum and boron-doped diamond. Electrochimica Acta 54 (7), 2077–2085.

Song, S., Liu, Z., He, Z., Li, Y., Chen, J., Li, C., 2009. Degradation of the biocide 4-chloro-3,5-dimethylphenol in aqueous medium with ozone in combination with ultraviolet irradiation: operating conditions influence and mechanism. Chemosphere 77 (8), 1043–1051.

Tamtam, F., Mercier, F., Le Bot, B., Eurin, J., Dinh, Q.T., Clément, M., Chevreuil, M., 2008. Occurrence and fate of antibiotics in the Seine River in various hydrological conditions. Science of the Total Environment 393 (1), 84–95.

Vieno, N., Tuhkanen, T., Kronberg, L., 2007. Elimination of pharmaceuticals in sewage treatment plants in Finland. Water Research 41 (5), 1001–1012.

Wang, P., He, Y.L., Huang, C.H., 2010. Oxidation of fluoroquinolone antibiotics and structurally related amines by chlorine dioxide: reaction kinetics, product and pathway evaluation. Water Research 44 (20), 5989–5998.

Zarei, M., Khataee, A.R., Ordijhani-Sevedlar, R., Fathinia, M., 2010. Photoelectro-Fenton combined with photocatalytic process for degradation of an azo dye using supported TiO_2 nanoparticles and carbon nanotube cathode: neural network modeling. Electrochimica Acta 55 (24), 7259–7265.

PAPER 2

Mineralization of the antibiotic chloramphenicol by solar photoelectro-Fenton: From stirred tank reactor to solar pre-pilot plant

Applied Catalysis B: Environmental 144 (2014) 588–598

Contents lists available at ScienceDirect

Applied Catalysis B: Environmental

journal homepage: www.elsevier.com/locate/apcatb

Mineralization of the antibiotic chloramphenicol by solar photoelectro-Fenton. From stirred tank reactor to solar pre-pilot plant

Sergi Garcia-Segura[a], Eliane Bezerra Cavalcanti[b], Enric Brillas[a,*]

[a] Laboratori d'Electroquímica dels Materials i del Medi Ambient, Departament de Química Física, Facultat de Química, Universitat de Barcelona, Martí i Franquès 1-11, 08028 Barcelona, Spain
[b] Instituto de Tecnologia e Pesquisa/ITP, Universidade Tiradentes/UNIT, Av. Murilo Dantas 300, CEP 49032-490 Aracaju, SE, Brazil

ARTICLE INFO

Article history:
Received 2 July 2013
Received in revised form 27 July 2013
Accepted 30 July 2013
Available online xxx

Keywords:
Antibiotics
Oxidation products
Solar photoelectro-Fenton
Solar photolysis
Water treatment

ABSTRACT

Chloramphenicol is a widely used broad-spectrum antibiotic, which has been detected as emerging pollutant in natural waters. The mineralization of this drug in a synthetic sulfate solution of pH 3.0 has been studied by anodic oxidation with electrogenerated H_2O_2 (AO-H_2O_2), electro-Fenton (EF), UVA photoelectro-Fenton (PEF) and solar photoelectro-Fenton (SPEF). Comparative electrolyses carried out with 100 mL stirred tank reactors equipped with a boron-doped diamond (BDD) or Pt anode and an air-diffusion cathode at constant current density showed the superiority of the processes with BDD because of the higher oxidation ability of •OH formed from water oxidation at the BDD surface. Total mineralization was rapidly reached for the most potent treatment of SPEF with BDD due to the additional oxidation by •OH produced from Fenton's reaction between added Fe^{2+} (0.5 mM) and H_2O_2 generated at the cathode, together the synergistic photolytic action of sunlight, much more intense than the 6 W UVA lamp used in PEF. Chloramphenicol decay always followed a pseudo-first-order kinetics. The influence of current density and substrate concentration on SPEF with BDD was examined. Nine aromatic products, thirteen hydroxylated derivatives and seven carboxylic acids were identified by different chromatographic techniques. While the initial Cl of the drug was released as chloride ion, its initial N was lost as nitrate ion and, in smaller proportion, as ammonium ion. From the detected products, a general reaction pathway for chloramphenicol mineralization is proposed. The viability of SPEF was confirmed in a 10 L pre-pilot plant with a Pt/air-diffusion filter-press reactor coupled to a solar CPCs photoreactor. After 180 min of electrolysis at 100 mA cm^{-2}, a 245 mg L^{-1} chloramphenicol solution in 0.05 M Na_2SO_4 with 0.5 mM Fe^{2+} at pH 3.0 underwent 89% mineralization with 36% current efficiency and 30.8 kWh m^{-3} energy cost.

1. Introduction

Recently, there exists an increasing attention on pharmaceuticals as potential bioactive chemicals in the aquatic environment. Many pharmaceutical drugs have been detected at relatively low contents up to μg L^{-1} level in soils, surface waters, ground waters and even drinking waters [1–3]. Antibiotics are the most commonly drugs found in the aquatic environment because their antimicrobial nature prevents effective removal in sewage treatment plants [4–6]. The occurrence and fate of antibiotics as well as their metabolites in water streams is recognized as one of the emerging issues in environmental chemistry [1,3,7,8]. Several authors reported that these pollutants can produce multi-resistant strains of microorganisms, can affect the endocrine systems of fishes and invertebrates, and are toxic on small invertebrates and algae [9–12]. Powerful oxidation treatments then need to be developed for the removal of antibiotics from waters and wastewaters to avoid their potential adverse health effects on humans and animals.

Several electrochemical advanced oxidation processes (EAOPs) are being currently developed for water prevention [12–17]. EAOPs are based on the *in situ* generation of hydroxyl radical (•OH), which is the second strongest oxidant known after fluorine since it has so high standard reduction potential (E°(•OH/H_2O) = 2.80 V/SHE) that can non-selectively react with organic pollutants up to their mineralization to CO_2, water and inorganic ions. The most potent EAOPs use both, heterogeneous and homogeneous •OH formed at the anode and in the solution bulk, respectively, as oxidizing agents. Mediated electro-oxidation with homogeneous •OH is usually achieved by decomposition of H_2O_2 generated from the two-electron cathodic reduction of injected O_2 [12,16]:

$$O_2 + 2H^+ + 2e^- \rightarrow H_2O_2 \quad (1)$$

* Corresponding author. Tel.: +34 93 4021223; fax: +34 93 4021231.
E-mail address: brillas@ub.edu (E. Brillas).

0926-3373/$ – see front matter © 2013 Elsevier B.V. All rights reserved.
http://dx.doi.org/10.1016/j.apcatb.2013.07.071

Good efficiencies for H_2O_2 generation from reaction (1) have been reported for carbonaceous cathodes such as carbon sponge [18], carbon nanotubes-polytetrafluoroethylene (PTFE) [19,20], carbon-felt [18,21–25], graphite-felt [26], boron-doped diamond (BDD) [27] and carbon-PTFE gas (O_2 or air) diffusion electrodes [21,22,28–32].

In our laboratory, we have checked the good oxidation ability of EAOPs like anodic oxidation with electrogenerated H_2O_2 (AO-H_2O_2) [28,32], electro-Fenton (EF) [21,22,28–31], UVA photoelectro-Fenton (PEF) [28–30] and solar photoelectro-Fenton (SPEF) [29,31] to destroy several antibiotics and other drugs in acidic solutions using small stirred tank reactors equipped with either a BDD or Pt anode and a gas-diffusion cathode. Our interest is to show that these EAOPs can be useful for the treatment of wastewaters contaminated with antibiotics. To do this and in view of the large variety of these drugs, it is necessary to know the degradative characteristics of more compounds. In this way, the scaling-up of EAOPs to a pre-pilot plant also needs to be assessed in order to demonstrate their possible viability at industrial level.

This paper aims to investigate the mineralization of the antibiotic chloramphenicol (2,2-dicloro-*N*-[1,3-dihydroxy-1-(4-nitrophenyl)propan-2-yl] acetamide) in acidic medium by AO-H_2O_2, EF, PEF and SPEF in order to clarify: (i) the role of generated •OH in the degradative processes using stirred Pt/air-diffusion and BDD/air-diffusion tank reactors of 100 mL under comparable conditions, (ii) the photolytic action of UVA and solar radiation in these systems, (iii) the effect of experimental parameters on substrate decay and mineralization rate, (iv) the products formed and their evolution to propose a general reaction pathway for chloramphenicol mineralization and (v) the viability of SPEF in a 10 L pre-pilot plant with a Pt/air-diffusion filter-press reactor coupled to a solar compound parabolic collectors (CPCs) photoreactor. Note that chloramphenicol is a broad-spectrum antibiotic, which is effective against a wide variety of Gram-positive and Gram-negative bacteria, including most anaerobic organisms. While in the developed countries it is currently prescribed only to treat bacterial conjunctivitis, chloramphenicol is widely used in developing countries. For this reason, it has been detected worldwide in ground waters, lakes, rivers and influents and effluents of sewage treatment plants [3,6–8,33–36]. However, less is known about the degradation of chloramphenicol from waters and its oxidation products formed from •OH attack have not been identified yet. It has been reported that it can be removed by UVC radiation [37], TiO_2/UV photocatalysis [38] and ozonation [39]. The electrochemical reduction of its nitro group to hydroxylamine or amine at a graphite cathode has also been described by means of cyclic voltammetry [40].

2. Experimental

2.1. Chemicals

Chloramphenicol (98% purity) was of reagent grade from Sigma–Aldrich. Carboxylic acids were of reagent grade from Panreac and Avocado. Anhydrous sodium sulfate and heptahydrated ferrous sulfate were of analytical grade from Fluka. Solutions treated in the stirred tank reactor were prepared with ultrapure water obtained from a Millipore Milli-Q system (resistivity > 18 MΩ cm at 25 °C). Solutions of 10 L to be degraded in the solar pre-pilot plant were prepared with deionized water. All solutions were adjusted to pH 3.0 with analytical grade sulfuric acid purchased from Merck. Other chemicals employed were of LC–MS, HPLC or analytical grade from Merck, Panreac and Sigma–Aldrich.

2.2. Electrochemical and photoelectrochemical systems

Experiments with 100 mL solutions were conducted in an undivided and cylindrical stirred tank reactor, with a double jacket in which external water circulated to maintain the solution temperature at 35 °C. The anode was either a BDD thin film electrode provided by Adamant Technologies or a Pt sheet of 99.99% purity supplied by SEMPSA. The cathode was a carbon-PTFE air-diffusion electrode purchased from E-TEK. The preparation of this cathode was described elsewhere [41] and was fed with air pumped at 300 mL min^{-1} for H_2O_2 generation from reaction (1). The area of both electrodes was 3 cm^2 and the interelectrode gap was ca. 1 cm. To remove the impurities of the BDD surface and activate the air-diffusion cathode prior use, they were polarized in 0.05 M Na_2SO_4 at 100 mA cm^{-2} for 60 min. All trials were carried out under vigorous stirring with a magnetic bar at 800 rpm to ensure homogenization and the transport of reactants toward/from the electrodes. For the PEF assays, a Philips 6-W black light blue tube was placed at 7 cm above the solution. This lamp emitted UVA light between 320 and 400 nm with λ_{max} = 360 nm, yielding a photoionization energy of 5 W m^{-2} as detected with a Kipp & Zonen CUV 5 global UV radiometer. In the SPEF assays, the tank reactor was directly exposed to solar radiation with a mirror placed at its bottom to better collect the sun rays.

A scheme of the solar pre-pilot plant operating in batch circulation mode was presented elsewhere [42]. For each EF or SPEF trial, the solution was introduced in the reservoir and continuously recirculated by a peristaltic pump at a flow rate of 200 L h^{-1} adjusted by a rotameter. The temperature was maintained at 35 °C by two heat exchangers. The electrolytic cell was an undivided filter-press reactor equipped with a Pt sheet anode from SEMPSA and a carbon-PTFE air-diffusion cathode from E-TEK. A PVC liquid compartment with a central window of 9.5 cm × 9.5 cm (90.2 cm^2) was used to contact the effluent with the outer faces of both electrodes, separated 1.2 cm. The inner face of the cathode was pressed to a Ni mesh as electrical connector in contact with a PVC gas chamber where circulated compressed air at a flow rate of 4.5 L min^{-1} regulated with a back-pressure gauge. The solar CPCs photoreactor with an area of 0.4 m^2 and concentration factor of 1 was composed of twelve borosilicate-glass tubes of 50.5 cm length × 1.82 cm inner diameter (irradiated volume 1.57 L), with connecting tubing and valves mounted in an aluminum frame on a platform tilted 41° to better collect the direct sun rays in our laboratory of Barcelona (latitude: 41°21′N, longitude: 2°10′E). In EF, the solar CPCs photoreactor was coated with a black plastic.

All solar trials were made for 240 min as maximal in sunny and clear days during summer 2012. The average solar UV radiation intensity (between 300 and 400 nm) was 30–32 W m^{-2}, as measured with a Kipp & Zonen CUV 5 global UV radiometer.

2.3. Apparatus and analytical procedures

The solution pH was measured with a Crison GLP 22 pH-meter. Galvanostatic electrolyses were performed with an Amel 2051 potentiostat–galvanostat for the tank reactor experiences and a Grelco GDL3020 power supply for the assays with the solar pre-pilot plant. Aliquots of 1 mL were withdrawn from electrolyzed solutions and filtered with 0.45 μm PTFE filters from Whatman before analysis. The mineralization of chloramphenicol solutions was monitored from their dissolved organic carbon (DOC) abatement, determined on a Shimadzu TOC-VCSN analyzer. Reproducible DOC values with an accuracy of ±1% were obtained by injecting 50 μL aliquots to the analyzer. Total nitrogen (TN) was determined with a Shimadzu TNM-1 unit coupled with the TOC analyzer.

The chloramphenicol decay was followed by reversed-phase HPLC using a Waters 600 LC fitted with a Spherisorb ODS2 5 μm (150 mm × 4.6 mm) column at 35 °C and coupled with a Waters 996 photodiode array detector selected at λ = 278.2 nm. Carboxylic acids were detected by ion-exclusion HPLC using the above LC fitted with a Bio-Rad Aminex HPX 87H (300 mm × 7.8 mm) column at 35 °C and the photodiode array detector set at λ = 210 nm. In the HPLC measurements, 20 μL aliquots were injected into the chromatograph and the mobile phase was either a 20:80 (v/v) acetonitrile/phosphate buffer (pH = 3.5) mixture at 0.4 mL min^{-1} for reversed-phase HPLC or 4 mM H_2SO_4 at 0.6 mL min^{-1} for ion-exclusion HPLC. The inorganic ions were quantified by ion chromatography using a Shimadzu 10 Avp HPLC coupled with a Shimadzu CDD 10 Avp conductivity detector. The NH_4^+ content was obtained with a Shodex IC YK-421 (125 mm × 4.6 mm) cation column at 40 °C, whereas the NO_3^- and Cl^- contents were determined with a Shim-Pack IC-A1S (100 mm × 4.6 mm) anion column at 40 °C. These analyses were made by injecting 25 μL aliquots and using mobile phases composed of a 5.0 mM tartaric acid, 1.0 mM dipicolinic acid, 24.2 mM boric acid and 1.5 mM crown ether solution at 0.8 mL min^{-1} for NH_4^+ and a 2.4 mM tris(hydroxymethyl)aminomethane and 2.5 mM phthalic acid solution of pH 4.0 at 1.5 mL min^{-1} for NO_3^- and Cl^-.

Products formed after 5–20 min of EF treatment of a 245 mg L^{-1} chloramphenicol solution in a BDD/air-diffusion tank reactor at 33.3 mA cm^{-2} were identified by LC–MS using a Shimadzu SIL-20AC LC coupled to a Shimadzu LCMS-2020 MS. The LC was fitted with a Teknokroma Mediterranean Sea C-18 3 μm (15 mm × 0.46 mm) column at 30 °C. The MS operated in the negative and positive modes with electrospray source ionization (ESI), by applying an interface voltage of −4.5 and 4.5 kV, respectively, and 60 V Q-array RF voltage. The DL temperature was 250 °C and pure N_2 was used as nebulising and dryer gas. Mass spectra were collected in the *m*/*z* range 50–420 using total ion current (TIC) acquisition. For these analyses, 15 μL aliquots were introduced into the LC, previously filtered with a Millipore filter of 0.22 μm, and the mobile phase was a 75:25 (v/v) acetonitrile/water (5.0 mM ammonium acetate) mixture at 0.2 mL min^{-1}.

3. Results and discussion

3.1. Comparative mineralization of chloramphenicol by EAOPs in a stirred tank reactor

The relative oxidation ability of AO-H_2O_2, EF, PEF and SPEF to destroy chloramphenicol was assessed by electrolyzing 100 mL of a synthetic solution with 245 mg L^{-1} drug (100 mg L^{-1} of DOC) and 0.05 M Na_2SO_4 at pH 3.0 using stirred Pt/air-diffusion and BDD/air-diffusion tank reactors at 33.3 mA cm^{-2} and 35 °C. The pH of 3.0 was chosen because it was found optimal for the treatment of other aromatics by these EAOPs [12,28–31] and treatments were made at 35 °C since this is the maximum temperature allowed in the open tank reactor without significant water evaporation from the solution during prolonged electrolysis [41]. For EF, PEF and SPEF, 0.5 mM Fe^{2+} was also added to the solution, which is the best catalyst concentration found for these processes under the conditions tested [28–31]. The chloramphenicol concentration checked was much higher than the usually detected in wastewaters, simply to better evaluate its mineralization behavior and identify its degradation products, as will be discussed below. In all these trials, the solution pH remained practically unchanged and decayed to values 2.7–2.8 after 360 min of the longer treatments, probably due to the formation of acidic products like short-chain carboxylic acids [12,16]. The cell voltage for BDD (17.0 V) was much higher than for Pt (8.3 V).

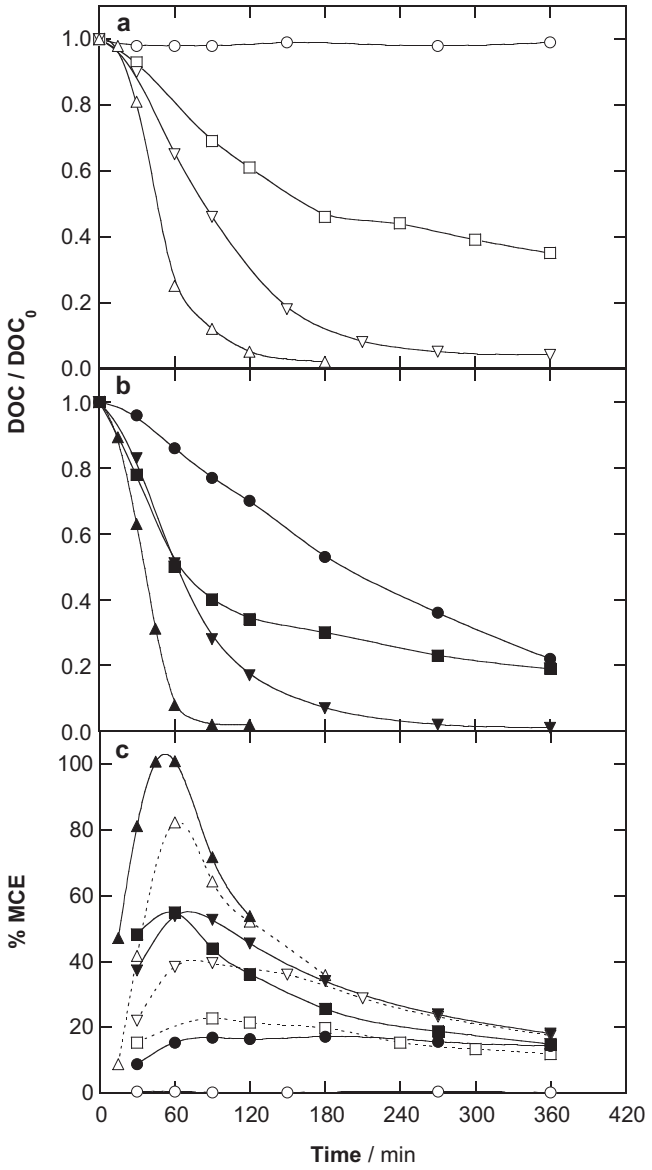

Fig. 1. Normalized DOC abatement with electrolysis time for the (○, ●) AO-H_2O_2, (□, ■) EF, (▽, ▼) PEF with a 6 W UVA light and (△, ▲) SPEF treatment of 100 mL of 245 mg L^{-1} chloramphenicol in 0.05 M Na_2SO_4 at pH 3.0, 33.3 mA cm^{-2} and 35 °C. In the three latter methods, the solution also contained 0.5 mM Fe^{2+}. (a) Pt/air-diffusion and (b) BDD/air-diffusion tank reactor. Plot (c) presents the mineralization current efficiency for the trials.

Fig. 1a and b depicts the change of normalized DOC for the above trials. For each EAOP, the chloramphenicol solution was more rapidly mineralized using a BDD than a Pt anode. In both systems, the relative oxidation ability of processes rose following the sequence AO-H_2O_2 < EF < PEF < SPEF. The lowest mineralization was achieved for AO-H_2O_2 because organics can only be slowly degraded by physisorbed Pt(•OH) or BDD(•OH) radicals formed from water oxidation at the Pt or BDD anode surface by reactions (2) and (3), respectively [15,28]:

$$Pt + H_2O \rightarrow Pt(^{\bullet}OH) + H^+ + e^- \quad (2)$$

$$BDD + H_2O \rightarrow BDD(^{\bullet}OH) + H^+ + e^- \quad (3)$$

The expected higher oxidation ability of BDD(•OH) than Pt(•OH) [15] then explains that the solution became more largely mineralized with a BDD anode. In fact, DOC was not practically removed

in the Pt/air-diffusion tank reactor (see Fig. 1a), whereas it was reduced by 78% at 360 min in the BDD/air-diffusion one (see Fig. 1b).

The mineralization rate of chloramphenicol increased in EF owe to the additional oxidative action of large amounts of •OH produced in the bulk from Fenton's reaction (4) between added Fe^{2+} and electrogenerated H_2O_2 [12,16,23,29]:

$$Fe^{2+} + H_2O_2 \rightarrow Fe^{3+} + {}^{\bullet}OH + OH^- \quad (4)$$

This reaction is catalytic and can be continuously propagated mainly from Fe^{3+} reduction to Fe^{2+} at the cathode. The fast reaction of organics with •OH can be confirmed in Fig. 1a, showing that DOC decayed up to 65% at the end of EF with Pt. The same behavior can be seen in Fig. 1b for EF with BDD, although in this case 81% of DOC was finally removed, a value very close to that of AO-H_2O_2 treatment. This can be related to the formation of Fe(III)-carboxylate complexes that are hardly destroyed by BDD(•OH) and •OH [21,28–31].

The chloramphenicol mineralization was more largely accelerated under UVA radiation with a 6-W light in PEF. This synergistic action can be related to two phenomena: (i) the photolysis of $Fe(OH)^{2+}$, the pre-eminent Fe^{3+} species near pH 3, regenerating Fe^{2+} and producing more •OH from reaction (5) and (ii) the photodecarboxylation of some generated Fe(III)-carboxylate species according to the general reaction (6) [12,16].

$$Fe(OH)^{2+} + h\nu \rightarrow Fe^{2+} + {}^{\bullet}OH \quad (5)$$

$$Fe(OOCR)^{2+} + h\nu \rightarrow Fe^{2+} + CO_2 + R^{\bullet} \quad (6)$$

The quick photolysis of Fe(III)-carboxylate species can then justify the almost total mineralization (96% DOC decay) and total mineralization (99% DOC decay) found for PEF with Pt and BDD, respectively. Fig. 1a and b also shows that the use of SPEF is much more effective, attaining total mineralization (98% DOC abatement) at 180 and 120 min of electrolysis using the Pt/air-diffusion and BDD/air-diffusion tank reactors, respectively. The greater UVA intensity of sunlight (about 30 W m^{-2}) in SPEF than of the 6-W lamp (5 W m^{-2}) in PEF can justify the superiority of the former process. The highest oxidation ability of SPEF with BDD is then due to the quickest destruction of organics under the synergistic action of BDD(•OH), •OH and sunlight.

For the above trials, the corresponding mineralization current efficiency (MCE) at given electrolysis time (t, in h) was estimated by the following equation [29]:

$$MCE(\%) = \frac{nFV_s\,\Delta(DOC)_{exp}}{4.32 \times 10^7 mIt} 100 \quad (7)$$

where F is the Faraday constant (96487 C mol^{-1}), V_s is the solution volume (L), $\Delta(DOC)_{exp}$ is the experimental DOC decay (mg L^{-1}), 4.32×10^7 is a conversion factor to homogenize units (3600 s h^{-1} × 12,000 mg mol^{-1}), m is the number of carbon atoms of chloramphenicol (11 carbon atoms) and I is the applied current (A). The number n of electrons consumed per chloramphenicol molecule was taken as 54 from reaction (8) considering its mineralization to CO_2 with loss of NO_3^- and Cl^- as main primary inorganic ions, as discussed below.

$$C_{11}H_{12}N_2Cl_2O_5 + 23H_2O \rightarrow 11CO_2 + 2NO_3^- + 2Cl^- + 58H^+ + 54e^- \quad (8)$$

Fig. 1c highlights the rise in MCE of the EAOPs tested in each system according to their relative oxidation ability, as well as the greater efficiency for all processes with BDD compared with the corresponding treatments with Pt. As expected, SPEF with BDD led to the highest MCE, with a maximum value near 100% between 45 and 60 min of electrolysis, further diminishing to 53% at 120 min.

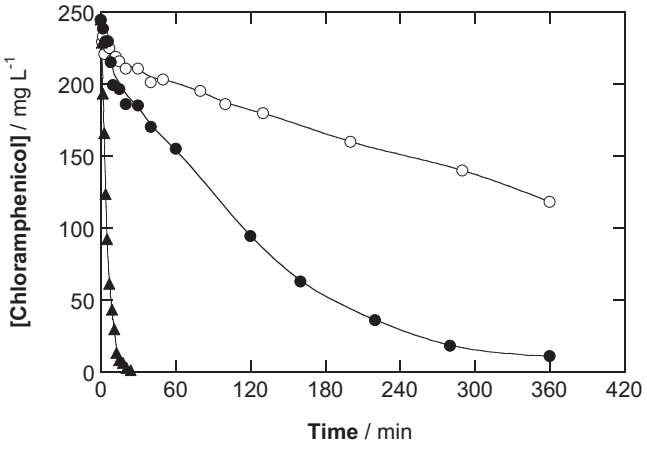

Fig. 2. Chloramphenicol concentration decay vs electrolysis time for the (○,●) AO-H_2O_2 and (▲) SPEF degradations under the conditions of Fig. 1 using a (○) Pt/air-diffusion or (●, ▲) BDD/air-diffusion tank reactor.

For most processes, maximum efficiency at short time, followed by its progressive loss with prolonging electrolysis, was also found. This decay in MCE can be accounted for by the presence of less organic matter as well as the gradual formation of more difficultly oxidizable products like short-chain carboxylic acids [12,15,16].

The role of Pt(•OH), BDD(•OH) and •OH was clarified by determining the kinetics of chloramphenicol decay in the above treatments by reversed-phase HPLC, where it displayed a well-defined peak with retention time (t_r) of 8.05 min. Blank experiments under direct UVA radiation without electrolysis corroborated that the drug was not directly photolyzed. Fig. 2 evidences a very slow removal of chloramphenicol concentration under the action of Pt(•OH), only passing from 245 to 118 mg L^{-1} in 360 min, whereas at the same time it was practically completely removed by BDD(•OH). This behavior confirms the much higher oxidation ability of BDD(•OH) in front of Pt(•OH) to destroy chloramphenicol and its oxidation products. Kinetic analysis of these concentration decays showed that they fit well with a pseudo-first-order reaction (data not shown), yielding an apparent rate constant (k_1) of 3.0×10^{-5} s^{-1} ($R^2 = 0.981$) for AO-H_2O_2 with Pt, which rose to 1.4×10^{-4} s^{-1} ($R^2 = 0.995$) for AO-H_2O_2 with BDD. In contrast, chloramphenicol was much more rapidly removed and with a quite similar rate operating with EF, PEF and SPEF, regardless of the anode used. In all these treatments, the drug disappeared in about 27 min, as exemplified in Fig. 2 for SPEF with BDD. The k_1 value obtained for the pseudo-first-order kinetics followed by this trial was 2.9×10^{-3} s^{-1} ($R^2 = 0.998$). All these findings demonstrate the preponderant action of •OH formed from Fenton's reaction (4) to oxidize not only the substrate, but also the aromatic species that are expected to be generated as its primary products. Besides, the similar decay kinetics determined for EF, PEF and SPEF indicates a low participation of photolytic reaction (5) to produce •OH in the two latter EAOPs. The fact that chloramphenicol is always removed following a pseudo-first-order kinetics suggests its reaction with a constant concentration of generated hydroxyl radicals in each treatment.

3.2. Effect of current density and chloramphenicol content on SPEF with BDD in a stirred tank reactor

The influence of key variable parameters such as current density (j) and substrate concentration on the SPEF process using a stirred BDD/air-diffusion tank reactor was examined from the DOC abatement of synthetic antibiotic solutions with 0.05 M Na_2SO_4 and 0.5 mM Fe^{2+} of pH 3.0. Fig. 3a shows the gradual quicker

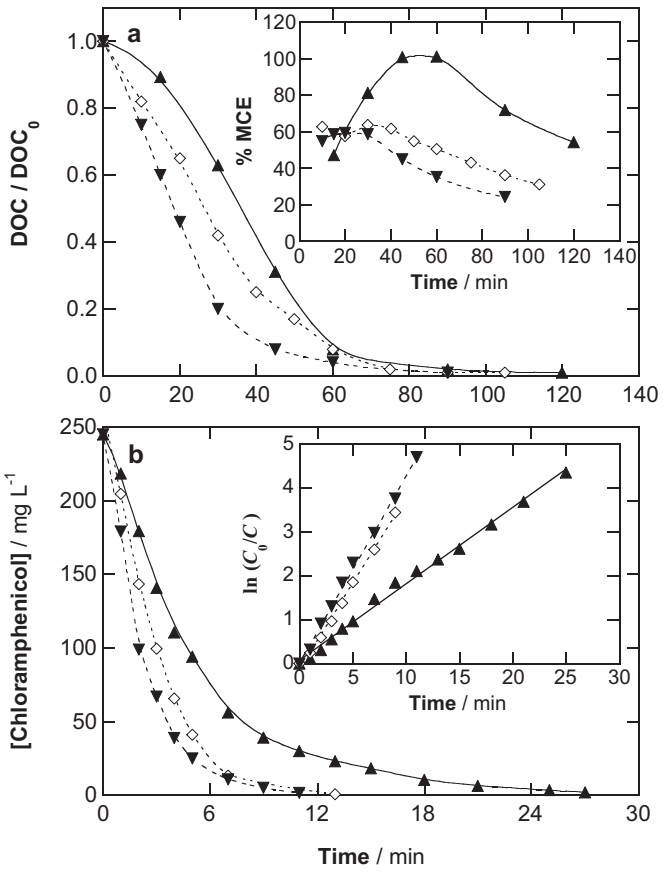

Fig. 3. Effect of current density on (a) normalized DOC removal and (b) substrate concentration decay with electrolysis time for the degradation of 100 mL of 245 mg L^{-1} chloramphenicol with 0.05 M Na_2SO_4 and 0.5 mM Fe^{2+} at pH 3.0 and 35 °C by SPEF using a BDD/air-diffusion tank reactor. Applied current density: (▲) 33.3 mA cm^{-2}, (◊) 66.6 mA cm^{-2} and (▼) 100 mA cm^{-2}. Inset panel: (a) mineralization current efficiency vs electrolysis time and (b) kinetic analysis assuming a pseudo-first-order reaction.

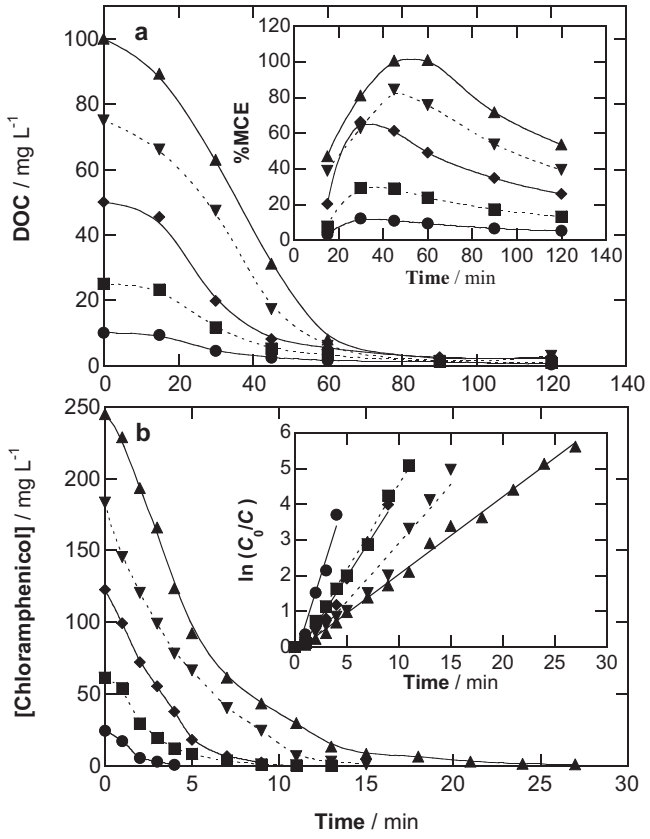

Fig. 4. Influence of initial chloramphenicol concentration on (a) DOC abatement and (b) substrate concentration abatement vs electrolysis time for the SPEF degradation of 100 mL of drug solutions in 0.05 M Na_2SO_4 with 0.5 mM Fe^{2+} at pH 3.0, 33.3 mA cm^{-2} and 35 °C using a BDD/air-diffusion tank reactor. Initial DOC content: (●) 24.5 mg L^{-1}, (■) 61.2 mg L^{-1}, (♦) 122.5 mg L^{-1}, (▼) 183.7 mg L^{-1} and (▲) 245 mg L^{-1}. Inset panel: (a) mineralization current efficiency vs electrolysis time and (b) analysis considering a pseudo-first-order kinetics.

mineralization obtained for 245 mg L^{-1} chloramphenicol with rising *j*, attaining total mineralization in 120, 105 and 90 min for 33.3, 66.6 and 100 mA cm^{-2}, respectively. This trend can be associated with the concomitant increase in rate of all electrode reactions leading to the production of higher amounts of BDD(•OH) from reaction (3) and •OH in the bulk from reaction (4) due to the enhancement of H_2O_2 generation from reaction (1) [43]. The faster destruction of organics with greater quantities of these radicals favors the formation of intermediates that are more rapidly photolyzed by solar radiation, thereby enhancing chloramphenicol mineralization. However, the opposite tendency can be observed in the inset panel of Fig. 3a for the calculated MCE from Eq. (7). Thus, the efficiency dropped as *j* increased and reached maximum values of 100%, 64% and 59% at 33.3, 66.6 and 100 mA cm^{-2}, respectively. This loss in efficiency can be related to a gradual loss in the relative quantity of generated BDD(•OH) and •OH due to the higher increase in rate of their non-oxidizing reactions, with the consequent fall in organic events making the mineralization more inefficient. These waste reactions involve primordially the oxidation of BDD(•OH) to O_2 via reaction (9), as well as the dimerization of •OH to H_2O_2 from reaction (10) and its reaction either with Fe^{2+} from reaction (11) or with H_2O_2 generating the weaker oxidant hydroperoxyl radical (HO_2•) from reaction (12) [15,16,23,30]. The relative amount of generated BDD(•OH) could also fall by the quicker formation of other weaker oxidants at the BDD anode such peroxodisulfate ($S_2O_8^{2-}$) ion by oxidation of SO_4^{2-} ion from the electrolyte by reaction (13) and ozone by reaction (14) [14,15].

$$2BDD(^{\bullet}OH) \rightarrow 2BDD + O_2 + 2H^+ + 2e^- \quad (9)$$

$$2^{\bullet}OH \rightarrow H_2O_2 \quad (10)$$

$$Fe^{2+} + {}^{\bullet}OH \rightarrow Fe^{3+} + OH^- \quad (11)$$

$$H_2O_2 + {}^{\bullet}OH \rightarrow HO_2{}^{\bullet} + H_2O \quad (12)$$

$$2SO_4{}^{2-} \rightarrow S_2O_8{}^{2-} + 2e^- \quad (13)$$

$$3H_2O \rightarrow O_3 + 6H^+ + 6e^- \quad (14)$$

It is important to remark that the oxidants produced in solution can also suffer chemical activation by irradiation (photocatalysis) and after that, other strong oxidant species can be produced by the combination of the oxidants produced with another species that leads to the production of very reactive species such as ozone and sulfate ion-radical. However, the undesired effect can be also observed because the effectiveness of the process could be reduced with a decrease of •OH concentration due to its combination by reaction (10).

Fig. 3b depicts that the increase in *j* accelerates the antibiotic abatement, which disappears in 27, 13 and 11 min for 33.3, 66.6 and 100 mA cm^{-2}. The inset panel of this figure presents the excellent linear correlations obtained from the analysis of such substrate decays for a pseudo-first-order kinetics, giving rise to increasing k_1

Table 1
Products and hydroxylated derivatives identified by LC–MS during chloramphenicol degradation by EF in a BDD/air-diffusion tank reactor.

Product	Chemical name	–OH groups added	m/z[a]	t_r[b] (min)
1	Chloramphenicol	–	321	9.917
			323	
			325	
		2	353	8.500
			355	
			357	
2	2,2-Dichloro-*N*-[1,3-dihydroxy-1-(4-hydroxyphenyl)propan-2-yl]acetamide	2	324	9.850
			326	
			328	
3	4-(2-Amino-1,3-dihydroxy-propanyl)-nitrobenzene	–	211	–
		1	227	11.250
		2	243	9.500
4	4-(2-Amino-1,3-dihydroxy-propanyl)-phenol	–	182	13.125
		3	230	9.135
5	4-(2-Nitro-1,3-dihydroxy-propanyl)-nitrobenzene	–	241	15.083
		2	273	8.653
		3	289	9.305
6	4-Nitro-(2*R*)-hydroxy(phenyl)ethanoic acid	–	212	8.430
		1	228	13.466
		2	244	9.325
7	4-Hydroxy-(2*R*)-hydroxy(phenyl)ethanoic acid	–	183	8.341
8	4-Nitrobenzoic acid	–	166	7.020
		1	182	13.041
		4	230	9.033
9	4-Hydroxybenzoic acid	–	137	6.500
		1	153	9.625
		2	169	9.157
		4	201	7.475
10	4-Nitrophenol	–	138	6.350
11	Dichloroacetic acid	–	127	7.568

[a] Negative ion with $z = 1$.
[b] Retention time.

values from 2.9×10^{-3} to 7.1×10^{-3} s^{-1} ($R^2 \sim 0.995$–0.998) when j changes from 33.3 to 100 mA cm^{-2}. This confirms the concomitant greater generation of •OH as the main oxidant of chloramphenicol.

The effect of substrate concentration on the oxidation ability of SPEF with BDD was explored for solutions containing 24.5–245 mg L^{-1} of chloramphenicol at 33.3 mA cm^{-2}. For these trials, Fig. 4a evidences that total mineralization (98% DOC abatement) was achieved at a similar time of 120 min in all cases. That means that the mineralization rate was accelerated at higher chloramphenicol concentration, thereby making the process more efficient. This behavior can be seen in the inset panel of Fig. 4a, where the maximum MCE values gradually increased from 12% for 24.5 mg L^{-1} to 100% for 245 mg L^{-1}. This suggests a progressive inhibition of parasitic reactions (9)–(14) to favor the attack of a larger proportion of BDD(•OH) and •OH on greater amounts of organics that are more rapidly mineralized and/or more quickly photolyzed by sunlight. The determination of substrate decay in these trials revealed that it disappeared at longer time at greater concentration, from 4 to 27 min, as depicted in Fig. 4b. Its inset panel evidences that chloramphenicol always followed a pseudo-first-order reaction, with decreasing k_1 values of 1.5×10^{-2} s^{-1} ($R^2 = 0.985$), 8.0×10^{-3} s^{-1} ($R^2 = 0.997$), 7.6×10^{-3} s^{-1} ($R^2 = 0.988$), 3.7×10^{-3} s^{-1} ($R^2 = 0.999$) and 2.9×10^{-3} s^{-1} ($R^2 = 0.998$) for increasing contents of 24.5, 61.2, 122.5, 183.7 and 245 mg L^{-1}. Note that the large drop in k_1 as chloramphenicol concentration rises is a surprising trend for a pseudo-first-order kinetics, since a rate constant independent of substrate content is theoretically expected. This may be related to the very short lifetime of hydroxyl radicals (about 4×10^{-9} s) [44] which need to be continuously produced from water oxidation by reaction (3) and Fenton's reaction (4) with participation of H_2O_2 and Fe^{2+}. The diffusion of all these species in the medium and their mass transport toward/from the electrodes then seem to limit the generation of BDD(•OH) and •OH giving a different constant concentration of them to attack chloramphenicol in each trial. This could explain that its decay always follows a pseudo-first-order kinetics but with a k_1 value depending on the experimental variables tested.

The aforementioned findings highlight the great oxidation ability of BDD(•OH), •OH and sunlight in SPEF with BDD, allowing the complete mineralization of acidic waters polluted with high contents of chloramphenicol. The efficiency of this EAOP improves with decreasing j and rising substrate content.

3.3. Identification and evolution of oxidation products

Since hydroxyl radicals (Pt(•OH), BDD(•OH) and •OH) are the main oxidants in the EAOPs tested, the same products are expected to be formed in all them. The primary intermediates were then detected from short electrolysis times of a solution with 245 mg L^{-1} chloramphenicol under EF with BDD at 33.3 mA cm^{-2} by liquid chromatography–mass spectrometry (LC–MS). Table 1 summarizes the products identified by this technique and their main characteristics. Apart from chloramphenicol (**1**), nine aromatic products (**2**–**10**) and thirteen hydroxylated derivatives along with dichloroacetic acid (**11**) were found.

The cleavage of the benzenic ring of aromatic products and the degradation of their lateral groups are expected to form short-chain carboxylic acids [12,16,18,28–32]. Ion-exclusion HPLC of all treated solutions revealed the generation of tartaric (**12**, $t_r = 8.24$ min), maleic (**13**, $t_r = 8.51$ min), acetic (**14**, $t_r = 14.96$ min), oxalic (**15**, $t_r = 7.00$ min), oxamic (**16**, $t_r = 9.39$ min) and formic (**17**, $t_r = 13.68$ min) acids. Oxidation of tartaric, maleic and acetic acids yields oxalic and formic acids [12,16], whereas oxamic acid can be formed from precedent amino compounds. Besides, oxalic, oxamic and formic acids are ultimate carboxylic acids since they are directly oxidized to CO_2 [16,45].

The evolution of detected carboxylic acids was determined for the treatment of a 245 mg L^{-1} chloramphenicol solution by

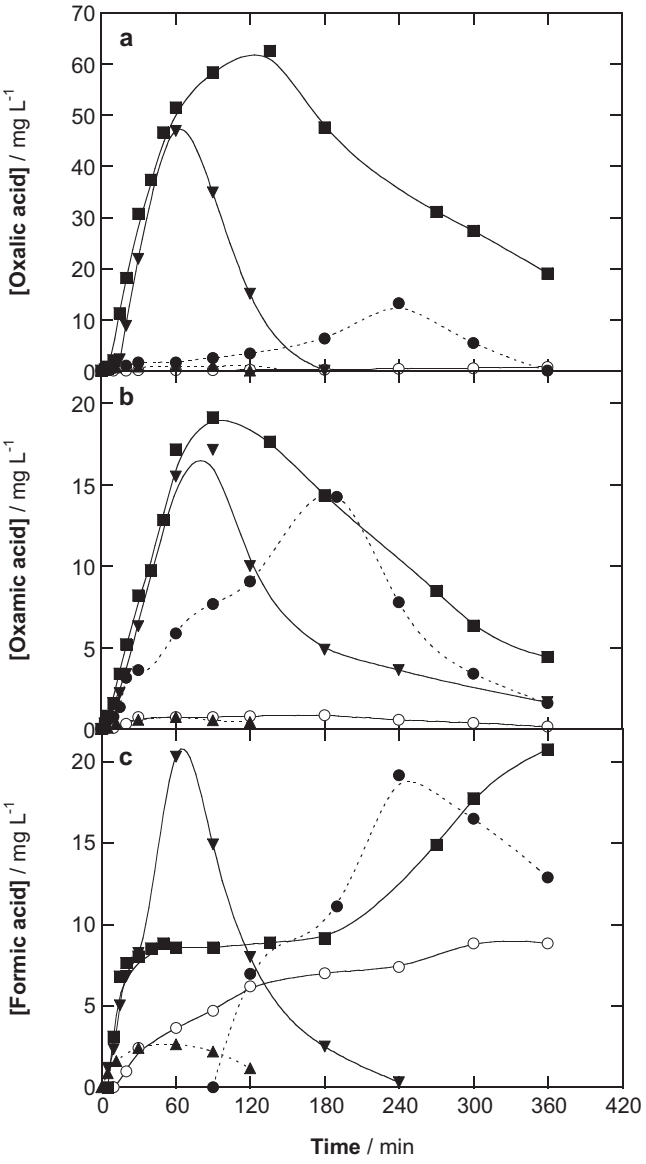

Fig. 5. Evolution of the concentration of (a) oxalic (**15**), (b) oxamic (**16**) and (c) formic (**17**) acids detected during the treatments of Fig. 1. Method: (○) AO-H_2O_2 with Pt, (●) AO-H_2O_2 with BDD, (■) EF with BDD, (▼) PEF with BDD and (▲) SPEF with BDD.

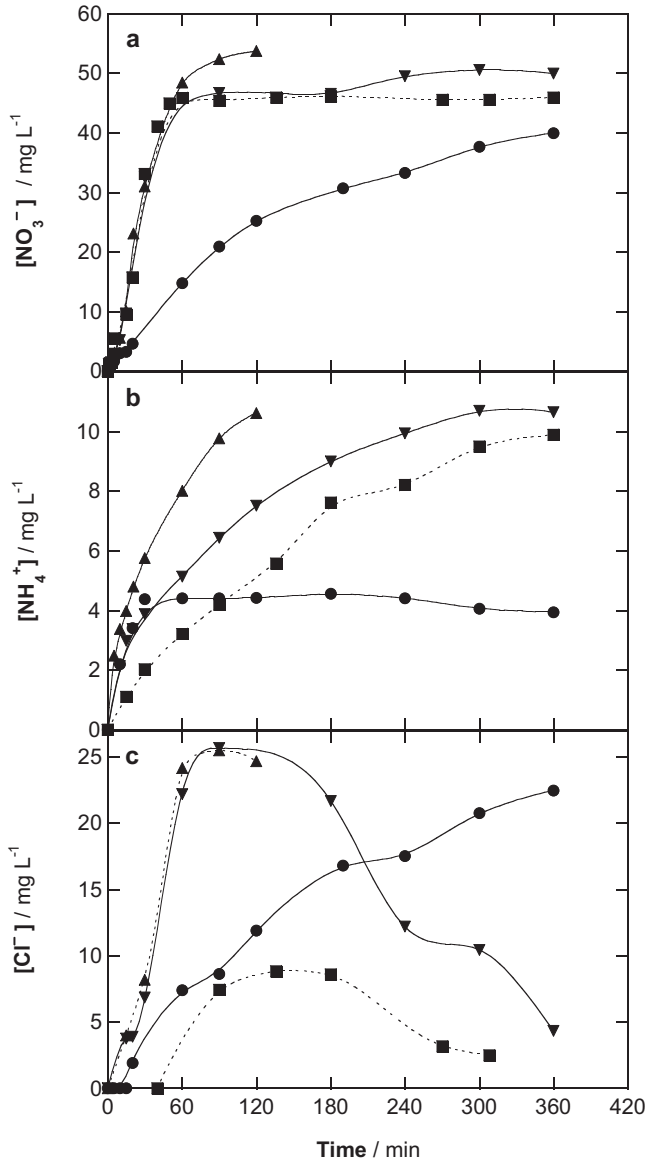

Fig. 6. Time-course of the concentration of: (a) nitrate, (b) ammonium and (c) chloride ions released during the degradations of Fig. 1 using a BDD/air-diffusion tank reactor. Method: (●) AO-H_2O_2, (■) EF, (▼) PEF and (▲) SPEF.

AO-H_2O_2 with Pt and BDD as well as EF, PEF and SPEF with BDD at 33.3 mA cm^{-2}. While only traces of **12**–**14** were found for the three latter methods, up to 8 mg L^{-1} of **12** were formed and completely removed at 360 min of both AO-H_2O_2 processes and **13** was continuously accumulated up to 2 mg L^{-1} in AO-H_2O_2 with Pt, being totally destroyed when using BDD. A very different behavior was obtained for the ultimate acids **15**–**17**, as shown in Fig. 5a–c. Thus, in AO-H_2O_2 with Pt, **15** and **16** were poorly produced (<0.8 mg L^{-1}) and up to 7.4 mg L^{-1} of **17** were continuously accumulated, according to the scarce DOC decay of this EAOP (see Fig. 1a). In contrast, the higher oxidation ability of AO-H_2O_2 with BDD allowed the faster destruction of precedent intermediates with larger accumulation of these three acids, which were also mineralized by BDD(•OH) at long electrolysis time, primordially **15** and **16**. The quicker destruction of aromatic products by •OH in EF with BDD favored the faster generation of the ultimate acids attaining maximum contents of 58.3 mg L^{-1} for **15**, 19.1 mg L^{-1} for **16** and 20.7 mg L^{-1} for **17**. Results of Fig. 5a–c evidence that Fe(III)-oxalate and Fe(III)-oxamate complexes were slowly removed from the attack of BDD(•OH) [16,45], whereas Fe(III)-formate species were more stable in solution. When PEF with BDD was used, these three Fe(III)-carboxylate complexes were rapidly photomineralized by UVA light from reaction (6), a process so rapid in SPEF with BDD that they were not practically accumulated. A simple mass balance at 120–135 min of AO-H_2O_2, EF, PEF and SPEF with BDD indicated that the ultimate acids contributed in 5.2, 23.2, 10.0 and 0.76 mg L^{-1} DOC, respectively, related to 7.4%, 68%, 59% and 38% of the organic matter contained in the final treated solution. All these results confirm the preponderant attack of •OH on aromatic products to produce carboxylic acids, which can be slowly decayed by BDD(•OH) and the potent photolytic action of sunlight quickly mineralizes Fe(III)-carboxylate complexes. This explains the highest oxidation ability of SPEF with BDD than the other EAOPs.

The conversion of the initial N of chloramphenicol (21.2 mg L^{-1}) into NO_3^- and NH_4^+ ions in the treatments with BDD was assessed by ion chromatography. Fig. 6a and b shows that NO_3^- ion was formed usually more rapidly and always in larger extent, as proposed in reaction (8). At the end of electrolyses, 40 mg L^{-1}

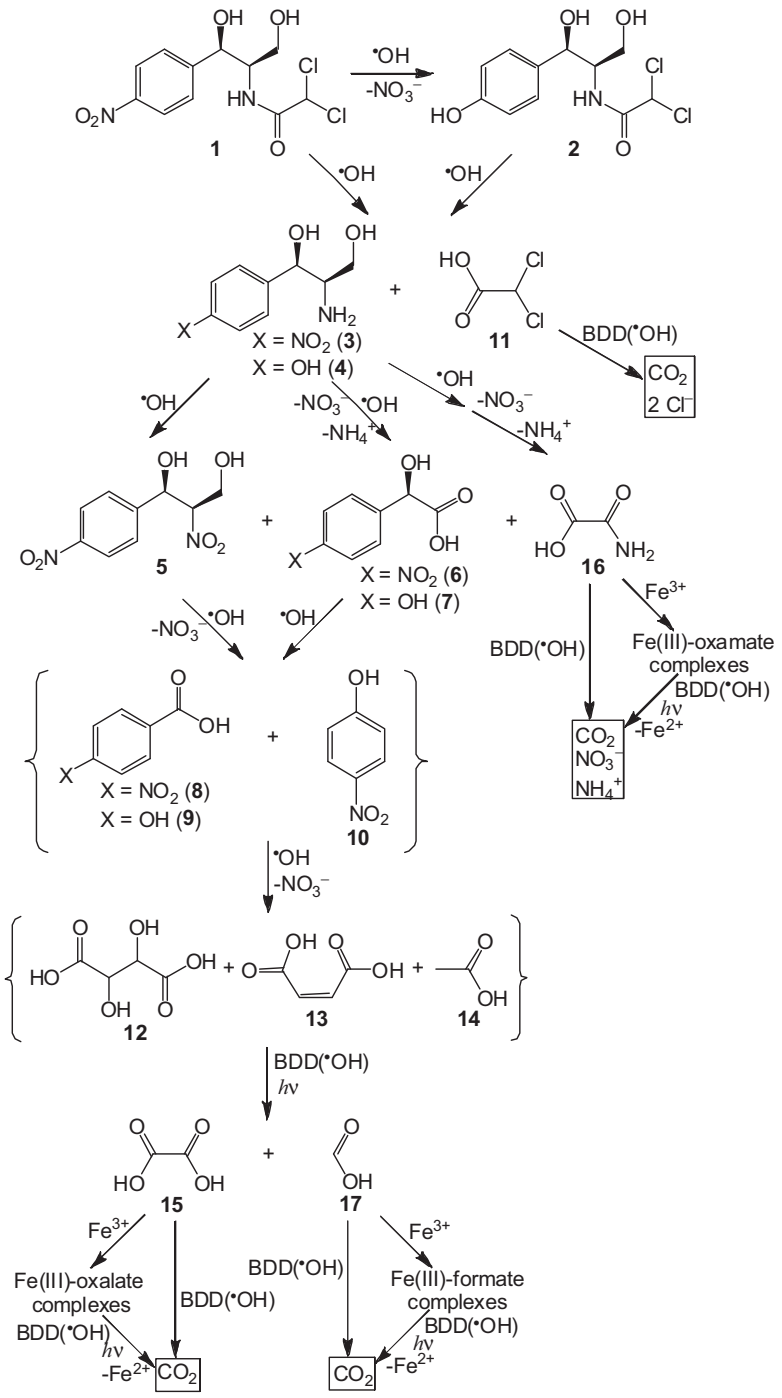

Fig. 7. General reaction sequence proposed for chloramphenicol mineralization by EAOPs in acidic aqueous medium.

NO_3^- (42% of initial N) and 4.1 mg L^{-1} NH_4^+ (15% of initial N) for AO-H_2O_2, 46 mg L^{-1} NO_3^- (49% of initial N) and 9.9 mg L^{-1} NH_4^+ (36% of initial N) for EF, 50 mg L^{-1} NO_3^- (53% of initial N) and 10.7 mg L^{-1} NH_4^+ (40% of initial N) for PEF and 54 mg L^{-1} NO_3^- (59% of initial N) and 10.7 mg L^{-1} NH_4^+ (40% of initial N) for SPEF were found. TN analysis of the final solution treated by AO-H_2O_2 revealed the presence of 61% of the initial N, in good agreement with 57% of initial N related to the sum of NO_3^- and NH_4^+ contents. This suggests the release of volatile N-derivatives in this process due to the smaller oxidation ability of BDD(•OH). The quicker oxidation of intermediates with •OH then favored their mineralization with larger release of inorganic ions, even enhanced under UVA and solar radiation. TN measurements then confirmed the presence of the initial N as NO_3^- and NH_4^+ ions in the final solution of the SPEF process. On the other hand, Fig. 6c shows that Cl^- ion was lost during the same trials, without reaching the initial Cl content of 53.7 mg L^{-1}. This ion was slowly accumulated in AO-H_2O_2 up to 24.7 mg L^{-1} since it was slowly generated from the BDD(•OH) attack on chloro-organics and oxidized to chlorine at the BDD anode [14,28]. This phenomenon can be better observed for both EF and PEF processes, where Cl^- ion was much more rapidly released due to the greater oxidation ability of •OH and practically disappeared in 360 min. That means that Cl^- ion is a primary inorganic ion formed in chloramphenicol mineralization, as stated in reaction (8).

3.4. Reaction sequence for chloramphenicol mineralization

Fig. 7 presents a general reaction pathway for chloramphenicol mineralization by the EAOPs tested. Only the detected aromatic species have been considered, but not their hydroxylated derivatives for sake of simplicity. These compounds are assumed to be mainly oxidized by •OH in EF, PEF and SPEF, although their slower destruction with either Pt(•OH) or BDD(•OH) takes place in the AO-H_2O_2 processes.

The sequence is initiated by the hydroxylation with denitration of **1** to give **2**, along with the hydroxylation of these two compounds yielding **3** and **4** with loss of **11**, which is mineralized with release of Cl^- ions. Further oxidation of the amino group of **3** to nitro group leads to **5**, whereas deamination of the lateral group of **3** and **4** gives the aromatics **6** and **7** and their parallel degradation leads to acid **16**. Subsequent oxidation of the lateral groups of **6** and **7** gives compounds **8**–**10**. The cleavage of the benzenic ring of the above aromatics and the destruction of their lateral groups yields the mixture of acids **12**–**14**, which are further transformed into **15** and **17**. All short-chain carboxylic acids can be slowly removed under the action of BDD(•OH) in AO-H_2O_2 with BDD, whereas in EF, PEF and SPEF they form Fe(III)-carboxylate species that are also slowly destroyed by BDD(•OH) but much more rapidly photolyzed by UVA and solar radiation in the two latter EAOPs. These alternative reactions are indicated for the ultimate acids **15**–**17** that are directly converted into CO_2. Acid **16** also releases NO_3^- and NH_4^+ ions during mineralization [45].

3.5. SPEF degradation with Pt in the solar pre-pilot plant

The most potent SPEF process was further scaled-up to a solar pre-pilot plant in order to assess its viability at industrial scale. A Pt anode was used to obtain a more economic process since gave a lower potential difference of the cell than using a BDD one. The pre-pilot plant then contained a Pt/air-diffusion filter-press cell coupled to the solar CPCs photoreactor. 10 L of 245 mg L^{-1} chloramphenicol with 0.05 M Na_2SO_4 and 0.5 mM Fe^{2+} at pH 3.0 and 35 °C were treated in batch circulation mode by applying up to 100 mA cm^{-2} and liquid flow rate of 200 L h^{-1}. Comparative EF in the dark was made to clarify the effect of irradiated sunlight.

As expected, the mineralization rate of the EF and SPEF processes increased when j rose. Fig. 8a exemplifies the normalized DOC decay found for 100 mA cm^{-2}. While DOC was slowly removed by EF only yielding 45% reduction in 360 min, it decayed much more rapidly by SPEF, being reduced by 89% in 180 min. This evidences the large synergistic action of sunlight using the CPCs photoreactor in SPEF. Besides, maximum MCE values of 19% for EF and 49% for SPEF were attained after 120 min of electrolysis, as can be seen in Fig. 8b. Comparison of these results with the total mineralization achieved at 180 min of SPEF at 33.3 mA cm^{-2} with maximum efficiency of 80% using the stirred tank reactor (see Fig. 1) allows concluding that the SPEF process is viable in the solar pre-pilot plant, although it has lower oxidation ability to mineralize chloramphenicol.

For the above trials, the energy cost per unit DOC mass removed (EC_{DOC}) was calculated from Eq. (15) [42,43]:

$$EC_{DOC}\left(\text{kWh g}^{-1}\text{ DOC}\right) = \frac{E_{cell} I t}{V_s\,\Delta(\text{DOC})_{exp}} \quad (15)$$

where E_{cell} is the average potential difference of the cell (11.4 V), I is the applied current (9 A), t is the electrolysis time (h), V_s is the solution volume (L) and $\Delta(DOC)_{exp}$ is the experimental DOC abatement (mg L^{-1}). Fig. 8c shows that the SPEF process was much more economic than the EF one. In both EAOPs, EC_{DOC} dropped from the starting of electrolysis reaching minimal of 0.676 and 0.255 kWh g^{-1} DOC after 2 h of EF and SPEF, respectively, just when

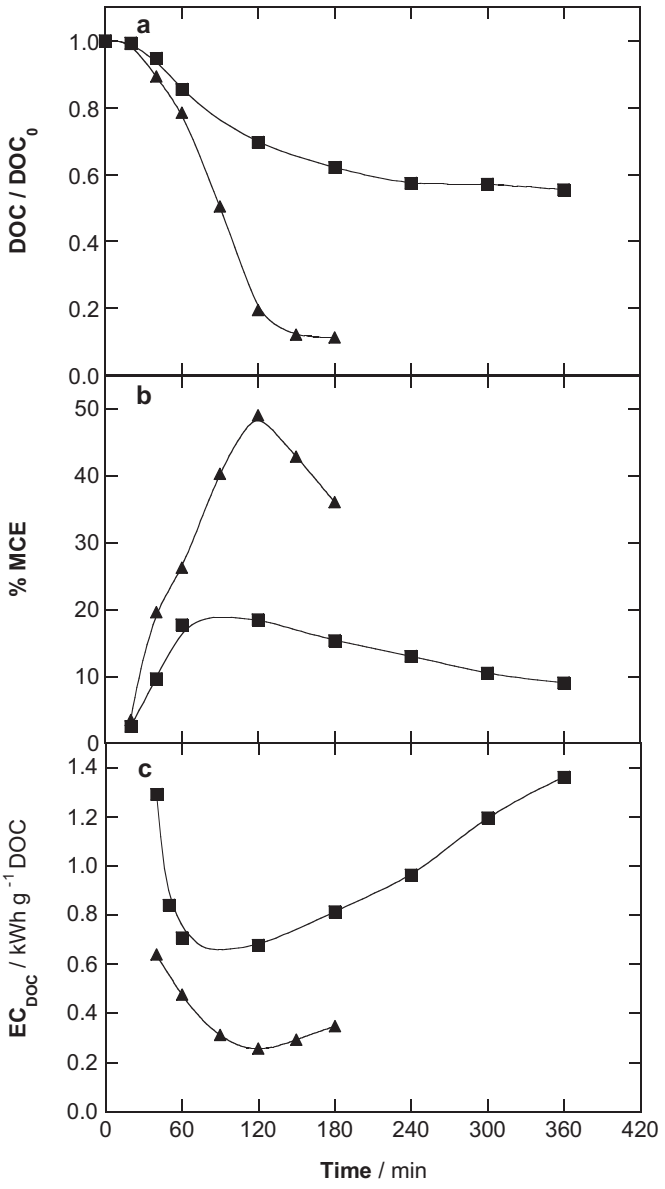

Fig. 8. Change of (a) normalized DOC, (b) mineralization current efficiency and (c) energy consumption per unit DOC mass for the (■) EF (in the dark) and (▲) SPEF treatments of a 245 mg L^{-1} chloramphenicol solution in 0.05 M Na_2SO_4 with 0.5 mM Fe^{2+} at pH 3.0, 100 mA cm^{-2} and 35 °C in the 10 L pre-pilot plant containing a Pt/air-diffusion filter-press reactor coupled to a solar CPCs photoreactor at liquid flow rate of 200 L h^{-1}.

their best efficiencies were attained (see Fig. 8b). At the end of SPEF (180 min), an EC_{DOC} value of 0.347 kWh g^{-1} DOC related to 30.8 kWh m^{-3} energy cost was obtained. Taking into account that the electrical energy cost of the Endesa, S.A., company in Spain is of about 0.141 € kWh^{-1}, one can estimate a cost of 4.35 € m^{-3} for the SPEF process. This low cost confirms its viability for possible application to industrial scale.

The chloramphenicol concentration decayed with similar rate in both EF and SPEF treatments, as can be seen in Fig. 9, where the antibiotic disappeared in about 60 min. The inset panel of this figure shows the excellent straight lines obtained considering a pseudo-first-order reaction, giving rise to k_1 values of 1.4×10^{-3} s^{-1} (R^2 = 0.994) for EF and 1.6×10^{-3} s^{-1} (R^2 = 0.994) for SPEF. This evidences again the small participation of photolytic reaction (5) to produce significant amounts of the main oxidant •OH in SPEF. The fact that a much greater k_1 value of 2.9×10^{-3} s^{-1} was obtained

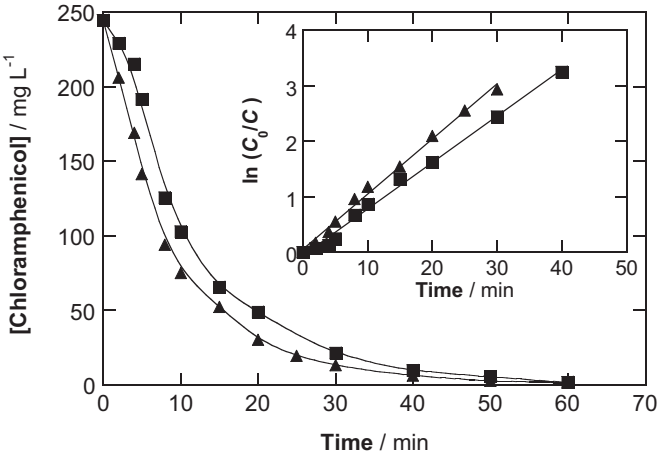

Fig. 9. Chloramphenicol concentration decay for the trials of Fig. 8. The inset panel presents the kinetic analysis assuming a pseudo-first-order reaction for the drug. Method: (■) EF and (▲) SPEF.

operating at lower j of 33.3 mA cm^{-2} in the stirred tank reactor, corroborates the formation of lower amounts of •OH from Fenton's reaction (4) in the solar pre-pilot plant, thereby making the SPEF process with Pt less efficient.

The time course of generated carboxylic acids for SPEF with Pt is depicted in Fig. 10a. While acids **12**, **13** and **15** disappeared completely during the 180 min of electrolysis, high amounts of **16** (15 mg L^{-1}) together only 1.8 mg L^{-1} of **14** and 2.6 mg L^{-1} of **17** remained in the solution. The amounts of these acids represent 5.5 mg L^{-1} DOC, i.e., a 50% of the DOC present in the final solution (see Fig. 8a), then being their main components. The greater persistence of Fe(III)-carboxylate complexes in the solar pre-pilot plant compared to the stirred tank reactor can be related to the poorer capture of solar radiation by the solution volume. Thus, the 100 mL cell was totally irradiated by sunlight in contrast to the very low irradiated volume/total volume ratio of 15.7% used in the 10 L pre-pilot plant at liquid flow rate of 200 L h^{-1}. Nevertheless, the latter system had a better solar radiation capture system from CPCs, which can use efficiently direct and diffuse solar irradiation, whereas the stirred tank reactor mostly used the direct radiation, although a very small part of diffuse UV radiation reflected by the mirror at the bottom of the cell reached the solution.

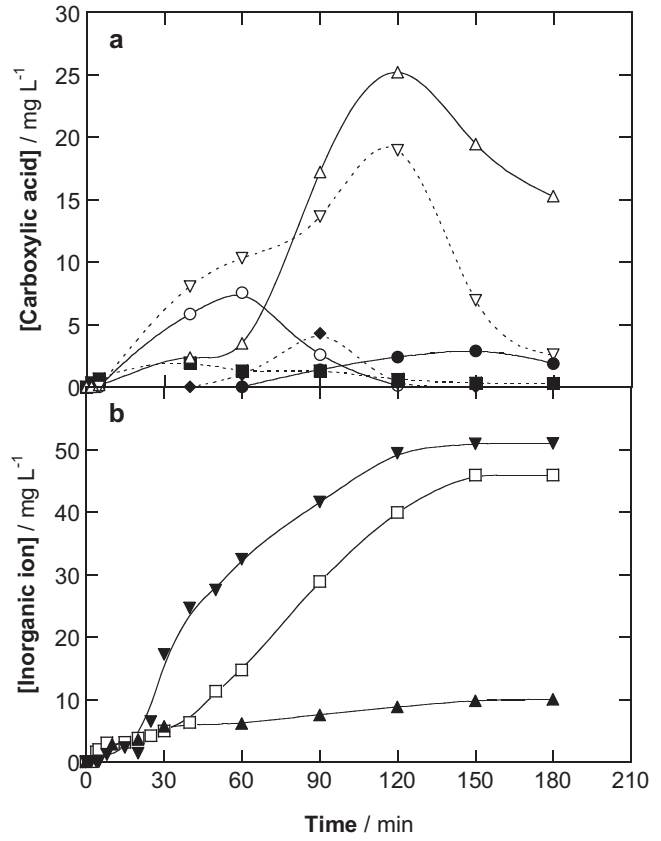

Fig. 10. Evolution of the concentration of (a) carboxylic acids and (b) inorganic ions formed during the experiment of Fig. 8 with a Pt/air-diffusion filter-press reactor. In plot (a), (♦) tartaric (**12**), (■) maleic (**13**), (●) acetic (**14**), (○) oxalic (**15**), (△) oxamic (**16**) and (▽) formic (**17**) acids. In plot (b), (▼) nitrate, (▲) ammonium and (□) chloride ions.

On the other hand, Fig. 10b confirms the release of NO_3^-, NH_4^+ and Cl^- ions during the SPEF treatment with Pt. NO_3^- ion was preferentially formed, being accumulated up to 51 mg L^{-1} (54% of initial N), whereas only 10 mg L^{-1} (36% of initial N) of NH_4^+ ion were formed. TN analysis of the final degraded solution confirmed that it contained all the initial N, which was distributed in the form of NO_3^- and NH_4^+ ions (90%) and the remaining **16** (10%). This indicates again the high oxidation of this EAOP to mineralize all *N*-compounds. In contrast, Cl^- ion was continuously accumulated up to a maximum content of 46 mg L^{-1} at about 150 min of electrolysis. This behavior differs from that found in the stirred tank reactor with a BDD anode (see Fig. 6c), suggesting a much slower destruction of chloroderivatives, like **11**, in the pre-pilot plant with a much slower oxidation of Cl^- ion to chlorine at the Pt anode.

4. Conclusions

It has been demonstrated that SPEF with BDD is the most potent EAOP for chloramphenicol mineralization at pH 3.0 using a 100 mL stirred BDD/air-diffusion tank reactor. Total mineralization of antibiotic solutions with 0.05 M Na_2SO_4 and 0.5 mM Fe^{2+} at pH 3.0 can be rapidly attained by the combined action of BDD(•OH), •OH and sunlight. PEF with BDD was less powerful due to the lower intensity of UVA radiation to photolyze generated Fe(III)-carboxylate species. EF and AO-H_2O_2 with BDD led to partial mineralization, the former being more potent because chloramphenicol and its aromatic products were more rapidly destroyed by •OH than BDD(•OH). Comparative treatments with a Pt anode yielded slower mineralization than using BDD because of the smaller oxidation ability of Pt(•OH), although total mineralization was also achieved for the SPEF process. In all these EAOPs, the antibiotic decayed following a pseudo-first-order reaction, with similar apparent constant rate in EF, PEF and SPEF since •OH formed from Fenton's reaction (4) was the main oxidant. For SPEF with BDD, the mineralization current efficiency was enhanced with decreasing j and increasing substrate concentration. The opposite trend was found for the apparent rate constant of the antibiotic decay. Nine aromatic products and thirteen hydroxylated derivatives were identified by LC–MS. Tartaric, maleic and acetic acids, along with oxalic, oxamic and formic as ultimate acids, were quantified by ion-exclusion HPLC. While the Fe(III)-carboxylate complexes of the three latter acids were slowly removed by BDD(•OH) in EF with BDD, they were rapidly photolyzed by UVA light in PEF with BDD and much more quickly photodecomposed by sunlight in SPEF with BDD. NO_3^- ion and, in smaller extent, NH_4^+ ion were released in all processes. Cl^- ion was also lost, but it was oxidized to chlorine at the BDD anode surface. From the detected products, a plausible general reaction sequence for chloramphenicol mineralization by EAOPs is proposed. The SPEF process with Pt was viable when it was scaled-up to a 10 L solar pre-pilot plant. This system showed less oxidation ability than the 100 mL stirred tank reactor, leading to partial

mineralization of a 245 mg L^{-1} antibiotic solution. After 180 min of electrolysis at 100 mA cm^{-2} and liquid flow rate of 200 L h^{-1}, 89% mineralization with 36% current efficiency and 30.8 kWh m^{-3} energy cost was obtained. Acetic, formic and primordially oxamic acids were the main components remaining in the final solution because of the poorer capture of solar radiation by the solution volume.

Acknowledgments

The authors gratefully acknowledge the financial support from MICINN (Ministerio de Ciencia e Innovación, Spain) under the Project CTQ2010-16164/BQU, co-financed with FEDER funds. S. Garcia-Segura thanks the grant awarded from MEC (Ministerio de Educación y Ciencia, Spain) and E.B. Cavalcanti acknowledges the financial support from CAPES/MEC/Brazil and Universidade Tiradentes/UNIT.

References

[1] K. Kümmerer, Chemosphere 75 (2009) 417–434.
[2] K. McClellan, R.U. Halden, Water Res. 44 (2010) 6011–6020.
[3] L.-J. Zhou, G.-G. Ying, S. Liu, J.-L. Zhao, B. Yang, Z.-F. Chen, H.-J. Lai, Sci. Total Environ. 452–453 (2013) 365–376.
[4] I. Kim, N. Yamashita, H. Tanaka, J. Hazard. Mater. 166 (2009) 1134–1140.
[5] V. Homem, L. Santos, J. Environ. Manage. 92 (2011) 2304–2347.
[6] P. Verlicchi, A. Galletti, M. Petrovic, D. Barceló, M. Al Aukidy, E. Zambello, Sci. Total Environ. 454–455 (2013) 411–425.
[7] Y. Xu, F. Luo, A. Pal, K.Y.-H. Gin, M. Reinhard, Chemosphere 83 (2011) 963–969.
[8] H.W. Leung, T.B. Minh, M.B. Murphy, J.C.W. Lam, M.K. So, M. Martin, P.K.S. Lam, J.B. Richardson, Environ. Int. 42 (2012) 1–9.
[9] R. Andreozzi, V. Caprio, C. Ciniglia, M. De Campore, R. Lo Giudice, R. Marotta, E. Zuccato, Environ. Sci. Technol. 38 (2004) 6832–6838.
[10] M. Crane, C. Watts, T. Boucard, Sci. Total Environ. 367 (2006) 23–41.
[11] F. Pomati, C. Orlandi, M. Clerici, F. Luciani, E. Zuccato, Toxicol. Sci. 102 (2008) 129–137.
[12] I. Sirés, E. Brillas, Environ. Int. 40 (2012) 212–229.
[13] C.A. Martínez-Huitle, S. Ferro, Chem. Soc. Rev. 35 (2006) 1324–1340.
[14] C.A. Martínez-Huitle, E. Brillas, Angew. Chem. Int. Ed. 47 (2008) 1998–2005.
[15] M. Panizza, G. Cerisola, Chem. Rev. 109 (2009) 6541–6569.
[16] E. Brillas, I. Sirés, M.A. Oturan, Chem. Rev. 109 (2009) 6570–6631.
[17] M. Klavarioti, D. Mantzavinos, D. Kassinos, Environ. Int. 35 (2009) 402–417.
[18] A. Özcan, Y. Sahin, A. Savas Koparal, M.A. Oturan, J. Electroanal. Chem. 616 (2008) 71–78.
[19] M. Zarei, A.R. Khataee, R. Ordikhani-Seyedlar, M. Fathinia, Electrochim. Acta 55 (2010) 7259–7265.
[20] M. Zarei, A. Niaei, D. Salari, A.R. Khataee, J. Hazard. Mater. 173 (2010) 544–551.
[21] I. Sirés, J.A. Garrido, R.M. Rodríguez, E. Brillas, N. Oturan, M.A. Oturan, Appl. Catal. B: Environ. 72 (2007) 382–394.
[22] I. Sirés, N. Oturan, M.A. Oturan, R.M. Rodríguez, J.A. Garrido, E. Brillas, Electrochim. Acta 52 (2007) 5493–5503.
[23] A. Ozcan, Y. Sahin, A.S. Koparal, M.A. Oturan, J. Hazard. Mater. 153 (2008) 718–727.
[24] A. Dirany, S. Efremova-Aaron, N. Oturan, I. Sirés, M.A. Oturan, J.-J. Aaron, Anal. Bioanal. Chem. 400 (2011) 353–360.
[25] A. Dirany, I. Sirés, N. Oturan, A. Özcan, M.A. Oturan, Environ. Sci. Technol. 46 (2012) 4074–4082.
[26] M. Panizza, M.A. Oturan, Electrochim. Acta 56 (2011) 7084–7087.
[27] K. Cruz-González, O. Torres-López, A. García-León, J.L. Guzmán-Mar, L.H. Reyes, A. Hernández-Ramírez, J.M. Peralta-Hernández, Chem. Eng. J. 160 (2010) 199–206.
[28] I. Sirés, F. Centellas, J.A. Garrido, R.M. Rodríguez, C. Arias, P.L. Cabot, E. Brillas, Appl. Catal. B: Environ. 72 (2007) 373–381.
[29] E. Guinea, J.A. Garrido, R.M. Rodríguez, P.L. Cabot, C. Arias, F. Centellas, E. Brillas, Electrochim. Acta 55 (2010) 2101–2115.
[30] S. Garcia-Segura, J.A. Garrido, R.M. Rodríguez, P.L. Cabot, F. Centellas, C. Arias, E. Brillas, Water Res. 46 (2012) 2067–2076.
[31] A. El-Ghenymy, P.L. Cabot, F. Centellas, J.A. Garrido, R.M. Rodríguez, C. Arias, E. Brillas, Chemosphere 91 (2013) 1324–1331.
[32] E.B. Cavalcanti, S. Garcia-Segura, F. Centellas, E. Brillas, Water Res. 47 (2013) 1803–1815.
[33] B. Kasprzyk-Hordern, R.M. Dinsdale, A.J. Guwy, Water Res. 42 (2008) 3498–3518.
[34] L. Tong, W. Ping, Y. Wang, K. Zhu, Chemosphere 74 (2009) 1090–1097.
[35] A.I. Okoh, E.O. Igbinosa, BMC Microbiol. 10 (2010) 143.
[36] H. Xu, W. Chen, C. Wang, J. Yang, L. Zhao, Fres. Environ. Bull. 21 (2012) 1619–1625.
[37] V. Suling, J. Wohlers, M. Reinhard, W. Thiemann, Vom Wasser 98 (2002) 145–158.
[38] A. Chatzitakis, C. Berberidou, I. Paspaltsis, G. Kyriakou, T. Sklaviadis, I. Poulios, Water Res. 42 (2008) 386–394.
[39] J. Wang, W. Sun, C. Xu, W. Liu, Int. J. Environ. Technol. Manage. 15 (2012) 180–192.
[40] M. Feng, D. Long, Y. Fang, Anal. Chim. Acta 363 (1998) 67–73.
[41] E. Brillas, M.A. Baños, S. Camps, C. Arias, P.L. Cabot, J.A. Garrido, R.M. Rodríguez, New J. Chem. 28 (2004) 314–322.
[42] L.C. Almeida, S. Garcia-Segura, N. Bocchi, E. Brillas, Appl. Catal. B: Environ. 103 (2011) 21–30.
[43] E.J. Ruiz, C. Arias, E. Brillas, A. Hernández-Ramírez, J.M. Peralta-Hernández, Chemosphere 82 (2011) 495–501.
[44] R. Roots, S. Okada, Radiat. Res. 64 (1975) 306–320.
[45] S. Garcia-Segura, E. Brillas, Water Res. 45 (2011) 2975–2984.

PAPER 3

Mineralization of the recalcitrant oxalic and oxamic acids by electrochemical advanced process using a boron-doped diamond anode

Available at www.sciencedirect.com

ScienceDirect

journal homepage: www.elsevier.com/locate/watres

Mineralization of the recalcitrant oxalic and oxamic acids by electrochemical advanced oxidation processes using a boron-doped diamond anode

*Sergi Garcia-Segura, Enric Brillas**

Laboratori d'Electroquímica de Materials i del Medi Ambient, Departament de Química Física, Facultat de Química, Universitat de Barcelona, Martí i Franquès 1-11, 08028 Barcelona, Spain

ARTICLE INFO

Article history:
Received 22 December 2010
Received in revised form
12 February 2011
Accepted 10 March 2011
Available online 21 March 2011

Keywords:
Carboxylic acids
Iron complexes
Anodic oxidation
Electro-Fenton
UVA light
Removal kinetics

ABSTRACT

Oxalic and oxamic acids are the ultimate and more persistent by-products of the degradation of *N*-aromatics by electrochemical advanced oxidation processes (EAOPs). In this paper, the kinetics and oxidative paths of these acids have been studied for several EAOPs using a boron-doped diamond (BDD) anode and a stainless steel or an air-diffusion cathode. Anodic oxidation (AO-BDD) in the presence of Fe^{2+} (AO-BDD-Fe^{2+}) and under UVA irradiation (AO-BDD-Fe^{2+}-UVA), along with electro-Fenton (EF-BDD), was tested. The oxidation of both acids and their iron complexes on BDD was clarified by cyclic voltammetry. AO-BDD allowed the overall mineralization of oxalic acid, but oxamic acid was removed much more slowly. Each acid underwent a similar decay in AO-BDD-Fe^{2+} and EF-BDD, as expected if its iron complexes were not attacked by hydroxyl radicals in the bulk. The faster and total mineralization of both acids was achieved in AO-BDD-Fe^{2+}-UVA due to the high photoactivity of their Fe(III) complexes that were continuously regenerated by oxidation of their Fe(II) complexes. Oxamic acid always released a larger proportion of NH_4^+ than NO_3^- ion, as well as volatile NO_x species. Both acids were independently oxidized at the anode in AO-BDD, but in AO-BDD-Fe^{2+}-UVA oxamic acid was more slowly degraded as its content decreased, without significant effect on oxalic acid decay. The increase in current density enhanced the oxidation power of the latter method, with loss of efficiency. High Fe^{2+} contents inhibited the oxidation of Fe(II) complexes by the competitive oxidation of Fe^{2+} to Fe^{3+}. Low current densities and Fe^{2+} contents are preferable to remove more efficiently these acids by the most potent AO-BDD-Fe^{2+}-UVA method.

1. Introduction

Recently, a large variety of advanced oxidation processes (AOPs) have been proposed for the remediation of wastewaters containing low contents of toxic and/or biorefractory organic pollutants (Andreozzi et al., 1999; Pera-Titus et al., 2004; Cañizares et al., 2008). These powerful oxidation methods include chemical, photochemical and electrochemical treatments based on the *in situ* generation of hydroxyl radical (•OH). This radical is the second most strong oxidizing species known after fluorine with a high standard reduction potential ($E°(•OH/H_2O) = 2.80$ V vs. SHE) that allows its non-selectively reaction with most organics leading to their overall mineralization to CO_2, water and inorganic ions. However, the effectiveness of AOPs is limited by the formation of recalcitrant carboxylic acids (Cañizares et al., 2003; Oturan et al., 2008; Serra

* *Corresponding author*. Tel.: +34 93 4021223; fax: +34 93 4021231.
E-mail address: brillas@ub.edu (E. Brillas).
0043-1354/$ – see front matter © 2011 Elsevier Ltd. All rights reserved.
doi:10.1016/j.watres.2011.03.017

et al., 2009). The most common ultimate by-product from aromatics is oxalic acid, which is hardly destroyed with $^{\bullet}OH$ largely prolonging the mineralization time with the consequent efficiency loss and/or greater operation cost of the treatment (Brillas et al., 2004; Pera-Titus et al., 2004; Diagne et al., 2007; Özcan et al., 2008). In the degradation of wastewaters with *N*-aromatics, a mixture of oxalic and oxamic acids is finally formed (Sirés et al., 2006; Hammami et al., 2008; Hamza et al., 2009; Brillas et al., 2010). Oxamic acid is even more recalcitrant than oxalic acid (Faria et al., 2008). While the removal rate of oxalic acid is strongly enhanced in photoassisted AOPs with iron ions (Zuo and Hoigné, 1992; Faust and Zepp, 1993; Zuo and Hoigné, 1994; Šima and Makáňová, 1997), less is known about the mineralization of oxamic acid by photochemical treatments.

The most typical electrochemical AOP (EAOP) is anodic oxidation (AO) in which organic pollutants contained in an electrolytic cell can be oxidized at the anode surface either by direct charge transfer and/or with $^{\bullet}OH$ generated from water oxidation at high current. For a boron-doped diamond (BDD) electrode, the formation of hydroxyl radical can be written as reaction (1) (Marselli et al., 2003; Sirés et al., 2008; Panizza and Cerisola, 2009; Brillas et al., 2010):

$$BDD + H_2O \rightarrow BDD(^{\bullet}OH) + H^+ + e^- \quad (1)$$

The BDD electrode has a much higher oxidation power than other conventional anodes and it is able to effectively mineralize oxalic acid (Gandini et al., 2000; Martínez-Huitle et al., 2004; Vandini et al., 2006; Weiss et al., 2007; Scialdone et al., 2008), but no information is available on the AO treatment of oxamic acid. The high oxidation power of BDD also allows generating reactive oxygen species (ROS) like H_2O_2 and ozone, as well as peroxo-derivatives coming from the oxidation of the anion of the background electrolyte (Cañizares et al., 2003; Panizza and Cerisola, 2009). In previous work (Guinea et al., 2009), we found that the presence of H_2O_2 in AO accelerates the mineralization process of carboxylic acids, although Fe(III)–oxalate complexes are quickly photolyzed by UVA light.

EAOPs based on Fenton's reaction chemistry have been recently developed (Brillas et al., 2009). In electro-Fenton (EF), H_2O_2 is continuously supplied to an acidic contaminated solution from the two-electron reduction of injected O_2 at a carbonaceous cathode, mainly carbon felt (Oturan et al., 2008; Balci et al., 2009) and carbon-PTFE gas-diffusion electrodes (Sirés et al., 2007; Ruiz et al., 2011), by reaction (2):

$$O_2 + 2H^+ + 2e^- \rightarrow H_2O_2 \quad (2)$$

Fe^{2+} ion is then added to the solution to react with H_2O_2 producing $^{\bullet}OH$ in the bulk and Fe^{3+} by Fenton's reaction (3) (Sun and Pignatello, 1993):

$$Fe^{2+} + H_2O_2 \rightarrow Fe^{3+} + {}^{\bullet}OH + OH^- \quad (3)$$

An advantage of EF is that Fe^{2+} can be regenerated from Fe^{3+} reduction at the cathode, thus accelerating Fenton's reaction (3) and the oxidation of organics with $^{\bullet}OH$ (Brillas et al., 2009). When a one-compartment cell with a BDD anode is used, the degradation of organic pollutants is additionally enhanced by the attack of BDD ($^{\bullet}OH$) formed from reaction (1) (Serra et al., 2009; Ruiz et al. 2011). The mineralization of aromatics can also be accelerated by exposing the contaminated solution to UVA light while is treated by EF (Brillas et al., 2004; Sirés et al., 2006; Ruiz et al., 2011). The main action of UVA irradiation is the photodecarboxylation of Fe(III)–carboxylate complexes.

The degradation of *N*-aromatics by EAOPs involves a high number of by-products that are simultaneously formed and destroyed by the different oxidizing species. Oxalic and oxamic acids are accumulated from the beginning of the process and their slow destruction limits the oxidation power of these methods. However, the influence of oxidants and/or UVA light on their removal, particularly of their iron species, is not well known yet.

To gain a better insight on the mineralization processes of oxalic and oxamic acids to better understand the degradation of *N*-aromatics, we report a study on the kinetics and oxidative paths of both acids by EAOPs with a BDD anode under typical treatment conditions of synthetic wastewaters with organics in sulfate medium. Special attention was taken on the action of Fe^{2+} and UVA light to clarify the destruction of their iron complexes. The oxidation of these compounds on BDD was analyzed by cyclic voltammetry (CV). The change in degradation rate of each acid when mixed in different proportions was examined. The effect of current density and Fe^{2+} content on oxamic acid removal was assessed. NH_4^+ and NO_3^- ions lost during the mineralization of oxamic acid were followed by ionic chromatography.

2. Materials and methods

2.1. Chemicals

Oxalic and oxamic acids were of analytical grade from Avocado. Anhydrous sodium sulfate, ferrous sulfate heptahydrate and ferric sulfate hydrate were of analytical grade from Fluka and Sigma. Solutions were prepared with high-purity water obtained from a Millipore Milli-Q system with resistivity > 18 MΩ cm at 25 °C. Organic solvents and other chemicals used were of HPLC or analytical grade from Aldrich, Lancaster, Merck and Panreac.

2.2. Apparatus

The solution pH was measured with a Crison GLP 22 pH-meter. CV was conducted with an Ecochemie Autolab PGSTAT100 potentiostat–galvanostat controlled by an Autolab Nova 1.5 software. Electrolyses were performed with an Amel 2053 potentiostat–galvanostat. The concentration of dissolved O_2 was determined with a Thermo Electron Corporation Orion 4 Star pH-DO portable with a Sensor Orion 083005MD DO probe. Total organic carbon (TOC) of solutions was measured with a Shimadzu VCSN TOC analyzer. Total nitrogen (TN) was determined with a Shimadzu TNM-1 unit coupled with the TOC analyzer. The concentration of oxalic and oxamic acids was quantified by ion-exclusion HPLC using a Waters 600 liquid chromatograph fitted with a Bio-Rad Aminex HPX 87H, 300 mm × 7.8 mm (i.d.), column at 35 °C,

coupled with a Waters 996 photodiode array detector at $\lambda = 210$ nm. Inorganic ions lost during oxamic acid degradation were detected by ionic chromatography using a Shimadzu 10 Avp HPLC coupled with a Shimadzu CDD 10 Avp conductivity detector. NH_4^+ concentration was obtained with a Shodex IC YK-421, 125 mm × 4.6 mm (i.d.), cation column at 40 °C, whereas NO_3^- content was determined with a Shim-Pack IC-A1S, 100 mm × 4.6 mm (i.d.), anion column at 40 °C.

2.3. Electrochemical systems

All electrolytic experiments were conducted in an open, undivided and thermostated cylindrical cell, so that all gases formed were directly released to the atmosphere. The anode was a BDD thin film provided by Adamant Technologies (La-Chaux-de-Fonds, Switzerland), while the cathode was either a stainless steel (AISI 304 grade) sheet (SS) or a carbon-PTFE air-diffusion electrode (ADE) from E-TEK (Somerset, NJ, USA). The preparation of the ADE cathode was described elsewhere (Brillas et al., 2004). It was fed with air pumped at 300 mL min^{-1} to generate H_2O_2 by reaction (2). The area of all electrodes was 3 cm^2 and the interelectrode gap was ca. 1 cm. To remove the impurities of the BDD surface and activate the ADE cathode, they were previously polarized in 0.05 M Na_2SO_4 at 300 mA for 60 min. The same cell without electrodes was used for the photochemical assays under UVA light.

Comparative photochemical and electrochemical degradations of 100 mL of 2.08 mM (50 mg L^{-1} of TOC) of oxalic (188 mg L^{-1}) or oxamic (185 mg L^{-1}) acid in 0.05 M Na_2SO_4 at pH 3.0 were performed. The photochemical assays with direct UVA exposition were made after addition of 0.5 mM Fe^{2+} (UVA-Fe^{2+}) or 0.5 mM Fe^{3+} (UVA-Fe^{3+}). The electrolytic methods were anodic oxidation with a BDD/SS cell (AO-BDD), the same treatment after addition of 0.5 mM Fe^{2+} (AO-BDD-Fe^{2+}) and under UVA illumination (AO-BDD-Fe^{2+}-UVA), and electro-Fenton with a BDD/ADE cell and 0.5 mM Fe^{2+} (EF-BDD). For the trials with UVA irradiation, a Philips TL/6W/08 fluorescent black light blue tube placed at 7 cm above the solution was employed. The tube emitted UVA light in the wavelength region 320–420 nm with $\lambda_{max} = 360$ nm, supplying a photoionization energy of 5 W m^{-2} as detected with a Kipp & Zonen CUV 5 radiometer. In all experiments, the solution was kept at 35.0 °C under vigorous stirring with a magnetic bar at 800 rpm to ensure its homogenization, as well as the transport of reactants towards/from the electrodes in the electrolytic assays.

CV measurements were carried out with a three-electrode one-compartment cell thermostated at 25 °C. The working electrode was a 0.40 cm^2 BDD, the counter reference was a Pt wire and the reference electrode was a Ag/AgCl/KCl (saturated) electrode ($E^\circ = 0.197$ V/SHE). Cyclic voltammograms were recorded at a scan rate of 100 mV s^{-1} under an Ar atmosphere after previous bubbling of this gas through the solution for 30 min.

2.4. Analytical procedures

Before analysis, aliquots withdrawn from treated solutions were filtered with 0.45 μm PTFE filters from Whatman. Reproducible TOC values with an accuracy of ±1% were found by injecting 50 μL aliquots to the TOC analyzer. The mineralization current efficiency (MCE) for electrolyzed solutions at time t (h) was then calculated by Eq. (4) (Hamza et al., 2009):

$$\mathrm{MCE}(\%) = \frac{nFV_s\Delta(\mathrm{TOC})_{exp}}{4.32 \times 10^7 mIt} \times 100 \quad (4)$$

where F is the Faraday constant (96487 C mol^{-1}), V_s is the solution volume (L), $\Delta(TOC)_{exp}$ is the experimental TOC removal (mg L^{-1}), 4.32×10^7 is a conversion factor (3600 s h^{-1} × 12,000 mg mol^{-1}), m is the number of carbon atoms of each acid (2 C atoms) and I is the current (A). The number of electrons (n) consumed was taken as 2 for oxalic acid and 10 for oxamic acid, assuming that their overall mineralization corresponds to reactions (5) and (6), respectively:

$$C_2H_2O_4 \rightarrow 2CO_2 + 2H^+ + 2e^- \quad (5)$$

$$C_2H_3NO_3 + 4H_2O \rightarrow 2CO_2 + NO_3^- + 11H^+ + 10e^- \quad (6)$$

The ion-exclusion HPLC measurements were made after injection of 20 μL aliquots into the liquid chromatograph and circulation of 4 mM H_2SO_4 at 0.6 mL min^{-1} as mobile phase. Ionic chromatography was performed with 25 μL aliquots using a mobile phase composed of 5.0 mM tartaric acid, 1.0 mM dipicolinic acid, 24.2 mM boric acid and 1.5 mM crown ether at 1.0 mL min^{-1} for NH_4^+ and 2.4 mM tris(hydroxymethyl)aminomethane and 2.5 mM phthalic acid of pH 4.0 at 1.5 mL min^{-1} for NO_3^-.

3. Results and discussion

3.1. CV behavior of oxalic and oxamic acids and their iron complexes

Fig. 1a shows the cyclic voltammograms obtained for the oxidation of 2.08 mM oxalic and oxamic acids in 0.05 M Na_2SO_4 on a BDD electrode at pH 3.0 and 100 mV s^{-1}. Both compounds display an irreversible peak, with an anodic peak potential (E_p^a) of 2.10 and 2.14 V for oxalic and oxamic acids, respectively, which partially overlap with that of water discharge to O_2 beginning at 2.2 V. The CV behaviour found for oxalic acid agrees with that reported by other authors (Martínez-Huitle et al., 2004; Weiss et al., 2007; Scialdone et al., 2008), who suggested the direct anodic oxidation of the acid at the BDD anode surface rather than its mediated reaction with BDD($^\bullet$OH) produced from reaction (1) to be converted into CO_2. This behavior can also be extended to the case of oxamic acid, which is oxidized at slightly higher potentials than oxalic acid and with a greater peak current due to the additional transformation of its $-NH_2$ group into inorganic ions.

The comparative cyclic voltammograms recorded for the above acids in the presence of 0.5 mM Fe^{2+} or 0.5 mM Fe^{3+} are depicted in Fig. 1b. Fe(II)– or Fe(III)–carboxylate complexes formed are oxidized at much more positive potentials than pure acids, clearly overlapping with the water discharge

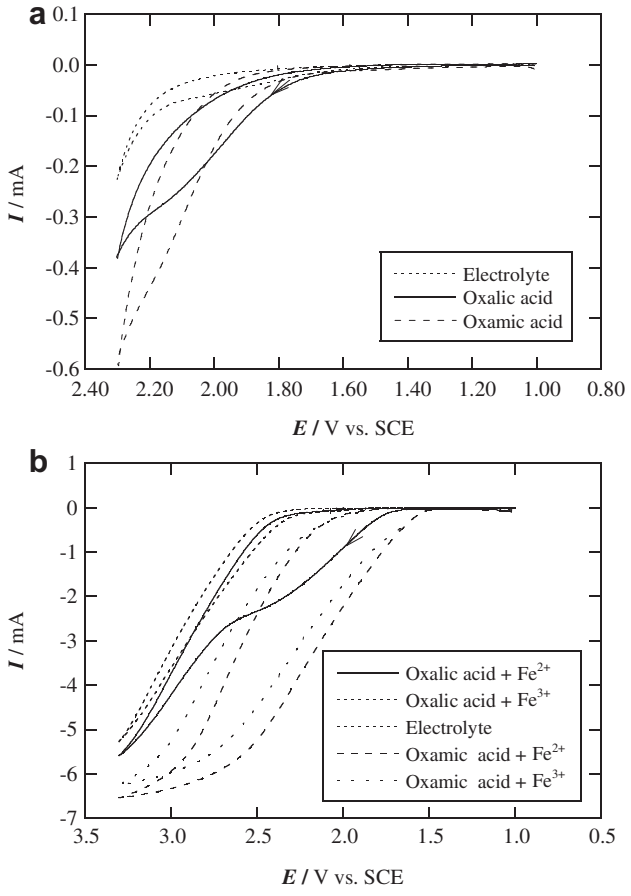

Fig. 1 – Cyclic voltammograms recorded for the oxidation of (a) 2.08 mM oxalic and oxamic acids and (b) their solutions with 0.5 mM Fe^{2+} or 0.5 mM Fe^{3+} in 0.05 M Na_2SO_4 of pH 3.0 on a 0.40 cm^2 boron-doped diamond (BDD) anode. Initial and final potentials 1.0 V, reversal potential: (a) 2.3 V and (b) 3.3 V. Scan rate 100 mV s^{-1}. Temperature 25 °C.

region. The irreversible peak for Fe(II)–oxalate complexes with $E_p^a = 2.31$ V has much higher height than that of oxalic acid (see Fig. 1a), as a result of the more complex oxidation of their electroactive species, predominantly $Fe^{II}(C_2O_4)_2^{2-}$ (Lan et al., 2010). In contrast, the dominant $Fe^{III}(C_2O_4)_3^{3-}$ and $Fe^{III}(C_2O_4)_2^{-}$ ions in the solution of Fe(III)–oxalate complexes (Balmer and Sulzberger, 1999; Kwan and Chu, 2007; Lan et al., 2010) are oxidized at so high potentials that any peak is displayed in CV. Fe(II)– and Fe(III)–oxamate complexes exhibit a similar irreversible peak, with high E_p^a of 2.54 and 2.72 V, respectively, suggesting that their ionic structures (not reported in literature) are analogous to those of iron–oxalate complexes, although the Fe(III)–oxamate species are more easily oxidizable. This is not surprising since oxamic like oxalic acid behaves as a bidentate ligand, coordinated with the amidic N, after ionization of one amidic H, and with the carboxylate O (Pardo et al., 2004). The fact that the iron complexes of oxalic and oxamic acids are destroyed in the water discharge zone indicates that they react predominantly with BDD(•OH) at the anode surface.

3.2. *Photochemical degradation of oxalic and oxamic acids and their iron complexes*

A series of trials were made to assess the degradation effect of the 6 W UVA light on 100 mL of the 2.08 mM acid solutions in the absence and presence of 0.5 mM Fe^{2+} or 0.5 mM Fe^{3+}. The evolution of each compound was monitored by ion-exclusion chromatography, which displayed a well-defined adsorption peak at retention time of 6.8 min for oxalic acid and 9.4 min for oxamic acid. Fig. 2a and b shows that both acids are very stable under UVA irradiation, as expected if they are not directly photolyzed. In contrast, their iron complexes are photodegraded at different rates depending on the acid and iron ion tested. The fastest removal was found for the UVA-Fe^{3+} treatment of oxalic acid, which disappears in about 150 min. Overall destruction of this acid is also feasible using UVA-Fe^{2+}, although a longer time close to 360 min is required. The kinetic analysis of these experiments showed good linear correlations for a pseudo first-order reaction. The pseudo first-order rate constant (k_{oxalic}) thus determined, along the corresponding square of regression coefficient, is collected in Table 1. The quick photodegradation of Fe(III)–oxalate

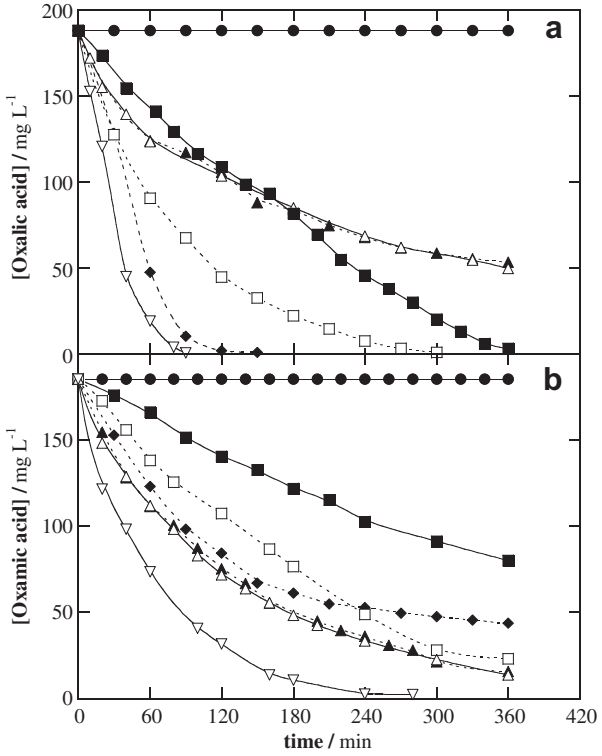

Fig. 2 – Decay of the concentration of (a) oxalic and (b) oxamic acids from 100 mL of 2.08 mM of each carboxylic acid in 0.05 M Na_2SO_4 at pH 3.0 and 35 °C. Method: (●) 6 W UVA irradiation (UVA), (■) 0.5 mM Fe^{2+} solution and UVA light (UVA-Fe^{2+}), (◆) 0.5 mM Fe^{3+} solution and UVA light (UVA-Fe^{3+}), (□) AO in BDD/stainless steel (SS) cell (AO-BDD), (△) AO-BDD with 0.5 mM Fe^{2+} (AO-BDD-Fe^{2+}), (▲) electro-Fenton (EF) in BDD/air-diffusion electrode (ADE) cell with 0.5 mM Fe^{2+} (EF-BDD) and (▽) AO-BDD with 0.5 mM Fe^{2+} under UVA irradiation (AO-BDD-Fe^{2+}-UVA). Current density of 33.3 mA cm^{-2} in all EAOPs.

Table 1 – Pseudo first-order rate constant and square regression coefficient (in parenthesis) for the decay of oxalic and oxamic acids during the degradation of 100 mL of 2.08 mM of each compound in 0.05 M Na_2SO_4 of pH 3.0 at 35 °C. The solution was irradiated with a 6 W UVA light and a current density of 33.3 mA cm^{-2} was applied in all EAOPs. The experiments with iron were carried out with 0.5 mM Fe^{2+} or 0.5 mM Fe^{3+}.

Method	$k_{oxalic} \times 10^4$ (s^{-1})	$k_{oxamic} \times 10^4$ (s^{-1})
UVA-Fe^{2+}	0.75 (0.995)	0.40 (0.978)
UVA-Fe^{2+} (O_2 sat.)	1.33 (0.988)	–[a]
UVA-Fe^{3+}	6.43 (0.985)	1.10 (0.996)
UVA-Fe^{3+} (O_2 sat.)	6.83 (0.984)	–[a]
AO-BDD	1.49 (0.999)	1.01 (0.993)
AO-BDD-Fe^{2+}	0.61 (0.986)	1.20 (0.998)
EF-BDD	0.61 (0.989)	1.15 (0.998)
AO-BDD-Fe^{2+}-UVA	9.01 (0.983)	2.82 (0.995)

a Not determined.

complexes can be accounted for by the high photoactivity of their dominant ionic species by reactions (7) and (8) (Faust and Zepp, 1993; Balmer and Sulzberger, 1999; Jeong and Yoon, 2005):

$$Fe^{III}(C_2O_4)_3^{3-} + h\nu \rightarrow Fe^{II}(C_2O_4)_2^{2-} + C_2O_4^{\bullet-} \quad (7)$$

$$Fe^{III}(C_2O_4)_2^{-} + h\nu \rightarrow Fe^{II}(C_2O_4) + C_2O_4^{\bullet-} \quad (8)$$

These reactions are photoredox processes with a ligand-to-metal charge transfer leading to the homolytic break of a Fe(III)–O coordination bond of the bidentate oxalate ligand (Šima and Makáňová, 1997). The anion radical $C_2O_4^{\bullet-}$ released yields CO_2 and the anion radical $CO_2^{\bullet-}$ by reaction (9), which then reacts with dissolved O_2 to produce the ion superoxide ($O_2^{\bullet-}$) from reaction (10). This species originates a cascade of other ROS like hydroperoxide radical ($HO_2^{\bullet}$) from reaction (11) and H_2O_2 from reaction (12). H_2O_2 can further oxidize the Fe(II) to Fe(III) complexes, as exemplified for $Fe^{II}(C_2O_4)_2^{2-}$ in reaction (13), at a rate about 1000 times higher than that of Fenton's reaction (3) (Faust and Zepp, 1993), thus closing the Fe(III)/Fe(II) catalytic loop. The large production of $^{\bullet}OH$ from the reaction (13), which does not attack the iron–oxalate complexes, has been well proven in photoassisted ferrioxalate systems (Jeong and Yoon, 2005; Rodríguez et al., 2007; Monteagudo et al., 2008).

$$C_2O_4^{\bullet-} \rightarrow CO_2 + CO_2^{\bullet-} \quad (9)$$

$$CO_2^{\bullet-} + O_2 \rightarrow CO_2 + O_2^{\bullet-} \quad (10)$$

$$O_2^{\bullet-} + H^+ \rightarrow HO_2^{\bullet} \quad (11)$$

$$O_2^{\bullet-} + HO_2^{\bullet} + H^+ \rightarrow H_2O_2 + O_2 \quad (12)$$

$$Fe^{II}(C_2O_4)_2^{2-} + H_2O_2 \rightarrow Fe^{III}(C_2O_4)_2^{-} + {}^{\bullet}OH + OH^- \quad (13)$$

The slow decay of oxalic acid in the UVA-Fe^{2+} system can then be related to the much lower photoactivity of Fe(II) complexes to be converted into Fe(III) ones, as exemplified by reaction (14) (Faust and Zepp, 1993; Kwan and Chu, 2007):

$$Fe^{II}(C_2O_4)_2^{2-} + h\nu \rightarrow Fe^{III}(C_2O_4)_2^{-} \quad (14)$$

Once the Fe(III)–oxalate complexes are formed, a photodegradation path similar to that described above for the UVA-Fe^{3+} treatment takes place, although the large preponderance of Fe(II)–oxalate complexes at the beginning of the process makes it slower.

The aforementioned experiments for oxalic acid were performed with 7.6 mg L^{-1} of dissolved O_2. To clarify the generation of ROS via reactions (10)–(12), the same trials were repeated with 28.0 mg O_2 L^{-1} in solution under O_2 bubbling at 0.5 L min^{-1}. Results of Table 1 confirm the increase in k_{oxalic} in both systems, much more for UVA-Fe^{2+} (1.77-fold) than for UVA-Fe^{3+} (1.06-fold). The excess of H_2O_2 formed under O_2 bubbling strongly accelerates the oxidation of $Fe^{II}(C_2O_4)_2^{2-}$ by reaction (13) in UVA-Fe^{2+}, while this reaction is only slightly enhanced in UVA-Fe^{3+} due to the much lower concentration of Fe(II) species.

Fig. 2b evidences that the very low photoactivity of Fe(II)– and Fe(III)–oxamate complexes only allows a 57% and 77% destruction of the acid after 360 min of UVA-Fe^{2+} and UVA-Fe^{3+} treatments, respectively. This is also reflected in the low pseudo first-order rate constant (k_{oxamic}) values obtained (see Table 1). As can be seen in Fig. 3, a larger percentage of its initial N is lost as NH_4^+ (43% for UVA-Fe^{2+} and 65% for UVA-Fe^{3+}) at the end of these trials, although the oxidation to NO_3^- is significant in both cases (9% of initial N for UVA-Fe^{2+} and 12% of initial N for UVA-Fe^{3+}). Note that for the UVA-Fe^{2+} system, about 5% of initial N is released as volatile compounds, probably NO_x species.

3.3. *Mineralization of oxalic acid by EAOPs*

Comparative degradations of 100 mL of 2.08 mM oxalic acid by different EAOPs were made at 33.3 mA cm^{-2}. Fig. 2a shows that

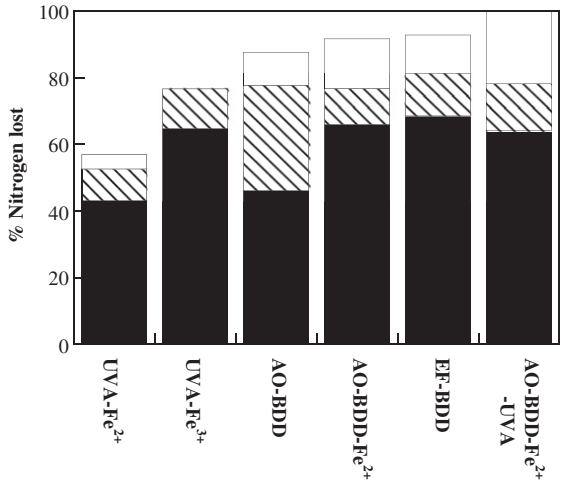

Fig. 3 – Percentage of nitrogen released as (■) NH_4^+ ion, (▨) NO_3^- ion and (▭) NO_x species at the end of the trials of Fig. 2b for oxamic acid.

this acid is completely removed at 300 min of the AO-BDD treatment, since it is transformed into CO_2 by direct oxidation at the anode, as stated above. When 0.5 mM Fe^{2+} is added to the solution, a strong inhibition of oxalic acid decay occurs during the AO-BDD-Fe^{2+} process, only being reduced by 72% after 360 min of electrolysis. A similar tendency can be observed in Fig. 2a for the EF-BDD system, where the large generation of H_2O_2 from the ADE cathode favors the rapid conversion of Fe(II)– into Fe(III)–oxalate complexes, e.g. via reaction (13). This suggests that in AO-BDD-Fe^{2+}, the initial Fe(II)–oxalate complexes are quickly oxidized to Fe(III)–oxalate species by BDD(•OH) at the anode surface. This oxidation is also feasible with H_2O_2 since it is produced in low amounts from dimerization of BDD(•OH) by reaction (15) (Guinea et al., 2009):

$$2BDD(^{\bullet}OH) \rightarrow 2BDD + H_2O_2 \quad (15)$$

The slow destruction of Fe(III)–oxalate complexes with BDD(•OH), as confirmed by CV (see Fig. 1b), then explains the similar and slow abatement of the acid in AO-BDD-Fe^{2+} and EF-BDD, without oxidation by •OH formed from Fenton's reaction (3). From these results, the effect of UVA illumination was studied for the AO-BDD-Fe^{2+}-UVA treatment. Fig. 2a shows that this EAOP leads to total destruction of the acid in only 90 min, as expected from the rapid photolysis of Fe(III)–oxalate complexes. Since a steady concentration of 13 mg O_2 L^{-1} was reached in this trial, significant amounts of H_2O_2 are formed from reaction (12), which contribute to the oxidation of Fe(II)– to Fe(III)–oxalate complexes.

The k_{oxalic} value obtained for the above EAOPs is listed in Table 1. It increased 1.40-fold for the most potent AO-BDD-Fe^{2+}-UVA system compared with UV-Fe^{3+}, as expected if the photoactive Fe(III)–oxalate species are more quickly regenerated, involving its oxidation with H_2O_2 from reaction (13) and with BDD(•OH) at the anode surface.

TOC was always removed in a similar way to oxalic acid due to the insignificant formation of by-products. For example, after 360 min of AO-BDD-Fe^{2+} and EF-BDD, TOC was reduced to 13 mg L^{-1}, corresponding to 49 mg L^{-1} oxalic acid in good agreement with 52 mg L^{-1} found for the final electrolyzed solutions (see Fig. 2a). Total mineralization was achieved after about 300 min of AO-BDD and close to 90 min of AO-BDD-Fe^{2+}-UVA, times similar to those required for the total removal of oxalic acid, as shown in Fig. 2a. The efficiency calculated from Eq. (4) decreased with electrolysis time by the gradual drop in oxalic acid content. For example, the MCE value decayed from 7.2% or 12.5% at 10 min to 1.6% or 6.7% at the end of the AO-BDD or AO-BDD-Fe^{2+}-UVA treatment.

From the above results, the reaction sequence of Fig. 4 is proposed for oxalic acid mineralization by AO-BDD-Fe^{2+}-UVA. It is initiated by the oxidation of $Fe^{II}(C_2O_4)_2^{2-}$ with BDD(•OH) to yield $Fe^{III}(C_2O_4)_2^-$, in equilibrium with $Fe^{III}(C_2O_4)_3^{3-}$. These ionic species are quickly photolyzed regenerating $Fe^{II}(C_2O_4)$ and $Fe^{II}(C_2O_4)_2^{2-}$, respectively, with the loss of CO_2 and $CO_2^{\bullet-}$. Further reaction of $CO_2^{\bullet-}$ with O_2 originates CO_2 and ROS. The catalytic loop between Fe(II)– and Fe(III)–oxalate complexes is then propagated by the continuous oxidation of $Fe^{II}(C_2O_4)_2^{2-}$ with BDD(•OH) and ROS (primordially H_2O_2). All ionic species can also be oxidized to CO_2 at the BDD anode, although reactions with BDD(•OH) are much slower than the photodegradation of Fe(III) species with UVA light. A slow oxidation of oxalic acid, in equilibrium with the above complexes, at the anode is also feasible.

3.4. Mineralization of oxamic acid by EAOPs

The degradation of 2.08 mM oxamic acid solutions by the same EAOPs always followed a pseudo first-order abatement. Fig. 2b evidences that AO-BDD-Fe^{2+} and EF-BDD processes yield the same decay rate for this acid, as expected if its Fe(II) complexes are oxidized by BDD(•OH) with insignificant participation of •OH in the bulk. Both treatments are more potent than AO-BDD because of the most effective destruction of Fe(III)–oxamate complexes by BDD(•OH) than that of oxamic acid by direct charge transfer. Comparison of Fig. 2a and b evidences that AO-BDD-Fe^{2+} and EF-BDD methods are more effective for the abatement of oxamic than oxalic acid, in agreement with the higher oxidation ability of Fe(III)–oxamate species at BDD (see Fig. 1b). Fig. 2b also shows that oxamic acid disappears in 270 min for AO-BDD-Fe^{2+}-UVA. Since k_{oxamic} for this method is 2.56 times higher than for UV-Fe^{3+} (see Table 1), one can infer that Fe(III)–oxamate species are rapidly formed from the oxidation of Fe(II)–oxamate ones with BDD(•OH) and generated H_2O_2 to be photolyzed by UVA light regenerating the Fe(II) species with loss of CO_2 and inorganic N products. Results of Table 1 indicate that $k_{oxalic} > k_{oxamic}$ for AO-BDD and AO-BDD-Fe^{2+}-UVA, while $k_{oxalic} < k_{oxamic}$ for AO-BDD-Fe^{2+} and EF-BDD. That means that oxamic acid is more recalcitrant than oxalic acid only in the two former methods, but not in the two latter. For the EAOPs tested, TOC was removed similarly to oxamic acid, indicating the formation of insignificant amounts of organic by-products during all mineralization processes. In addition, the progressive loss in oxidizable organic matter caused a continuous fall in MCE.

Fig. 3 illustrates the predominance of N lost as NH_4^+ ion at the end of all EAOPs tested to mineralize the 2.08 mM oxalic acid solution at 33.3 mA cm^{-2}. The larger proportion of N lost as NO_3^- ion is found for AO-BDD, indicating that NH_4^+ ion is preferentially formed during the oxidation of Fe(III)–oxamate species than oxamic acid. TN analysis of final electrolyzed solutions confirmed the release of N as NO_x species. For AO-BDD-Fe^{2+}-UVA, for example, the initial 29.6 mg L^{-1} of N was reduced to 23.1 mg L^{-1} in 270 min, i.e. when all oxamic acid is mineralized, corresponding to a loss of 21.9% of N as NO_x species, a value close to 21.8% determined from the N obtained for NH_4^+ (64%) and NO_3^- (14.2%), as depicted in Fig. 3.

3.5. Mineralization of mixtures of oxalic and oxamic acids by EAOPs

Since a mixture of oxalic and oxamic acids is obtained as ultimate by-product of the degradation of N-aromatics by EAOPs (Sirés et al., 2006; Hammami et al., 2008; Hamza et al., 2009), the possible influence of the relative proportion of both acids on their removal rate was investigated. To do this, 8%, 25% and 43% of oxamic acid were added to the 2.08 mM oxalic acid solution to be treated by AO-BDD, AO-BDD-Fe^{2+} and AO-BDD-Fe^{2+}-UVA at 33.3 mA cm^{-2}, after adding 0.5 mM Fe^{2+} in the two latter methods. The k_{oxamic} and k_{oxalic} values

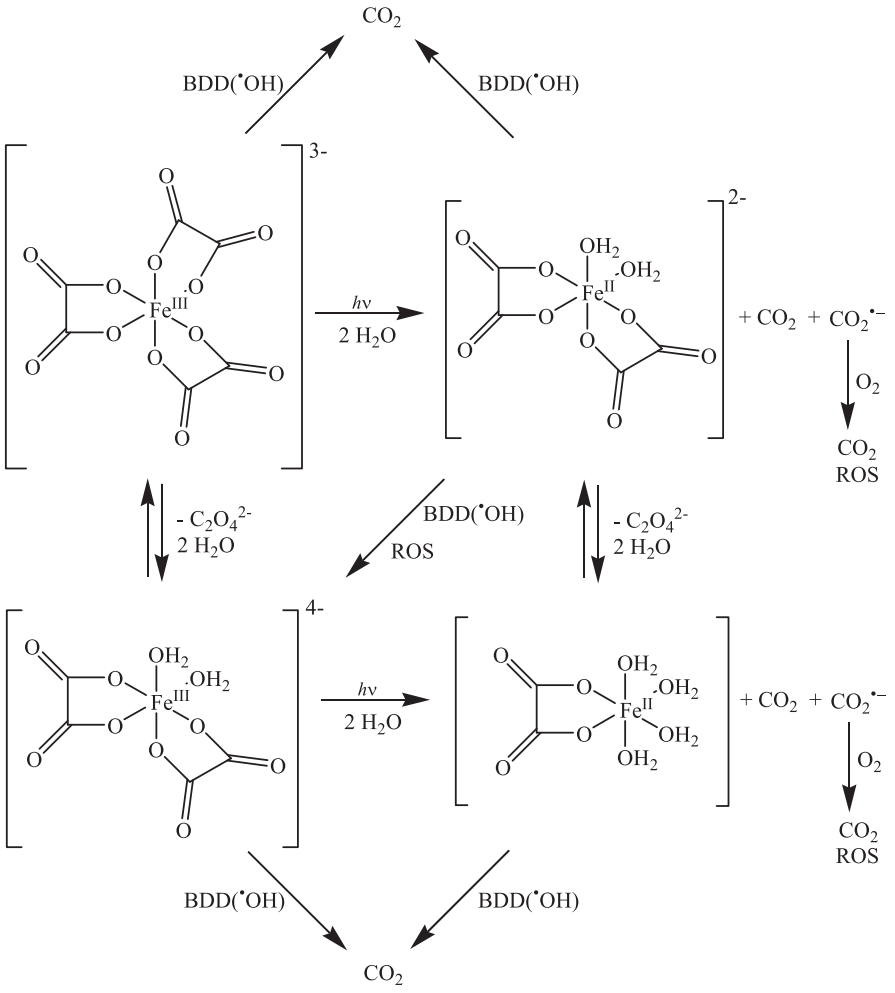

Fig. 4 – Proposed reaction sequence for the mineralization of Fe(III)–oxalate complexes in acidic aqueous medium by EAOPs with Fe^{2+} as catalyst under UVA irradiation using a BDD anode.

determined simultaneously for these experiments are summarized in Table 2.

For AO-BDD, similar $k_{oxamic} \sim 1.1 \times 10^{-4}\ s^{-1}$ and $k_{oxalic} \sim 1.5 \times 10^{-4}\ s^{-1}$ to that of pure solutions (see Table 1) are found, evidencing that both acids are independently oxidized at the BDD anode via direct charge transfer. In contrast, the competition between Fe(III)–oxamate and Fe(III)–oxalate complexes causes a change in the removal rate of acids in the EAOPs with Fe^{2+}. Thus, for AO-BDD-Fe^{2+}, k_{oxalic} gradually decays with decreasing the percentage of oxamic acid, while $k_{oxamic} \sim 1.3 \times 10^{-4}\ s^{-1}$ is similar to $1.2 \times 10^{-4}\ s^{-1}$ for pure iron–oxamate complexes (see Table 1). This deceleration of oxalic acid removal is due to the progressive formation of a larger proportion of Fe(III)–oxalate complexes that are more difficultly oxidized with BDD(•OH). The much faster destruction of Fe(III)–oxamate species with this radical explains the slight change in k_{oxamic} in all mixtures. The smaller amount of Fe(III)–oxamate species formed and the rise in Fe(III)–oxalate ones with decreasing the percentage of oxamic acid are also reflected in AO-BDD-Fe^{2+}-UVA, where the low photoactivity of the former accounts for the drop in k_{oxamic}, whereas the much greater photoactivity of the latter justifies the slight increase in k_{oxalic}. A slower removal of oxamic acid is then expected as its content decreases, without significant effect on oxalic acid decay.

Table 2 – Pseudo first-order rate constant and square regression coefficient (in parenthesis) determined for the decay of oxamic and oxalic acids during the degradation of 100 mL solutions of 2.08 mM oxalic acid and different percentages of oxamic acid by several EAOPs at 33.3 mA cm^{-2}.

% Oxamic acid	AO-BDD		AO-BDD-Fe^{2+}		AO-BDD-Fe^{2+}-UVA	
	$k_{oxamic} \times 10^4$ (s^{-1})	$k_{oxalic} \times 10^4$ (s^{-1})	$k_{oxamic} \times 10^4$ (s^{-1})	$k_{oxalic} \times 10^4$ (s^{-1})	$k_{oxamic} \times 10^4$ (s^{-1})	$k_{oxalic} \times 10^4$ (s^{-1})
43	1.05 (0.989)	1.53 (0.998)	1.33 (0.987)	1.03 (0.995)	2.27 (0.992)	7.65 (0.990)
25	1.12 (0.997)	1.54 (0.996)	1.27 (0.989)	0.97 (0.980)	2.00 (0.999)	7.62 (0.993)
8	1.12 (0.993)	1.50 (0.998)	1.36 (0.991)	0.72 (0.988)	1.61 (0.993)	7.90 (0.981)

3.6. Effect of current density and Fe^{2+} content on the mineralization of oxamic acid by AO-BDD-Fe^{2+}-UVA

The abatement of TOC and oxamic acid content between 16.6 and 100 mA cm^{-2} for the most potent AO-BDD-Fe^{2+}-UVA process is presented in Fig. 5a and b, respectively. The rise in current density accelerates the decay of both parameters, enhancing the oxidation power of the process. The time required for overall mineralization (see Fig. 5a) is slightly longer than that needed for total destruction of the acid (see Fig. 5b), as expected if very low amounts of more recalcitrant by-products are formed. A progressive loss in MCE as current density increases can be observed in the inset panel of Fig. 5a, whereas the opposite trend is found for k_{oxamic} in the inset panel of Fig. 5b, which gradually increases from 1.48×10^{-4} s^{-1} ($R^2 = 0.999$) for 16.6 mA cm^{-2} to 3.15×10^{-4} s^{-1} ($R^2 = 0.996$) for 100 mA cm^{-2}. This behavior agrees with the expected production of more amounts of oxidant BDD(•OH) from reaction (1) at greater current density (Brillas et al., 2009; Panizza and Cerisola, 2009), accelerating the oxidation of Fe(II) into Fe(III) complexes to be more quickly photolyzed by UVA light. The loss in efficiency evidences that the excess of generated BDD(•OH) is mainly wasted by oxidation to O_2 via reaction (16) (Marselli et al., 2003; Panizza and Cerisola, 2009):

$$2\text{BDD}(^{\bullet}\text{OH}) \rightarrow 2\ \text{BDD} + \text{O}_2 + 2\text{H}^+ + 2\text{e}^- \quad (16)$$

The evolution of NH_4^+ and NO_3^- ions detected during 360 min in the above experiments is shown in Fig. 6a and b, respectively. NH_4^+ ion is continuously accumulated up to 33.3 mA cm^{-2}, but it undergoes a gradual drop as electrolysis time is prolonged at current densities $\geq$ 66.6 mA cm^{-2}. The fast removal of NH_4^+ ion at 100 mA cm^{-2} is accompanied by a large NO_3^- accumulation, while much lower contents of this ion are found at lower current densities. Increasing percentages of N lost as NO_x species of 15.3%, 21.8%, 44.0% and 55.5% were thus determined for 16.6, 33.3, 66.6 and 100 mA cm^{-2}, also confirmed from TN analysis of final electrolyzed solutions. These findings suggest that high current densities accelerate the parasite oxidation of NH_4^+ to NO_3^- ion with the greater amounts of BDD(•OH) produced, increasing the loss of NO_x species. This suggestion was corroborated by electrolyzing a $(NH_4)_2SO_4$ solution with 20 mg L^{-1} of N under similar conditions. For 100 mA cm^{-2}, NH_4^+ ion was totally removed in 270 min generating 4.6 mg L^{-1} of N as NO_3^- ion and releasing 78% of N as NO_x species. In contrast, after 360 min of electrolysis at 33.3 mA cm^{-2}, 11.3 mg L^{-1} of N as NH_4^+ ion and 1.2 mg L^{-1} of N as NO_3^- ion were found, with loss of 37% of N as NO_x species. Note that NH_4^+ is converted into NO_3^- in larger extent in the treatment of $(NH_4)_2SO_4$ than oxamic acid,

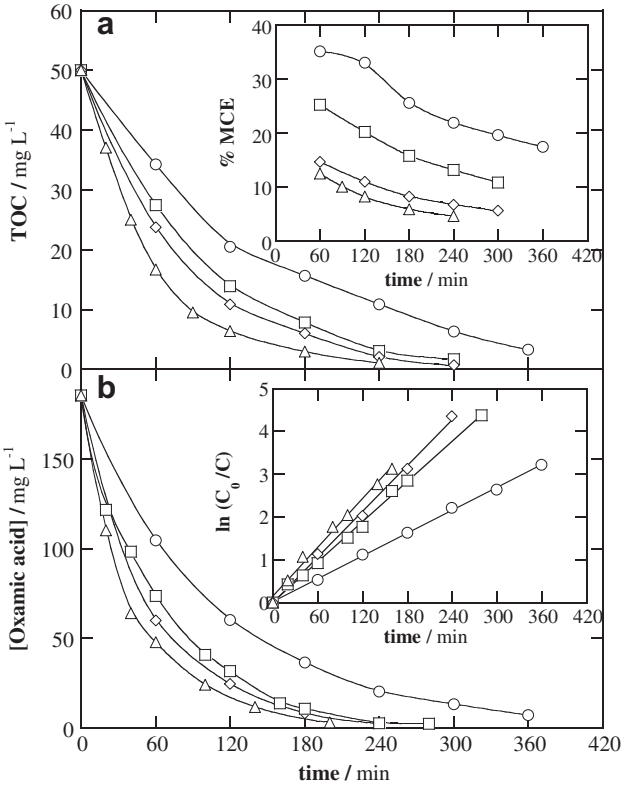

Fig. 5 – Effect of current density on (a) TOC removal and (b) concentration decay for the AO-BDD-Fe^{2+}-UVA treatment of 100 mL of 2.08 mM oxamic acid in 0.05 M Na_2SO_4 with 0.5 mM Fe^{2+} at pH 3.0 and 35 °C. Current density: (○) 16.6 mA cm^{-2}, (□) 33.3 mA cm^{-2}, (◇) 66.6 mA cm^{-2} and (△) 100 mA cm^{-2}. The inset panels show (a) the mineralization current efficiency calculated from Eq. (4) and (b) the kinetic analysis assuming a pseudo first-order reaction for oxamic acid.

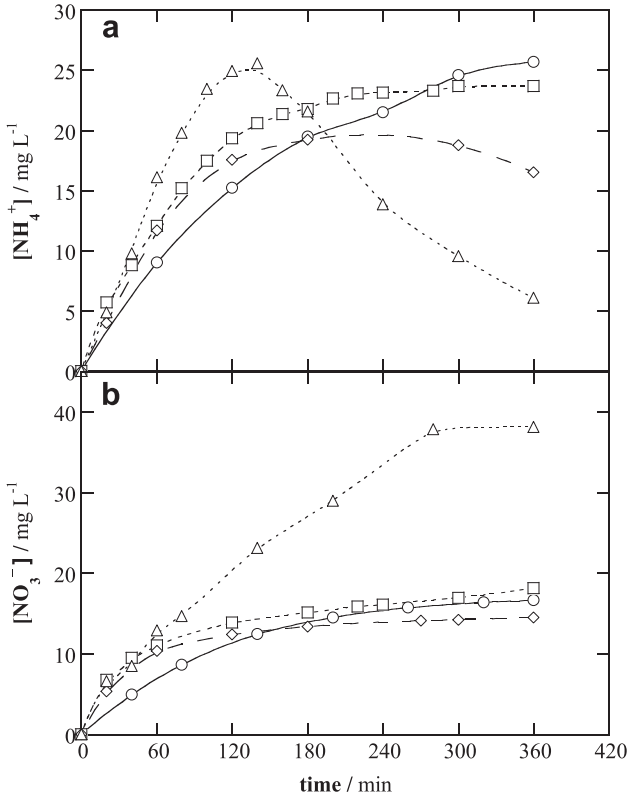

Fig. 6 – Evolution of the concentration of (a) ammonium and (b) nitrate ions released during the experiments of Fig. 5.

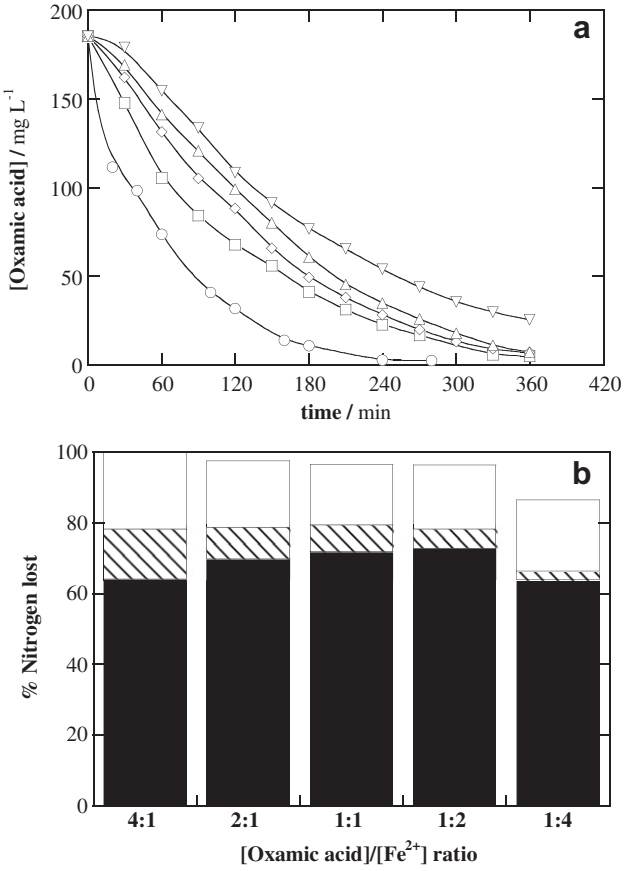

Fig. 7 – (a) Effect of Fe^{2+} content on the decay of oxamic acid concentration for the AO-BDD-Fe^{2+}-UVA degradation of 100 mL of 2.08 mM of the carboxylic acid in 0.05 M Na_2SO_4 at pH 3.0, 33.3 mA cm^{-2} and 35 °C. [Oxamic acid]/[Fe^{2+}] ratio: (○) 4:1, (□) 2:1, (◇) 1:1, (△) 1:2 and (▽) 1:4. (b) Percentage of nitrogen lost as (■) NH_4^+ ion, (▨) NO_3^- ion and (▭) NO_x species vs. [oxamic acid]/[Fe^{2+}] ratio at the end of these experiments.

probably because NH_4^+ ion is gradually released to the medium in the latter case and its oxidation at the BDD anode competes with that of iron–oxamate complexes.

Fig. 7a evidences that oxamic acid removal is inhibited with increasing Fe^{2+} content. This trend can be related to a gradual decay in rate of the reaction between Fe(II)–oxamate species and BDD(•OH), decelerating its conversion into photoactive Fe(III) complexes, due to the competition of the oxidation of larger amounts of free Fe^{2+} to Fe^{3+} ion at the anode (Sirés et al., 2007). The reduction of Fe^{3+} ion at the SS cathode regenerates the Fe^{2+} ion and maintains the equilibrium between both ions in solution (Brillas et al., 2009). The loss of oxidation ability of the system is also reflected in Fig. 7b, where higher Fe^{2+} content causes a gradual decay in the percentage of N lost as NO_3^- ion and a larger proportion of N lost as NH_4^+ ion, with a similar percentage of N lost as NO_x species. The presence of small amounts of Fe^{2+} in solution then minimizes the undesired oxidation of Fe^{2+} at the anode, favouring the rapid conversion of Fe(II)–oxamate complexes into photoactive Fe(III)–oxamate species.

4. Conclusions

Oxalic and oxamic acids were efficiently mineralized by AO-BDD-Fe^{2+}-UVA, as a result of the high photoactivity of their Fe(III) complexes that are continuously regenerated by oxidation of their Fe(II) complexes with BDD(•OH) formed at the anode surface and H_2O_2 generated from O_2 reduction or BDD(•OH) dimerization. In this method, oxamic acid was more recalcitrant by the lower photoactivity of its Fe(III) complexes, releasing a larger proportion of NH_4^+ than NO_3^- ion. The loss of volatile NO_x species was confirmed from TN analysis of the final electrolyzed solutions. Each acid underwent a similar decay in AO-BDD-Fe^{2+} and EF-BDD since its iron complexes were not attacked with •OH in the bulk. AO-BDD also allowed the total conversion of oxalic acid into CO_2 by direct charge transfer at the anode. This process explained the slower destruction of oxamic acid by this method. In contrast, oxamic acid was less recalcitrant in AO-BDD-Fe^{2+} and EF-BDD, since Fe(III)–oxamate complexes were oxidized more quickly with BDD(•OH) than Fe(III)–oxalate ones. TOC always decayed similarly to the corresponding acid, indicating a insignificant formation of by-products. While both acids when mixed were independently oxidized at the anode in AO-BDD, the proportion of their Fe(III) complexes and their ability to be oxidized and/or photolyzed affected their degradation rate in the EAOPs with Fe^{2+}. For the most potent AO-BDD-Fe^{2+}-UVA, a lower oxamic acid content decelerated its degradation, without significant effect on oxalic acid decay. Greater current density enhanced the oxidation power of this method since oxamic acid removal was accelerated, but losing efficiency. High Fe^{2+} contents inhibited the oxidation of Fe(II)–oxamate complexes by the competitive oxidation of free Fe^{2+} to Fe^{3+}. Low current densities and Fe^{2+} contents are then preferable for the more efficient removal of these acids in AO-BDD-Fe^{2+}-UVA.

Acknowledgements

The authors acknowledge financial support from MICINN (Ministerio de Ciencia e Innovación, Spain) under the project CTQ2010-16164/BQU, cofinanced with FEDER funds. S. G.-S. thanks the grant awarded from MEC (Ministerio de Educación y Ciencia, Spain).

REFERENCES

Andreozzi, R., Caprio, V., Insola, A., Marotta, R., 1999. Advanced oxidation processes (AOP) for water purification and recovery. Catal. Today 53 (1), 51–59.

Balci, B., Oturan, N., Cherrier, R., Oturan, M.A., 2009. Degradation of atrazine in aqueous medium by electrocatalytically generated hydroxyl radicals. A kinetic and mechanistic study. Water Res. 43 (7), 1924–1934.

Balmer, M.E., Sulzberger, B., 1999. Atrazine degradation in irradiated iron/oxalate systems: effects of pH and oxalate. Environ. Sci. Technol. 33 (14), 2418–2424.

Brillas, E., Baños, M.A., Camps, S., Arias, C., Cabot, P.L., Garrido, J.A., Rodríguez, R.M., 2004. Catalytic effect of Fe^{2+}, Cu^{2+} and UVA

light on the electrochemical degradation of nitrobenzene using an oxygen-diffusion cathode. New J. Chem. 28 (2), 314–322.
Brillas, E., Sirés, I., Oturan, M.A., 2009. Electro-Fenton process and related electrochemical technologies based on Fenton's reaction chemistry. Chem. Rev. 109 (12), 6570–6631.
Brillas, E., Garcia-Segura, S., Skoumal, M., Arias, C., 2010. Electrochemical incineration of diclofenac in neutral aqueous medium by anodic oxidation using Pt and boron-doped diamond anodes. Chemosphere 79 (6), 605–612.
Cañizares, P., García-Gómez, J., Lobato, J., Rodrigo, M.A., 2003. Electrochemical oxidation of aqueous carboxylic acid wastes using diamond thin-film electrodes. Ind. Eng. Chem. Res. 42 (5), 956–962.
Cañizares, P., Beteta, A., Saez, C., Rodríguez, L., Rodrigo, M.A., 2008. Use of electrochemical technology to increase the quality of the effluents of bio-oxidation processes. A case studied. Chemosphere 72 (7), 1080–1085.
Diagne, M., Oturan, N., Oturan, M.A., 2007. Removal of methyl parathion from water by electrochemically generated Fenton's reagent. Chemosphere 66 (5), 841–848.
Faria, P.C.C., Órfão, J.J.M., Pereira, M.F.R., 2008. Activated carbon catalytic ozonation of oxamic and oxalic acids. Appl. Catal. B: Environ. 79 (3), 237–243.
Faust, B.C., Zepp, R.G., 1993. Photochemistry of aqueous iron(III)-polycarboxylate complexes: roles in the chemistry of atmospheric and surface waters. Environ. Sci. Technol. 27 (12), 2517–2522.
Gandini, D., Mahé, E., Michaud, P.A., Haenni, W., Perret, A., Comninellis, Ch, 2000. Oxidation of carboxylic acids at boron-doped diamond electrodes for wastewater treatment. J. Appl. Electrochem. 30 (12), 1345–1350.
Guinea, E., Centellas, F., Garrido, J.A., Rodríguez, R.M., Arias, C., Cabot, P.L., Brillas, E., 2009. Solar photoassisted anodic oxidation of carboxylic acids in presence of Fe^{3+} using a boron-doped diamond electrode. Appl. Catal. B: Environ. 89 (3–4), 459–468.
Hammami, S., Bellakhal, N., Oturan, N., Oturan, M.A., Dachraoui, M., 2008. Degradation of acid orange 7 by electrochemically generated ·OH radicals in acidic aqueous medium using a boron-doped diamond or platinum anode. A mechanistic study. Chemosphere 73 (5), 678–684.
Hamza, M., Abdelhedi, R., Brillas, E., Sirés, I., 2009. Comparative electrochemical degradation of the triphenylmethane dye methyl violet with boron-doped diamond and Pt anodes. J. Electroanal. Chem. 627 (1–2), 41–50.
Jeong, J., Yoon, J., 2005. pH effect on OH radical production in photo/ferrioxalate system. Water Res. 39 (13), 2893–2900.
Kwan, C.Y., Chu, W., 2007. The role of organic ligands in ferrous-induced photochemical degradation of 2,4-dichlorophenoxyacetic acid. Chemosphere 67 (8), 1601–1611.
Lan, Q., Li, F.B., Sun, C.X., Liu, C.S., Li, X.Z., 2010. Heterogeneous photodegradation of pentachlorophenol and iron cycling with goethite, hematite and oxalate under UVA illumination. J. Hazard. Mater. 174 (1–3), 64–70.
Martínez-Huitle, C.A., Ferro, S., De Battisti, A., 2004. Electrochemical incineration of oxalic acid: role of electrode material. Electrochim. Acta 49 (22–23), 4027–4034.
Marselli, B., García-Gómez, J., Michaud, P.A., Rodrigo, M.A., Comninellis, Ch, 2003. Electrogeneration of hydroxyl radicals on boron-doped diamond electrodes. J. Electrochem. Soc. 150 (3), D79–D83.
Monteagudo, J.M., Durán, A., López-Almodóvar, C., 2008. Homogeneus ferrioxalate-assisted solar photo-Fenton degradation of orange II aqueous solutions. Appl. Catal. B: Environ. 83 (1–2), 46–55.
Oturan, M.A., Pimentel, M., Oturan, N., Sirés, I., 2008. Reaction sequence for the mineralization of the short-chain carboxylic acids usually formed upon cleavage of aromatics during electrochemical Fenton treatment. Electrochim. Acta 54 (2), 173–182.
Özcan, A., Şahin, Y., Koparal, A.S., Oturan, M.A., 2008. Propham mineralization in aqueous medium by anodic oxidation using boron-doped diamond anode. Experimental parameters' influence on degradation kinetics and mineralization efficiency. Water Res. 42 (12), 2889–2898.
Panizza, M., Cerisola, G., 2009. Direct and mediated anodic oxidation of organic pollutants. Chem. Rev. 109 (12), 6541–6569.
Pardo, E., Lloret, F., Carrasco, R., Muñoz, M.C., Temporal-Sánchez, T., Ruiz-García, R., 2004. Chemistry and reactivity of dinuclear iron oxamate complexes: alkane oxidation with hydrogen peroxide catalysed by an oxo-bridged diiron(III) complex with amide and carboxylate ligation. Inorg. Chim. Acta 357 (9), 2713–2720.
Pera-Titus, M., García-Molina, V., Baños, M.A., Giménez, J., Esplugas, S., 2004. Degradation of chlorophenols by means of advanced oxidation processes: a general review. Appl. Catal. B: Environ. 47 (4), 219–256.
Rodríguez, E., Mimbrero, M., Masa, F.J., Beltrán, F.J., 2007. Homogeneous iron-catalyzed photochemical degradation of muconic acid in water. Water Res. 41 (6), 1325–1333.
Ruiz, E.J., Arias, C., Brillas, E., Hernández-Ramírez, A., Peralta-Hernández, J.M., 2011. Mineralization of acid yellow 36 azo dye by electro-Fenton and solar photoelectro-Fenton processes with a boron-doped diamond anode. Chemosphere 82 (4), 495–501.
Scialdone, O., Galia, A., Guarisco, C., Randazzo, S., Filardo, G., 2008. Electrochemical incineration of oxalic acid at boron doped diamond anodes: role of operative parameters. Electrochim. Acta 53 (5), 2095–2108.
Serra, A., Domènech, X., Arias, C., Brillas, E., Peral, J., 2009. Oxidation of α-methylphenylglycine under Fenton and electro-Fenton conditions in the dark and in the presence of solar light. Appl. Catal. B: Environ. 89 (1–2), 12–21.
Šima, J., Makáňová, J., 1997. Photochemistry of iron(III) complexes. Coord. Chem. Rev. 160, 161–189.
Sirés, I., Garrido, J.A., Rodríguez, R.M., Cabot, P.L., Centellas, F., Arias, C., Brillas, E., 2006. Electrochemical degradation of paracetamol from water by catalytic action of Fe^{2+}, Cu^{2+}, and UVA light on electrogenerated hydrogen peroxide. J. Electrochem. Soc. 153 (1), D1–D9.
Sirés, I., Centellas, F., Garrido, J.A., Rodríguez, R.M., Arias, C., Cabot, P.L., Brillas, E., 2007. Mineralization of clofibric acid by electrochemical advanced oxidation processes using a boron-doped diamond anode and Fe^{2+} and UVA light as catalysts. Appl. Catal. B: Environ. 72 (3–4), 373–381.
Sirés, I., Brillas, E., Cerisola, G., Panizza, M., 2008. Comparative depollution of mecoprop aqueous solutions by electrochemical incineration using BDD and PbO_2 as high oxidation power anodes. J. Electroanal. Chem. 613 (2), 151–159.
Sun, Y., Pignatello, J.J., 1993. Photochemical-reactions involved in the total mineralization of 2,4-D by Fe^{3+}/H_2O_2/UV. Environ. Sci. Technol. 27 (2), 304–310.
Vandini, T.A., Rao, T.N., Fujishima, A., Einaga, Y., 2006. Electrochemical oxidation of oxalic acid at highly boron-doped diamond electrodes. Anal. Chem. 78 (10), 3467–3471.
Weiss, E., Groenen-Serrano, K., Savall, A., Comninellis, Ch, 2007. A kinetic study of the electrochemical oxidation of maleic acid on boron doped diamond. J. Electroanal. Chem. 37 (1), 41–47.
Zuo, Y., Hoigné, J., 1992. Formation of hydrogen peroxide and depletion of oxalic acid in atmospheric water by photolysis of iron(III)-oxalato complexes. Environ. Sci. Technol. 26 (5), 1014–1022.
Zuo, Y., Hoigné, J., 1994. Photochemical decomposition of oxalic, glyoxalic and pyruvic acid catalysed by iron in atmospheric waters. Atmos. Environ. 28 (7), 1231–1239.

Electrochemical Advanced Oxidation Processes applied to the treatment of wastewaters polluted with azo dyes

During the last years our research group LEMMA has started to investigate the remediation of industrial effluents from dying industries (Ruiz et al., 2011; Salazar et al., 2011; Almeida et al., 2012; Moreira et al., 2013; Ramírez et al., 2013). Large volumes of these coloured wastewaters are discharged into water bodies such as lakes and rivers, where they cause aesthetic problems and serious health and environmental risks because of the toxicity, carcinogenic and mutagenic properties of dyes and its by-products (Sharma et al., 2007; Umbuzeiro et al., 2005). Even at low concentrations, these pollutants are able to dye completely huge water volumes.

Azo dyes, which are characterized by the presence of one or more azo bonds as chromophore group, represent about 70 % of the world dye production. Azo dyes are highly persistent under ambient conditions and hardly removed under biological conventional treatments in sewage treatment plants (Robinson et al., 2001). One of the main targets on dyes treatment is the color removal which is the most visible pollution effect. So, powerful oxidation processes are required for the destruction of these POPs to avoid their adverse impact and EAOPs emerge as promising technologies that allows the decolorization and removal of these polluted water bodies.

This section reports the degradation of synthetic wastewaters polluted with four azo dyes Acid Orange 7 (AO7), Acid Red 151 (AR151), Direct Blue 71 (DB71) and Direct Yellow 4 (DY4) by several EAOPs. The color removal process has received special attention due to its industrial interest. The SPEF process for DY4 solutions was scaled-up to a 10 L pre-pilot flow plant completely autonomous with electric energy provided by a 50 W solar photovoltaic panel, evidencing the possibility of the renewable energy use and maintenance costs reduction. Lastly, due to the identification of phthalic acid and their derivatives during the naphthalenic rings cleavage (Isarain-Chávez et al., 2011; Moreira et al., 2013), a genuine study on phthalic acid degradation by the EAOPs tested with a complete characterization of by-products was carried out. Phthalic acid and phthalate derivatives are the major industrial materials used as plasticisers to manufacture plastic products. These products are classified as priority pollutants by USEPA (United States Environmental Protection Agency 7407, 1994) due to their adverse effects on living beings (Oishi and Hiraga, 1980; Makoto et al., 1997). Consequently, their removal study is of great interest by itself as well as to better understand the degradation pathways of azo dyes with naphthalenic groups.

The decolorization process represents the first step for the remediation of waters containing azo dyes and in some cases the generated by-products are biodegradable and less toxic. This process was deeply studied by trying to clarify the influence of the number of azo bonds per dye molecule. For this purpose, the destruction of the monoazo AO7, diazo AR151 and triazo DB71 was tested by EF. These azo dyes present similar structures with equal functional groups such as –OH and $–SO_3^-$ groups.

The role of $^{\bullet}OH$ generated in EF was assessed by comparison with the direct AO using Pt/ADE, BDD/ADE, Pt/graphite and BDD/graphite cells. From these results, the reduction of the azo bond on the graphite cathode was demonstrated, but it cannot take place on the ADE because this cathode mainly involves the bielectronic reduction of O_2 to H_2O_2. That fact is of extreme relevance since the reduction processes usually affect negatively the degradation processes (El-Ghenymy et al., 2012, 2013a), which are avoidable using an ADE cathode. The comparison of these four AO processes with the EF treatment showed that the main oxidant of the azo dyes is the $^{\bullet}OH$ produced in the bulk from Fenton's reaction (10), instead of the radicals formed at the anode surface.

The results obtained for the decolorization of solutions evidenced the high photostability of azo dyes that were not discoloured by UVA radiation (Martínez-Huitle and Brillas, 2009) since they were only degraded by the action of $^{\bullet}OH$ radicals generated in the processes.

The effect of the number of azo bonds on the decolorization process was assessed from the change of the azo dye concentration and the applied current density. For this purpose, the color removal vs time, the k_{dec} value calculated as the slope of the corresponding $\ln(A_0/A)$-t plot and the real pseudo-first order rate determined from the dye concentration decay were determined. Furthermore, a new comparative parameter so-called initial decoloration rate (δ_0) was introduced, being defined as the slope of the linear fitting between the percentage of color removal and t at the beginning of the process, i.e. up to 20-25% of the absorbance decay when the dye is the main responsible of the solution color because of the low content of intermediates generated.

The plot of δ_0 with dye concentration revealed a gradual and quick decay when the dye concentration increased. The initial decolorization rate decreased in the sequence monoazo > diazo> triazo indicating that $^{\bullet}OH$ reacts more slowly at higher number of azo bonds, thereby making the decolorization process less potent. If the same δ_0 results were

plotted versus the azo bond concentration in solution instead of the dye concentration, higher differences were found in the same sequence (monoazo> diazo > triazo). This was justified by the greater activation energy needed for the electrophilic attack of •OH radicals when the number of azo bonds per molecule increases due to the formation of larger and more stable conjugated π systems.

Table 11 shows a similar δ_0 value for the diazos DY4 and AR151 at the same azo bond concentration in solution and applied density current, evidencing the high influence of the number of azo bonds as a control parameter. The diazo dye AR151 contains two benzenic and one naphthalenic ring, whereas the DY4 contains four benzenic rings. The increase in aromatic conjugated rings is a structural effect that increases the stabilization of the π systems decreasing the decolorization rate, although this effect is not appreciable in this case. As far as it is known, naphthalene rings introduce higher stability than benzenic rings, but the presence of an additional benzenic ring in the DY4 structure compensates the additional stabilisation of the naphtalene ring in AR151 and hence, the stabilisation of both dyes by their π systems is quite similar.

The δ_0 determined for DY4 in the pre-pilot flow plant was almost the half value obtained for the stirred tank reactor (**Table 11**). This difference was related to the different electrode area/volume ratio that is appreciably lower in the pre-pilot flow plant where a considerably higher volume is treated and consequently, a lower concentration of •OH is active to attack the organic matter. The lower concenration of •OH and the greater volumes treated in the pre-pilot plant make the process slower justifying the smaller δ_0 values found, which would be enhanced coupling more electrochemical cells.

Table 11. *Initial decolorization rate (δ_0) determined for the EF treatment of 100 mL of solutions of the azo dyes AO7, AR151, DB71and DY4 with a concentration equivalent to 0.600 mM of azo bonds in 0.05 mM Na_2SO_4 with 0.50 mM Fe^{2+} at pH 3.0, 35 ºC and 33.3 mA cm^{-2}. Initial decolorization rate for 10 L of 0.600 mM azo bonds concentration of DY4 in the pre-pilot plant by SPEF treatment under the same conditions.*

	AO7	AR151	DB71	DY4	DY4 pre-pilot plant
δ_0 / s^{-1}	0.175	0.121	0.091	0.122	0.055

In the case of the SPEC treatment, the maximum dye concentrations treatable and the times needed to achieve a complete color removal were very far away from the highly efficient EAOPs. For 15 mg L^{-1} AO7 in 0.05 M Na_2SO_4 of pH 7, complete color removal was achieved in 120 min by SPEC, whereas SPC and AO showed only 21% and 41% of color removal after 300 min. These findings confirmed that the SPEC process was synergistic and not cumulative from the SPC and AO processes because only 45% was attained form the sum of both treatments at 120 min.

The dye concentration affects directly the efficiency of the SPEC treatment showing that greater concentration results in a gradual loss in color removal. This behaviour can be associated with the increasing consumption of $^{\bullet}OH$ by more amounts of organics formed on the TiO_2 surface, along with a fall in photogeneration efficiency because of the loss of solution transparency with rising dye content (Fujishima et al., 2008). The results evidenced good color removal rates up to 15 mg L^{-1} of AO7, which can be taken as the best concentration for SPEC application.

The influence of applied current density was also evaluated for the EAOPs. The δ_0-j plots showed a linear relationship between 16.7 and 83.3 mA cm^{-2} for all the azo dyes, but with lower relative increases for each dye in the sequence monoazo> diazo> triazo. This smaller reactivity was related to an increase in rate of the parasitic reactions of $^{\bullet}OH$ because of the greater stability of the dyes with higher number of azo bonds per molecule. The decolorization pseudo-first order rate (k_{dec}) determined from the absorbance decay and the pseudo-first-order rate constant (k_1) found from the compound decay using HPLC increased when j rose. Both parameters showed a similar trend to that predicted for δ_0 confirming the validity of the analysis performed with this parameter on the decolorization ability of EF. However, k_{dec} cannot be used to predict the comparative total decolorization of the initial dye due to the large accumulation of more recalcitrant colored intermediates that induce an appreciable error. The difference between the concentration decay and the absorbance abatement evidenced that the solution color was not related to the dye concentration by the Lambert-Beer law because of the generation of some by-products with the same or similar λ_{max} to the treated dye. This effect was well reflected in the UV-vis spectra of the DY4 solution registered at different times, as can be seen in **Fig. 13,** where the intensity of both bands dropped rapidly during the first 20-25 min of electrolysis, as expected if non-conjugated molecules are gradually formed. Besides, the maximal of 400 nm of the major band was

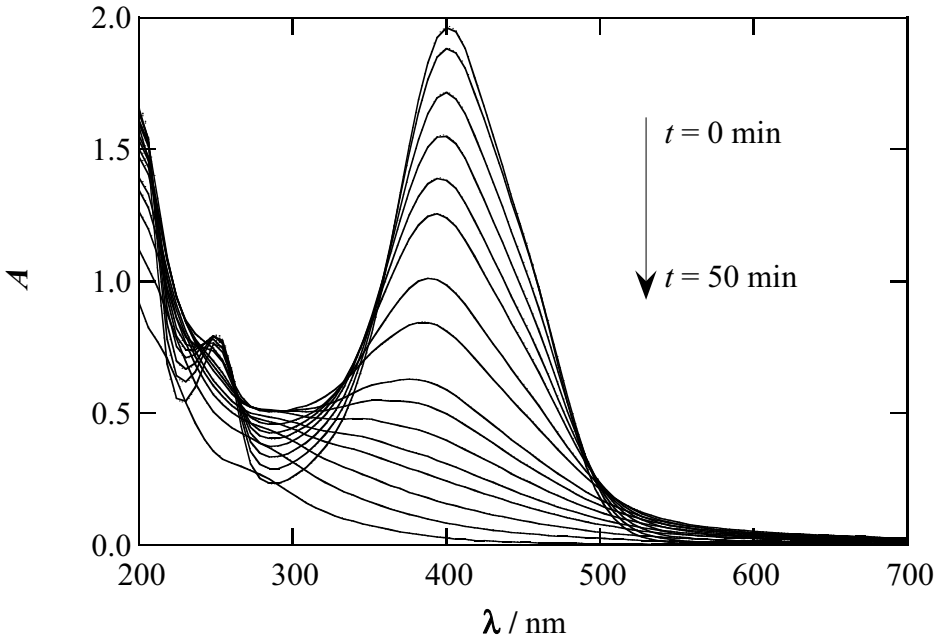

Figure 13. *UV–vis spectra recorded for the DY4 solution up to 50 min of electrolysis for the degradation of 100 mL of a 200 mg L^{-1} DY4 solution in 0.05 M Na_2SO_4 with 0.5 mM Fe^{2+} at pH 3.0, 33.3 mA cm^{-2} and 35 ºC by EF.*

progressively shifted to a lower value of 348 nm and this band was simultaneously widened, suggesting the generation of colored by-products.

When the effect of the anodic current density on decolorization and decay kinetics was studied for SPEC, it showed that a j_{anod} as low as 0.23 mA cm^{-2} enhanced strongly the decolorization efficiency of the solution compared with SPC. The increase of j_{anod} to 1.0 mA cm^{-2} caused a quicker color removal owing to a faster electron-hole separation at the photoanode. The dye concentration decay showed a similar behaviour as well as increasing k_1 values at higher j_{anod}. Even though it cannot compete with the quicker removal of EAOPs, the remarkably lower energy consumption in comparison makes it an interesting process to study and improve.

The evaluation of the mineralization during the EAOPs of solutions containing 200 mg L^{-1} of DY4 in 0.05 M Na_2SO_4 with 0.5 mM Fe^{2+} at pH 3.0 and 35 ºC confirmed the feasibility of these electrochemical processes for wastewater remediation. The knowledge obtained for the EF and PEF processes in previous works with drugs and carboxylic acids allowed us the better understanding of the photo-Fenton process and the proposal of a new process so-called photo-assisted electro-Fenton (PA-EF). Complete color removal

was obtained at 40 min of treatment at j = 33.3 mA cm^{-2}. The time required for total decolorization decreased with rising j. The DOC evolution showed almost a complete removal by PEF and only an 83% by EF, as expected by the accumulation of carboxylic acids. The innovative PA-EF process consisted in stop the electrochemical process and start the solution irradiation when all the carboxylic acids are generated and accumulated and no aromatic compounds remain in solution. So, the PA-EF process attained a similar mineralization degree to PEF although with a considerable lower energy consumption.

The carboxylic acid analysis sheds light on the role played by UVA irradiation. It revealed, for example, that maleic acid is not photolyzed by UVA but it is efficiently oxidized by $^{\bullet}$OH. In contrast, the complexes of Fe(III) and oxalic acid, accumulated in major extent, justifies the efficiency of the PA-EF process. Unexpectedly, oxamic acid was largely produced under UVA light, probably by photolysis of some *N*-intermediates that accelerates its production helping to achieve the total mineralization.

The slower mineralization in the pre-pilot plant by SPEF facilitated the identification of more carboxylic acids as DY4 intermediates. These acids had longer chains than the recalcitrant oxalic acid and were quickly destroyed by the action of generated $^{\bullet}$OH. Their fast removal justified their difficult identification in the tank reactor system. Although longer times were required in the pre-pilot plant for the treatment of high volumes of dying effluents, the SPEF treatment was suitable for their remediation. Furthermore, the use of photovoltaic energy that is environmentally friendly and a renewable energy source evidenced that SPEF could be applied without energy consumption making it really interesting and affordable.

During the SPEC treatment of AO7, phthalic, tartaric, succinic, acetic and oxamic acids were detected as generated carboxylic acids. The sum of the DOC of these species represented the 86% of DOC of the final solution. Except oxamic acid, all these acids were formed from the beginning of the SPEC treatment. These findings corroborate the low ability of $^{\bullet}$OH produced in the SPEC process to destroy the recalcitrant carboxylic acids, where the last carboxylic acid, oxalic acid, was not generated.

Under EF and PEF conditions, only the 30% of total N contained in DY4 remained in solution, corresponding to a similar concentration of NH_4^+ and NO_3^-, about 6 and 7 mg L^{-1}, respectively. In contrast, the PA-EF process yielded a higher N concentration of 44.6 % in solution due to a higher accumulation of both NH_4^+ and NO_3^- ions (around 9 mg L^{-1}

in both cases). These findings demonstrate that the *N* remaining in solution is mainly transformed into inorganic ions, although the major part of N of DY4 is lost as volatile derivatives (such as N_2 and NOx species) as it is usual in azo-compounds (Moreira et al., 2013). The smaller accumulation of ions in EF and PEF than in PA-EF suggests that the *N*-volatile derivatives proceed from the oxidation with $^{\bullet}OH$ and BDD($^{\bullet}OH$).

When the evolution of N was analyzed for the SPEF process in the pre-pilot plant, higher percentages of N were transformed into NH_4^+. This phenomenon could be related to the higher photoefficiency of the CPC photoreactor that allows a major generation of inorganic species, like in the case of PA-EF.

The same effect as in EF and PEF occurred in SPEC, where the major part of N (80.8%) was loss as volatile derivatives like N_2 or NOx. This large loss of N as volatile species could be explained by the main rupture of azo bond releasing highly stable N_2.

LC-MS analysis of initially electrolyzed DY4 solutions by SPEF allowed the identification of eleven aromatic compounds and twenty two hydroxylated derivatives. By-products formed by the consecutive breaking of the two azo bonds of the dye and from the deamination, desulfonation, hydroxylation, nitration and carboxylation of their benzenic groups were detected and a complete degradation pathway from these results was proposed.

The breakage of naphthalenic rings of azo dyes led to phthalic acid as by-product (Özcan et al., 2009; Isarain-Chávez et al., 2011; Moreira et al., 2013) and due to their toxicity, a further study of this compound was carried out for a better knowledge of its mineralization pathway by EAOPs. The phthalic acid decay by AO, EF and SPEF was analyzed by HPLC using iron and copper ions and their mixtures as Fenton's catalysts. Phthalic acid was removed at similar rates by all the methods mainly because the poor reduction of Fe^{3+} and Cu^{2+} to the catalytic species Fe^{2+} and Cu^{+} decreasing the production of $^{\bullet}OH$ by Fenton's reaction (10) and making the BDD($^{\bullet}OH$) radical as the main oxidizing species. The DOC removal evidenced higher efficiencies for SPEF due to the quick removal of metal-carboxylate complexes by photolysis. The treatment in the presence of Cu^{2+} yielded lower and slower photodegradation than with Fe^{3+}. Surprisingly, however, the assays realized with mixtures of both metallic ions led to

Table 12. *Stability constants for carboxylic acids generated as intermediates and complexed with iron or copper ions at different ionic strengths (Smith and Martell, 1977).*

Acid	Metallic center	Complexes	Log k, 25 ºC, I=0.1	Log k, 25 ºC, I=1.0	Log k, 25 ºC, I=0
Acetic	Cu^{2+}	[ML]/ [M][L]	1.83	1.71	2.22
		$[ML_2]/ [M][L]^2$	3.09	2.71	3.63
		$[ML_3]/ [M][L]^3$	--	3.10	3.58
		$[ML_4]/ [M][L]^4$	--	2.90	3.30
	Fe^{2+}	[ML]/ [M][L]	--	--	1.40
	Fe^{3+}	[ML]/ [M][L]	3.38	3.20	--
Formic	Cu^{2+}	[ML]/ [M][L]	1.38	1.40	2.00
		$[ML_2]/ [M][L]^2$	--	2.30	--
		$[ML_3]/ [M][L]^3$	--	2.68	--
		$[ML_4]/ [M][L]^4$	--	1.90	--
	Fe^{3+}	[ML]/ [M][L]	--	3.10	--
Fumaric	Cu^{+}	[ML]/ [M][L]	--	--	2.51
	Cu^{2+}	[ML]/ [M][L]	3.96	--	--
Maleic	Cu^{+}	[ML]/ [M][L]	3.05	--	--
	Cu^{2+}	[ML]/ [M][L]	3.40	--	--
		$[ML_2]/ [M][L]^2$	5.48	--	--
		$[ML_3]/ [M][L]^3$	6.20	--	--
Malic	Cu^{2+}	[ML]/ [M][L]	3.42	--	--
	Fe^{3+}	[ML]/ [M][L]	7.10	--	--
Malonic	Cu^{2+}	[ML]/ [M][L]	5.03	4.63	5.70
	Fe^{2+}	[ML]/ [M][L]	--	2.17	--
		$[ML_2]/ [M][L]^2$	--	3.21	--
	Fe^{3+}	[ML]/ [M][L]	7.57	7.50	--
		$[ML_2]/ [M][L]^2$	--	13.04	--
		$[ML_3]/ [M][L]^3$	--	16.60	--
Oxalic	Cu^{2+}	[ML]/ [M][L]	4.85	5.53	6.23
		$[ML_2]/ [M][L]^2$	9.81	9.54	10.27
	Fe^{2+}	[ML]/ [M][L]	--	3.05	--
		$[ML_2]/ [M][L]^2$	--	5.15	--
	Fe^{3+}	[ML]/ [M][L]	7.53	7.58	7.74
		$[ML_2]/ [M][L]^2$	13.64	13.81	
		$[ML_3]/ [M][L]^3$	18.49	18.6	
Pyruvic	Cu^{2+}	[ML]/ [M][L]	1.40	2.20	1.35
		$[ML_2]/ [M][L]^2$	2.60	4.90	2.05
	Fe2+	[ML]/ [M][L]	--	0.69	--
Tartaric	Cu^{2+}	[ML]/ [M][L]	2.5	2.65	--
		$[ML_2]/ [M][L]^2$	--	4.38	--
	Fe^{2+}	[ML]/ [M][L]	2.24	1.43	--
		$[ML_2]/ [M][L]^2$	--	2.50	--
	Fe^{3+}	[ML]/ [M][L]	--	5.73	--
Tartronic	Cu^{2+}	[ML]/ [M][L]	5.31	--	--
Succinic	Cu^{2+}	[ML]/ [M][L]	2.60	--	3.28
	Fe2+	[ML]/ [M][L]	1.40	--	--
	Fe^{3+}	[ML]/ [M][L]	6.88	--	--

faster and higher removal rates due to synergistic effects involving photodecarboxylation with Fe^{2+} regeneration and enhancement of $^{\bullet}OH$ production which is able to mineralize the Cu(II) complexes (Flox et al., 2006; Salazar et al., 2012). In some cases, the Cu(II) complexes are preferentially formed compared to the iron ones (see **Table 12**) and are faster mineralized by $^{\bullet}OH$ and BDD($^{\bullet}OH$) and poorly photolyzed. In contrast, the Fe(III) complexes are slowly mineralized by BDD($^{\bullet}OH$) and quickly photolyzed (Guinea et al., 2009; Garcia-Segura and Brillas, 2011). Using a mixture of 0.125 mM of Cu^{2+} and 0.375 mM of Fe^{3+}, DOC was reduced by 99% in 240 min while phthalic acid disappeared in less than 60 min, illustrating the high efficiency of SPEF for this pollutant remediation. From LC-MS, eleven aromatic by-products of phthalic acid were detected, while ion-exclusion HPLC allowed identifying six short-linear carboxylic acids. From all these oxidation products, a plausible degradation pathway, which will be applicable whenever phthalic acid or phthalates would be found as by-products of azo dyes, was finally proposed.

PAPER 4

Comparative decolorization of monoazo, diazo and triazo dyes by electro-Fenton process

Electrochimica Acta 58 (2011) 303–311

Contents lists available at SciVerse ScienceDirect

Electrochimica Acta

journal homepage: www.elsevier.com/locate/electacta

Comparative decolorization of monoazo, diazo and triazo dyes by electro-Fenton process

Sergi Garcia-Segura, Francesc Centellas, Conchita Arias, José A. Garrido, Rosa M. Rodríguez, Pere L. Cabot[1], Enric Brillas*,[1]

Laboratori d'Electroquímica dels Materials i del Medi Ambient, Departament de Química Física, Facultat de Química, Universitat de Barcelona, Martí i Franquès 1-11, 08028 Barcelona, Spain

ARTICLE INFO

Article history:
Received 29 July 2011
Received in revised form
17 September 2011
Accepted 19 September 2011
Available online 29 September 2011

Keywords:
Acid Orange 7
Acid Red 151
Direct Blue 71
Decolorization rate
Electro-Fenton

ABSTRACT

The decolorization process of the monoazo Acid Orange 7, diazo Acid Red 151 and triazo Direct Blue 71, with similar aromatics and functional groups, has been comparatively studied by electro-Fenton. Solutions of 100 cm^3 of each azo dye in 0.05 mol dm^{-3} Na_2SO_4 with 0.5 mmol dm^{-3} Fe^{2+} of pH 3.0 were electrolyzed in an undivided BDD/air-diffusion cell under galvanostatic conditions. Organics were oxidized with hydroxyl radicals formed at the BDD anode from water oxidation and mainly in the bulk from Fenton's reaction between cathodically generated H_2O_2 and added Fe^{2+}. A simple parameter so-called initial decolorization rate was used to analyze the behaviour of the azo dyes at the beginning of the process. This parameter decreased with increasing initial azo bonds concentration due to the oxidation of more organic matter with similar amounts of hydroxyl radicals. It rose linearly with current density by the greater production of these oxidants, even when similar color removal was found at long electrolysis times, indicating that the process was mass-transfer controlled. The initial decolorization rate became lower as the number of azo bonds in the molecule increased owing to their smaller reactivity with hydroxyl radicals. Reversed-phase HPLC of electrolyzed solutions revealed the total removal of all azo dyes following a pseudo first-order kinetics with rate constants that showed the same trends as those predicted by initial decolorization rates. The pseudo first-order rate constants for decolorization obtained from absorbance decay also showed similar tendencies, but they were not useful to describe the comparative total decolorization of azo dye solutions because of the slower and parallel destruction of colored conjugated intermediates formed during the electro-Fenton treatment.

1. Introduction

Azo dyes are mainly used in textile and food industries and represent about 70% of the world dye production. The chemical structure of these compounds contains one or various azo groups (–N=N–) as chromophore, conjugated with aromatic systems [1]. Acid azo dyes, for example, have sulfonic groups that allow a strong attachment to the cationic groups of fibers. Moreover, they are used for manufacturing paints, inks, plastics and leather. The main problem of azo dyes is that they are discharged in large quantities in the environment from industrial effluents. The entrance of these pollutants in natural waters causes esthetic problems because of the visible colorization of the water even at low concentration, as well as serious health risks due to their toxicity to aquatic organisms and humans [2,3]. Azo dyes are very stable in the environment owing to their persistence under natural oxidation and reduction conditions, light exposure and biodegradation [1,4].

Different methods have been tested to remove azo dyes from waters to avoid their environmental problems and hazardous effects on living beings. Several studies have reported that physicochemical treatments like coagulation [5], adsorption [6] or filtration by selective membranes [7] enable the decolorization of dyeing wastewaters, but generating large volumes of sludge or requiring regular maintenance for adsorbents or membranes regeneration. Some biotreatments [8,9] have also been applied to decolorize these wastewaters. However, fast and even total decolorization of dyeing wastewaters has been found using powerful oxidation methods like ozonation [7,8] and advanced oxidation processes (AOPs) [1,4,10].

Recently, electrochemical AOPs (EAOPs) have received great attention for water remediation. The most typical EAOP is anodic oxidation (AO) in which organics are destroyed by hydroxyl radicals generated at the surface of a high O_2-overpotential anode like

* Corresponding author. Tel.: +34 93 4021223; fax: +34 93 4021231.
E-mail address: brillas@ub.edu (E. Brillas).
[1] ISE Active Member.

0013-4686/$ – see front matter © 2011 Elsevier Ltd. All rights reserved.
doi:10.1016/j.electacta.2011.09.049

boron-doped diamond (BDD) from water oxidation by reaction (1) [11–15]:

$$BDD + H_2O \rightarrow BDD(^{\bullet}OH) + H^+ + e^- \quad (1)$$

where BDD(•OH) denotes the in situ hydroxyl radical formed. The •OH radical has so high standard reduction potential (E°(•OH/H_2O) = 2.80 V vs SHE) that can non-selective react with most organics until overall mineralization, that is, conversion into CO_2, water and inorganic ions. It has been found that BDD thin-film electrodes are preferable for AO because they interact very weakly with generated •OH resulting in a much greater O_2-overpotential than other conventional anodes such as PbO_2 [16] or Pt [17] and in an enhancement of organic removal with reactive BDD(•OH), thus being potent enough to mineralize aromatic pollutants and their generated carboxylic acids up to CO_2 [1,15,18,19].

The most common EAOP based on Fenton's reaction chemistry is the electro-Fenton (EF) process, which enhances the degradation of organics compared with AO [20–22]. In EF, H_2O_2 is continuously supplied to a contaminated acidic solution by the two-electron reduction of injected O_2 at the cathode from reaction (2), whereas Fe^{2+} ion is added to react with this species to generate Fe^{3+} ion and •OH in the bulk from Fenton's reaction (3), which is mainly propagated by the cathodic reduction of Fe^{3+} ion to Fe^{2+} ion from reaction (4) [22,23]:

$$O_2 + 2H^+ + 2e^- \rightarrow H_2O_2 \quad (2)$$

$$Fe^{2+} + H_2O_2 \rightarrow Fe^{3+} + {}^{\bullet}OH + OH^- \quad (3)$$

$$Fe^{3+} + e^- \rightarrow Fe^{2+} \quad (4)$$

Cathodes like carbon nanotubes-PTFE [24–26], carbon nanotubes on graphite [27], carbon felt [23,28–32], carbon cloth [33], carbon fiber [34], BDD [35] and carbon-PTFE gas (O_2 or air) diffusion [36–42] have shown a good efficiency for H_2O_2 generation from reaction (2). When an undivided cell with a BDD anode is used in EF, organics can be destroyed simultaneously by BDD(•OH) formed from reaction (1) and •OH produced in the bulk from Fenton's reaction (3) [22,30,32,36,37,41].

The effectiveness of EF to decolorize waters containing dyes, including some monoazo dyes, has been well proven [20,28–30,33–35,40–42]. The decolorization process represents a first step for the remediation of such waters because by-products with oxygenated functional are produced, which are usually biodegradable and much less toxic than the starting dyes [1,22]. However, the EF treatment of dyes with various azo bonds has not been reported. The clarification of these processes can be of interest because it can offer relevant information on the oxidation power of hydroxyl radicals on complex azo molecules. To do this, we have undertaken a study on the decolorization of the monoazo Acid Orange 7 (AO7), diazo Acid Red 151 (AR151) and triazo Direct Blue 71 (DB71) by EF. Note that using TiO_2/UV photocatalysis, it has been found that the reactivity of similar aromatic azo dyes with hydroxyl radicals is affected by the number of –OH substituents, without significant influence of the number of $–SO_3^-$ groups present in the molecule [43]. To minimize these effects, the azo dyes tested were chosen with analogous aromatics, one –OH group and one or various $–SO_3^-$ substituents, as can be seen in Table 1 where their characteristics are also summarized. AO7 and AR151 are widely used for dyeing natural fibers like wool, silk and cotton, as well as synthetic fibers like polyesters and acrylics, whereas DB71 is used in biology for the detection of proteins by staining [44]. Contradictory trends for their comparative decolorization have been described by other technologies. Thus, any relationship between the number of azo bonds and degradation kinetics was found from TiO_2 photocatalysis [45], while longer decolorization time with increasing the number of azo bonds was obtained by applying ozonation [46,47]. In contrast, bioremoval with brown-rot fungi decolorized more rapidly waters with the diazo dye AR151 than the monoazo dye AO7 [48].

In this article, we present the results obtained for the comparative decolorization of AO7, AR151 and DB71 by EF using an undivided BDD/air-diffusion cell. The effect of the number of azo bonds on the decolorization process was assessed from the change of both, the azo dye concentration and applied current density. A new and simple parameter so-called initial decolorization rate (δ_0) was used to analyze the behaviour of the above compounds at the beginning of the EF process. Its predicted trends were compared with those established from the pseudo first-order rate constant for decolorization (k_{dec}) and for dye decay (k_1), determined from the absorbance and concentration decays measured by UV–vis spectroscopy and reversed-phase high-performance liquid chromatography (HPLC), respectively.

2. Experimental

2.1. Chemicals

Commercial pure azo dyes AO7 and DB71 supplied by Acros Organics España (Madrid, Spain) and AR151 purchased from TCI Europe (Antwerp, Belgium) were used as received. Iron (II) sulfate heptahydrate, used as catalyst, and anhydrous sodium sulfate, used as background electrolyte, were of analytical grade from Fluka (Buchs, Switzerland) and Merck (Darmstad, Germany), respectively. Solutions were prepared with pure water obtained from a Millipore Milli-Q system (Molsheim, France) with resistivity >18 MΩ cm at 25 °C. All solutions were adjusted to pH 3.0 with analytical grade sulfuric acid from Merck. All the other chemicals employed were either of HPLC or analytical grade from Panreac (Barcelona, Spain) and Acros Organics España.

2.2. Electrochemical system

All the electrolytic experiments were conducted in an undivided and cylindrical cell of 150 cm^3 capacity, with a double jacket in which external water circulated to maintain the solution temperature at 35 °C. The anode was a BDD thin film provided by Adamant Technologies (La Chaux-de-Fonds, Switzerland), while the cathode was a carbon-PTFE air-diffusion electrode from E-TEK (Somerset, NJ, USA). The preparation of this cathode was described elsewhere [49]. It was fed with air pumped at 300 $cm^3\ min^{-1}$ to generate H_2O_2 from reaction (2). The area of both electrodes was 3 cm^2 and the interelectrode gap was ca. 1 cm. To remove the impurities of the BDD surface and activate the air-diffusion cathode, they were previously polarized in 0.05 mol dm^{-3} Na_2SO_4 at a current density (j) of 100 mA cm^{-2} for 60 min. Comparative electrochemical degradations of 100 cm^3 of 0.018–1.0 mmol dm^{-3} dye solutions in 0.05 mol dm^{-3} Na_2SO_4 with 0.5 mmol dm^{-3} Fe^{2+} at pH 3.0 were performed. The influence of j from 8.3 to 100 mA cm^{-2} on dye decolorization was also examined. The oxidative role of electrogenerated hydroxyl radicals was clarified from comparative trials using a 3 cm^2 Pt sheet of 99.99% purity from SEMPSA (Barcelona, Spain) as anode and a 3 cm^2 graphite rod from Sofacel (Sant Feliu, Spain) as cathode. All experiments were carried out under vigorous stirring with a magnetic bar at 800 rpm to ensure homogenization and the transport of reactants towards/from the electrodes.

2.3. Apparatus and analytical procedures

The solution pH was determined with a Crison 2000 pH meter (Alella, Spain). Galvanostatic electrolyses were performed with an Amel 2053 potentiostat-galvanostat (Milano, Italy). Before analysis, the aliquots were alkalinized to stop the degradation process and filtered with 0.45 μm PTFE filters from Whatman (Maidstone, UK).

Table 1
Chemical structure and characteristics of azo dyes tested.

Chemical structure	Color index name	Chemical name	Color index number	λ_{max} (nm)	M/g mol^{-1}
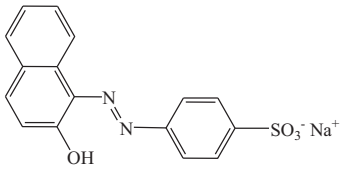	Acid Orange 7 (AO7)	Sodium 4-[(2E)-2-(2-oxonaphthalen-1-ylidene)hydrazinyl]benzenesulfonate	15510	484	350.32
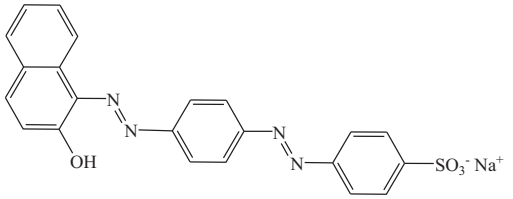	Acid Red 151 (AR151)	Sodium 4-(4-(2-hydroxynaphthalenylazo) phenylazo)benzene sulphonate	26900	500	454.45
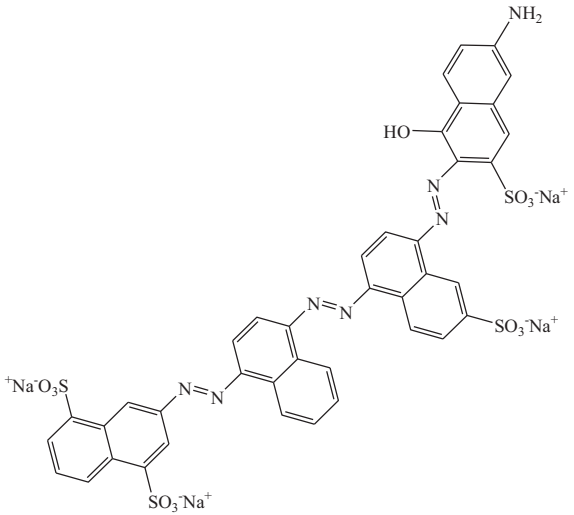	Direct Blue 71 (DB71)	Tetrasodium 3-[[4-[[4-[(6-amino-1-hydroxy-3-sulphonato-2-naphthyl)azo]-6-sulphonato-1-naphthyl]azo]-1-naphthyl] azo]naphthalene-1,5-disulphonate	34140	584	1029.86

The decolorization process of azo dye solutions was monitored from the decay of the absorbance (A) at the maximum wavelength in the visible region of λ_{max} = 484 nm for AO7, λ_{max} = 500 nm for AR151 and λ_{max} = 584 nm for DB71, measured on the spectra recorded with a Shimadzu 1800 UV–vis spectrophotometer (Kyoto, Japan) at 35 °C. The percentage of color removal for each dye was then calculated from Eq. (5) [1]:

$$\%\text{Color removal} = \frac{A_0 - A}{A_0} \times 100 \quad (5)$$

where A_0 and A are the absorbance at initial time and time t at the corresponding λ_{max}, respectively. The parameter δ_0 was then determined as the slope of the linear fitting between % color removal and t at the beginning of the process up to 20–25% of the absorbance decay, that is, when practically the dye alone is degraded because of the low content of intermediates generated. The k_{dec} value was calculated as the slope of the corresponding $\ln(A_0/A) - t$ plot while a linear correlation was verified.

The decay of dye concentration was followed by reversed-phase HPLC using a Waters 600 liquid chromatograph (Milford, MA, USA) fitted with a Spherisorb ODS2 5 μm (150 mm × 4.6 mm (i.d.)) column at 35 °C, and coupled with a Waters 996 photodiode array detector, which was selected at λ = 310.2 nm for AO7, λ = 229.9 nm for AR151 and λ = 289.0 nm for DB71. These wavelengths corresponded to the maximal of their UV bands that are sharper and better defined than their visible bands, thereby allowing more accurate measurements for dye decays. For these analyses, 20 μL aliquots were injected into the liquid chromatograph and the mobile phase was a 30:70 (v/v) acetonitrile/water mixture for AO7 and DB71 and a 50:50 (v/v) acetonitrile/water mixture for AR151, both with 2.4 mmol dm^{-3} n-butylamine and circulating at 0.6 cm^3 min^{-1}. The recorded chromatograms displayed well-defined absorption peaks with a retention time of 7.6 min for AO7, 5.4 min for AR151 and 2.0 min for DB71.

3. Results and discussion

3.1. Oxidative role of electrogenerated hydroxyl radicals in electro-Fenton

The action of hydroxyl radicals produced in the EF process to decolorize the azo dyes was ascertained by determining the percentage of color removal of a 0.400 mmol dm^{-3} AO7 in a 0.05 mol dm^{-3} Na_2SO_4 solution at pH 3.0 and 35 °C using different electrolytic systems at 50 mA cm^{-2}. Prior to these trials, it was found that the addition of 5 mmol dm^{-3} H_2O_2 to the above AO7 solution did not cause any decolorization, indicating that H_2O_2 does not react directly with the azo dye. Fig. 1 presents that the use of BDD/air-diffusion and Pt/air-diffusion cells under AO conditions yields a similar, but poor decolorization of the 0.400 mmol dm^{-3} AO7, only leading to ca. 15% color removal at 30 min. This evidences that BDD (•OH) or Pt(•OH) radicals formed in the above systems from the corresponding reaction (1) react very slowly with the azo dye. When the air-diffusion cathode was replaced by a graphite one, a larger acceleration of the decolorization process can be observed in Fig. 1 achieving 35% and 37% of color decay after 30 min of AO treatment in the BDD/graphite and Pt/graphite cells without H_2O_2 accumulation, respectively. This enhancement can be related to the parallel reduction of the azo dye on the graphite cathode, which does not take place on the air-diffusion cathode because it mainly involves the bielectronic reduction of O_2 to H_2O_2 from reaction (2) [1,22]. However, by adding 0.5 mmol dm^{-3} Fe^{2+} to the AO7 solution, a very quick and almost overall decolorization was attained in only 23 min working with both BDD/air-diffusion and Pt/air-diffusion cells, as can be seen in Fig. 1. This means that in EF, the •OH radical formed in the bulk from reaction (3) is the main oxidant of the azo dyes tested since it is produced in much greater concentration than at the anode surface. This phenomenon has been reported for the oxidation of a high number of aromatics by this procedure [1,22].

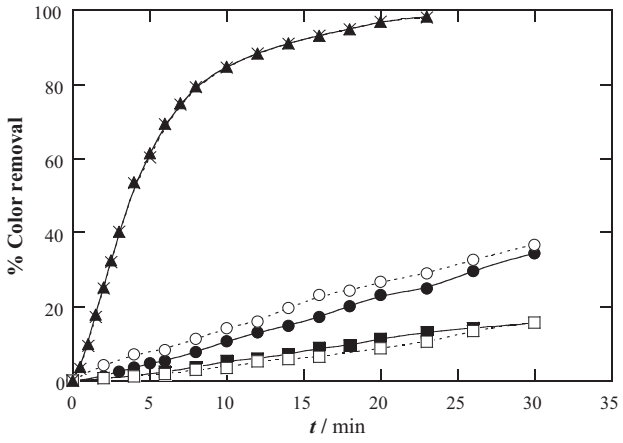

Fig. 1. Change of the percentage of color removal with electrolysis time for the treatment of 100 cm^3 of 0.400 mmol dm^{-3} Acid Orange 7 (AO7) solutions in 0.05 mol dm^{-3} Na_2SO_4 at pH 3.0 and 35 °C by anodic oxidation (AO) with (○) Pt/graphite, (●) BDD/graphite, (□) Pt/air-diffusion and (■) BDD/air-diffusion cells and by electro-Fenton (EF) with 0.5 mmol dm^{-3} Fe^{2+} using (×) Pt/air-diffusion and (▲) BDD/air-diffusion cells. The area of all electrodes was 3.0 cm^2 and a current density of 50 mA cm^{-2} was always applied.

3.2. Effect of the azo dye content on the decolorization process

Several electrolyses were performed for each azo dye to check the influence of its concentration in a 0.05 mol dm^{-3} Na_2SO_4 and 0.5 mmol dm^{-3} Fe^{2+} solution of pH 3.0 at 35 °C on the decolorization power of EF using a BDD/air-diffusion cell at 33.3 mA cm^{-2} for 20 min. These values of Fe^{2+} concentration and pH were chosen since they were found optimal for the treatment of other dyes by this EAOP [41,42]. In these trials, the solution pH always remained practically constant, but large changes in the color of solutions were observed. Thus, the strong orange color of the initial AO7 solutions lost rapidly intensity and gradually turned in a dark brown color, which further became clearer giving rise to a colorless solution for azo dye contents < 0.400 mmol dm^{-3}. The red AR151 solutions darkened initially and further, they underwent a progressive loss in color intensity up to yield practically colorless solutions. Similarly, the color of DB71 solutions varied consecutively from intense blue to purple blue, purple, red and clear brown, before obtaining almost colorless solutions. All these findings evidence the formation of different colored conjugated intermediates by the attack of hydroxyl radicals on the three azo dyes during their decolorization process.

Fig. 2 depicts the increase in the percentage of color removal determined from Eq. (5) with prolonging electrolysis time for the above assays. As can be seen in Fig. 2a, the color decay for AO7 solutions is gradually decelerated when its concentration rises. Thus, only the 0.200 mmol dm^{-3} solution becomes colorless after 12 min of EF treatment, whereas the most concentrated solution with 1.0 mmol dm^{-3} AO7 attains 80% color removal at 20 min. The same behaviour can be observed in Fig. 2b for AR151, although in this case lower percentages of color removal are achieved at the end of electrolysis decreasing from 88% for 0.100 mmol dm^{-3} to 76% for 0.500 mmol dm^{-3}. The progressive loss in color removal at long electrolysis time with rising AO7 and AR151 contents can be explained by the decay in their reaction rate with the same amount of generated hydroxyl radicals due to the presence of more organic matter. In contrast, Fig. 2c shows a fluctuant change in color removal between 68% for the lower 0.018 mmol dm^{-3} of DB71

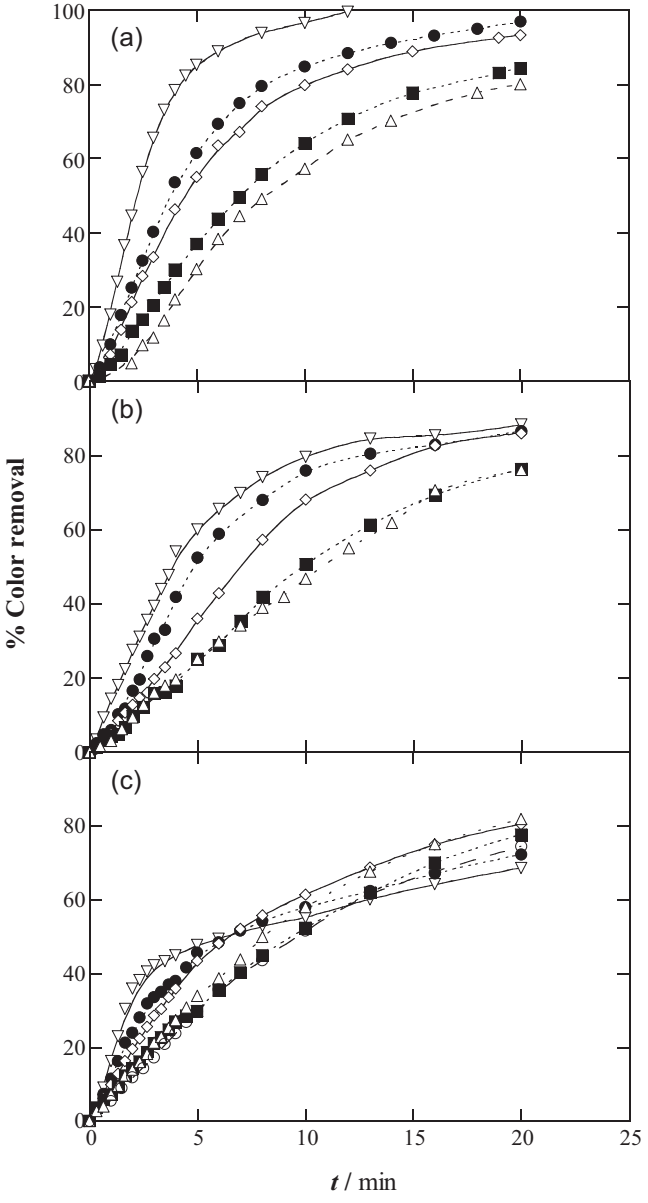

Fig. 2. Variation of the percentage of color removal with electrolysis time for the EF degradation of 100 cm^3 of azo dye solutions in 0.05 mol dm^{-3} Na_2SO_4 with 0.5 mmol dm^{-3} Fe^{2+} at pH 3.0 and 35 °C using a BDD/air-diffusion cell at 33.3 mA cm^{-2}. (a) AO7 concentration: (▽) 0.200 mmol dm^{-3}, (●) 0.400 mmol dm^{-3}, (◊) 0.600 mmol dm^{-3}, (■) 0.800 mmol dm^{-3} and (△) 1.0 mmol dm^{-3}. (b) Acid Red 151 (AR151) concentration: (▽) 0.100 mmol dm^{-3}, (●) 0.200 mmol dm^{-3}, (◊) 0.300 mmol dm^{-3}, (■) 0.400 mmol dm^{-3} and (△) 0.500 mmol dm^{-3}. (c) Direct Blue 71 (DB71) concentration: (▽) 0.018 mmol dm^{-3}, (●) 0.036 mmol dm^{-3}, (◊) 0.053 mmol dm^{-3}, (■) 0.072 mmol dm^{-3}, (△) 0.090 mmol dm^{-3} and (○) 0.200 mmol dm^{-3}.

and 80% for the higher content of 0.200 mmol dm^{-3} at 20 min. This anomalous behaviour can be related to the production of colored by-products with λ_{max} similar to that of the initial azo dye, which are difficultly oxidized with hydroxyl radicals but are formed in relative less extent at greater azo dye concentrations.

From the above results, the corresponding initial decolorization rates were calculated and the values obtained are presented as a function of the azo dye and initial azo bonds concentrations in Fig. 3a and b, respectively. In addition, the δ_0 values found for 0.133 and 0.266 mmol dm^{-3} DB71 solutions are also given in both figures to better compare the behaviour of this parameter. A gradual and quick decay in δ_0 can be observed for each compound when its

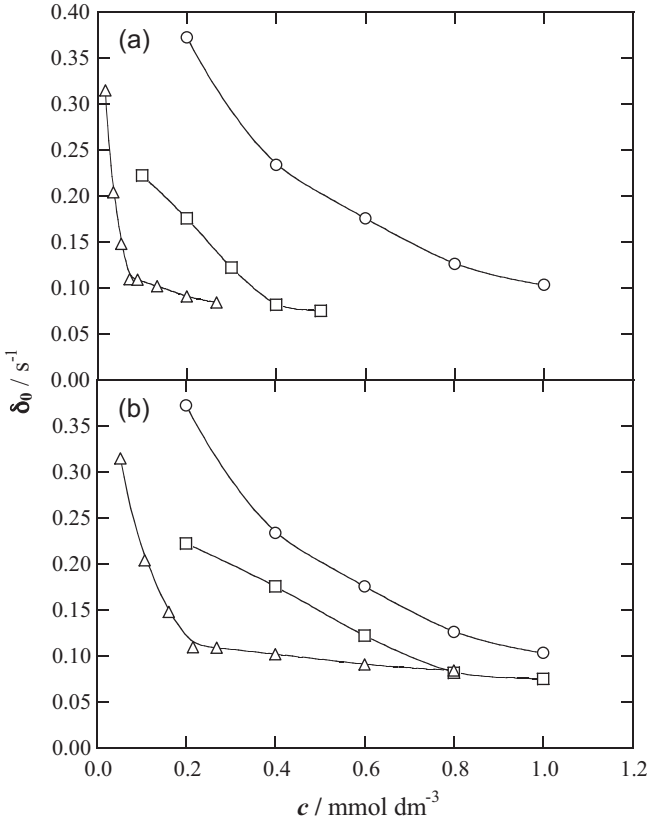

Fig. 3. Initial decolorization rate determined for the experiments of Fig. 2 vs concentration of (a) azo dye and (b) initial azo bonds. Compound: (○) AO7, (□) AR151 and (△) DB71. Data obtained for 0.133 and 0.266 mmol dm^{-3} DB71 solutions are also included.

concentration increases, as expected if less relative quantity of azo dye is destroyed by the same quantity of generated hydroxyl radicals. This tendency agrees with that found for the change in percentage of color removal at long time for AO7 and AR151 (see Fig. 2a and b), suggesting that the decolorization process of such azo dyes involves mainly their disappearance from the medium. However, it differs from the fluctuant variation of color removal obtained for DB71 under similar conditions (see Fig. 2c), since the parameter δ_0 is determined when the content of colored and refractory intermediates is very low and does not affect significantly the absorbance of the solution.

Results of Fig. 3a and b also show that the initial decolorization rate decreases in the sequence AO7 > AR151 > DB71, indicating that hydroxyl radicals react more slowly with the azo dyes as their number of azo bonds rises making the EF process less potent for their decolorization. Fig. 3b shows that this trend is more notable at lower initial azo bonds concentrations when dyes are more rapidly decolorized. Thus, at 0.200 mmol dm^{-3} of initial azo bonds, decreasing δ_0 values of 0.37, 0.22 and 0.11 s^{-1} are found for AO7, AR151 and DB71, respectively, whereas at 0.800 mmol dm^{-3} a smaller decay of this parameter in 0.13, 0.08 and 0.08 s^{-1} is obtained. Note that for DB71, δ_0 decreases very slowly between both contents of initial azo bonds, making less significant the difference of this parameter between the three azo dyes as their content rises (see Fig. 3b). These findings evidence a large influence of the number of azo bonds on the reactivity of the molecules tested with hydroxyl radicals and hence, on their decolorization process. When the number of azo bonds in the dye increases, a larger and more stable conjugated π system is formed (see Table 1) and greater activation energy for the electrophilic attack of hydroxyl radicals is then expected. This originates a decrease in the reaction rate

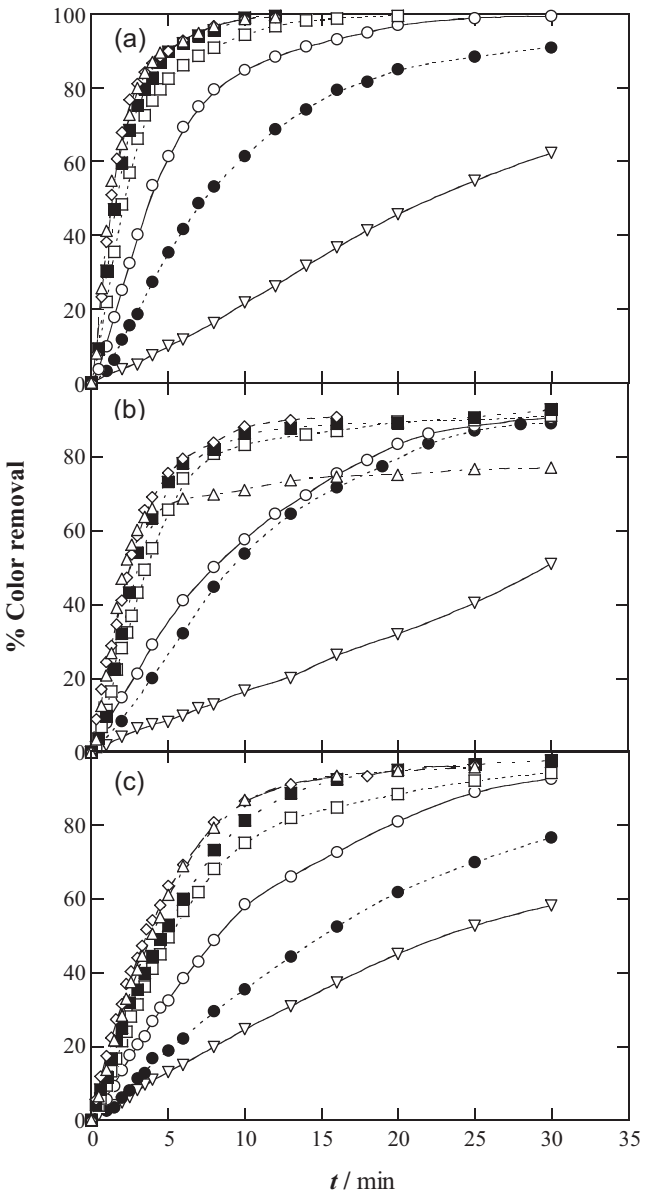

Fig. 4. Change of the percentage of color removal with electrolysis time for the EF treatment of 100 cm^3 of solutions containing 0.400 mmol dm^{-3} of initial azo bonds in 0.05 mol dm^{-3} Na_2SO_4 and 0.5 mmol dm^{-3} Fe^{2+} at pH 3.0 and 35 °C. Azo dye: (a) AO7, (b) AR151 and (c) DB71. Applied current density: (▽) 8.3 mA cm^{-2}, (●) 16.7 mA cm^{-2}, (○) 33.3 mA cm^{-2}, (□) 50 mA cm^{-2}, (■) 66.7 mA cm^{-2}, (◊) 83.3 mA cm^{-2} and (△) 100 mA cm^{-2}.

between both species, as reflected by the lower initial decolorization rates shown in Fig. 3b.

3.3. Effect of current density on the decolorization process of azo dyes

To gain a better knowledge of the decolorization power of EF for each azo dye tested, the influence of j on the process was investigated. To do this, solutions with 0.400 mmol dm^{-3} of initial azo bonds, 0.05 mol dm^{-3} Na_2SO_4 and 0.5 mmol dm^{-3} Fe^{2+} at pH 3.0 were electrolyzed between 8.3 and 100 mA cm^{-2} for 30 min. Fig. 4a–c show a gradual rise in the percentage of color removal with increasing j from 8.3 to 50 mA cm^{-2} for AO7, AR151 and DB71, respectively, due to the acceleration in the production of BDD (•OH) from reaction (1) [14–17] and •OH from Fenton's reaction (3) by the greater H_2O_2 electrogeneration from reaction (2) and higher Fe^{2+} regeneration from reaction (4) [21,22,38–42], indicating that the process is mass-transfer controlled. However, similar percentages of color removal are attained operating between 50 and 100 mA cm^{-2} for AO7 (see Fig. 4a) and DB71 (see Fig. 4c) and between 50 and 83.3 mA cm^{-2} for AR151 (see Fig. 4b). Under these conditions, AO7 is completely decolorized in 12 min, but only 92% and 97% color decay are obtained as maximal for AR151 and DB71, respectively. These findings indicate that the current density of 50 mA cm^{-2} is optimal to decolorize the three dyes.

The fact that the quicker color removal found for each azo dye from 50 mA cm^{-2} is practically independent of j, could be related to the enhancement of parasitic reactions of hydroxyl radicals and the formation of colored conjugated by-products. It is expected that an increase in j causes greater amounts of hydroxyl radicals, but also accelerates more largely their waste reactions reducing the relative quantity of these oxidants with the consequent decrease in organic events [14,22]. These parasite reactions involve, for example, the O_2 evolution from the anodic oxidation of BDD(•OH) by reaction (6) and the attack of •OH on H_2O_2 to yield the weaker oxidant hydroperoxyl radical (HO_2•) by reaction (7) or the dimerization of this radical by reaction (8) [16,22,37,39]:

$$2\text{BDD}(^{\bullet}\text{OH}) \rightarrow 2\text{BDD} + 2O_2 + 2H^+ + 2e^- \quad (6)$$

$$H_2O_2 + {}^{\bullet}\text{OH} \rightarrow HO_2{}^{\bullet} + H_2O \quad (7)$$

$$2\,{}^{\bullet}\text{OH} \rightarrow H_2O_2 \quad (8)$$

The relative loss of reactive hydroxyl radicals with rising j could also be due to the larger enhancement of other anodic reactions such as the oxidation of generated H_2O_2 to O_2 by reaction (9) and of Fe^{2+} ion to Fe^{3+} ion by reaction (10), as well as the formation of peroxodisulfate ion from sulfate ion of the electrolyte by reaction (11) and ozone from water oxidation by reaction (12) [14,22]:

$$H_2O_2 \rightarrow O_2 + 2H^+ + 2e^- \quad (9)$$

$$Fe^{2+} \rightarrow Fe^{3+} + e^- \quad (10)$$

$$2SO_4{}^{2-} \rightarrow S_2O_8{}^{2-} + 2e^- \quad (11)$$

$$3H_2O \rightarrow O_3 + 6H^+ + 6e^- \quad (12)$$

Nevertheless, it seems more reasonable to consider that the decolorization ability of EF for $j > 50$ mA cm^{-2} is limited by the slower oxidation with hydroxyl radicals of generated colored conjugated molecules with λ_{max} close to that of initial compound. This is supported by the fact that the 92% color removal achieved for the AR151 solution at 83.3 mA cm^{-2} is reduced to 77% at 100 mA cm^{-2} (see Fig. 4b), as expected by the formation of very recalcitrant colored by-products that are produced in much lesser extent at lower current densities. The much smaller generation of such kind of by-products with increasing current for AO7 could explain the fast and overall decolorization attained for the EF treatment of this compound (see Fig. 4a), whereas greater amounts of such recalcitrant by-products could be formed in the case of DB71 that are more slowly removed from 66.7 mA cm^{-2} (see Fig. 4c).

A very different behaviour was found when the beginning of the decolorization processes was analyzed by means of δ_0 where practically the azo dye alone is destroyed. Fig. 5 shows that at a given $j \geq 16.7$ mA cm^{-2} this parameter decreases in the sequence AO7 > AR151 > DB71, as expected by the lower reactivity of generated oxidants hydroxyl radicals with longer conjugated π molecules, as pointed out above. Moreover, δ_0 and j show a linear relationship between 16.7 and 83.3 mA cm^{-2} for all the azo dyes. For this increase in 5 times of the current density, δ_0 rises 5.2, 4.0 and 3.2 times for AO7, AR151 and DB71, respectively. The fact that δ_0 and j vary in a similar way for AO7 indicates that it reacts with a similar relative quantity of hydroxyl radicals generated at each current density. However, the smaller reactivity as current density

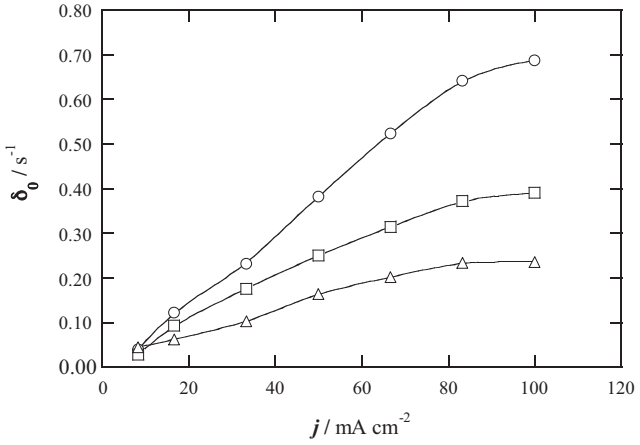

Fig. 5. Initial decolorization rate for the trials of Fig. 4 vs applied current density. Azo dye: (◯) AO7, (□) AR151 and (△) DB71.

rises for AR151 and DB71 can be accounted for the loss of reactive hydroxyl radicals by the acceleration of waste reactions (6)–(8), which is more significant for a higher number of azo bonds due to their slower reaction with hydroxyl radicals. The large enhancement of these parasitic reactions can also explain the quite similar δ_0 value found at 83.3 and 100 mA cm^{-2} for AR151 and DB71 (see Fig. 5).

The above considerations allow inferring that the parameter δ_0 can serve to describe the reactivity of azo dyes with hydroxyl radicals produced in the EF process. In contrast, the decolorization ability of this method is rather limited by the parallel destruction of some colored conjugated by-products, which are formed in larger extent in the diazo and triazo dyes than in the monoazo one.

3.4. Decay kinetics for the azo dyes

The kinetics for the reaction of each azo dye with generated hydroxyl radicals in EF was studied to check the comparative trends established with the parameter δ_0 for their initial decolorization. This was made by electrolyzing the solutions with 0.400 mmol dm^{-3} of initial azo bonds between 16.7 and 66.7 mA cm^{-2} and measuring the concentration decay of each compound from the reversed-phase chromatograms recorded.

Fig. 6a shows a fast and total decay of AO7 under the EF conditions tested. The removal of this azo dye is strongly accelerated with increasing j owing to the generation of greater quantities of BDD(•OH) at the anode from reaction (1) and mainly of •OH in the bulk from Fenton's reaction (3). This causes that AO7 disappears at decreasing times of about 26, 16, 6 and 4 min for increasing current densities of 16.7, 33.3, 50 and 66.7 mA cm^{-2}, respectively. The above concentration decays were analyzed from kinetic equations related to simple reaction orders and excellent fits were obtained for a pseudo first-order reaction, as can be seen in the inset panel of Fig. 6a. The k_1 value with the corresponding square of the linear regression coefficient (R^2) thus determined for the different current densities tested are collected in Table 2. As can be seen, k_1 varies linearly with j up to 50 mA cm^{-2}, whereas its value further increases two-folds at 66.7 mA cm^{-2}. Using the BDD/air-diffusion cell under AO conditions, it was found that the pseudo first-order rate constant for the reaction of AO7 with BDD(•OH) changed from 1.10×10^{-4} s^{-1} for 50 mA cm^{-2} to 1.87×10^{-4} s^{-1} for 66.7 mA cm^{-2}, which are two magnitude orders lower than the k_1 values found under EF conditions (see Table 2), in agreement with results shown in Fig. 1. Note that the percentage of color removal in EF is quite similar when j rises from 50 to 66.7 cm^{-2} (see Fig. 4a), suggesting that in both cases, the colored by-products are removed

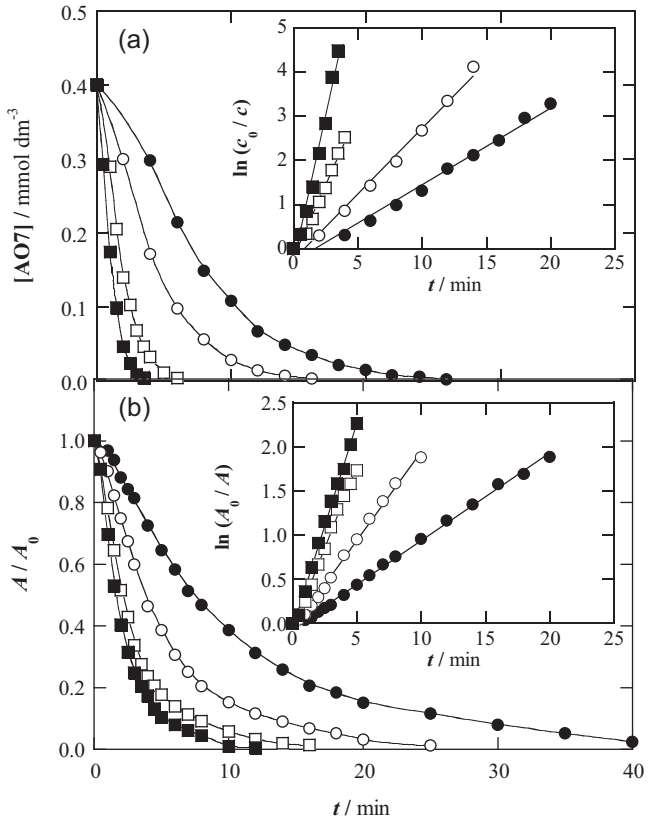

Fig. 6. (a) Time-course of the decay of AO7 concentration determined by reversed-phase HPLC for the EF treatment of 100 cm^3 of solutions with 0.400 mmol dm^{-3} initial azo bonds in 0.05 mol dm^{-3} Na_2SO_4 and 0.5 mmol dm^{-3} Fe^{2+} at pH 3.0 and 35 °C. (b) Change of the normalized absorbance at λ = 484 nm with electrolysis time for the above trials. Applied current density: (●) 16.7 mA cm^{-2}, (◯) 33.3 mA cm^{-2}, (□) 50 mA cm^{-2} and (■) 66.7 mA cm^{-2}. The inset panels present the corresponding kinetic analysis assuming a pseudo first-order reaction.

by similar contents of the main oxidant •OH formed in the bulk. So, the relative greater amounts of •OH generated at 66.7 mA cm^{-2} could react in much larger extent with the initial AO7 concentration causing the large enhancement in k_1 found at this current density.

The decolorization process of the above trials was also followed from the normalized absorbance of the solution at the λ_{max} of the

Table 2
Pseudo first-order rate constant for dye decay (k_1) and for decolorization (k_{dec}) and initial decolorization rate (δ_0) determined for the EF treatment of 100 cm^3 of solutions of the azo dyes AO7, AR151 and DB71 with a concentration equivalent to 0.400 mmol dm^{-3} of azo bonds in 0.05 mol dm^{-3} Na_2SO_4 with 0.50 mmol dm^{-3} Fe^{2+} at pH 3.0, 35 °C and different current densities. The square of the linear regression coefficient (R^2) is given in parenthesis.

j (mA cm^{-2})	AO7	AR151	DB71
		$k_1 \times 10^3$ (s^{-1})	
16.7	2.90 (0.992)	0.99 (0.999)	0.80 (0.995)
33.3	4.96 (0.995)	1.78 (0.997)	1.49 (0.999)
50.0	11.1 (0.992)	2.83 (0.997)	2.64 (0.999)
66.7	22.2 (0.991)	7.94 (0.996)	6.41 (0.999)
		$k_{dec} \times 10^3$ (s^{-1})	
16.7	1.65 (0.998)	1.40 (0.998)	0.81 (0.995)
33.3	3.36 (0.996)	1.42 (0.998)	1.39 (0.996)
50.0	6.15 (0.995)	3.81 (0.989)	2.31 (0.997)
66.7	7.76 (0.996)	4.58 (0.990)	2.75 (0.998)
		δ_0 (s^{-1})	
16.7	0.12 (0.993)	0.09 (0.998)	0.06 (0.990)
33.3	0.23 (0.993)	0.18 (0.986)	0.10 (0.996)
50.0	0.38 (0.997)	0.25 (0.996)	0.16 (0.993)
66.7	0.53 (0.987)	0.31 (0.987)	0.20 (0.992)

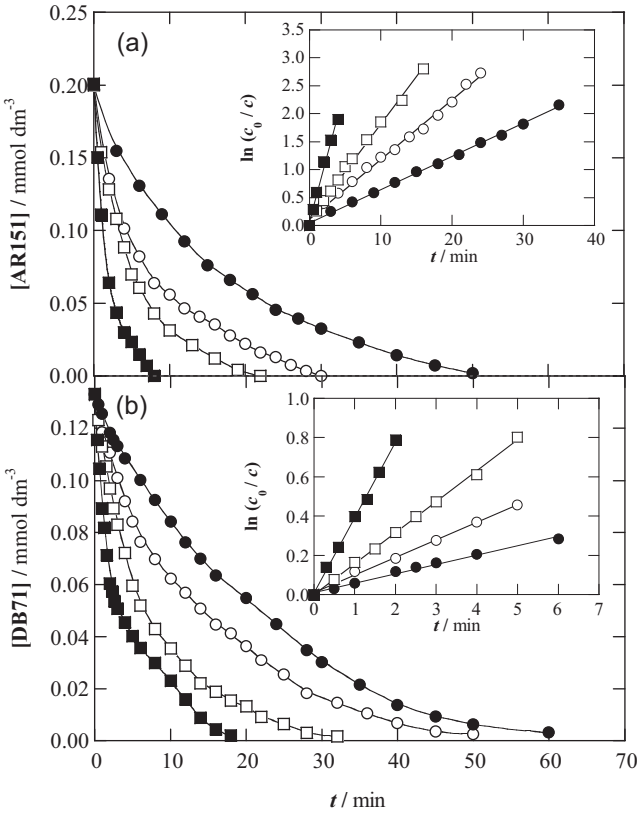

Fig. 7. Decay of the concentration of (a) AR151 and (b) DB71 with electrolysis time obtained by reversed-phase HPLC under the same EF conditions of Fig. 6a. The kinetic analysis considering a pseudo first-order reaction for each dye is shown in the inset panels.

azo dye. Fig. 6b shows the decay of this parameter with electrolysis time and its inset panel presents the good linear $\ln(A_0/A) - t$ plots obtained up to about the half of the time needed to attain total decolorization. The corresponding k_{dec} values calculated from these plots are listed in Table 2. Comparison of Fig. 6a and 6b allows concluding that the time required for the total removal of AO7 is always much shorter than that needed for the overall decolorization of the solution, thereby corroborating the formation of more recalcitrant colored conjugated by-products with λ_{max} similar to that of the azo dye during the EF process. This is also reflected by the much lower k_{dec} value obtained for decolorization compared with the k_1 value determined for azo dye removal at each j (see Table 2), since the former process becomes much slower by the parallel oxidation of such colored intermediates with hydroxyl radicals.

The same behaviour was found for the removal of the diazo AR151 and triazo DB71, as well as the decolorization of their solutions. Fig. 7a and b depict the concentration decays up to total removal of these compounds, respectively, whereas the excellent linear correlations considering that they follow a pseudo first-order kinetics are shown in the inset panels. The k_1 and k_{dec} values calculated from these analyses are also collected in Table 2. For each compound, these results indicate that both, the azo dye decay and solution decolorization are strongly enhanced with increasing j and that the former is always much faster than the latter as a result of the slower destruction of generated colored by-products with λ_{max} similar to that of each azo dye. As in the case of AO7, a strong increase in k_1 for AR151 and BD71 decays when passing from 50 to 66.7 mA cm^{-2} can also be observed in Table 2. This can be related to their faster reactions with greater relative amounts of •OH in the bulk formed at 66.7 mA cm^{-2} because in both current densities the colored by-products are destroyed at similar rate, as deduced from the analogous percentages of color removal depicted in Fig. 4b and 4c.

From the k_1 values given in Table 2, one can infer that the reactivity of azo dyes with generated hydroxyl radicals in EF decreases in the order AO7 > AR151 > DB71, so prolonging the time required for their disappearance (see Figs. 6 and 7). This is the same trend as predicted from the initial decolorization rates at the beginning of the process, also collected in Table 2, thereby confirming the validity of the analysis performed with this parameter on the oxidation ability of EF for increasing number of azo bonds in Sections 3.2 and 3.3. Note that the changes in k_{dec} of Table 2 also seem to verify the same tendency for the decolorization process of monoazo, diazo and triazo dyes. However, this rate constant cannot be used to predict the comparative total decolorization of these compounds since it does not describe adequately the behaviour of solutions after about 50–60% of the absorbance decay due to the large accumulation of more recalcitrant colored intermediates, which are generated in different extent depending on the dye, its concentration and the applied j (see Figs. 2 and 4).

4. Conclusions

The decolorization process of azo dyes by EF showed a marked influence of the number of azo bonds present in the molecule. The initial decolorization rate decreased with rising initial azo bonds concentration due to the oxidation of more organic matter with similar amounts of generated hydroxyl radicals. A linear increase of δ_0 with applied current density was found as a result of the greater production of these oxidants, even when similar color removal was determined at long electrolysis times for high j values. This parameter became lower when the number of azo bonds increased, indicating the existence of a smaller reactivity with hydroxyl radicals because larger and more stable conjugated π systems are formed. In contrast, the decolorization ability of EF was limited by the slower and parallel destruction of colored conjugated by-products, formed in larger extent in the diazo and triazo dyes than in the monoazo one, because poly-azo dyes do not decolorize when the first azo functional group is removed. HPLC analysis of electrolyzed solutions confirmed the total removal of all azo dyes by EF treatment. They disappeared in shorter times as j rose and the number of azo bonds decreased. The k_1 values determined by this technique showed the same trends as those predicted by δ_0, thereby evidencing that the latter simple parameter is suitable to analyze the reactivity of azo dyes. The k_{dec} values obtained from the absorbance decay also showed similar tendencies, but they did not describe the comparative total decolorization of azo dye solutions because of the complex degradative behaviour of colored intermediates, which depends on the compound tested and experimental conditions used. An optimum current density of 50 mA cm^{-2} was found to decolorize the three dyes.

Acknowledgements

The authors acknowledge financial support from MICINN (Ministerio de Ciencia e Innovación, Spain) under the project CTQ2010-16164/BQU, co-financed with FEDER funds. S. Garcia-Segura thanks the grant awarded from MEC (Ministerio de Educación y Ciencia, Spain) to do this work.

References

[1] C.A. Martínez-Huitle, E. Brillas, Appl. Catal. B: Environ. 87 (2009) 105.
[2] D. Brown, Ecotox. Environ. Safe 13 (1987) 139.
[3] K.P. Sharma, S. Sharma, S.P. Sharma, K. Singh, S. Kumar, R. Grover, P.K. Sharma, Chemosphere 69 (2007) 48.
[4] E. Forgacs, T. Cserhati, G. Oros, Environ. Int. 30 (2004) 953.
[5] A. Szygula, E. Guibal, M. Ruiz, A.M. Sastre, Colloids Surf. A 330 (2008) 219.

[6] M.M. Dávila-Jiménez, M.P. Elizalde-González, A.A. Pelaéz-Cid, Colloids Surf. A 254 (2005) 107.
[7] J. Wu, C. Liu, K.H. Chu, S. Suen, J. Membrane Sci. 309 (2008) 239.
[8] E. Franciscon, A. Zille, F. Dias, C. Ragagnin de Menezes, L.R. Durrant, A. Cavaco-Paulo, Int. Biodeterior. Biodegrad. 63 (2009) 280.
[9] G. Buitrón, M. Quezada, G. Moreno, Bioresour. Technol. 92 (2004) 143.
[10] T.A. Özbelge, F. Erol, Chem. Eng. Commun. 169 (2009) 39.
[11] D. Gandini, E. Mahé, P.A. Michaud, W. Haenni, A. Perret, Ch. Comninellis, J. Appl. Electrochem. 30 (2000) 1345.
[12] P.A. Michaud, M. Panizza, L. Ouattara, T. Diaco, G. Foti, Ch. Comninellis, J. Appl. Electrochem. 33 (2003) 151.
[13] B. Marselli, J. García-Gomez, P.A. Michaud, M.A. Rodrigo, Ch. Comninellis, J. Electrochem. Soc. 150 (2003) D79.
[14] M. Panizza, G. Cerisola, Chem. Rev. 109 (2009) 6541.
[15] E. Brillas, S. Garcia-Segura, M. Skoumal, C. Arias, Chemosphere 79 (2010) 605.
[16] I. Sirés, E. Brillas, G. Cerisola, M. Panizza, J. Electroanal. Chem. 613 (2008) 151.
[17] M. Hamza, R. Abdelhedi, E. Brillas, I. Sirés, J. Electroanal. Chem. 627 (2009) 41.
[18] C. Zhang, J. Wang, T. Murakami, A. Fujishima, D. Fu, Z. Gu, J. Electroanal. Chem. 638 (2010) 91.
[19] S. Garcia-Segura, E. Brillas, Water Res. 45 (2011) 2975.
[20] N. Daneshvar, S. Aber, V. Vatanpour, M.H. Rasoulifard, J. Electroanal. Chem. 615 (2008) 165.
[21] E. Guinea, C. Arias, P.L. Cabot, J.A. Garrido, R.M. Rodríguez, F. Centellas, E. Brillas, Water Res. 42 (2008) 499.
[22] E. Brillas, I. Sirés, M.A. Oturan, Chem. Rev. 109 (2009) 6570.
[23] M. Diagne, N. Oturan, M.A. Oturan, Chemosphere 66 (2007) 841.
[24] A.R. Khataee, M. Zarei, L. Moradkhannejhad, Desalination 258 (2010) 112.
[25] M. Zarei, A.R. Khataee, R. Ordikhani-Seyedlar, M. Fathinia, Electrochim. Acta 55 (2010) 7259.
[26] A.R. Khataee, M. Zarei, S.K. Asl, J. Electroanal. Chem. 648 (2010) 143.
[27] A.R. Khataee, M. Safarpour, M. Zarei, S. Aber, J. Electroanal. Chem. 659 (2011) 63.
[28] S. Hammami, N. Bellakhal, N. Oturan, M.A. Oturan, M. Dachraoui, Chemosphere 73 (2008) 678.
[29] A. Özcan, Y. Sahin, A.S. Koparal, M.A. Oturan, J. Electroanal. Chem. 616 (2008) 71.
[30] A. Özcan, M.A. Oturan, N. Oturan, Y. Sahin, J. Hazard. Mater. 163 (2009) 1213.
[31] B. Balci, N. Oturan, R. Cherrier, M.A. Oturan, Water Res. 43 (2009) 1924.
[32] A. Dirany, I. Sirés, N. Oturan, M.A. Oturan, Chemosphere 81 (2010) 594.
[33] J.M. Peralta-Hernández, Y. Meas-Vong, F.J. Rodríguez, T.W. Chapman, M.I. Maldonado, L.A. Godínez, Dyes Pigments 76 (2008) 656.
[34] A. Wang, J. Qu, H. Liu, J. Ru, Appl. Catal. B: Environ. 84 (2008) 393.
[35] K. Cruz-González, O. Torres-López, A. García-León, J.L. Guzmán-Mar, L.H. Reyes, A. Hernández-Ramírez, J.M. Peralta-Hernández, Chem. Eng. J. 160 (2010) 199.
[36] I. Sirés, F. Centellas, J.A. Garrido, R.M. Rodríguez, C. Arias, P.L. Cabot, E. Brillas, Appl. Catal. B: Environ. 72 (2007) 373.
[37] M. Skoumal, C. Arias, P.L. Cabot, F. Centellas, J.A. Garrido, R.M. Rodríguez, E. Brillas, Chemosphere 71 (2008) 1718.
[38] M. Panizza, G. Cerisola, Electrochim. Acta 54 (2008) 876.
[39] M. Skoumal, R.M. Rodríguez, P.L. Cabot, F. Centellas, J.A. Garrido, C. Arias, E. Brillas, Electrochim. Acta 54 (2009) 2077.
[40] M. Panizza, G. Cerisola, Water Res. 43 (2009) 339.
[41] E.J. Ruiz, C. Arias, E. Brillas, A. Hernández-Ramírez, J.M. Peralta-Hernández, Chemosphere 82 (2011) 495.
[42] R. Salazar, S. Garcia-Segura, M.S. Ureta-Zañartu, E. Brillas, Electrochim. Acta 56 (2011) 6371.
[43] A.R. Khataee, M.B. Kasiri, J. Mol. Catal. A: Chem. 328 (2010) 8.
[44] H.Y. Hong, G.S. Yoo, J.K. Choi, Electrophoresis 21 (2000) 841.
[45] C.G. Silva, W. Wang, J.L. Faria, J. Photochem. Photobiol. A: Chem. 181 (2006) 314.
[46] M. Muthukumar, D. Sargunamani, N. Selvakumar, Dyes Pigments 65 (2005) 151.
[47] M. Muthukumar, N. Selvakumar, Dyes Pigments 62 (2004) 221.
[48] N. Ali, A. Hameed, S. Ahmed, Braz. J. Microbiol. 41 (2010) 907.
[49] E. Brillas, M.A. Baños, S. Camps, C. Arias, P.L. Cabot, J.A. Garrido, R.M. Rodríguez, New J. Chem. 28 (2004) 314.

PAPER 5

Comparative degradation of the diazo dye Direct Yellow 4 by electro-Fenton, photoelectron-Fenton and photo-assisted electro-Fenton

Journal of Electroanalytical Chemistry 681 (2012) 36–43

Contents lists available at SciVerse ScienceDirect

Journal of Electroanalytical Chemistry

journal homepage: www.elsevier.com/locate/jelechem

Comparative degradation of the diazo dye Direct Yellow 4 by electro-Fenton, photoelectro-Fenton and photo-assisted electro-Fenton

Sergi Garcia-Segura, Abdellatif El-Ghenymy, Francesc Centellas, Rosa M. Rodríguez, Conchita Arias, José A. Garrido, Pere L. Cabot, Enric Brillas *

Laboratori d'Electroquímica de Materials i del Medi Ambient, Departament de Química Física, Facultat de Química, Universitat de Barcelona, Martí i Franquès 1-11, 08028 Barcelona, Spain

ARTICLE INFO

Article history:
Received 8 May 2012
Received in revised form 1 June 2012
Accepted 6 June 2012
Available online 15 June 2012

Keywords:
Direct Yellow 4
Electro-Fenton
Mineralization
Oxidation by-products
Photo-assisted electro-Fenton
Photoelectro-Fenton

ABSTRACT

The degradation of 100 ml of a 200 mg l^{-1} Direct Yellow 4 (DY4) solution in 0.05 M Na_2SO_4 with 0.5 mM Fe^{2+} of pH 3.0 has been comparatively studied by electro-Fenton (EF), photoelectro-Fenton (PEF) with UVA light and a novel photo-assisted EF (PA–EF). The latter method consists of the application of EF for a given time, followed by UVA illumination alone. Electrolytic experiments were made with a boron-doped diamond (BDD) anode and an air-diffusion cathode generating H_2O_2 at constant current density. In this system, oxidant ·OH was produced at the BDD surface from water oxidation and in the bulk from Fenton's reaction. The DY4 solution was rapidly decolorized in EF and PEF due to the action of ·OH. The PEF process yielded an almost total mineralization of DY4, being more powerful than EF that only allowed partial mineralization. The proposed PA–EF was as potent as PEF if the initial electrolysis was prolonged until the production of intermediates that can be mineralized by UVA light. At 33.3 mA cm^{-2}, the best PA–EF was found by stopping the electrolysis and starting UVA irradiation at 120 min. The PA–EF process was always more economic than PEF and even less expensive than EF at high current density. Oxalic and oxamic acids were detected as ultimate by-products by ion-exclusion HPLC. The Fe(III) complexes of both acids were slowly mineralized with ·OH in EF, but rapidly photolyzed by UVA light in PEF and PA–EF. In these processes, the photolysis of *N*-intermediates produced oxamic acid. NH_4^+ ion was released in much larger proportion than NO_3^- ion, but the major part of the initial N was lost as volatile *N*-compounds. The photolytic removal of Fe(III)-oxalate complexes and *N*-intermediates accounts for the high effectiveness of the PEF and PA–EF processes.

1. Introduction

Azo dyes are characterized by one or more azo bonds (—N=N—) as chromophore group in association with aromatic structures containing functional groups such as —OH and —SO_3H, among others [1,2]. They represent about 70% of the world dye production and are extensively used in textile industries, which produce large volumes of wastewater effluents with high dye contents coming from the dyeing processes. These colored effluents are discharged into water bodies such as lakes and rivers, where they cause esthetic problems and serious health and environmental risks because of the toxicity, carcinogenic and mutagenic properties of dyes and its by-products [3,4]. Azo dyes are very stable in the environment and persist under ambient conditions due to the difficulty of their removal under conventional aerobic treatments in wastewater treatment plants [5]. Powerful oxidation processes are then needed to be developed for the destruction of these pollutants from industrial wastewaters to avoid their adverse impact.

Advanced oxidation processes (AOPs) are powerful chemical, photochemical, photocatalytic and electrochemical processes that are being applied to degrade toxic and/or biorefractory organics in wastewaters [6–9]. The common feature of AOPs is the in situ generation of hydroxyl radical (·OH) as strong oxidant of the organic matter in waters. The high standard reduction potential of ·OH ($E°$(·OH/H_2O) = 2.80 V/SHE) makes possible its non-selective reaction with most organics yielding dehydrogenated or hydroxylated derivatives, which can be in turn completely mineralized, i.e. converted into CO_2, water and inorganic ions. Recently, electrochemical AOPs (EAOPs) have received great attention by their environmental compatibility, versatility, high efficiency, amenability of automation and safety because they operate at mild conditions [10–13].

Electro-oxidation or anodic oxidation (AO) is the most popular EAOP due to its simplicity. In this procedure, the pollutants are oxidized by direct electron transfer to the anode and/or mediated oxidation with heterogeneous ·OH formed from water discharge at the

* Corresponding author. Tel.: +34 93 4021223; fax: +34 93 4021231.
E-mail address: brillas@ub.edu (E. Brillas).

1572-6657/$ - see front matter © 2012 Elsevier B.V. All rights reserved.
http://dx.doi.org/10.1016/j.jelechem.2012.06.002

anode surface at high current [10,12,14]. Non-active boron-doped diamond (BDD) thin-film electrodes are the best anodic materials for AO because they interact very weakly with physisorbed BDD(·OH) produced from reaction (1) and promote a much greater O_2-overpotential than other conventional anodes like Pt and PbO_2 [15,16], enhancing the removal of aromatics like azo dyes [17–24].

$$BDD + H_2O \rightarrow BDD(\cdot OH) + H^+ + e^- \quad (1)$$

The efficiency of AO can be enhanced using EAOPs based on Fenton's reaction chemistry like electro-Fenton (EF) and photoelectro-Fenton (PEF) [13]. These procedures involve the continuous supply of H_2O_2 to an acidic contaminated solution from the two-electron cathodic reduction of injected O_2 from following reaction:

$$O_2 + 2H^+ + 2e^- \rightarrow H_2O_2 \quad (2)$$

Carbonaceous cathodes like carbon nanotubes-polytetrafluoroethylene (PTFE) [25–27], carbon nanotubes on graphite [28], carbon felt [29–33], activated carbon fiber [34], carbon sponge [35], BDD [36,37] and carbon-PTFE gas (O_2 or air) diffusion [38–46] have demonstrated a good efficiency for H_2O_2 generation in the EF and PEF treatments. In these EAOPs, Fe^{2+} ion is added as catalyst to react with H_2O_2 giving homogeneous ·OH and Fe^{3+} ion from Fenton's reaction:

$$Fe^{2+} + H_2O_2 \rightarrow Fe^{3+} + \cdot OH + OH^- \quad (3)$$

EF is more efficient than the classical chemical Fenton process because reaction (3) can be mainly propagated by the cathodic reduction of Fe^{3+} to Fe^{2+} from following reaction [13]:

$$Fe^{3+} + e^- \rightarrow Fe^{2+} \quad (4)$$

Moreover, when an undivided cell with a BDD anode is used in EF, organics can be attacked by heterogeneous BDD(·OH) formed from reaction (1) and by ·OH produced in the bulk from Fenton's reaction (3). In previous work, our group reported that the EF treatment of many aromatics like azo dyes do not allow total mineralization owing to the formation of very recalcitrant by-products such as several Fe(III)-carboxylate complexes that react very slowly with generated ·OH [38–41,43–46]. We have also found that the PEF process involving the simultaneous exposition of the treated solution to UVA light accelerates strongly the mineralization process of aromatics mainly due to the photolysis of Fe(III)-carboxylate complexes by following reaction [43–46]:

$$Fe(OOCR)^{2+} + h\nu \rightarrow Fe^{2+} + CO_2 + R^{\cdot} \quad (5)$$

Although the PEF process seems preferable to the EF one, its application to water remediation is limited by the high electrical energy requirements of both, the electrochemical cell and the artificial UVA lamp working during all electrolysis time. A much more economic EAOP could be designed by combining partially EF and UVA light in the so-called photo-assisted EF (PA–EF) method. In this technique, the EF process will be applied only during the time needed for the conversion of most pollutants into intermediates such as Fe(III)-carboxylate complexes that can be photolyzed under UVA illumination and mineralized, thereby strongly reducing the electrical energy consumed. To check the possible viability of the proposed PA–EF method for wastewater treatment, we have undertaken a study on the degradation of the diazo dye Direct Yellow 4 (DY4), which has not been previously treated by EAOPs. The characteristics of this diazo dye are collected in Table 1.

This paper presents the comparative results obtained for the decolorization and mineralization of a 200 mg l^{-1} DY4 solution by EF, PEF and PA–EF using a BDD/air-diffusion cell. The combined action of applied current density and UVA irradiation was explored to find the best experimental conditions for the PA–EF process. The evolution of generated carboxylic acids was followed by HPLC to clarify the role of generated hydroxyl radicals and UVA light on the mineralization process. The fate of initial N was assessed by determining the concentration of released nitrogen ions like NH_4^+ and NO_3^- by ion chromatography.

2. Materials and methods

2.1. Chemicals

Commercial pure azo dye DY4 was supplied by Sigma–Aldrich. Anhydrous sodium sulfate and heptahydrated iron(II) sulfate were of analytical grade from Fluka and Sigma, respectively. Oxalic, oxamic and maleic acids were of analytical grade from Avocado. Organic solvents and other chemicals used were of HPLC or analytical grade from Aldrich, Lancaster, Merck and Panreac. Solutions were prepared with high-purity water obtained from a Millipore Milli-Q system with resistivity >18 MΩ cm at 25 °C.

2.2. Electrochemical systems

All electrolytic trials were conducted in an open and undivided cylindrical cell of 150 ml capacity with a double jacket for circulation of external thermostated water to regulate the solution temperature using a Thermo Electron Corporation HAAKE DC 10 thermostat. The anode was a BDD thin film provided by Adamant Technologies (La-Chaux-de-Fonds, Switzerland). The cathode was a carbon-PTFE air-diffusion electrode from E-TEK (Somerset, NJ, USA), mounted as described elsewhere [39]. This cathode was fed with air pumped at 300 ml min^{-1} to continuously generate H_2O_2 by the two-electron reduction of injected O_2 from reaction (2). The geometric area of all electrodes was 3 cm^2 and the interelectrode

Table 1
Chemical structure and characteristics of diazo dye Direct Yellow 4.

Chemical structure	Chemical formula	Color index name	Chemical name	Color index number	λ_{max}/nm	M/g mol^{-1}
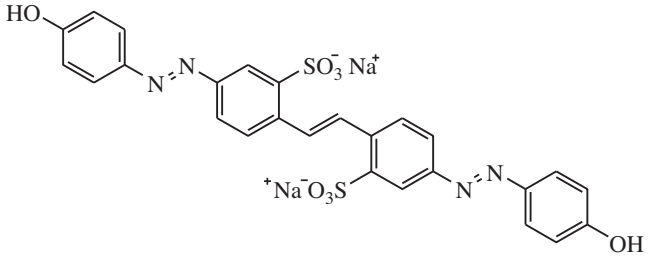	$Na_2C_{26}H_{18}N_4O_8S_2$	Direct Yellow 4 (DY4)	Disodium 5-[2-(4-oxocyclohexa-2,5-dien-1-ylidene)hydrazinyl]-2-[(E)-2-[4-[2-(4-oxocyclohexa-2,5-dien-1-ylidene) hydrazinyl]-2-sulphonatophenyl]ethenyl] benzenesulphonate	24890	400	624.55

gap was ca. 1 cm. All the experiments were performed at constant current density (j) provided by an Amel 2053 potentiostat–galvanostat. To remove the impurities of the BDD anode surface and activate the air-diffusion cathode, they were previously polarized in a 0.05 M Na_2SO_4 solution at 100 mA cm^{-2} for 60 min.

Comparative EF, PEF and PA–EF treatments were made using 100 ml of solutions containing 200 mg l^{-1} DY4 (equivalent to 100 mg l^{-1} of total organic carbon (TOC)) in 0.05 M Na_2SO_4 as background electrolyte and 0.5 mM Fe^{2+} as catalyst at pH 3.0. This Fe^{2+} concentration was chosen since it was found optimal for the EF and PEF degradations of other aromatics [39–41,43]. The solution was always kept at 35.0 °C, which is the maximum temperature that can be used in the cell without significant water evaporation during prolonged electrolysis [38]. The solution was vigorously stirred with a magnetic bar at 800 rpm to ensure its mixing and the transport of reactants towards/from the electrodes. For the PEF and PA–EF processes under UVA irradiation, a Philips TL/6 W/08 fluorescent black light blue tube placed at 7 cm above the solution was employed. The tube emitted UVA light in the wavelength region 320–400 nm with λ_{max} = 360 nm, supplying a photoionization energy of 5 W m^{-2} as detected with a Kipp & Zonen CUV 5 radiometer.

2.3. Apparatus and analytical procedures

The solution pH was measured with a Crison GLP 22 pH-meter. Samples were withdrawn at regular time intervals from the treated solution, then alkalinized to stop the degradation process and microfiltered with 0.45 μm PTFE filters from Whatman before analysis. The decolorization of DY4 solutions was monitored from the absorbance (A) decrease at the maximum visible wavelength (λ_{max}) of 400 nm, measured from the spectra recorded on a Shimadzu 1800 UV/Vis spectrophotometer at 35 °C. The mineralization of solutions was monitored from their TOC decay using a Shimadzu VCSN TOC analyzer. Reproducible TOC values with a precision of ±1% were obtained by injecting 50 μl aliquots into the TOC analyzer. Total nitrogen (TN) was determined with a Shimadzu TNM-1 unit coupled with the TOC analyzer.

Generated carboxylic acids were identified and quantified by ion-exclusion HPLC using a Waters 600 LC fitted with a Bio-Rad Aminex HPX 87H, 300 mm × 7.8 mm (i.d.), column at 35 °C and coupled with a Waters 996 photodiode array detector at λ = 210 nm. These measurements were made by injecting 20 μl aliquots into the LC under circulation of 4 mM H_2SO_4 at 0.6 ml min^{-1} as mobile phase. NH_4^+ and NO_3^- ions formed during dye degradation were detected by ionic chromatography using a Shimadzu 10 Avp HPLC coupled with a Shimadzu CDD 10 Avp conductivity detector. The NH_4^+ concentration was determined with a Shodex IC YK-421, 125 mm × 4.6 mm (i.d.), cation column at 40 °C, whereas the NO_3^- content was obtained with a Shim-Pack IC-A1S, 100 mm × 4.6 mm (i.d.), anion column at 40 °C. These analyses were performed with 25 μl aliquots using a mobile phase composed of 5.0 mM tartaric acid, 1.0 mM dipicolinic acid, 24.2 mM boric acid and 1.5 mM corona ether at 1.0 ml min^{-1} for NH_4^+ and 2.4 mM tris(hydroxymethyl)aminomethane and 2.5 mM phthalic acid of pH 4.0 at 1.5 ml min^{-1} for NO_3^-.

3. Results and discussion

3.1. Color removal of the DY4 solution in EF and PEF

The 200 mg l^{-1} DY4 solution in 0.05 M Na_2SO_4 with 0.5 mM Fe^{2+} at pH 3.0 and 35 °C was decolorized at similar rate in EF and PEF for the same current density. An increase in j decreased the time required for achieving total decolorization. For each trial, the percentage of color removal was calculated from the expression [13]:

$$\%\ \text{color removal} = \frac{A_0 - A_t}{t_0} \times 100 \quad (6)$$

where A_0 and A_t are the absorbances at initial time and time t for λ_{max} = 400 nm, respectively. Fig. 1a exemplifies the variation of this parameter with electrolysis time for EF at j = 33.3 mA cm^{-2}. As can be seen, the initially yellow DY4 solution underwent a quick color removal, becoming colorless at 40 min of treatment. This behavior can be confirmed from the change in its UV–Vis spectrum depicted in Fig. 1b. Two broad bands centered at 252 and 400 nm can be observed for the initial solution. The minor band at 252 nm can be ascribed to the aromatic rings, whereas the major one is related to the $\pi \rightarrow \pi*$ transition of the large conjugated chromophore system with three benzenic rings, one —C=C— bond and two —N=N— bonds (see the formula of DY4 in Table 1). Fig. 1b also shows that the intensity of both bands falls rapidly during the first 20–25 min of electrolysis, as expected if non-conjugated molecules are gradually formed [44–46]. Besides, the maximal of 400 nm of the major band is progressively shifted to a lower value of 348 nm, suggesting the generation of colored by-products with shorter conjugation prior to the cleavage of the conjugated systems.

Note that the high efficiency of the air-diffusion cathode to generate H_2O_2 from reaction (2) [13,44] avoids the significant reduction of —N=N— bonds on its surface, as found for metallic cathodes [2]. The fast and similar decolorization of the DY4 solution by EF and PEF can then be associated with the combined oxidative attack of ·OH formed from Fenton's reaction (3) and

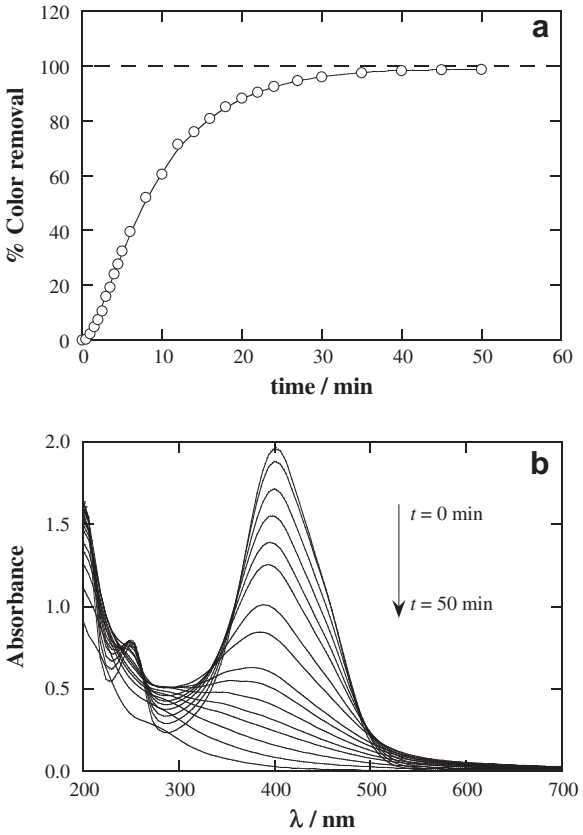

Fig. 1. (a) Percentage of color removal with electrolysis time for the degradation of 100 ml of a 200 mg l^{-1} DY4 solution in 0.05 M Na_2SO_4 with 0.5 mM Fe^{2+} at pH 3.0, 33.3 mA cm^{-2} and 35 °C by electro-Fenton (EF). The cell contained a 3 cm^2 BDD anode and a 3 cm^2 air-diffusion electrode. (b) UV–vis spectra recorded for the DY4 solution from 0 to 50 min of electrolysis.

BDD(·OH) produced from reaction (1), as well as the direct oxidation of DY4 and its primary by-products at the BDD anode, without significant photolysis of organics by UVA light in PEF. Higher j values accelerate all electrode reactions, producing more oxidant hydroxyl radicals and shorting the time required for total decolorization. These oxidation reactions also yield the gradual mineralization of intermediates to CO_2 and inorganic ions, as will be discussed in subsections below.

3.2. Comparative TOC removal of the DY4 solution by EF, PEF and PA–EF

Fig. 2a highlights that direct exposition of the above 200 mg l^{-1} DY4 solution to UVA light without current circulation did not yield any TOC decay, indicating that the diazo dye is not photodecomposed. In contrast, a gradual mineralization with prolonging electrolysis always took place under EF and PEF conditions. After 360 min at 33.3 mA cm^{-2} (see Fig. 2a), TOC was only reduced by 83% in EF process, whereas an almost total mineralization with 97% TOC decay was achieved by the more potent PEF method. In both treatments, DY4 and its intermediates are destroyed by ·OH in the bulk and BDD(·OH) at the anode surface, along with their direct oxidation on BDD, as pointed out above. The higher mineralization attained by PEF can then be related to the synergistic action of UVA light that promotes the photolysis of several intermediates, like Fe(III)-carboxylate complexes [43–46], accelerating their conversion into CO_2.

To check the oxidation ability of H_2O_2 produced in EF, a run was made by stopping the current density of 33.3 mA cm^{-2} at 60 min and further measuring the change of TOC up to 360 min. As can be seen in Fig. 2a, the remaining TOC of 69 mg l^{-1} after 60 min of EF was reduced to 55 mg l^{-1} at 180 min, whereupon it remained constant. This decay in 14 mg l^{-1} of TOC without pass of current can be accounted for by the oxidative action of ·OH formed from Fenton's reaction (3) until the consumption of H_2O_2 accumulated in solution during the first hour of electrolysis. A gradual accumulation of H_2O_2 generated from a gas-diffusion electrode during EF and PEF treatments of other aromatics has been reported previously [41].

From the aforementioned considerations, several trials were designed to assess the oxidation power of the proposed PA–EF process. The treatment of the 200 mg l^{-1} DY4 solution was initiated operating under EF conditions at 33.3 mA cm^{-2} for 30, 60 and 120 min, being subsequently irradiated with UVA light until 360 min. Fig. 2b illustrates that for these runs, TOC was finally reduced by 41%, 82% and 97%, respectively. Note that by stopping the EF treatment at 60 min, the oxidation action of UVA light with 82% TOC decay was much more effective than that of ·OH formed from accumulated H_2O_2 with only 45% TOC decay (see Fig. 2a), indicating that a large proportion of intermediates is already able to be photolyzed. When the electrolysis time of EF was prolonged to 120 min reaching about 60% of TOC removal (see Fig. 2b), the PA–EF process became as potent as the PEF one, giving rise to a similar almost total mineralization of 97% at 360 min. That means that once attained 60% TOC decay in EF, most of remaining intermediates can be easily photolyzed by UVA light and transformed into CO_2, so that, no oxidant hydroxyl radicals are needed for their mineralization. A 60% TOC removal can then be considered the best experimental condition to stop the EF treatment during the PA–EF process.

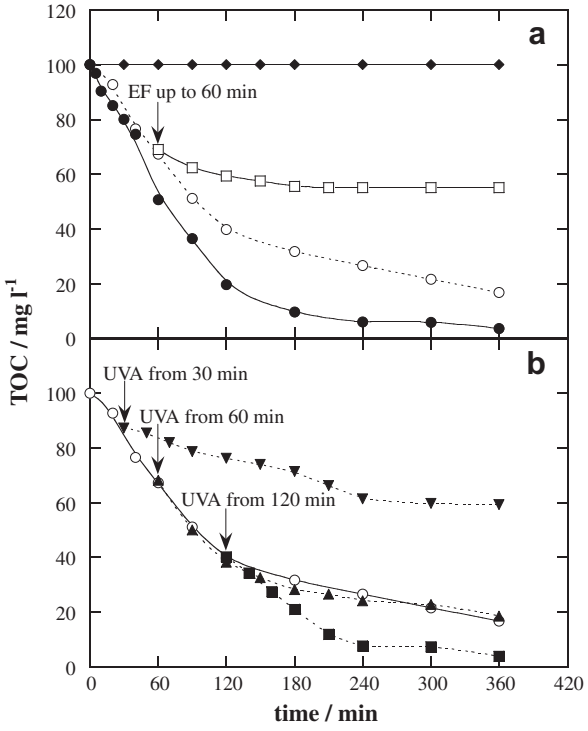

Fig. 2. TOC abatement vs electrolysis time for 100 ml of a 200 mg l^{-1} DY4 solution in 0.05 M Na_2SO_4 with 0.5 mM Fe^{2+} at pH 3.0, 33.3 mA cm^{-2} and 35 °C. In plot (a), (♦) UV irradiation without current and (○) EF and (●) photoelectro-Fenton (PEF) with 6 W UVA light of λ_{max} = 360 nm. (□) EF process up to 60 min, whereupon the resulting solution remained without any treatment. In plot (b), (○) EF process and photo-assisted EF (PA–EF) degradation where only UVA irradiation was applied to the solution after: (▼) 30 min, (▲) 60 min and (■) 120 min of electrolysis.

3.3. Effect of current density on TOC decay

The current density is a key parameter of the EAOPs because it limits the amount of generated hydroxyl radicals that can oxidize the organic matter [13]. The influence of this variable on the degradation rate of DY4 in EF and PEF was studied by electrolyzing the 200 mg l^{-1} diazo dye solution between 16.6 and 100 mA cm^{-2}. Fig. 3a and b shows that TOC removal increased with increasing j from 16.6 to 66.6 mA cm^{-2} due to the concomitant acceleration in the production of BDD(·OH) from reaction (1) and ·OH from Fenton's reaction (3) as a result of the greater H_2O_2 electrogeneration [41,44] by reaction (2) and Fe^{2+} regeneration by reaction (4). However, similar TOC abatements were found in both treatments for 66.6 and 100 mA cm^{-2}, indicating that at j > 66.6 mA cm^{-2}, the electrolytic systems achieved their maximum oxidation power with maximum generation of reactive hydroxyl radicals. Comparison of Fig. 3a and b evidences that the PEF process is more potent than the EF one for all j values because of the additional photolytic destruction of intermediates by UVA light. For example, after 240 min of electrolysis, TOC was reduced by 59%, 68%, 74%, 85% and 83% for EF and 72%, 91%, 94%, 95% and 97% for PEF at increasing j of 16.6, 25.0, 33.3, 66.6 and 100 mA cm^{-2}.

To better clarify the role of generated hydroxyl radicals, the mineralization current efficiency (MCE) for the above trials was estimated as follows [44,45]:

$$\mathrm{MCE}\ (\%) = \frac{nFV_s\Delta(\mathrm{TOC})_{\mathrm{exp}}}{4.32\times10^7\ mIt}\times 100 \qquad (7)$$

where F is the Faraday constant (96487 C mol^{-1}), V_s is the solution volume (l), $\Delta(\mathrm{TOC})_{\mathrm{exp}}$ is the experimental TOC decay (mg l^{-1}), 4.32×10^7 is an homogenization factor (3600 s h^{-1} × 12000 mg mol^{-1}), m is the number of carbon atoms of DY4 (26 carbon atoms), I is the applied current (A) and t is the electrolysis time (h). The number of electrons (n) consumed per molecule

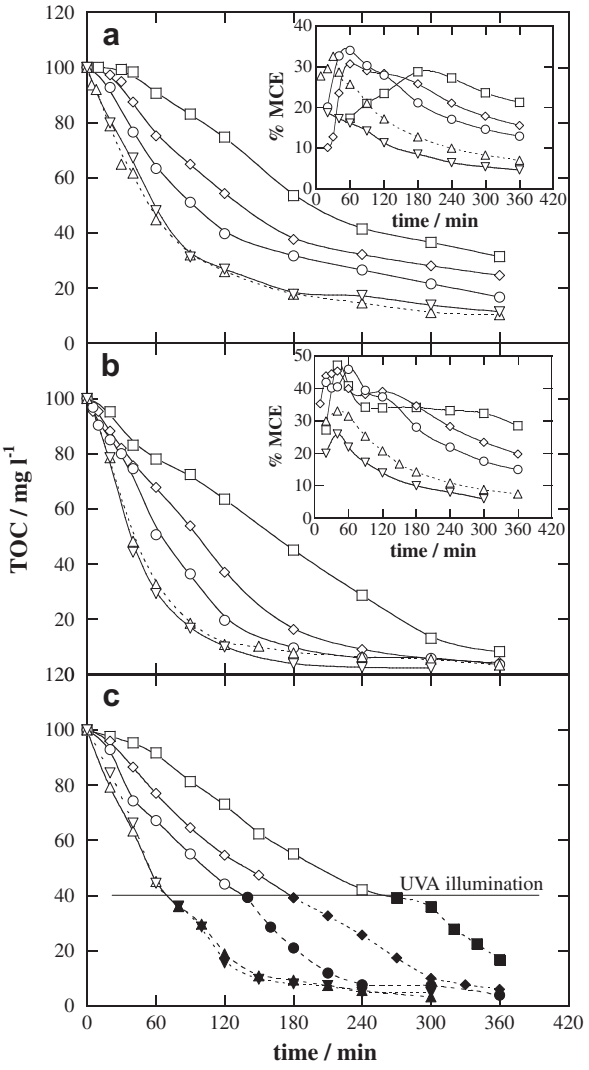

Fig. 3. Effect of current density on TOC decay with electrolysis time for the treatments of 100 ml of 200 mg l^{-1} DY4 solution in 0.05 M Na_2SO_4 with 0.5 mM Fe^{2+} at pH 3.0 and 35 °C. by means of (a) EF, (b) PEF and (c) PA–EF by stopping applied current density and starting UVA irradiation at 60% of mineralization. Current density: (□) 16.6 mA cm^{-2}, (◇) 25.0 mA cm^{-2}, (○) 33.3 mA cm^{-2}, (△) 66.6 mA cm^{-2} and (▽) 100 mA cm^{-2}. In plot (c), the black symbols correspond to data obtained under UVA light. The inset panels present the corresponding mineralization current efficiencies calculated from Eq. (7).

mineralized was taken as 108 assuming that DY4 is converted into carbon dioxide, and sulfate and ammonium ions from reaction (8):

$$C_{26}H_{18}N_4O_8S_2^{2-} + 52H_2O \rightarrow 26CO_2 + 2SO_4^{2-} + 4NH_4^+ + 106H^+ + 108e^- \quad (8)$$

The formation of sulfate ion is expected from the oxidation behavior of sulfonated compounds [42], whereas the initial nitrogen is mainly mineralized to NH_4^+ ion, as will be discussed below.

The inset panels of Fig. 3a and b present the MCE values calculated from Eq. (7) for the corresponding EF and PEF trials. As expected, greater efficiencies were comparatively obtained for the PEF process owing to its higher oxidation power. The lower j = 16.6 mA cm^{-2} yielded smaller MCE values than 25.0 and 33.3 mA cm^{-2} during the first 120 min of both treatments, suggesting the slower mineralization of organics by the lower production of BDD(·OH) and ·OH. Maximum efficiencies of 28–34% for EF and 37–45% for PEF were found for 25.0 and 33.3 mA cm^{-2} up to 120 min, although such efficiencies diminished gradually with raising j. Moreover, at longer electrolysis time the MCE values undergo a dramatic fall, more pronounced as j increases. This phenomenon can be ascribed to the gradual loss in organic matter and the accumulation of low amounts of intermediates that are hardly oxidizable with hydroxyl radicals [12,13]. The fact that maximum and similar efficiencies were determined for each EAOP at 25.0 and 33.3 mA cm^{-2} up to 120 min, decreasing strongly for 66.6 and 100 mA cm^{-2}, as well as the progressive decay in MCE at longer times when j increases from 16.6 to 100 mA cm^{-2}, seems contradictory to the higher production of hydroxyl radicals suggested by the concomitant acceleration of the mineralization process shown in Fig. 3a and b. This behavior indicates that hydroxyls radicals are mainly consumed in parasitic non-oxidizing reactions at higher j. Such waste reactions involve the direct oxidation of BDD(·OH) to O_2 by reaction (9), the dimerization of ·OH to H_2O_2 by reaction (10) and its destruction with H_2O_2 by reaction (11) giving the weaker oxidant hydroperoxyl radical (HO_2·) [12–14]:

$$2BDD(\cdot OH) \rightarrow 2BDD + O_{2(g)} + 2H^+ + 2e^- \quad (9)$$

$$2\cdot OH \rightarrow H_2O_2 \quad (10)$$

$$H_2O_2 + \cdot OH \rightarrow HO_2^{\cdot} + H_2O \quad (11)$$

Moreover, BDD(·OH) generation can also be inhibited by the parallel production of weaker oxidants like $S_2O_8^{2-}$ ion from SO_4^{2-} ion oxidation by reaction (12) and O_3 by reaction (13) [8,12]:

$$2SO_4^{2-} \rightarrow S_2O_8^{2-} + 2e^- \quad (12)$$

$$3H_2O \rightarrow O_{3(g)} + 6H^+ + 6e^- \quad (13)$$

The production of ·OH in the bulk from Fenton's reaction (3) could also be decelerated at higher j by the increase in rate of H_2 evolution at the cathode taking place in parallel to H_2O_2 generation by reaction (2).

The effect of current density on the PA–EF degradation of the DY4 solution was further investigated. To do this, the initial EF treatment was applied for each j until the optimum 60% TOC removal was reached, then the solution being illuminated with UVA light. For these trials, Fig. 3c depicts that the electrolysis ran for 270, 180, 140, 80 and 80 min at 16.6, 25.0, 33.3, 66.6 and 100 mA cm^{-2}, respectively. While only 83% mineralization was reached for 16.6 mA cm^{-2} at 360 min, higher TOC removals of 90–93% were obtained for the j values of 33.3, 66.6 and 100 mA cm^{-2} at 240 min, slightly lower than those determined for PEF (see Fig. 3b). This indicates again that the PA–EF process rapidly mineralizes the solution because the major part of remaining organics can be photolyzed by UVA light, being as potent as PEF. To confirm that the former method is more economic, the specific energy consumption per unit TOC mass (EC) of each trial was estimated from the expression [13]:

$$EC(kW\ h\ g^{-1}TOC) = \frac{(IE_{cell}t_1 + 6t_2)}{\Delta(TOC_{exp})V_s} \quad (14)$$

where E_{cell} is the average potential difference of the cell (V), 6 is the power of the UVA lamp (W), t_1 and t_2 are the corresponding times for the electrolysis and UVA irradiation (h), $\Delta(TOC)_{exp}$ is the experimental TOC decay (mg l^{-1}) and V_s is the solution volume (l). From Eq. (14), one obtains for j = 33.3 mA cm^{-2} (E_{cell} = 12.0 V) during 4 h of treatment, a cost of 0.64 kW h g^{-1} TOC for EF (t_1 = 4 h, t_2 = 0), 3.06 kW h g^{-1} TOC for PEF (t_1 = 4 h, t_2 = 4 h) and 1.39 kW h g^{-1} TOC for PA–EF (t_1 = 2.66 h, t_2 = 1.33 h). It is then apparent that the PA–EF method is much less expensive than the PEF one, but EF is more economic although it yields lower mineralization (see Fig. 3a and c). However, at high j this trend is inverted due to the

great increase in E_{cell}. For example, at 100 mA cm^{-2} (E_{cell} = 28.9 V), energy consumptions of 4.18, 6.05 and 3.55 kW h g^{-1} TOC are obtained for the above EF, PEF and PA–EF treatments, respectively. Consequently, the PA–EF process is always more economic than PEF and can also be less expensive than EF at high *j*.

3.4. Evolution of generated carboxylic acids and released inorganic nitrogen ions

It is well-known that the mineralization of aromatics by EAOPs leads to short-linear carboxylic acids, which are present in the solution as Fe(III) complexes [2,13,41,43–46]. The formation of these products from DY4 was corroborated for the EF, PEF and PA–EF treatments at 33.3 mA cm^{-2}. Ion-exclusion HPLC chromatograms of electrolyzed solutions exhibited well-defined peaks related to oxalic, maleic and oxamic acids at retention times of 6.9, 8.2 and 9.4 min, respectively. Maleic acid is formed from the cleavage of the benzenic rings of aromatic intermediates, subsequently being oxidized to oxalic acid [2,13]. This acid is largely accumulated because it is the final product of precedent longer linear acids, whereas oxamic acid is formed in much smaller extent from the breaking of the heteroaromatic moieties with a —NH_2 group. Oxalic and oxamic acids are ultimate carboxylic acids because they are directly oxidized to CO_2 [47].

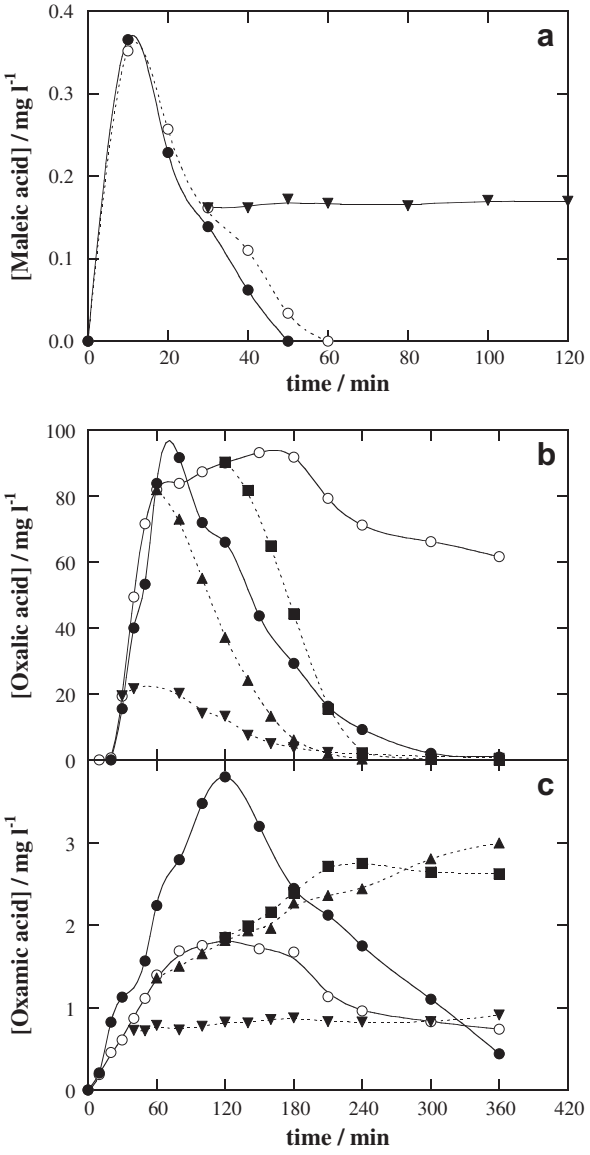

Fig. 4. Evolution of (a) maleic, (b) oxalic and (c) oxamic acids detected during the treatment of 100 ml of a 200 mg l^{-1} DY4 solution in 0.05 M Na_2SO_4 with 0.5 mM Fe^{2+} at pH 3.0, 33.3 mA cm^{-2} and 35 °C. Method: (○) EF, (●) PEF and PA–EF where only UVA irradiation started at: (▼) 30 min, (▲) 60 min and (■) 120 min of electrolysis.

Fig. 4a illustrates that maleic acid was accumulated in small extent, 0.36 mg l^{-1} as maximum, and removed at similar rate by EF and PEF, disappearing from the medium in 50–60 min. It can also be observed that when the electrolysis was stopped at 30 min of the PA–EF treatment, the concentration of maleic acid (0.16 mg l^{-1}) remained constant under UVA irradiation. This indicates that Fe(III)-maleate complexes are efficiently oxidized by ·OH and BDD(·OH), but not directly photolyzed by UVA light. The fast destruction of such complexes by hydroxyl radicals then explains the quick removal of maleic acid in these EAOPs.

A very different behavior can be seen in Fig. 4b for oxalic acid. In EF, this acid was gradually and largely accumulated up to 93 mg l^{-1} in 150 min, whereupon it decayed slowly to 62 mg l^{-1} in 360 min. This trend evidences a very slow destruction of Fe(III)-oxalate complexes with hydroxyl radicals, mainly with BDD(·OH) [47]. In contrast, a maximum content of 91 mg l^{-1} for this acid was already found after only 80 min of PEF, practically disappearing at 360 min, i.e. when the solution reached 97% mineralization (see Fig. 2a). This indicates that larger amounts of Fe(III)-oxalate complexes are more quickly generated from the photolysis of longer carboxylic acids, then being much more rapidly photodecarboxylated by UVA light than oxidized with hydroxyl radicals [43–47]. Fig. 4b also shows that in PA–EF, all the oxalic acid accumulated after 30, 60 and 120 min of electrolysis was completely removed by applying UVA irradiation up to 360 min. A simple mass balance of this process at 120 min reveals that the 90 mg l^{-1} of oxalic acid accumulated corresponds to 24 mg l^{-1} TOC, that is, only 60% of the 40 mg l^{-1} TOC of the remaining solution (see Fig. 2b). Since 97% TOC removal is attained at the end of this PA–EF treatment, one can infer that large quantities of other undetected intermediates, different from carboxylic acids, are mineralized under the action of UVA light.

Fig. 4c depicts a more complex behavior for oxamic acid. In EF, this acid was accumulated up to 1.8 mg l^{-1} in 120 min and further very slowly removed to a final value of 0.7 mg l^{-1} because of the small reaction rate of their Fe(III) complexes with ·OH and BDD(·OH) [47]. In PEF, however, oxamic acid was much more largely produced, up to 3.8 mg l^{-1} in 120 min, and much more rapidly removed at 360 min. This can be related to the synergistic action of UVA light, which photolyzes several *N*-intermediates accelerating the production of oxamic acid, as well as the Fe(III)-oxamate complexes enhancing their mineralization. Surprisingly, Fig. 4c shows that in all the PA–EF treatments, the oxamic acid concentration increased during the UVA illumination step. For example, the 1.8 mg l^{-1} of this acid present in the solution after 120 min of electrolysis rose up to 2.6 mg l^{-1} at the end of the process. This suggest the generation of large amounts of *N*-derivatives from DY4 that are difficulty removed by hydroxyl radicals but easily photolyzed by UVA light accelerating their conversion into oxamic acid and/or their mineralization. This fact, along with the quick photodecomposition of Fe(III)-oxalate complexes (see Fig. 4b), could explain the almost total mineralization reached by this PA–EF process.

Ionic chromatograms of electrolyzed solutions confirmed the release of NH_4^+ and NO_3^- ions from the initial N contained in DY4 (21.4 mg l^{-1}) by the EAOPs tested. No other inorganic nitrogen ions, like NO_2^- ion, were detected by this technique. Table 2 shows that after 360 min of electrolysis at 33.3 mA cm^{-2}, a similar concentration of each ion was found for both EF and PEF treatments, but with a much larger proportion of NH_4^+ (ca. 22% of initial N) than NO_3^- ion (ca. 8% of initial N), as proposed in reaction (8). In contrast, the

Table 2
Concentration of *N*-compounds formed, percentage of initial N released to solution and total nitrogen (TN) determined after 360 min of treatment of 100 ml of a 200 mg l^{-1} DY4 solution in 0.05 M Na_2SO_4 with 0.5 mM Fe^{2+} at pH 3.0 and 35 °C in a BDD/air-diffusion cell at 33.3 mA cm^{-2} by EF, PEF and PA–EF.

Process	Oxamic acid[a] (mg l^{-1})	NH_4^+ ion[a] (mg l^{-1})	NO_3^- ion[a] (mg l^{-1})	% initial N released to solution	TN[b] (mg l^{-1})
EF	0.74 (0.55)	5.90 (21.44)	6.82 (7.19)	29.18	6.40 (29.89)
PEF	0.44 (0.33)	6.06 (22.02)	8.28 (8.73)	31.08	6.67 (31.17)
PA–EF[c]	2.62 (1.87)	9.03 (32.80)	9.38 (9.89)	44.56	9.51 (44.39)

[a] In parenthesis: percentage of initial N in the *N*-compound.
[b] In parenthesis: percentage of total nitrogen respect to initial N.
[c] In parenthesis: stop of EF and start of UVA illumination at 120 min.

PA–EF process by stopping the electrolysis at 120 min yielded greater contents of both inorganic ions, being accumulated about 33% and 10% of initial N as NO_4^+ and NO_3^- ions, respectively (see Table 2). Taking into account the concentration of oxamic acid shown in Fig. 4c, Table 2 evidences that the percentage of initial N released to the solution is near 30% for EF and PEF and 44% for PA–EF, in good agreement with the TN values determined for the corresponding final treated solutions, as expected if they mainly contain oxamic acid and NH_4^+ and NO_3^- ions as *N*-compounds. These findings demonstrate that the initial N is mainly mineralized to NH_4^+, although its major part is loss as volatile derivatives, probably N_2 and NO_x species. The smaller production of inorganic nitrogen ions in the EF and PEF processes than in the PA–EF one suggests that volatile *N*-derivatives proceed from the oxidation of *N*-intermediates with generated hydroxyl radicals, whereas their photolytic reactions favor the mineralization via NH_4^+ and NO_3^- production.

4. Conclusions

A solution with 200 mg l^{-1} DY4 was rapidly decolorized at the same rate by EF and PEF, indicating that generated hydroxyl radicals are the main oxidants of the diazo dye. The PEF process was much more powerful due to the synergistic action of UVA light yielding an almost total mineralization, whereas the EF one only allowed a partial mineralization. The proposed PA–EF treatment was as potent as the PEF one if the initial electrolysis was performed during a sufficiently long time to produce intermediates that can be mineralized by photolysis with UVA light. At 33.3 mA cm^{-2}, the best PA–EF process was found by stopping the electrolysis and starting UVA irradiation at 120 min. The increase in j from 16.6 to 100 mA cm^{-2} enhanced both EF and PEF treatments because of the larger production of hydroxyl radicals. Maximum MCE values were obtained during the first 120 min of both EAOPs at 25.0 and 33.3 mA cm^{-2}, decreasing with increasing j by the acceleration of parasitic reactions of hydroxyl radicals. The PA–EF process was also very effective from j = 25.0 mA cm^{-2}, always being more economic than PEF and even less expensive than EF at high j. Maleic, oxalic and oxamic acids were detected as generated carboxylic acids. While Fe(III)-maleate complexes were quickly removed with hydroxyl radicals, the Fe(III) complexes of the two latter acids were photodecomposed by UVA light in PEF and PA–EF. In these processes, oxamic acid was formed in larger extent from the photolysis of *N*-intermediates. NH_4^+ ion was accumulated in much larger proportion than NO_3^- ion, although the major part of the initial N was lost as volatile *N*-compounds. The high effectiveness of PEF and PA–EF treatments can be ascribed to the photolytic removal of Fe(III)-oxalate complexes and *N*-intermediates. PA–EF method can then be an excellent EAOP for the remediation of industrial textile wastewaters.

Acknowledgements

The authors thank the financial support from MICINN (Ministerio de Ciencia e Innovación, Spain) under the project CTQ2010-16164/BQU, co-financed with FEDER funds. The grants given to S. Garcia-Segura and A. El-Ghenymy awarded from MEC (Ministerio de Educación y Ciencia, Spain) are acknowledged.

References

[1] E. Forgacs, T. Cserháti, G. Oros, Environ. Int. 30 (2004) 953–971.
[2] C.A. Martínez-Huitle, E. Brillas, Appl. Catal. B: Environ. 87 (2009) 105–145.
[3] S.M.A.G. Ulson de Souza, E. Forgiarini, A.A. Ulson de Souza, J. Hazard. Mater. 147 (2007) 1073–1078.
[4] K.P. Sharma, S. Sharma, S. Sharma, P.K. Singh, S. Kumar, R. Grover, P.K. Sharma, Chemosphere 69 (2007) 48–54.
[5] T. Robinson, G. McMullan, R. Marchant, P. Nigam, Bioresour. Technol. 77 (2001) 241–255.
[6] E. Brillas, J.C. Calpe, P.L. Cabot, Appl. Catal. B-Environ. 46 (2003) 381–391.
[7] M. Pera-Titus, V. García-Molina, M.A. Baños, J. Giménez, S. Esplugas, Appl. Catal. B-Environ. 47 (2004) 219–256.
[8] C.A. Martínez-Huitle, E. Brillas, Angew. Chem. Int. Ed. 47 (2008) 1998–2005.
[9] M. Klavarioti, D. Mantzavinos, D. Kassinos, Environ. Int. 35 (2009) 402–417.
[10] C.A. Martínez-Huitle, S. Ferro, Chem. Soc. Rev. 35 (2006) 1324–1340.
[11] A. Anglada, A. Urtiaga, I. Ortiz, J. Chem. Technol. Biotechnol. 84 (2009) 1747–1755.
[12] M. Panizza, G. Cerisola, Chem. Rev. 109 (2009) 6541–6569.
[13] E. Brillas, I. Sirés, M.A. Oturan, Chem. Rev. 109 (2009) 6570–6631.
[14] B. Marselli, J. Garcia-Gomez, P.A. Michaud, M.A. Rodrigo, Ch. Comninellis, J. Electrochem. Soc. 150 (2003) D79–D83.
[15] I. Sirés, E. Brillas, G. Cerisola, M. Panizza, J. Electroanal. Chem. 613 (2008) 151–159.
[16] C. Flox, C. Arias, E. Brillas, A. Savall, K. Groenen-Serrano, Chemosphere 74 (2009) 1340–1347.
[17] M. Faouzi, P. Cañizares, A. Gadri, J. Lobato, B. Nasr, R. Paz, M.A. Rodrigo, C. Saez, Electrochim. Acta 52 (2006) 325–331.
[18] C. Flox, P.L. Cabot, F. Centellas, J.A. Garrido, R.M. Rodríguez, C. Arias, E. Brillas, Chemosphere 64 (2006) 892–902.
[19] L.S. Andrade, L.A.M. Ruotolo, R.C. Rocha-Filho, N. Bocchi, S.R. Biaggio, J. Iniesta, V. García-Garcia, V. Montiel, Chemosphere 66 (2007) 2035–2043.
[20] E. Butrón, M.E. Juárez, M. Solis, M. Teutli, I. González, J.L. Nava, Electrochim. Acta 52 (2007) 6888–6894.
[21] M. Panizza, G. Cerisola, J. Hazard. Mater. 153 (2008) 83–88.
[22] E. Brillas, S. Garcia-Segura, M. Skoumal, C. Arias, Chemosphere 79 (2010) 605–612.
[23] J. Sun, H. Lu, L. Du, H. Lin, H. Li, Appl. Surf. Sci. 257 (2011) 6667–6671.
[24] J.M. Aquino, M.A. Rodrigo, R.C. Rocha-Filho, C. Sáez, P. Cañizares, Chem. Eng. J. 184 (2012) 221–227.
[25] A.R. Khataee, M. Zarei, S.K. Asl, J. Electroanal. Chem. 648 (2010) 143–150.
[26] M. Zarei, A.R. Khataee, R. Ordikhani-Seyedlar, M. Fathinia, Electrochim. Acta 55 (2010) 7259–7265.
[27] M. Iranifam, M. Zarei, A.R. Khataee, J. Electroanal. Chem. 659 (2011) 107–112.
[28] A.R. Khataee, M. Safarpour, M. Zarei, S. Aber, J. Electroanal. Chem. 659 (2011) 63–68.
[29] N. Oturan, M.A. Oturan, Agron. Sustain. Dev. 25 (2005) 267–270.
[30] S. Hammami, N. Oturan, N. Bellakhal, M. Dachraoui, M.A. Oturan, J. Electroanal. Chem. 610 (2007) 75–84.
[31] A. Özcan, Y. Şahin, A.S. Koparal, M.A. Oturan, Appl. Catal. B-Environ. 89 (2009) 620–626.
[32] I. Sirés, N. Oturan, M.A. Oturan, Water Res. 44 (2010) 3109–3120.
[33] M.A. Oturan, N. Oturan, M.C. Edelahi, F.I. Podvorica, K. El Kacemi, Chem. Eng. J. 171 (2011) 127–135.
[34] A. Wang, J. Qu, H. Liu, J. Ru, Appl. Catal. B-Environ. 84 (2008) 393–399.
[35] A. Özcan, Y. Sahin, A.S. Koparal, M.A. Oturan, J. Electroanal. Chem. 616 (2008) 71–78.
[36] K. Cruz-González, O. Torres-López, A. García-León, J.L. Guzmán-Mar, L.H. Reyes, A. Hernández-Ramírez, J.M. Peralta-Hernández, Chem. Eng. J. 160 (2010) 199–206.
[37] K. Cruz-González, O. Torres-Lopez, A.M. García-León, E. Brillas, A. Hernández-Ramírez, J.M. Peralta-Hernández, Desalination 286 (2012) 63–68.
[38] B. Boye, M.M. Dieng, E. Brillas, Electrochim. Acta 48 (2003) 781–790.
[39] E. Brillas, M.A. Baños, S. Camps, C. Arias, P.L. Cabot, J.A. Garrido, R.M. Rodríguez, New J. Chem. 28 (2004) 314–322.

[40] S. Ammar, R. Abdelhedi, C. Flox, C. Arias, E. Brillas, Environ. Chem. Lett. 4 (2006) 229–233.
[41] C. Flox, J.A. Garrido, R.M. Rodríguez, P.L. Cabot, F. Centellas, C. Arias, E. Brillas, Catal. Today 129 (2007) 29–36.
[42] M. Panizza, G. Cerisola, Water Res. 43 (2009) 339–344.
[43] M. Skoumal, R.M. Rodríguez, P.L. Cabot, F. Centellas, J.A. Garrido, C. Arias, E. Brillas, Electrochim. Acta 54 (2009) 2077–2085.
[44] E.J. Ruiz, A. Hernández-Ramírez, J.M. Peralta-Hernández, C. Arias, E. Brillas, Chem. Eng. J. 171 (2011) 385–392.
[45] R. Salazar, S. Garcia-Segura, M.S. Ureta-Zañartu, E. Brillas, Electrochim. Acta 56 (2011) 6371–6379.
[46] L.C. Almeida, S. Garcia-Segura, N. Bocchi, E. Brillas, Appl. Catal. B: Environ. 103 (2011) 21–30.
[47] S. Garcia-Segura, E. Brillas, Water Res. 45 (2011) 2975–2984.

PAPER 6

Solar photoelectrocatalytic degradation of Acid Orange 7 azo dye using a highly stable TiO_2 photoanode synthesized by atmospheric plasma spray

Applied Catalysis B: Environmental 132–133 (2013) 142–150

Contents lists available at SciVerse ScienceDirect

Applied Catalysis B: Environmental

journal homepage: www.elsevier.com/locate/apcatb

Solar photoelectrocatalytic degradation of Acid Orange 7 azo dye using a highly stable TiO_2 photoanode synthesized by atmospheric plasma spray

Sergi Garcia-Segura[a], Sergi Dosta[b], Josep M. Guilemany[b], Enric Brillas[a,*]

[a] Laboratori d'Electroquímica dels Materials i del Medi Ambient, Departament de Química Física, Facultat de Química, Universitat de Barcelona, Martí i Franquès 1-11, 08028 Barcelona, Spain

[b] CPT Thermal Spray Centre, Materials Engineering, Departament d'Enginyeria Química i Metal.lúrgia, Universitat de Barcelona, Martí i Franquès 1-11, 08028 Barcelona, Spain

ARTICLE INFO

Article history:
Received 16 August 2012
Received in revised form
17 November 2012
Accepted 22 November 2012
Available online 1 December 2012

Keywords:
Acid Orange 7
Photocatalysis
Photoelectrocatalysis
Sunlight
Water treatment

ABSTRACT

A TiO_2 coating composed of 29% rutile, 9% anatase and 62% of Ti_7O_{13} on stainless steel support has been prepared by atmospheric plasma spray technology. This novel photoanode was coupled to an air-diffusion cathode that generates H_2O_2 in a photoelectrochemical cell submitted to direct sunlight irradiation to degrade 100 mL of Acid Orange 7 (AO7) azo dye solutions in 0.05 M Na_2SO_4 by solar photoelectrocatalysis (SPEC). The photoanode presented excellent mechanical properties as well as large stability and long durability up to 2.0 mA cm^{-2}. The decolorization process in SPEC was synergistic of the individual processes in solar photocatalysis and anodic oxidation with generated H_2O_2 under comparable conditions owing to the larger production of •OH from the higher amounts of photogenerated holes that can be separated of photogenerated electrons. The best operating variables for SPEC were 15 mg L^{-1} AO7, pH 7.0 and anodic current density (j_{anod}) of 1.0 mA cm^{-2}. Under these conditions, the azo dye disappeared in 100 min and the solution was totally decolorized in 120 min, but only 40% mineralization was attained after 240 min of electrolysis. The AO7 decay followed a pseudo-first-order reaction as found by reversed-phase HPLC and it was accelerated with increasing j_{anod} due to the higher amounts of •OH generated from the production of more photogenerated holes and the enhancement of anodic oxidation of water. Ion-exclusion HPLC allowed the identification of generated carboxylic acids like phthalic, tartaric, succinic, acetic and oxamic, which were the main components of long-time electrolysis. Their persistence explains the low mineralization of AO7 in SPEC. The initial N of the azo dye was mineralized as NH_4^+ ion, in larger proportion than NO_3^- ion, although it was mainly loss as volatile species.

1. Introduction

Azo dyes are widely used in textile and food industries in Mt quantity and represent about 70% of the world dye production. These colored compounds contain one or more azo bonds (—N=N—) as chromophore group linked to aromatic structures with functional groups such as —OH and —SO_3H, among others [1,2]. The dyeing process of textile industries produces large volumes of wastewater effluents with high dye contents, which are discharged into water bodies such as lakes and rivers. Azo dyes are very stable in the aquatic environment and usually persist under ambient conditions because they are difficultly removed in conventional wastewater treatment plants due to their high stability under sunlight and high resistance to biodegradation in aerobic conditions [3]. This contamination is dangerous not only by the esthetic problems caused in waters, but also by the potential health and environmental risks due to the toxic, carcinogenic and mutagenic properties of azo dyes and their by-products [4–6]. To avoid their environmental problems and hazardous effects on living beings, physicochemical treatments like coagulation [7], adsorption [8] or filtration by selective membranes [9], as well as some biotreatments [10], have been applied to decolorize dyeing wastewaters. However, faster and even total decolorization of these effluents can be obtained using advanced oxidation processes (AOPs) [1,2,11]. AOPs are chemical, photochemical, photocatalytic and electrochemical techniques based on the in situ production of hydroxyl radical (•OH) as strong non-selective oxidant of organic pollutants in waters [2,12–14].

In recent years, TiO_2 photocatalysis (PC) has been widely used for the removal of organics, including several dyes, in waters [2,15–25]. This AOP involves the irradiation of TiO_2 nanoparticles, mainly crystallized in the anatase form, in colloidal suspension or deposited as a thin film on Ti by UV photons of sufficient energy

* Corresponding author. Tel.: +34 934021223; fax: +34 934021231.
E-mail address: brillas@ub.edu (E. Brillas).

0926-3373/$ – see front matter © 2012 Elsevier B.V. All rights reserved.
http://dx.doi.org/10.1016/j.apcatb.2012.11.037

($\lambda < 380$ nm) to promote an electron from the filled valence band to the empty conduction band (e_{cb}^-) with an energy gap of 3.2 eV generating a positively charged vacancy or hole (h_{vb}^+) as follows [2,18,19]:

$$TiO_2 + h\nu \rightarrow e_{cb}^- + h_{vb}^+ \quad (1)$$

Organics can then be either reduced by the generated electron or oxidized by the hole as well as by heterogeneous •OH formed between the photogenerated vacancy and adsorbed water or OH^-:

$$h_{vb}^+ + H_2O \rightarrow {}^\bullet OH + H^+ \quad (2)$$

$$h_{vb}^+ + OH^- \rightarrow {}^\bullet OH \quad (3)$$

In addition, other weaker reactive oxygen species (ROS) like superoxide radical ion ($O_2^{\bullet -}$), hydroperoxyl radical ($HO_2^\bullet$) and H_2O_2, as well as more •OH, can be produced from the photoinjected electron by the following reactions [2,19]:

$$e_{cb}^- + O_2 \rightarrow O_2^{\bullet -} \quad (4)$$

$$O_2^{\bullet -} + H^+ \rightarrow HO_2^\bullet \quad (5)$$

$$2HO_2^\bullet \rightarrow H_2O_2 + O_2 \quad (6)$$

$$e_{cb}^- + H_2O_2 \rightarrow {}^\bullet OH + OH^- \quad (7)$$

$$H_2O_2 + O_2^{\bullet -} \rightarrow {}^\bullet OH + OH^- + O_2 \quad (8)$$

When sunlight is used as energy source, the procedure is so-called solar PC (SPC) [17,23,25]. The major loss of efficiency in PC or SPC is due to the recombination of electrons promoted to the valence band either with unreacted holes or with adsorbed hydroxyl radicals [2,12]:

$$e_{cb}^- + h_{vb}^+ \rightarrow TiO_2 + \text{heat} \quad (9)$$

$$e_{cb}^- + {}^\bullet OH \rightarrow OH^- \quad (10)$$

Heterogeneous PC, where the TiO_2 photocatalyst is immobilized onto a solid support matrix mainly by sol-gel, thermal treatment, chemical vapor deposition, electrodeposition and anodization methods, causes a loss of specific area available for photoreaction (1) and the enhancement of the electron-hole pair recombination by reaction (9) that consumes the reductive and oxidant species to destroy organics [22]. However, the efficiency of immobilized TiO_2 can be strongly improved when it acts as photoanode in a photoelectrochemical system leading to the so-called photoelectrocatalysis (PEC) process under UV irradiation or solar PEC (SPEC) process under sunlight illumination [2,26–36]. These electrochemical AOPs (EAOPs) consists of the application of either a constant bias anodic potential or a low constant anodic current density (j_{anod}) to the TiO_2 photoanode subjected to illumination in order to continuously extract the photoinduced electrons by an external electrical circuit. This causes the inhibition of reactions (4)–(10) favoring the production of higher amounts of holes from reaction (1) and heterogeneous •OH from reaction (2) or (3), thereby largely enhancing organics oxidation compared to PC or SPC. In PEC or SPEC, the rutile form of TiO_2 immobilized onto a conductive substrate also shows significant photocatalytic oxidative efficiency, although lower than that of the anatase form [26,28,35].

In this paper, we report the synthesis of a novel TiO_2 photoanode from the deposition of a TiO_2 coating on a stainless steel substrate using the atmospheric plasma spray (APS) technology [37–39]. This photoanode presented excellent mechanical properties and long durability to the pass of relatively high j_{anod} values in SPEC. Its oxidation ability on azo dyes was tested in a photoelectrochemical reactor under direct solar irradiation by studying the decolorization and degradation of Acid Orange 7 (AO7 or Orange II, see formula and characteristics in Table 1) as representative model compound, since it is non-biodegradable and commonly used in

Table 1
Chemical structure and characteristics of Acid Orange 7 azo dye.

Chemical structure	Chemical formula	Color index name	Chemical name	Color index number	λ_{max}/nm	M/g mol^{-1}
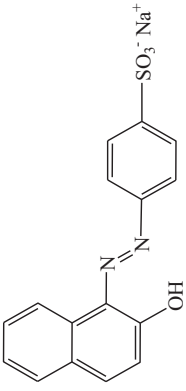	$NaC_{16}H_{10}N_2O_4S$	Acid Orange 7 (AO7)	Sodium 4-[(2E)-2-(2-oxonaphthalen-1-ylidene)hydrazinyl] benzenesulfonate	15510	484	350.32

textile industries. The degradation of AO7 by PC [15] and SPC [16] with TiO_2 in suspension, as well as by PEC with UVA light and SPEC with TiO_2 deposited on transparent conducting substrates [31], has been reported. Note that azo dyes can be reduced at the cathode of an electrochemical and photoelectrochemical system, depending on the nature of the cathodic material [2]. For this reason and to avoid the possible competitive cathodic reduction of AO7 and its intermediates, a carbon-polytetrafluoroethylene (PTFE) air-diffusion cathode was chosen in the present work since it inhibits organic reduction because efficiently generates H_2O_2 from injected O_2 as follows [40–43]:

$$O_2 + 2H^+ + 2e^- \rightarrow H_2O_2 \quad (11)$$

The comparative decolorization efficiency for AO7 solutions using SPC, electrochemical oxidation or anodic oxidation with generated H_2O_2 (AO-H_2O_2) and SPEC was examined. The best operating variables like pH, dye content and applied j_{anod} for the decolorization process in SPEC were determined. The decay kinetics for AO7 and the evolution of generated carboxylic acids and released inorganic nitrogen ions were followed by chromatographic techniques.

2. Experimental

2.1. Chemicals

Pure AO7 azo dye was purchased from Acros Organics and used as received. Phthalic, tartaric, succinic, oxamic and acetic acids were of analytical grade from Panreac and Avocado. Anhydrous sodium sulphate used as background electrolyte was of analytical grade from Fluka. Synthetic dye solutions were prepared with high-purity water obtained from a Millipore Milli-Q system with resistivity >18 MΩ cm at 25 °C and their pH was adjusted with either analytical grade sulphuric acid or analytical sodium hydroxide, both supplied by Merck. Organic solvents and other chemicals employed were of either HPLC or analytical grade from Merck, Fluka and Sigma-Aldrich.

2.2. Preparation of TiO_2 coating onto stainless steel by APS

TiO_2 powder supplied by Sulzer Metco was used as feedstock to synthesize the final coating onto stainless steel by APS technology using an F4 plasma torch with a Sultzer Metco A-3000S system. APS consists of heating up, mixing and homogenization of the feedstock powder particles during their short residence time in the hot zone of the plasma jet. The molten droplets are then accelerated and quenched onto the substrate to produce the coating layer by layer [37–39]. A flat 316L stainless steel (50 mm x 30 mm × 5 mm) was used as substrate, which was previously degreased with acetone and grit blasted with white corundum at 5.6 bar and 45° using a blasting distance of 250 mm. The grit blasted substrate had a mean roughness (Ra) of about 5 μm. The spraying parameters for the TiO_2 coating were taken within the following intervals: argon flow plasma (20–40 L min^{-1}), hydrogen flow plasma (10–15 L min^{-1}), applied current (550–650 A), spray distance (80–160 mm) and feed rate (10–30 g min^{-1}).

2.3. SPC, AO-H_2O_2 and SPEC systems

Fig. 1 illustrates a sketch of the set-up used for the SPEC degradation of 100 mL of AO7 solutions. The photoelectrochemical reactor was an undivided, open and cylindrical cell with a double jacket in which external water circulated to maintain the solution temperature at 35 °C using a Thermo Electron Corporation HAAKE DC 10 thermostat. This temperature was chosen because it is the maximum value allowed in the reactor with insignificant water evaporation during prolonged treatment. The photoanode was the above-synthesized TiO_2 electrode with 5 cm^2 area, whereas the cathode was a 3 cm^2 carbon-PTFE air-diffusion electrode supplied by E-TEK and mounted as described elsewhere [44]. This cathode was fed with air pumped at 300 mL min^{-1} to generate H_2O_2 from reaction (11) and the interelectrode gap was about 1 cm. The electrochemical assays were performed at constant j_{anod} provided with an Amel 2053 potentiostat-galvanostat. The same system was used for the experiments of AO-H_2O_2 in the dark and SPC without pass of current. Prior to the electrolytic trials, the air-diffusion cathode was activated by polarization in 0.05 M Na_2SO_4 using the same reactor with a 3 cm^2 Pt anode at j_{anod} = 100 mA cm^{-2} for 60 min. All experiments were carried out under vigorous stirring with a magnetic bar at 800 rpm to ensure homogenization and the transport of reactants towards/from the TiO_2 electrode or photocatalyst.

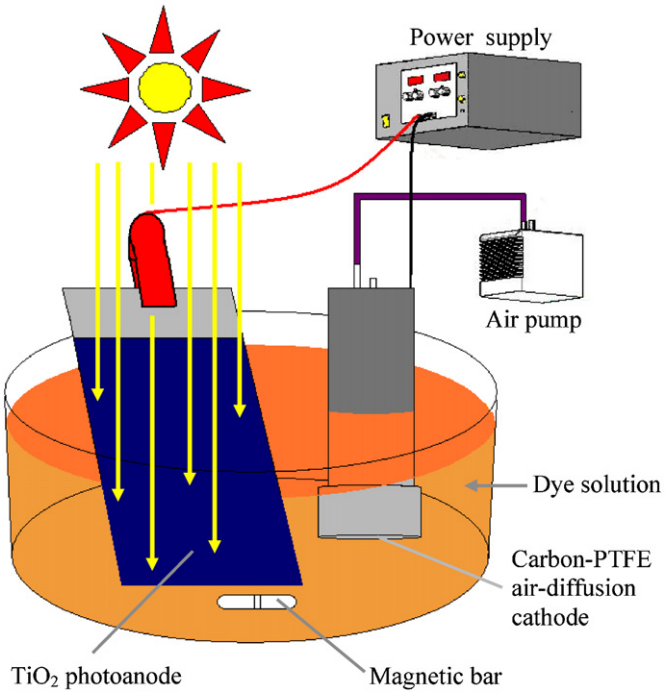

Fig. 1. Sketch of the experimental set-up used for the degradation of 100 mL of Acid Orange 7 (AO7) solutions by solar photoelectrocatalysis (SPEC). The photoelectrochemical reactor contained a TiO_2 photoanode of 5 cm^2 area, which was prepared by TiO_2 deposition on a stainless steel substrate by atmospheric plasma spray technology. The air-diffusion cathode of 3 cm^2 area supplied continuously H_2O_2 to the dye solution from O_2 reduction. The solution was thermostated at 35 °C.

In the SPC and SPEC trials, the immersed TiO_2 photocatalyst was tilted 41° from the solution surface to better collect the direct sun rays in our laboratory of Barcelona (latitude: 41° 21′N, longitude: 2° 10′E). Solar assays were made for 300 min as maximal in sunny and clear days during the summer of 2011, with similar average UV irradiation intensities between 300 and 400 nm of 30.3 and 31.2 W m^{-2}, as measured with a Kipp & Zonen CUV 5 radiometer.

All SPC, AO-H_2O_2 and SPEC experiments were made with solutions containing 0.05 M Na_2SO_4 as background electrolyte. This environmentally friendly medium was chosen because it is usually employed in electrochemical systems to clarify the oxidation role of generated •OH radicals [2]. The best conditions for AO7 decolorization in SPEC were found by studying the effect of pH between 3.0 and 11.0, azo dye concentration up to 45 mg L^{-1} and j_{anod} up to 2.0 mA cm^{-2}.

2.4. Apparatus and analytical procedures

The particle size distribution of the feedstock TiO_2 powder was measured by laser scattering using a Beckman Coulter LS equipment. Scanning electron microscopy (SEM) images of the initial and deposited TiO_2 were obtained using a Jeol 5510 system, which was coupled with an energy dispersive X-ray spectrometry (EDS) phase analyzer from Röntec. More accurate phase analysis of the starting powder and coating was performed by X-ray diffractometry (XRD) using a Siemens D500 system type Bragg-Brentano $\theta/2\theta$ by applying a Cu $K\alpha_{1+2}$ radiation ($\lambda(\alpha_1) = 0.154060$ nm and $\lambda(\alpha_2) = 0.154443$ nm) at 40 kV and 30 mA current. The ratio between the obtained crystalline phases was calculated from their reference intensity ratio (RIR) by the Chung's method [45] and applying the X'pert HighScore Plus software. The porosity of the coating was measured with a Matrox Inspector software image analyzer. Its microroughness was determined with a Mitutoyo Surftest 301 equipment and its adhesion was measured with a Servosis MCH-102ME system through the ASTM C633 standard. Cross-sectional microhardness measurements were performed with a Matsuzawa MXT-α system by Vickers indentation at 300 g load using the UNE 7-423/2 standard. Indentations were determined with a Leica DMI 5000 M optical microscope to increase their accuracy.

The pH of AO7 solutions was measured with a Crison GLP 22 pH-meter. Before analysis, the aliquots were filtered with 0.45 μm PTFE filters from Whatman. The decolorization process of azo dye solutions in SPC, AO-H_2O_2 and SPEC was monitored from the decay of the absorbance (A) at the maximum wavelength (λ_{max} = 484 nm) of AO7 (see Table 1), measured on the spectra recorded with a Shimadzu 1800 UV–vis spectrophotometer at 35 °C. The percentage of color removal or decolorization efficiency was then calculated from the following equation [42,43]:

$$\%\text{Color removal} = \frac{A_0 - A_t}{A_0} 100 \quad (12)$$

where A_0 and A are the absorbance at initial time and time t at the λ_{max} of the azo dye, respectively.

The concentration of accumulated H_2O_2 was determined from the light absorption of its Ti(IV) colored complex at λ = 409 nm [46] using the above spectrophotometer thermostated at 35 °C. The mineralization of azo dye solutions was determined from the abatement of their TOC, measured on a Shimadzu VCSN analyzer. Reproducible TOC values with an accuracy of ±1% were obtained by injecting 50 μL aliquots to the analyzer. Total nitrogen (TN) was determined with a Shimadzu TNM-1 unit coupled to the above TOC analyzer.

The decay of AO7 concentration in SPEC was followed by reversed-phase HPLC using a Waters 600 LC fitted with a Spherisorb ODS2 5 μm (150 mm x 4.6 mm) column at 35 °C and coupled to a Waters 996 photodiode array detector selected at the λ_{max} of the azo dye. Generated carboxylic acids in SPEC were detected by ion-exclusion HPLC using the above LC fitted with a Bio-Rad Aminex HPX 87H (300 mm × 7.8 mm) column at 35 °C and the photodiode array detector set at λ = 210 nm. For these measurements, 20 μL aliquots were injected into the LC and the mobile phase was either a 30:70 (v/v) acetonitrile/water mixture with 2.4 mM *n*-butylamine at 0.6 mL min^{-1} for reversed-phase HPLC or 4 mM H_2SO_4 at 0.6 mL min^{-1} for ion-exclusion HPLC. The inorganic nitrogen ions released in SPEC treatment were quantified by ionic chromatography with a Shimadzu 10 Avp HPLC coupled with a Shimadzu CDD 10 Avp conductivity detector. The NH_4^+ concentration was determined with a Shodex IC YK-421 (125 mm × 4.6 mm) cation column at 40 °C under circulation of a 5.0 mM tartaric acid, 1.0 mM dipicolinic acid, 24.2 mM boric acid and 1.5 mM crown ether solution at 1.0 mL min^{-1} as mobile phase. The NO_3^- content was obtained with a Shim-Pack IC-A1S (100 mm × 4.6 mm) anion column at 40 °C using a mobile phase of 2.4 mM tris(hydroxymethyl)aminomethane and 2.5 mM phthalic acid of pH 4.0 at 1.5 mL min^{-1}.

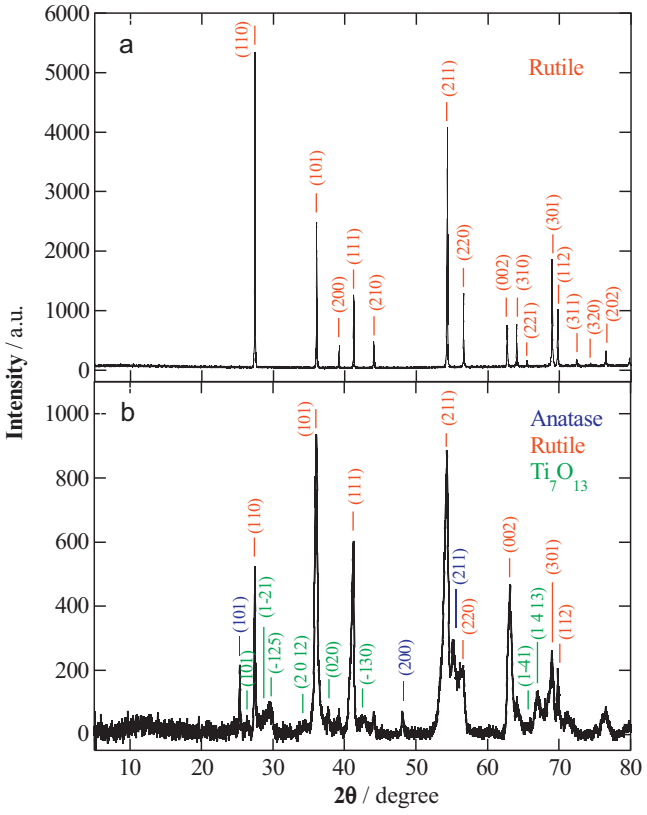

Fig. 2. X-ray diffractograms of (a) the semiconductor TiO_2 powder composed of 100% rutile and (b) the prepared TiO_2 photoanode by atmospheric plasma spray technology composed of 29% rutile, 9% anatase and 62% of non-stoichiometric phase of Ti_7O_{13}. The corresponding crystallographic planes for each phase are assigned.

3. Results and discussion

3.1. Characterization of the TiO_2 coating prepared by APS

Figs. 2 and 3 depict the X-ray diffractograms and SEM images obtained for both, the TiO_2 feedstock powder and the resulting coating by APS, respectively. As can be seen in Fig. 2a, the starting powder prepared by a sintering and crushing process was only composed of rutile phase [47]. The SEM image of Fig. 3a shows that the free-surface of the initial powder exhibited an irregular blocky morphology only composed of TiO_2 microparticles, also corroborated by its EDS analysis. The particle size distribution of this powder measured by laser scattering ranged between 20 and 50 μm, with a mean particle size of 32 μm.

Fig. 2b shows the XRD pattern for the TiO_2 coating on stainless steel. Crystallographic planes related to the rutile [47] and anatase [48] forms, along with those ascribed to a non-stoichiometric Ti_7O_{13} [49], are also given in Fig. 2b to show that a part of the initial rutile is conserved, but another part of it is transformed into anatase and Ti_7O_{13} under APS deposition. Moreover, the peaks for the TiO_2 coating were wider than those of pure compounds due to formation of the non-stoichiometric phase and a grain size reduction, as typically found for coatings obtained by APS. Analysis of the crystallographic phases revealed that the 100% rutile-TiO_2 phase powder was converted after the APS process into a coating containing 29% of rutile, 9% of anatase and 62%

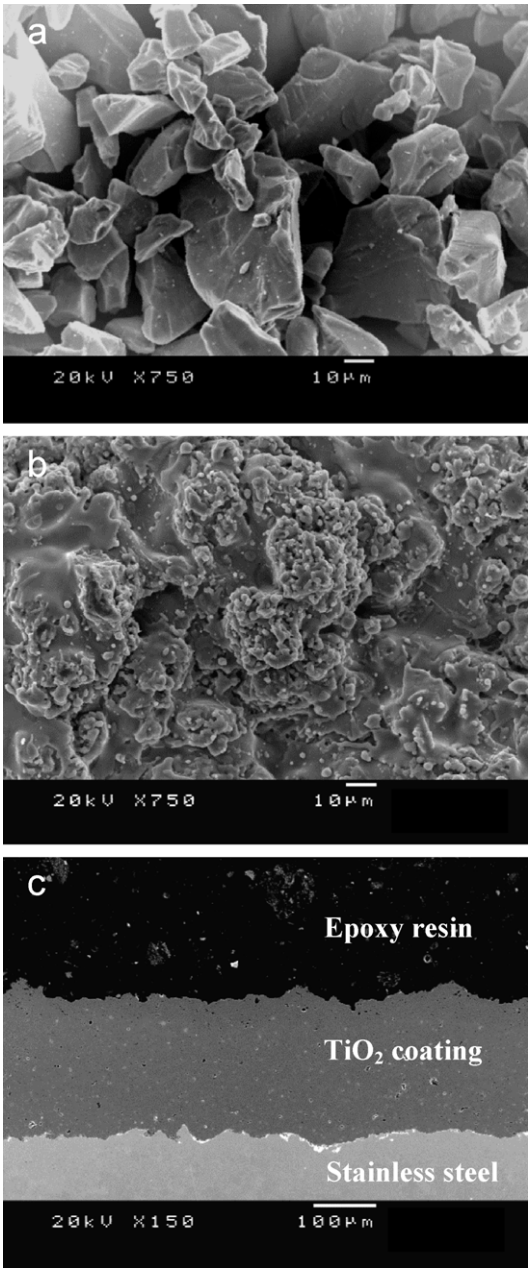

Fig. 3. Scanning electron microscopy (SEM) images of (a) the free-surface micrograph of the initial TiO_2 powder, (b) the free-surface micrograph of the microparticulated TiO_2 coating prepared by atmospheric plasma spray and (c) the cross section of the TiO_2 coating on stainless steel substrate.

of Ti_7O_{13}. An anatase-to-rutile ratio of 0.31 was then formed at the coating. The SEM image of Fig. 3b of its free surface also confirms that some microparticles were fully melted during the APS process. The excellent deposition obtained by this technique can be observed in the SEM cross-section of Fig. 3c, showing a homogeneous microstructure with a thickness of 211 ± 21 μm. It was found that its porosity was of 4.0 ± 1.7%, with a microroughness of 8.1 ± 1.5 μm. Moreover, the adhesion of the coating was 39.8 ± 3.8 MPa and its HVN microhardness was 842 ± 28. The coating failed by the substrate interface after the C633 adhesion test.

The TiO_2 coating on stainless steel synthesized by APS then presented excellent mechanical properties and also showed large stability and long durability to the current pass. Thus, using the SPEC system of Fig. 1 with 100 mL of 0.05 M Na_2SO_4 as background

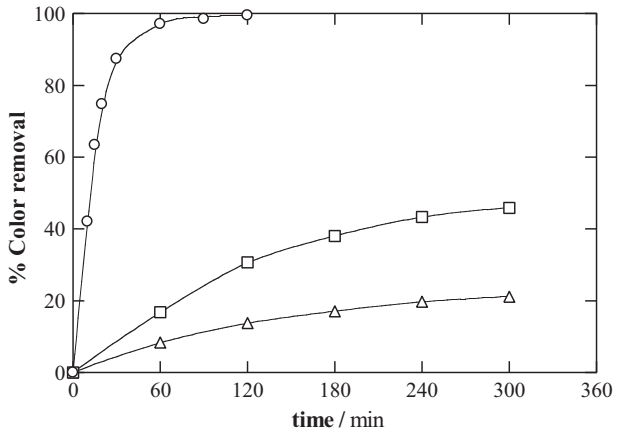

Fig. 4. Variation of percentage of color removal with time for the treatment of 100 mL of a 15 mg L^{-1} AO7 solution in 0.05 M Na_2SO_4 at pH 7.0 and 35 °C. (△) Solar photocatalysis (SPC) with the synthesized TiO_2 coating, (□) anodic oxidation with generated H_2O_2 (AO-H_2O_2) using the TiO_2/air-diffusion cell at anodic current density (j_{anod}) of 1.0 mA cm^{-2} in the dark and (○) SPEC under the same conditions but exposing the photoelectrochemical cell directly to sunlight.

electrolyte, no change in the characteristics of the TiO_2 photoanode was found operating up to $j_{anod} = 2.0$ mA cm^{-2}, where a bias anodic potential of about 1.75 V vs SCE was attained. This anodic current density was chosen as maximal for the AO-H_2O_2 and SPEC trials performed with this electrode. All experiments reported below were comparatively made with the same TiO_2 deposit.

3.2. Comparative color removal of AO7 solutions by SPC, AO-H_2O_2 and SPEC

The comparative oxidation ability of SPC, AO-H_2O_2 and SPEC on AO7 solutions was clarified from their corresponding decolorization efficiencies, which are typically used to check the effectiveness of an azo dye treatment. Fig. 4 illustrates the color removal obtained for 15 mg L^{-1} AO7 in 0.05 M Na_2SO_4 of pH 7.0 under the application of these processes using the synthesized TiO_2 photocatalyst. For AO-H_2O_2 and SPEC, a $j_{anod} = 1.0$ mA cm^{-2} (bias anodic potential of about 1.35 V vs SCE) was applied. In all these trials, the solution pH remained practically unchanged.

As can be seen in Fig. 4, the slowest decolorization took place in SPC, where only 21% color removal was achieved in 300 min. The low effectiveness of this procedure can be associated with the fast recombination of the photogenerated oxidizing holes and reducing electrons by reaction (9), then being largely inhibited the reaction of holes with water to form •OH from reaction (2), which is the main oxidant of organics at neutral pH [17,19]. Fig. 4 shows that AO-H_2O_2 in the dark decolorized more quickly the azo dye solution, leading to 46% color removal in 300 min. The destruction of AO7 in this method can be ascribed to the action of heterogeneous •OH generated at the TiO_2 anode surface as intermediate of the anodic oxidation of water to O_2 by the following reaction [2,50]:

$$H_2O \rightarrow {}^{\bullet}OH + H^+ + e^- \quad (13)$$

The slow decolorization found in AO-H_2O_2 can then be accounted by the expected small production of reactive •OH on TiO_2 anode from reaction (13), which is pH independent [50]. In contrast, Fig. 4 evidences that the AO7 solution was very quickly discolored, with total color removal in about 120 min, using SPEC. This behavior indicates that the application of a current allows a very effective separation of the electron-hole pair formed from reaction (1) on the TiO_2 photoanode subjected to sunlight illumination, being the electrons driven to the cathode and strongly enhancing the reaction (2) between holes and water to produce large quantities of oxidant

•OH that destroy AO7 and its by-products [35]. Results of Fig. 4 confirm that the SPEC process is synergistic, but not cumulative of the individual processes, because when total color removal is attained at 120 min of SPEC, only 45% decolorization efficiency is achieved from the sum of both SPC and AO-H_2O_2 treatments.

Note that H_2O_2 formed at the cathode from reaction (11) was accumulated in large extent in the solution during the AO-H_2O_2 and SPEC trials. A blank experiment was performed by adding 10 mM H_2O_2 to 100 mL of 15 mg L^{-1} AO7 in 0.05 M Na_2SO_4 adjusted to pH 7.0, but no significant decolorization of this solution was found after 60 min of solar illumination, indicating that H_2O_2 does not oxidize the azo dye. After 180 min of SPEC at j_{anod} = 1.0 mA cm^{-2}, 1.66 mM of H_2O_2 were detected in solution, a value lower than 2.76 mM expected from reaction (11) assuming 100% current efficiency for H_2O_2 production. This decay in accumulated H_2O_2 may be related to its slow reaction with photogenerated electrons from reaction (7), but it can be more probably due to its oxidation to O_2 at the TiO_2 photoanode giving rise to the weaker oxidant HO_2• as follows [2]:

$$H_2O_2 \rightarrow HO_2^{\bullet} + H^+ + e^- \quad (14)$$

Reaction (14) is also expected in AO-H_2O_2, but the low decolorization rate found for this process (see Fig. 4) suggests a small participation of HO_2• in azo dye removal.

The above results indicate that the SPEC process with the TiO_2 photoanode synthesized by APS is very effective for AO7 decolorization. The influence of variables like pH, azo dye concentration and j_{anod} on this EAOP was then examined to clarify the best experimental decolorization conditions, as will be discussed in subsections below.

3.3. Effect of pH on the AO7 decolorization in SPEC process

The change of percentage of color removal with electrolysis time for 15 mg L^{-1} AO7 solutions in the pH range 3.0–11.0 by using SPEC at j_{anod} = 1.0 mA cm^{-2} for 180 min as maximal is depicted in Fig. 5a. In these trials, no significant change of solution pH with electrolysis time was detected. As can be seen, complete decolorization was only feasible after 120 min of electrolysis at neutral pH 7.0, which is the optimum pH for this treatment. A similar color removal rate to pH 7.0 was also determined during the first 60 min at pH 9.0, reaching 96% decolorization, but prolonging the electrolysis the absorbance at λ = 484 nm rose gradually decreasing the color decay to 68% at 180 min. The same behavior, with maximum color removal of 80% and 40% at 60 min, was also found for pH 5.0 and 11.0, respectively. A different trend can be observed in Fig. 5a for pH 3.0, where the solution was progressively decolorized, but only attaining 65% color removal in 180 min.

The complex effect of pH shown in Fig. 5a is difficult to justify from the change in the electrostatic interactions between the azo dye and the amphoteric TiO_2 surface [19,21], because the former is always charged negatively due to its sulfonic group while the TiO_2 photocatalyst is always subjected to a positive charge in SPEC. The variation of AO7 decolorization with pH can be rather related to the change of the oxidation ability of the photogenerated holes [19] and the different products formed from azo dye degradation. Thus, the removal of AO7 followed by the progressive formation of products that present a high residual absorbance at 484 nm can explain the volcano shape of the decolorization curves at pH 5.0, 9.0 and 11.0 shown in Fig. 5a, as can be deduced from the UV-Vis spectra recorded for the final treated solutions and presented in Fig. 5b.

In aqueous solution, AO7 presents two tautomeric forms in equilibrium, the azo form (see Table 1) and the hydrazone one, where the hydroxyl group appears as carbonyl group being its hydrogen linked to the azo group [16]. The hydrazone form is the major

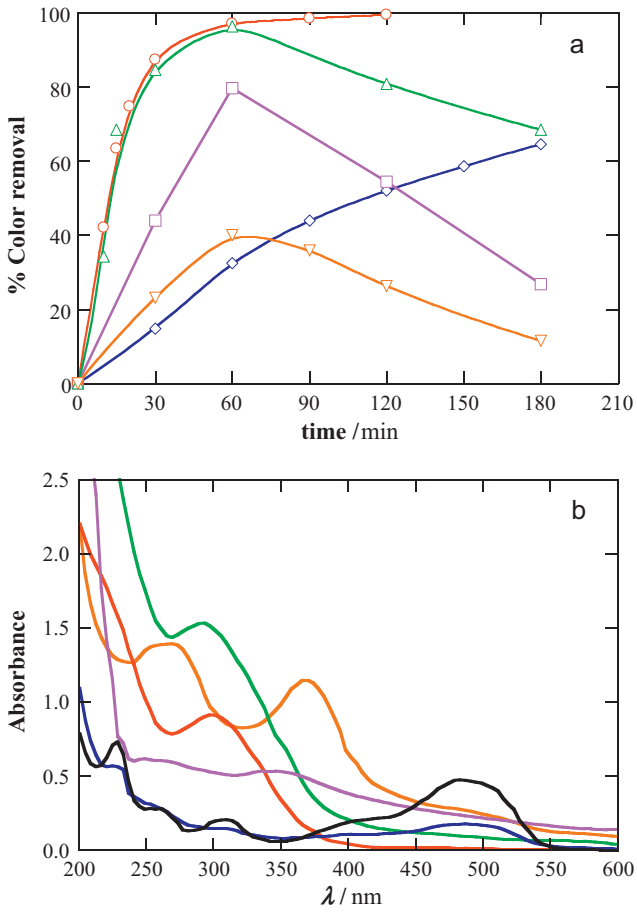

Fig. 5. (a) Effect of pH on the change of percentage of color removal with time for the SPEC treatment of 100 mL of solutions containing 15 mg L^{-1} of AO7 in 0.05 M Na_2SO_4 at j_{anod} = 1.0 mA cm^{-2} and 35 °C. Solution pH: (◊) 3.0, (□) 5.0, (○) 7.0, (△) 9.0 and (▽) 11.0. (b) UV–vis spectra of the initial solution (in black) at pH 7.0 and the above final treated solutions after further adjustment to pH 7.0.

species giving a strong visible band with λ_{max} = 484 nm (characteristic of AO7), whereas the azo form yields a much weaker shoulder near 430 nm. These bands can be observed in the UV–vis spectrum of the initial 15 mg L^{-1} AO7 solution of pH 7.0 depicted in Fig. 5b, along with two other bands in the ultraviolet region centred at 230 and 305 nm due to the benzene and naphthalene groups of AO7, respectively [16]. The same four bands with analogous intensity were detected for all initials solutions in the pH range 3.0–11.0, indicating the presence of the two forms of AO7 in all them and in similar proportion. During the SPEC treatment, the bands of the two forms of AO7 were always reduced at similar rate up to disappear, except for pH 3.0 where they still persisted at 180 min (see Fig. 5b). The slower oxidation of AO7 found at pH 3.0 suggests that in this medium, organics are predominantly destroyed by photogenerated holes from reaction (1), which are weaker oxidizing agents than •OH [19]. In contrast, at higher pH the holes produce large amounts of •OH, from reaction (2) at pH 5.0 and 7.0 and/or from reaction (3) at pH 9.0 and 11.0, removing much more rapidly AO7, but giving different products depending on pH as a result of its non-selective attack on organics. Thus, Fig. 5b shows a strong band at 300 nm, related to naphthalenic derivatives, in the final solution of pH 7.0, without any absorbance for λ > 400 nm. A similar strong band can be observed for pH 9.0, but with residual absorbance in the visible region probably due to the formation of low amounts of colored aromatic intermediates, thus avoiding the total decolorization of solution. A significant absorbance in the visible region was also found at pH 5.0 and 11.0, although in the latter medium

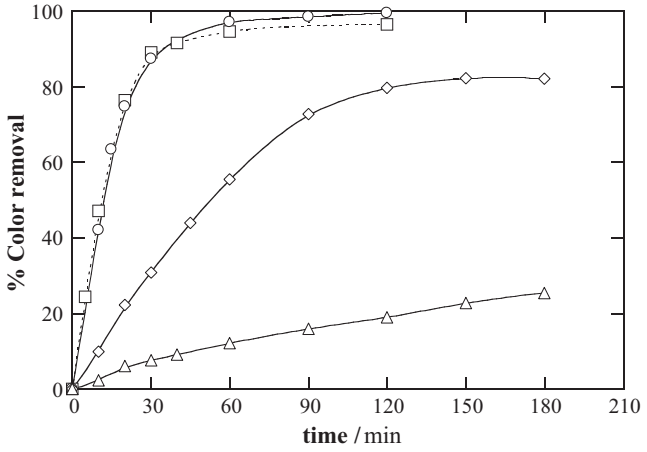

Fig. 6. Influence of dye concentration on the decolorization rate for 100 mL of AO7 solutions in 0.05 M Na_2SO_4 at pH 7.0 by SPEC at j_{anod} = 1.0 mA cm^{-2} and 35 °C. Dye concentration: (□) 5 mg L^{-1}, (○) 15 mg L^{-1}, (◊) 30 mg L^{-1} and (△) 45 mg L^{-1}.

two other bands at 263 and 365 nm due to the formation of other products were detected. The progressive increase of the residual absorbance at 484 nm after 60 min of SPEC at pH 5.0, 9.0 and 11.0 explains the volcano shape with gradual decay in color removal shown in Fig. 5a.

3.4. Influence of azo dye concentration on its decolorization in SPEC process

The effect of initial AO7 concentration on color removal in SPEC was tested at the optimum neutral pH 7.0 and applying 1.0 mA cm^{-2}. Under these conditions, a maximum content of 45 mg L^{-1} was studied because of the limited oxidation ability of this method for higher azo dye concentrations. The decolorization efficiency-time plots thus obtained are presented in Fig. 6. A similar decay of the percentage of color removal for 5 and 15 mg L^{-1} of the azo dye can be observed giving rise to total decolorization in about 120 min. However, further increase of AO7 concentration resulted in a gradual loss in color removal, reaching 82% and only 25% decolorization after 180 min of electrolysis for 30 and 45 mg L^{-1}. Under these conditions, the disappearance of the strong band at λ_{max} = 484 nm of the azo dye became progressively slower and a more rapid raise of the residual absorbance in the visible region due to colored intermediates was detected. This behavior can be mainly associated with the increasing consumption of generated •OH to oxidize the greater amounts of organics formed on the TiO_2 photoanode surface, thereby decreasing the amount of this radical to attack the azo dye [33,34]. Moreover, the transparency of the solution decreases at greater AO7 concentration because UV irradiation of sunlight is more strongly absorbed by the azo dye and its aromatic products yielding lower photogeneration of holes with the consequent loss of •OH production that decreases the oxidation ability of SPEC [27]. Results of Fig. 6 evidence that SPEC is able to completely decolorize solutions of pH 7.0 containing low AO7 contents up to 15 mg L^{-1}, which can be taken as the best concentration for this treatment.

3.5. Effect of anodic current density on decolorization and decay kinetics of AO7 in SPEC process

The applied j_{anod} is a key parameter in SPEC because it limits the separation of photogenerated holes and electrons and hence, the oxidation action of the former on the organic matter. The influence of this variable on AO7 decolorization was checked for a solution containing the best content of 15 mg L^{-1} of azo dye at the optimum pH 7.0. Fig. 7a shows that a j_{anod} as low as 0.25 mA cm^{-2} already enhanced strongly the decolorization efficiency of the solution compared with that of the SPC process, as expected if the transport of photoelectrons to the cathode allows the fast generation of oxidant •OH from holes by reaction (2) [33–35]. Fig. 7a also evidences that the increase in j_{anod} from 0.25 to 1.0 mA cm^{-2} caused a quicker color removal owing to a faster electron-hole separation at the TiO_2 photoanode, as well as a faster oxidation of water from reaction (13), giving rise to higher •OH production, which is able to completely decolorize the solution after 120 min of electrolysis at 1.0 mA cm^{-2}. For 2.0 mA cm^{-2}, however, a decay in color removal can be observed after 50 min of SPEC treatment when 90% decolorization was already reached. This is due to the existence of an increasing residual absorbance in the visible region of the UV-vis spectrum of the solution, suggesting that the generation of an excess of oxidant •OH with a higher decrease of the local pH in the vicinity of the TiO_2 electrode at 2.0 mA cm^{-2} favors

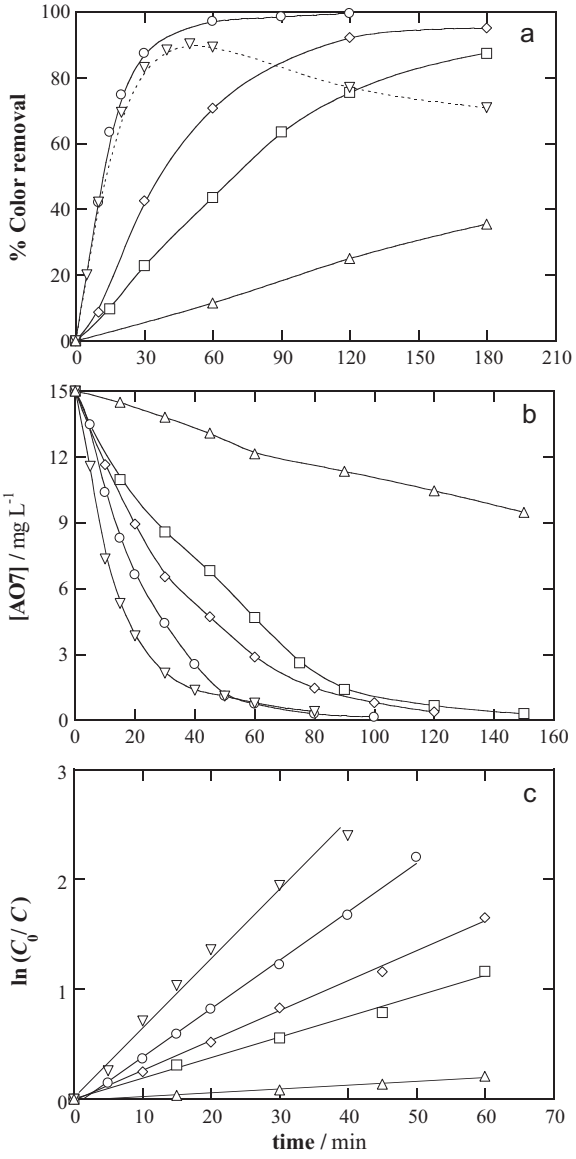

Fig. 7. Effect of anodic current density on (a) the percentage of color removal and (b) the dye concentration decay determined by reversed-phase HPLC with time for the treatment of 100 mL of a 15 mg L^{-1} AO7 solution in 0.05 M Na_2SO_4 at pH 7.0 and 35 °C. (△) SPC and SPEC at j_{anod}: (□) 0.25 mA cm^{-2}, (◊) 0.50 mA cm^{-2}, (○) 1.0 mA cm^{-2} and (▽) 2.0 mA cm^{-2}. In plot (c), kinetic analysis of data given in plot (b) assuming that AO7 verifies a pseudo-first-order reaction.

the formation of colored aromatic intermediates. Unfortunately, these compounds could not be identified by reversed-phase HPLC. Consequently, 1.0 mA cm^{-2} is the best j_{anod} needed to decolorize the optimized AO7 solution in SPEC.

The decay kinetics for AO7 in the above trials was followed by reversed-phase HPLC, where it displayed a well-defined peak with retention time (t_r) of 7.6 min. Fig. 7b shows that while the azo dye was very slowly removed by SPC, it was quickly destroyed by SPEC, much more rapidly with increasing j_{anod} from 0.25 to 2.0 mA cm^{-2}. Thus, AO7 was only reduced by 36% after 150 min of SPC, but disappeared in decreasing times of 150, 120, 100 and 80 min for increasing current densities of 0.25, 0.50, 1.0 and 2.0 mA cm^{-2}. This trend agrees with the expected larger production of oxidizing species (mainly •OH) when j_{anod} rises due to the faster separation of photogenerated holes and electrons on the TiO_2 photoanode and the quicker anodic oxidation of water. Comparison of Figs. 7a and 7b evidences that the decolorization process in SPEC is always slower than AO7 decay, as expected if colored aromatic intermediates that absorb at λ = 484 nm are formed during its degradation.

The concentration decays of Fig. 7b were analyzed using kinetic equations related to simple reaction orders and excellent linear correlations were only found for a pseudo-first-order reaction, as illustrated in Fig. 7c. From this analysis, increasing pseudo rate constants (k_{SPEC}) of 3.1×10^{-4} s^{-1} ($R^2 = 0.993$) at 0.25 mA cm^{-2}, 4.5×10^{-4} s^{-1} ($R^2 = 0.997$) at 0.50 mA cm^{-2}, 7.4×10^{-4} s^{-1} ($R^2 = 0.993$) at 1.0 mA cm^{-2} and 1.0×10^{-3} s^{-1} ($R^2 = 0.992$) at 2.0 mA cm^{-2} were determined for the SPEC process, which were, as expected, much greater than the pseudo rate constant (k_{SPC}) of 5.8×10^{-5} s^{-1} ($R^2 = 0.982$) obtained for SPC. This behavior suggests a constant production of oxidizing agents (mainly photogenerated holes and •OH) in both SPC and SPEC treatments. Taking into account the above k_{SPEC} and k_{SPC} values, the extent of the electrochemical enhancement (E, in %) was estimated from the following expression [33]:

$$E = \frac{k_{SPEC} - k_{SPC}}{k_{SPEC}} 100 \quad (15)$$

Very high values for E were thus obtained, which increased gradually in 81%, 87%, 92% and 94% with increasing j_{anod} values of 0.25, 0.50, 1.0 and 2.0 mA cm^{-2}. This confirms the relevant role of j_{anod} in SPEC to accelerate the production of oxidants.

3.6. AO7 mineralization and identification and evolution of generated carboxylic acid and released inorganic nitrogen ions

The 15 mg L^{-1} azo dye solution in 0.05 M Na_2SO_4 of pH 7.0 was slowly mineralized in the TiO_2/air-diffusion photoelectrochemical cell under SPEC at j_{anod} = 1.0 mA cm^{-2}. In these optimized conditions, the initial TOC of 8.22 mg L^{-1} was only reduced to 4.93 mg L^{-1} in 240 min, corresponding to 40% of mineralization. That means that although AO7 is completely removed in 100 min (see Fig. 7b), it forms more recalcitrant by-products that react very hardly with •OH. It is expected the formation of the same kind of by-products by SPEC and SPC because the same oxidizing agents act in both system. However, the larger production of photogenerated holes and •OH in the former treatment accelerates strongly the destruction of intermediates affecting their distribution in relation to the second one.

Ion-exclusion chromatograms of the above treated solution displayed well-defined peaks ascribed to carboxylic acids such as tartaric (t_r = 8.51 min), oxamic (t_r = 9.41 min), succinic (t_r = 11.7 min), acetic (t_r = 14.9 min) and phthalic acid (t_r = 27.7 min). Tartaric, succinic and acetic acids can be formed from the cleavage of the benzene ring of aromatic intermediates [2,50], whereas oxamic acid is expected to be produced from the degradation of *N*-derivatives. Phthalic acid is an aromatic dicarboxylic acid

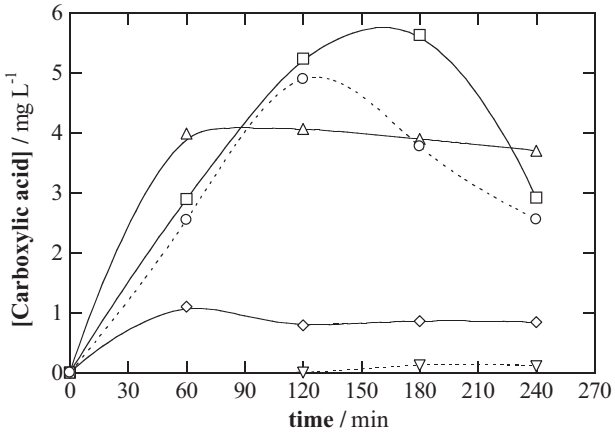

Fig. 8. Time-course of the concentration of: (○) phthalic, (□) tartaric, (△) succinic, (◊) acetic and (▽) oxamic acids detected during the SPEC degradation of 100 mL of a 15 mg L^{-1} AO7 solution in 0.05 M Na_2SO_4 at pH 7.0 and j_{anod} = 1.0 mA cm^{-2} and 35 °C.

coming from the oxidation of the naphthalene moiety. Note that this latter by-product and succinic acid have also been detected in the degradation of AO7 by SPC with TiO_2 in suspension [16].

Fig. 8 highlights that most carboxylic acids, except oxamic acid, were formed from the beginning of the SPEC treatment and attained their maximum content at about 120 min of electrolysis. At longer times up to 240 min, tartaric acid decayed from 5.63 to 2.90 mg L^{-1} and phthalic acid dropped from 4.89 to 2.56 mg L^{-1}, whereas succinic and acetic acids remained with contents practically constants near 3.70 and 0.84 mg L^{-1}, respectively. In contrast, oxamic acid only reached 0.11 mg L^{-1} at the end of SPEC, being detected for times > 120 min. A simple mass balance of carboxylic acids accumulated at 240 min revealed that they account for by 4.23 mg L^{-1} TOC, i.e. 86% of the TOC contained in the remaining solution (4.93 mg L^{-1}). This indicates that the detected carboxylic acids are the main components of the final treated solution, which contains other minority unidentified organics only related to 14% of its TOC. Results of Fig. 8 corroborate the low ability of •OH produced in the SPEC process to remove the recalcitrant carboxylic acids generated, thereby explaining the low mineralization of the AO7 solution in this treatment.

Ionic chromatograms of the electrolyzed solutions revealed the release of NH_4^+ and NO_3^- ions in the mineralization of the initial N contained in AO7 (1.20 mg L^{-1}). No other inorganic nitrogen ions, like NO_2^- ion, were detected by this technique. After 240 min of SPEC, 0.16 mg L^{-1} of NH_4^+ ion (10.4% of initial N) and 0.54 mg L^{-1} of NO_3^- ion (1.0% of initial N) were found, indicating that the former ion was produced in larger proportion. The TN analysis of this solution evidenced that it only contained 0.23 mg L^{-1} of N, corresponding to 19.2% of initial N. This suggests that during AO7 degradation in SPEC, the major part of its N (80.8%) is loss as volatile derivatives, probably N_2 and NOx species. Taking into account that NH_4^+ and NO_3^- ions, as well as 0.11 mg L^{-1} of oxamic acid (1.4% of initial N), are detected as *N*-compounds in the final solution, one can concluded that 6.4% of initial N is retained in it in other recalcitrant unidentified *N*-derivatives.

4. Conclusions

It has been demonstrated that a novel TiO_2 photoanode synthesized by APS can decolorize efficiently solutions with low contents of AO7 azo dye and 0.05 M Na_2SO_4 using SPEC under direct sunlight irradiation in a photoelectrochemical cell with an air-diffusion cathode that generates H_2O_2. The photoanode presented excellent mechanical properties and showed large stability and long

durability up to 2.0 mA cm^{-2}. The SPEC process was synergistic of individual SPC and AO-H_2O_2 ones under comparable conditions as a result of the larger production of •OH from the higher amounts of photogenerated holes that can be separated of photogenerated electrons. Colored aromatic intermediates were formed in SPEC depending on pH, azo dye content and applied j_{anod}. The best operating variables were 15 mg L^{-1} AO7, pH 7.0 and j_{anod} = 1.0 mA cm^{-2}. Under these conditions, the azo dye disappeared in 100 min and the solution was completely decolorized in 120 min, but its TOC was much more slowly removed only attaining 40% mineralization after 240 min of electrolysis. The AO7 decay followed a pseudo-first-order reaction, which was accelerated with increasing j_{anod} due to the higher •OH generation from the production of more photogenerated holes and the faster anodic oxidation of water. Detected carboxylic acids like phthalic, tartaric, succinic, acetic and oxamic accounted for 86% of the TOC contained in the solution electrolyzed for 240 min and their large persistence explains the low mineralization degree achieved for the azo dye in SPEC. The initial N of AO7 was mineralized as NH_4^+ ion and in a smaller proportion of NO_3^- ion, although it was mainly loss as volatile species. These results point to the use of SPEC followed by a biological treatment for the remediation of waters containing AO7, because the latter method can efficiently remove the large amounts of carboxylic acids formed from the application of the former one, thereby strongly increasing the mineralization degree of the azo dye.

Acknowledgements

The authors thank the financial support from MICINN (Ministerio de Ciencia e Innovación, Spain) through project CTQ 2010-16164/BQU, co-financed with Feder funds, and from AGAUR (Agència de Gestió d'Ajuts Universitaris i de Recerca, Generalitat de Catalunya, Spain) through project 2009 SGR 00390. The grant awarded to S. Garcia-Segura by MEC (Ministerio de Educación y Ciencia, Spain) is also acknowledged.

References

[1] E. Forgacs, T. Cserháti, G. Oros, Environment International 30 (2004) 953–971.
[2] C.A. Martínez-Huitle, E. Brillas, Applied Catalysis B: Environmental 87 (2009) 105–145.
[3] T. Robinson, G. McMullan, R. Marchant, P. Nigam, Bioresource Technology 77 (2001) 241–255.
[4] G.A. Umbuzeiro, H.S. Freeman, S.H. Waren, D.P. Oliveira, Y. Terão, T. Watanabe, L.D. Claxton, Chemosphere 60 (2005) 55–64.
[5] S.M.A.G. Ulson de Souza, E. Forgiarini, A.A. Ulson de Souza, Journal of Hazardous Materials 147 (2007) 1073–1078.
[6] K.P. Sharma, S. Sharma, S. Sharma, P.K. Singh, S. Kumar, R. Grover, P.K. Sharma, Chemosphere 69 (2007) 48–54.
[7] A. Szygula, E. Guibal, M. Ruiz, A.M. Sastre, Colloids and Surfaces A 330 (2008) 219–226.
[8] M.M. Dávila-Jiménez, M.P. Elizalde-González, A.A. Pelaéz-Cid, Colloids and Surfaces A 254 (2005) 107–114.
[9] J. Wu, C. Liu, K.H. Chu, S. Suen, Journal of Membrane Science 309 (2008) 239–245.
[10] E. Franciscon, A. Zille, F. Dias Guimaro, C. Ragagnin de Menezes, L.R. Durrant, A. Cavaco-Paulo, International Biodeterioration and Biodegradation 63 (2009) 280–288.
[11] T.A. Özbelge, F. Erol, Chemical Engineering Communications 169 (2008) 39–55.
[12] R. Andreozzi, V. Caprio, A. Insola, R. Marotta, Catalysis Today 53 (1999) 51–59.
[13] E. Brillas, J.C. Calpe, P.L. Cabot, Applied Catalysis B: Environmental 46 (2003) 381–391.
[14] M. Pera-Titus, V. García-Molina, M.A. Baños, J. Giménez, S. Esplugas, Applied Catalysis B: Environmental 47 (2004) 219–256.
[15] F. Kiriakidou, D.I. Kondarides, X.E. Verykios, Catalysis Today 54 (1999) 119–130.
[16] M. Stylidi, D.I. Kondarides, X.E. Verykios, Applied Catalysis B: Environmental 40 (2003) 271–286.
[17] S. Malato, J. Blanco, D.C. Alarcón, M.I. Maldonado, P. Fernández-Ibañez, W. Gernjak, Catalysis Today 122 (2007) 137–149.
[18] A. Fujishima, X. Zhang, D.A. Tryk, Surface Science Reports 63 (2008) 515–582.
[19] U.G. Akpan, B.H. Hameed, Journal of Hazardous Materials 170 (2009) 520–529.
[20] R. Pourata, A.R. Khataee, S. Aber, N. Daneshvar, Desalination 249 (2009) 301–307.
[21] D. Friedmann, C. Mendive, D. Bahnemann, Applied Catalysis B: Environmental 99 (2010) 398–406.
[22] A.Y. Shan, T.I.M. Ghazi, S.A. Rashid, Applied Catalysis A: General 389 (2010) 1–8.
[23] L.A. Ioannou, E. Hapeshi, M.I. Vasquez, D. Mantzavinos, D. Fatta-Kassinos, Solar Energy 85 (2011) 1915–1926.
[24] J.H.O.S. Pereira, V.J.P. Vilar, M.T. Borges, O. González, S. Esplugas, R.A.R. Boaventura, Solar Energy 85 (2011) 2732–2740.
[25] V.M. Daskalaki, Z. Frontistis, D. Mantzavinos, A. Katsounis, Catalysis Today 161 (2011) 110–114.
[26] W.H. Leng, Z. Zhang, J.Q. Zhang, Journal of Molecular Catalysis A: Chemical 206 (2003) 239–252.
[27] P.A. Carneiro, M.E. Osugi, J.J. Sene, M.A. Anderson, M.V.B. Zanoni, Electrochimica Acta 49 (2004) 3807–3820.
[28] M.G. Neelavannan, C.A. Basha, Separation and Purification Technology 61 (2008) 168–174.
[29] K. Esquivel, L.G. Arriaga, F.J. Rodríguez, L. Martínez, L.A. Godínez, Water Research 43 (2009) 3593–3603.
[30] J. Marugán, P. Christensen, T. Egerton, H. Purnama, Applied Catalysis B: Environmental 89 (2009) 273–283.
[31] P.S. Shinde, P.S. Patil, P.N. Bhosale, A. Brueger, G. Nauer, M. Neumann-Spallart, C.H. Bhosale, Applied Catalysis B: Environmental 89 (2009) 288–294.
[32] H.G. Oliveira, D.C. Nery, C. Longo, Applied Catalysis B: Environmental 93 (2010) 205–211.
[33] Z. Frontistis, V.M. Daskalaki, A. Katsaounis, I. Poulios, D. Mantzavinos, Water Research 45 (2011) 2996–3004.
[34] R. Daghrir, P. Drogui, I. Ka, M.A. El Khakani, Journal of Hazardous Materials 199–200 (2012) 15–24.
[35] R. Daghrir, P. Drogui, D. Robert, Journal of Photochemistry and Photobiology A: Chemistry 238 (2012) 41–52.
[36] L. Yu, Z. Wang, L. Shi, S. Yuan, Y. Zhao, J. Fang, W. Deng, Applied Catalysis B: Environmental 113–114 (2012) 318–325.
[37] S. Dosta, I.G. Cano, J.R. Miguel, J.M. Guilemany, Journal of Thermal Spray Technology 17 (2008) 360–364.
[38] J. Suffner, H. Hahn, S. Dosta, I.G. Cano, J.M. Guilemany, Surface and Coatings Technology 204 (2009) 149–156.
[39] J. Suffner, H. Sieger, H. Hahn, S. Dosta, I.G. Cano, J.M. Guilemany, P. Klimczyk, L. Jaworska, Materials Science and Engineering A 506 (2009) 180–186.
[40] S. Ammar, R. Abdelhedi, C. Flox, C. Arias, E. Brillas, Environmental Chemistry Letters 4 (2006) 229–233.
[41] L.C. Almeida, S. Garcia-Segura, N. Bocchi, E. Brillas, Applied Catalysis B: Environmental 103 (2011) 21–30.
[42] E.J. Ruiz, C. Arias, E. Brillas, A. Hernández-Ramírez, J.M. Peralta-Hernández, Chemosphere 82 (2011) 495–501.
[43] S. Garcia-Segura, F. Centellas, C. Arias, J.A. Garrido, R.M. Rodríguez, P.L. Cabot, E. Brillas, Electrochimica Acta 58 (2011) 303–311.
[44] E. Brillas, M.A. Baños, S. Camps, C. Arias, P.L. Cabot, J.A. Garrido, R.M. Rodríguez, New Journal of Chemistry 28 (2004) 314–322.
[45] F.H. Chung, Journal of Applied Crystallography 7 (1974) 519–525.
[46] F.J. Welcher (Ed.), Standard Methods of Chemical Analysis, vol. 2, Part B, 6th ed, R.E. Krieger Publishers Co., Huntington, New York, 1975, p. 1827.
[47] R. Restori, D. Schwarzenbach, J.R. Schneider, Acta Crystallographica 43B (1987) 251–257.
[48] E. Sánchez, T. López, R. Gómez, X. Bokhimi, A. Morales, O.J. Novaro, Journal of Solid State Chemistry 122 (1996) 309–314.
[49] Y. Le Page, P. Strobel, Journal of Solid State Chemistry 44 (1982) 273–281.
[50] M. Panizza, G. Cerisola, Chemical Reviews 109 (2009) 6541–6569.

PAPER 7

Advances in solar photoelectron-Fenton: Decolorization and mineralization of the Direct Yellow 4 azo dye using an autonomous solar pre-pilot plant

Advances in solar photoelectro-Fenton: Decolorization and mineralization of the Direct Yellow 4 diazo dye using an autonomous solar pre-pilot plant

Sergi Garcia-Segura, Enric Brillas[1,]*

Laboratori d'Electroquímica dels Materials i del Medi Ambient, Departament de Química Física, Facultat de Química, Universitat de Barcelona, Martí i Franquès 1-11, 08028-Barcelona, Spain

Article submitted to be published in Electrochimica Acta

* Corresponding author: Tel.: +34 934021223, Fax: +34 934021231

E-mail address: brillas@ub.edu (E. Brillas)

[1] ISE Active Member

Abstract

Here, an overview on the advances in solar photoelectro-Fenton (SPEF) is initially presented to show that it is the more potent electrochemical advanced oxidation process based on Fenton's reaction chemistry to remove organic pollutants from waters, due to the synergistic action of generated hydroxyl radicals and solar irradiation. As a novel advance for SPEF, an autonomous solar pre-pilot plant is proposed to make an energetically inexpensive process that can be viable at industrial level. The plant of 10 dm^3 capacity contained a Pt/air-diffusion cell with 90.2 cm^2 electrode area, coupled to a solar compound parabolic collectors (CPCs) photoreactor of 1.57 dm^3 irradiation volume and to a solar photovoltaic panel that provides a maximum average current of 5.0 A. The oxidation ability of this plant was assessed by studying the degradation of Direct Yellow 4 (DY4) diazo dye, which involved the predominant destruction of organics by $^{\bullet}OH$ formed from Fenton's reaction between H_2O_2 generated at the cathode and added Fe^{2+}, along with the photolysis of Fe(III) complexes with products by sunlight in the CPCs photoreactor. The effect of Fe^{2+} and dye contents as well as current on decolorization rate, substrate decay and mineralization rate was examined. About 96-97% mineralization was rapidly attained using 0.50 mmol dm^{-3} Fe^{2+} and up to 0.32 mmol dm^{-3} DY4 at 5.0 A. The DY4 decay always obeyed a pseudo-first-order kinetics. Eleven aromatic products, twenty two hydroxylated derivatives and nine short-linear carboxylic acids were identified as intermediates. The Fe(III) complexes of most acids were rapidly removed, pre-eminently photolyzed by sunlight, except those of acetic and oxamic acids that were slowly destroyed. The initial N of the dye was mainly released as NH_4^+ ion and its initial S was lost as SO_4^{2-} ion. A plausible reaction sequence for DY4 mineralization involving all the detected products was finally proposed.

Keywords: Autonomous solar pre-pilot plant; Direct Yellow 4; Oxidation products; Solar photoelectro-Fenton; Water treatment

1. Introduction

Over the past fifteen years, electrochemical advanced oxidation processes (EAOPs) have received increasing attention for the removal of toxic and non-biodegradable organic contaminants from waters [1-6]. These treatments are based on the in situ generation of hydroxyl radical ($^{\bullet}OH$), which has so high standard reduction potential (E^{o} = 2.80 V/SHE) that reacts with most organics yielding dehydrogenated or hydroxylated derivatives, which can be in turn mineralized. The most typical EAOP is anodic oxidation (AO), where pollutants are oxidized by electron transfer to the anode M and/or mediated oxidation with heterogeneous M($^{\bullet}OH$) formed from water discharge at the anode surface at high current [2,4,7]:

$$M + H_2O \rightarrow M(^{\bullet}OH) + H^+ + e^- \quad (1)$$

Boron-doped diamond (BDD) electrodes are the best anodes for AO because they interact very weakly with physisorbed BDD($^{\bullet}OH$) produced from reaction (1) and promote a much greater O_2-overpotential than other conventional anodes like Pt, enhancing the removal of organics [8-10].

Other EAOPs based on Fenton's reaction chemistry are electro-Fenton (EF) and photoelectro-Fenton (PEF), in which H_2O_2 is supplied to an acidic contaminated solution from the two-electron reduction of injected O_2, for example, at a carbon-PTFE gas (O_2 or air) diffusion cathode [5,6,11]:

$$O_2 + 2\,H^+ + 2\,e^- \rightarrow H_2O_2 \quad (2)$$

In both EAOPs, Fe^{2+} ion is added as catalyst to react with H_2O_2 to give Fe^{3+} ion and $^{\bullet}OH$ from Fenton's reaction with optimum pH 2.8 [5,12-17]:

$$Fe^{2+} + H_2O_2 \rightarrow Fe^{3+} + {}^{\bullet}OH + OH^- \quad (3)$$

Reaction (3) is catalytic and can be mainly propagated from Fe^{3+} reduction to Fe^{2+} at the cathode. When an undivided cell is used in EF, organics can be attacked by heterogeneous M(•OH) formed from reaction (1) and by •OH produced in the bulk from Fenton's reaction (3). In PEF, the degradation rate is enhanced under the simultaneous irradiation of the solution with UV light due to: (i) the greater Fe^{2+} regeneration and •OH production by photolysis of $Fe(OH)^{2+}$, the pre-eminent Fe^{3+} species in solution at pH near 3, by reaction (4) and (ii) the photodecarboxylation of complexes of Fe(III) with generated carboxylic acids, which are hardly attacked with •OH, by the global reaction (5) [15,16,18-23].

$$Fe(OH)^{2+} + h\nu \rightarrow Fe^{2+} + {}^{\bullet}OH \quad (4)$$

$$Fe(OOCR)^{2+} + h\nu \rightarrow Fe^{2+} + CO_2 + R^{\bullet} \quad (5)$$

An important drawback of PEF is the high electrical cost of the UV lamps used. To solve this problem, we have proposed the alternative use of the SPEF method in which the solution is directly irradiated with sunlight as an inexpensive and renewable energy source with $\lambda > 300$ nm [24,25]. The higher intensity of UV radiation supplied by sunlight and the additional absorption at $\lambda > 400$ nm, e.g. for the photolysis of Fe(III)-carboxylate complexes, enhance the mineralization process of SPEF compared with PEF.

Despite the more cost-effective treatment by SPEF, the electrolytic systems used spent energy from a power supply that provides the electric current to the electrolytic cell and this still represents an economical problem for its possible application to water remediation at industrial level. For this reason, we have designed a novel autonomous solar pre-pilot plant in which the electrical energy needed for the electrolytic cell is supplied by a solar photovoltaic panel, making thereby an energetically inexpensive SPEF process. The ability of such autonomous plant for organic removal has been assessed by

studying the decolorization and mineralization of a typical diazo dye such as Direct Yellow 4 (DY4), whose chemical structure and characteristics are collected in Table 1.

This paper presents, in the first place, a brief overview over the advances in SPEF to show more clearly the interest of using the designed autonomous solar pre-pilot plant of 10 dm^3 capacity containing a Pt/air-diffusion cell coupled to a compound parabolic collectors (CPCs) photoreactor and controlled by a 50 W photovoltaic panel. The degradation of synthetic DY4 solutions in 0.05 mol dm^{-3} Na_2SO_4 at pH 3.0 by SPEF using such a plant is later reported to check the high effectiveness of this EAOP. The effect of Fe^{2+} content, applied current and DY4 concentration on the decolorization rate, substrate decay and mineralization rate and degree was examined. The decay kinetics for DY4 was followed by high-performance liquid chromatography (HPLC). Aromatic intermediates were detected by liquid chromatography-mass spectrometry (LC-MS) and generated short-linear carboxylic acids and released inorganic ions were quantified by different chromatographic techniques. From these results, a plausible reaction pathway for DY4 mineralization is finally proposed.

2. Advances in the solar photoelectro-Fenton process

The degradation of the drugs salicylic acid [26], ibuprofen [27], enrofloxacin [28] and chloramphenicol [29], as well as of the pharmaceutical precursor α-methylphenylglycine [30] and the dye Sunset Yellow CFC (SY) [31], has been comparatively studied by SPEF and other EAOPs using a 100 cm^3 stirred and thermostated tank reactor with a BDD or Pt anode and a gas (O_2 or air) diffusion cathode, all with 3 cm^2 area. In EF, PEF and SPEF, 0.05 or 0.10 mol dm^{-3} Na_2SO_4 was used as background electrolyte and 0.5 mol dm^{-3} Fe^{2+} was usually added as catalyst. The PEF trials were made with a 6 W UVA lamp of λ_{max} = 360 nm and the SPEF ones under direct

solar irradiation with an average UV intensity of ca. 31 W m^{-2}. The performance of each EAOP increased using a BDD anode instead of Pt, indicating the higher oxidizing power of BDD(•OH) than Pt(•OH) formed from reaction (1) to remove the contaminants. Although UV light enhanced the degradation, almost total mineralization was more rapidly achieved in SPEF due to the higher intensity of sunlight. It was found an optimum pH of 3.0 for EF, PEF and SPEF treatments, near the optimum pH of 2.8 for Fenton's reaction (3), as expected if •OH was the main oxidant of organics. Moreover, a Fe^{2+} content of 0.5-1.0 mM was found optimal for all processes. The amount of total organic carbon (TOC) removed always increased at higher current density and greater pollutant concentration, and so, the efficiency of SPEF rose when current decreased and more contaminant was present in the solution. The decay kinetics for pollutants always followed a pseudo-first-order reaction, with rate constants much higher for SPEF than for EF and PEF, due to the additional production of •OH induced by reaction (4). GC-MS and HPLC analysis of treated solutions allowed the detection of aromatic intermediates like 2,3-, 2,5- and 2,6-dihidroxy-benzoic acids for salicylic acid, 34 products for chloramphenicol and 48 products for SY. Oxalic acid was always the ultimate generated carboxylic more largely accumulated, which was not removed in EF but rapidly destroyed in PEF and much more quickly in SPEF by the fast photolysis of its Fe(III) complexes by reaction (5). This phenomenon explained the higher mineralization ability of the SPEF process. For enrofloxacin and α-methylphenylglycine, the initial N was mainly converted into NH_4^+ ion and in smaller proportion into NO_3^- ion. However, the opposite trend was found for chloramphenicol.

The SPEF treatment of organics has been scaled-up to a recirculation pre-pilot plant of 2.5 dm^3 with a BDD/O_2-diffusion cell coupled to a flat solar photoreactor composed of a polycarbonate box of 600 dm^3 of irradiated volume. The electrodes of 20 cm^2 area

were separated about 1.2 cm. Solutions with 50-200 mg dm^{-3} of TOC in 0.05-0.10 mol dm^{-3} Na_2SO_4 with 0.5 mmol dm^{-3} Fe^{2+} at pH 3.0, 50 mA cm^{-2} and flow rate of 180-200 L h^{-1} were tested. SPEF was much more potent to mineralize organics than AO and EF, as found for the herbicide mecoprop [24], *o*-, *m*- and *p*-cresol [25] and the dyes Acid Yellow 36 (AY36) [15], Acid Red 88 (AR88) [32], Acid Yellow 9 (AY9) [32], Disperse Red 1 (DR1) [33] and Disperse Red 3 (DR3) [33]. For all these compounds, the SPEF efficiency rose at lower current density and higher pollutant content, being much more cost-effective than the compared EF one. The performance of SPEF was slightly enhanced from the combined use of Fe^{2+} and Cu^{2+} as co-catalysts as found for Disperse Blue 3 (DB3) [34] since mineralization was accelerated by the attack of $^{\bullet}OH$ on Cu(II)-carboxylate species, competitively formed with Fe(III)-carboxylate ones. A drawback of this plant, however, was the high energy consumption of the BDD/air-diffusion cell as a result of its great potential difference between electrodes. For this reason, more recent studies with the 2.5 dm^3 solar pre-pilot plant were focused to the degradation of the sulfa compounds sulfanilic acid [35] and sulfanilamide [36] using a more economic Pt/air-diffusion cell because of its smaller potential difference compared with the BDD/air-diffusion one. For the SPEF process of sulfanilic acid, the application of response surface methodology allowed obtaining 100 mA cm^{-2}, 0.5 mmol dm^{-3} Fe^{2+} and pH 4.0 as optimum variables, yielding 76% mineralization with 275 kWh kg^{-1} TOC energy cost and 52% current efficiency at 120 min. For the SPEF treatment of 239-1195 mg dm^{-3} sulfanilamide solutions of pH 3.0, 91-94% mineralization was achieved after 240 min at 100 mA cm^{-2} with energy consumptions < 470 kWh kg^{-1} TOC. All the initial compounds decayed at similar rate in EF and SPEF following a pseudo-first-order kinetics and their rate constant increased with raising current density and decreasing pollutant content. Consequently, the solar photoreactor did not favored the $^{\bullet}OH$ generation from reaction (4). Analysis of final

carboxylic acids confirmed the quick removal of oxalic acid by photolysis of its Fe(III) complexes in SPEF, but the formation of other more recalcitrant carboxylic acids like acetic and oxamic slowed the mineralization process. The initial N of all *N*-products was pre-eminently transformed into NH_4^+ ion.

In order to reduce the energy consumption for the SPEF process, a larger solar pre-pilot plant of 10 dm^3 was built-up with an electrolytic reactor of 90.2 cm^2 electrode area coupled to a 1.57 dm^3 solar compound parabolic collectors (CPCs) photoreactor, much more efficient than the solar flat photoreactor previously used. With this plant, acidic solutions with 100 mg dm^{-3} TOC of the beta-blockers atenolol, metoprolol tartrate and propranolol hydrochloride at pH 3.0 were treated using single Pt/air-diffusion and BDD/air-diffusion cells and also their combination with Pt/carbon-felt cell to enhance Fe^{2+} regeneration from Fe^{3+} reduction [37]. Although the use of a BDD anode led to quicker TOC reduction, the lowest cost of 80 kWh kg^{-1} TOC with 88-93% mineralization was found for the combined Pt/air-diffusion-Pt/carbon-felt cell, but only giving a slightly lower consumption than the single Pt/air-diffusion one. From these results, we concluded that a Pt/air-diffusion reactor was the most viable cell for SPEF in the 10 dm^3 pre-pilot plant. The good effectiveness of this system was later confirmed by studying the treatment of 186 mg dm^{-3} of the herbicide 4-chloro-2-methylphenoxyacetic acid [38] and 157 mg dm^{-3} of the drug paracetamol [39] by response surface methodology. In both cases, the optimum variables were 5.0 A, 0.4-1.0 mol dm^{-3} Fe^{2+} and pH 3.0. Under these conditions, 75% mineralization with 71% current efficiency and an energy consumption as low as 88 kWh kg^{-1} TOC were obtained at 120 min for 4-chloro-2-methylphenoxyacetic acid, whereas the same mineralization degree with a current efficiency of 71% and a similar energy cost of 93 kWh kg^{-1} TOC was found also at 120 min for paracetamol.

In view of the excellent expectative of using the above 10 dm^3 solar pre-pilot plant for the SPEF process, we have introduced in it a new component, a solar photovoltaic panel to provide the electric energy to the electrolytic cell in order to obtain an energetically inexpensive treatment for waters. The assessment of this novel autonomous solar pre-pilot plant is reported below.

3. Experimental

3.1. Chemicals

Pure DY4 diazo dye was purchased from Sigma-Aldrich. Maleic, malic, tartronic, malonic, glycolic, acetic, formic, oxalic and oxamic acids were of analytical grade supplied by Panreac and Avocado. Anhydrous sodium sulfate, used as background electrolyte, and heptahydrated Fe(II) sulfate, used as catalyst, were of analytical grade purchased from Fluka and Sigma-Aldrich, respectively. Organic solvents and other chemicals employed were of LC-MS, HPLC or analytical grade purchased from Teknokroma, Merck and Sigma-Aldrich. All solutions were prepared with deionized water and their initial pH was adjusted to 3.0 with analytical grade sulfuric acid purchased from Merck.

3.2. Autonomous solar pre-pilot plant

A scheme of the pre-pilot plant designed for the SPEF process is depicted in Fig. 1. In each trial, a volume of 10 dm^3 of a DY4 solution in 0.05 mol dm^{-3} Na_2SO_4 of pH 3.0 was introduced in the reservoir and recirculated through the plant with a magnetic drive centrifugal pump from Iwaki at a liquid flow rate of 200 L h^{-1} regulated by a flowmeter. The solution then passed through the electrochemical reactor, the solar photoreactor and two heat exchangers to maintain the temperature at 35 ºC to finally back to the reservoir. The electrochemical cell was a one-compartment filter-press reactor with components of

12 cm × 18 cm in dimension, separated with Viton gaskets to avoid leakages. The anode was a Pt sheet of 99.99% purity purchased from SEMPSA and the cathode was a carbon-PTFE air-diffusion electrode supplied by E-TEK. Both electrodes were of 10 cm × 10 cm in dimension. A PVC liquid compartment with a central window of 9.5 cm × 9.5 cm (90.2 cm^2) was used to contact the effluent with the outer faces of both electrodes separated a distance of 1.2 cm. The inner face of the cathode was pressed onto a Ni mesh as electrical connector and contacted with a PVC gas chamber where circulated compressed air at a flow rate of 4.5 dm^3 min^{-1}, regulated with a back-pressure gauge, to continuously generate H_2O_2 from O_2 reduction. The electric energy to the cell was provided by a 50 W solar photovoltaic panel supplied by Nousol. The applied current and potential difference between electrodes were directly measured by an ammeter, coupled in series, and a voltmeter, coupled in parallel. The solar CPCs photoreactor had an area of 0.4 m^2 and concentration factor of 1, being composed of 12 borosilicate-glass tubes of 50.5 cm length × 1.82 cm inner diameter (1.57 dm^3 irradiated volume), with connecting tubing and valves mounted in an aluminium frame. Both the solar photovoltaic panel and CPCs photoreactor were placed on separated platforms tilted 41º to better collect the sun rays.

All the SPEF experiments were run for 4 h from the noon in sunny and clear days during the summer of 2013 in our laboratory of Barcelona, Spain (latitude: 41º 21'N; longitude: 2º 10'E). The average solar UV radiation intensity (between 300 and 400 nm) was about 31 W m^{-2}, as measured with a Kipp & Zonen CUV 5 global UV radiometer. Under these conditions, the photovoltaic panel provided average values of 5.0 A and 10.0 V. Part of this panel was covered with a black plastic to operate at average values of 3.0 A and 7.3 V. Before the degradation tests, the air-diffusion cathode was activated by electrolyzing 10 dm^3 of 0.05 mol dm^{-3} Na_2SO_4 at pH 3.0 and 5.0 A for 240 min.

3.3. Apparatus and analytical procedures

The solution pH was determined with a Crison GLP 22 pH-meter. Prior to analysis, the samples withdrawn from electrolyzed solutions were neutralized at pH 7-8 to stop the degradation process and filtered with 0.45 μm PTFE filters purchased from Whatman. The mineralization of DY4 was monitored from the abatement of its dissolved organic carbon (DOC), measured with a Shimadzu TOC-VCSN analyzer. Reproducible TOC values with ±1% accuracy were found by injecting 50 μl aliquots into the analyzer. Total nitrogen (TN) was determined with a Shimadzu TNM-1 unit coupled with the TOC analyzer. The mineralization current efficiency (MCE) for each trial at average current I (in A) and electrolysis time t (in h) was then estimated as follows [15,24]:

$$\text{MCE (\%)} = \frac{n\,F\,V_s\,\triangle(\text{DOC})_{exp}}{4.32\times10^7\,m\,I\,t} \times 100 \qquad (6)$$

where F is the Faraday constant (96,487 C mol^{-1}), V_s is the solution volume (10 dm^3), $\triangle(DOC)_{exp}$ is the experimental DOC decay (in mg dm^{-3}), 4.32×10^7 is a conversion factor to homogenize units (3,600 s h^{-1} × 12,000 mg mol^{-1}) and m is the number of carbon atoms of the dye (26 carbon atoms). The number of electrons consumed per each DY4 molecule (n) was taken as 106, considering that mineralization involves its conversion into CO_2 with release of NH_4^+ and SO_4^{2-} as major inorganic ions, as will be discussed below, according to reaction (7):

$$C_{26}H_{16}N_4O_8S_2^{2-} + 52\ H_2O \rightarrow 26\ CO_2 + 4\ NH_4^+ + 2\ SO_4^{2-} + 104\ H^+ + 106\ e^- \qquad (7)$$

The DY4 decay was followed by reversed-phase HPLC using a Waters 600 LC fitted with a Spherisorb ODS2 5 μm, 150 mm × 4.6 mm, column at 35 ºC and coupled with a Waters 996 photodiode array detector selected at λ_{max} = 400 nm. In these measurements, 20 μl aliquots were injected into the chromatograph and the mobile phase was a 50:50 (v/v) acetonitrile/water mixture with 2.4 mmol dm^{-3} n-butylamine at 0.3 cm^3 min^{-1}, displaying the dye at a retention time of 5.15 min. The change in concentration of

generated carboxylic acids was determined by ion-exclusion HPLC using a the same LC fitted with a Bio-Rad Aminex HPX 87H, 300 mm × 7.8 mm, column at 35 °C and setting the photodiode array detector at λ = 210 nm. For these analyses, 20 μl aliquots were also injected into the LC, 4 mmol dm^{-3} H_2SO_4 at 0.6 cm^3 min^{-1} was employed as mobile phase and the peaks appeared at retention times of 7.0 min for oxalic acid, 7.9 min for tartronic acid, 8.3 min for maleic acid, 9.4 min for oxamic acid, 9.5 min for malic acid, 9.8 min for malonic acid, 12.2 min for glycolic acid, 13.4 min for formic acid and 15.1 min for acetic acid. The released inorganic ions were quantified by ion chromatography with a Shimadzu 10 Avp LC coupled with a Shimadzu CDD 10 Avp conductivity detector. The NH_4^+ concentration was analyzed with a Shodex IC YK-421, 125 mm × 4.6 mm, cation column at 40 ºC, whereas the NO_3^- and SO_4^{2-} contents were obtained with a Shim-Pack IC-A1S, 100 mm × 4.6 mm, anion column also at 40 ºC. These analyses were made by injecting 25 μl samples and circulating mobile phases composed of a 5.0 mmol dm^{-3} tartaric acid, 1.0 mmol dm^{-3} dipicolinic acid, 24.2 mmol dm^{-3} boric acid and 1.5 mmol dm^{-3} crown ether solution at 1.0 cm^3 min^{-1} for NH_4^+ and a 2.4 mmol dm^{-3} tris(hydroxymethyl)-aminomethane and 2.5 mmol dm^{-3} phthalic acid solution of pH 4.0 at 1.5 cm^3 min^{-1} for NO_3^- and SO_4^{2-}.

Aromatic intermediates formed after 5-30 min of SPEF treatment of a 0.16 mmol dm^{-3} DY4 solution in the autonomous solar pre-pilot plant at average current of 5.0 A were identified by LC–MS using a Shimadzu SIL-20ACLC coupled with a Shimadzu LCMS-2020 MS. The LC was fitted with a Teknokroma Mediterranean Sea C-18 3 μm, 15 mm × 0.46 mm, column at 30 ºC. The MS operated in the negative mode with electrospray source ionization (ESI), by applying an interface voltage of −4.5 V and 60 V Q-array RF oltage. The DL temperature was 250 ºC and pure N_2 was used as nebulising and dryer gas. Mass spectra were collected in the *m/z* range 50–820 using total ion current (TIC)

acquisition. For these analyses, 30 μl aliquots were introduced into the LC, previously filtered with a Millipore filter of 0.22 μm, and the mobile phase was a 75:25 (v/v) acetonitrile/water (5.0 mmol dm^{-3} ammonium acetate) mixture at 0.2 cm^3 min^{-1}.

4. Results and discussion

4.1. Effect of Fe^{2+} concentration on the solar photoelectro-Fenton degradation

A first series of experiments was made by electrolyzing 10 dm^3 of 0.16 mmol dm^{-3} DY4 (corresponding to 50 mg dm^{-3} DOC) in 0.05 mol dm^{-3} Na_2SO_4 with Fe^{2+} content between 0.25 and 5.0 mmol dm^{-3} at pH 3.0 and 35 ºC using the autonomous solar pre-pilot plant for 240 min. The system operated under steady conditions since the solar photovoltaic panel provided to the Pt/air-diffusion cell the maximum average current of 5.0 A, within a fluctuation of 0.1 A. In these trials, the initial yellow solutions were rapidly decolorized and their pH did not vary significantly during electrolysis time, attaining final values near 2.7-2.8, suggesting the formation of acidic products like short-linear carboxylic acids [5,6].

Fig. 2a evidences that the decolorization rate of the dye increased gradually with increasing Fe^{2+} content from 0.25 to 5.0 mmol dm^{-3}. Thus, 99% and 97% of color removal were achieved at 60 min of treatment with 0.25 and 0.50 mmol dm^{-3} Fe^{2+}, respectively, whereas the use of 2.0 and 5.0 mmol dm^{-3} Fe^{2+} only yielded 92% and 84% color removal at 120 min, respectively. This deceleration in decolorization can be related to the concomitant loss of $^{\bullet}OH$ produced from Fenton's reaction (3) and induced by photolytic reaction (4) due to the increase in rate of the following parasitic reaction with raising amounts of Fe^{2+} [40]:

$$Fe^{2+} + {}^{\bullet}OH \rightarrow Fe^{3+} + OH^{-} \quad (8)$$

To better clarify this behavior, the decay of DY4 concentration was followed by reversed-phase HPLC and the results obtained are presented in Fig. 2b. In all cases, the dye was completely removed at much higher rate than decolorized. That means that the decolorization process involves the formation of colored conjugated products with λ_{max} similar to that of the dye, which are more difficultly destroyed, particularly for Fe^{2+} contents ≥ 2.0 mmol dm^{-3} when lesser amounts of oxidant •OH are available in the medium. Surprisingly, Fig. 2b also shows that the dye disappeared more quickly from 0.25 to 0.50 mmol dm^{-3} Fe^{2+}. This evidences that Fenton's reaction (3) is accelerated, generating more •OH up to 0.50 mmol dm^{-3} Fe^{2+}, but at higher catalyst content this radical is progressively loss under the action of reaction (8). The drop in decolorization efficiency when dye content rises from 0.25 to 0.50 mmol dm^{-3} Fe^{2+} points to the formation of Fe(III) complexes among the colored conjugated products formed. Analysis of the above concentration decays revealed that the dye obeyed a pseudo-first-order kinetics, as can be observed in the inset panel of Fig. 2b. The greater apparent rate constant (k_1) of 3.5×10^{-3} s^{-1} (R^2 = 0.999) was found for 0.50 mmol dm^{-3} Fe^{2+}, dropping slightly to 3.0×10^{-3} s^{-1} (R^2 = 0.998) for 0.25 mmol dm^{-3}, and much more strongly to 1.9×10^{-3} s^{-1} (R^2 = 0.998) for 2.0 mmol dm^{-3} and 7.3×10^{-4} s^{-1} (R^2 = 0.999) for 5.0 mmol dm^{-3}. This behavior suggests that the dye is always attacked by a constant but different amount of •OH in all cases, as expected if the plant operates under steady conditions.

Fig. 2c depicts that the solution DOC was also destroyed more rapidly for 0.50 mmol dm^{-3} Fe^{2+}, attaining 96% mineralization after 180 min of SPEF process. A mineralization degree of 95% was also achieved for 0.25 mmol dm^{-3} Fe^{2+} but at 240 min, whereas the use of 2.0 mmol dm^{-3} Fe^{2+} led to 94% DOC reduction at the end of treatment. In contrast, the much lower oxidation ability for 5.0 mmol dm^{-3} Fe^{2+} only allowed reaching 85% mineralization. The greater production of •OH then favors the faster destruction of

organics and the formation of Fe(III) complexes that can be more quickly photolyzed by sunlight in the CPCs photoreactor.

The aforementioned findings indicate that the optimum Fe^{2+} concentration for the SPEF degradation of DY4 in the autonomous pre-pilot plant is 0.50 mmol dm^{-3}, which was used in the next experiments. Besides, the large influence of this catalyst on the destruction of organics evidences that •OH formed in the medium is the predominant oxidizing agent, being much more potent than Pt(•OH) formed at the anode surface from reaction (1), as found for other aromatic treated by EAOPs based on Fenton's reaction chemistry [5,6,18,19,32].

4.2. Influence of applied current on the solar photoelectro-Fenton process

The applied current is a key parameter in the EAOPs because it controls the amount of •OH able to oxidize organic pollutants. The influence of this experimental variable on the SPEF process using the autonomous solar pre-pilot plant was investigated for 10 dm^3 of a 0.16 mmol dm^{-3} DY4 solution with 0.05 mol dm^{-3} Na_2SO_4 at optimum 0.50 mmol dm^{-3} Fe^{2+} and pH 3.0 by applying average current values of 3.0 and 5.0 A.

Fig. 3a illustrates that the increase in current upgrades dye decolorization, thereby attaining 97% color removal after 90 min of applying 3.0 A, but only after 60 min at 5.0 A. This can be accounted for by the acceleration of the electrode reactions involving the direct and/or mediated generation of hydroxyl radical, allowing the production of more amounts of Pt(•OH) from reaction (1) as well as of H_2O_2 from reaction (2) [15], which enhances Fenton's reaction (3) leading to greater quantities of •OH in the bulk. The positive effect on degradation as current rises can be better observed in Fig. 3b, where the decay kinetics for the dye is comparatively depicted. The substrate disappeared in 40 min at 3.0 A and at a shorter time of 20 min at 5.0 A. These times were much shorter than

those needed for attaining 97% decolorization efficiency, indicating the generation of colored conjugated products that persisted largely to the attack of •OH in the bulk. As can be seen in the inset panel of Fig. 3b, good linear correlations were obtained assuming a pseudo-first-order reaction for the kinetic analysis of concentration decays. The k_1 value rose from 2.0×10^{-3} s^{-1} (R^2 = 0.995) for 3.0 A to 3.5×10^{-3} s^{-1} (R^2 = 0.999) for 5.0 A, in agreement with the expected attack of the dye by a constant and increasing amount of oxidizing hydroxyl radicals.

An almost complete mineralization of 96% as maximal was found for both currents, but a longer time of 240 min was needed for 3.0 A compared to 180 min for 5.0 A, as shown in Fig. 3c. This agrees with the greater generation of Pt(•OH) and •OH at higher current with the concomitant acceleration of organics removal. However, the opposite trend can be seen in the inset panel of Fig. 3c for the corresponding MCE values calculated from. Eq. (6). For 3.0 A, the current efficiency attained its maximum value of 56% at 120 min to be further reduced to 35% at the end of the SPEF treatment, whereas for 5.0 A, a lower current efficiency of 28% at 180 min was determined after passing by a maximal of 41% at 90 min. The drop in MCE at long electrolysis time can be ascribed to the presence of less organic matter along with the formation of more recalcitrant products [4]. Besides, the gradual decay in current efficiency as current rises can be accounted for by a progressive loss in the relative amount of •OH formed as a result of the higher acceleration of its parasitic reactions with the consequent fall in organic events decelerating the mineralization process. These non-oxidizing reactions involve, for example, the destruction of •OH by Fe^{2+} from reaction (8) [40] and by H_2O_2 from reaction (9), generating the weaker oxidant hydroperoxyl radical ($HO_2^•$) [5], as well as its dimerization to H_2O_2 by reaction (10) [32]:

$$H_2O_2 + {}^•OH \rightarrow HO_2^• + H_2O \quad (9)$$

$$2\ {}^{\bullet}OH \rightarrow H_2O_2 \quad (10)$$

The above results are indicative of a good effectiveness of the SPEF process for DY4 mineralization using the autonomous solar pre-pilot plant. The treatment becomes more efficient at smaller currents, but longer time is required for achieving the maximum mineralization of 96%. For this reason, the maximum average current of 5.0 A provided by the solar photovoltaic panel can be taken as the best current for SPEF under the present experimental conditions.

4.3. Effect of dye concentration on the solar photoelectro-Fenton treatment

The substrate concentration is another important experimental variable since it can inform about the ability of EAOPs to produce reactive oxidizing species and to treat high pollutant concentrations. To clarify this effect for the autonomous solar pre-pilot plant, 10 dm^3 of solutions with DY4 concentrations between 0.08 and 0.32 mmol dm^{-3} with 0.05 mol dm^{-3} Na_2SO_4 and 0.50 mmol dm^{-3} Fe^{2+} at pH 3.0 were degraded at 5.0 A.

Fig. 4a highlights that longer time, from 30 to 90 min, was needed for reaching 97-99% color removal as dye content rises from 0.08 and 0.32 mmol dm^{-3}. This is the behavior expected if more organic matter is attacked by a similar amount of oxidizing agents that are formed under steady conditions. Note that a similar decolorization efficiency was found for 0.16 and 0.24 mmol dm^{-3}, indicating that analogous quantities of colored conjugated intermediates are formed in this concentration range. The longer duration of the attack of Pt(${}^{\bullet}OH$) and primordially ${}^{\bullet}OH$ over greater DY4 concentrations was confirmed by determining their decay kinetics. As can be seen in Fig. 4b, the dye was completely removed at increasing times of about 15, 20, 40 and 60 min for higher dye contents of 0.08, 0.16, 0.24 and 0.32 mmol dm^{-3}. According to this, the k_1 value decreased gradually from 5.1×10^{-3} s^{-1} (R^2 = 0.987) at 0.08 mmol dm^{-3} to 1.6×10^{-3} s^{-1} (R^2 = 0.998) at 0.32 mmol dm^{-3}. The large drop in k_1 evidences that the reaction of the dye

with hydroxyl radicals does not obey a true pseudo-first-order kinetics, since an apparent rate constant independent of substrate content is theoretically predicted in such a case. This complex behavior may be ascribed to the very short lifetime of hydroxyl radicals (about 4×10^{-9} s [41]), which need to be continuously produced at the Pt anode from water oxidation by reaction (1) and in the medium from reactions (3) and (4) with participation of H_2O_2 and Fe^{2+}, also continuously generated at the cathode. The diffusion of all these species in the medium and their mass transport toward/from the electrodes then seem to limit the generation of Pt(•OH) and •OH giving rise to a different constant concentration to attack DY4 in each trial. This can justify the pseudo-first-order kinetics always followed by the dye but with a k_1 value that falls as substrate content rises due to the slower diffusion and mass transport control of the species generating these oxidants by the presence of more organic matter.

The good oxidation ability of the SPEF process to mineralize the different DY4 solutions is shown in Fig. 4c. An almost total mineralization related to 96-97% DOC abatement was found in all cases, which was reached at longer time with increasing substrate concentration. For the higher content of 0.32 mmol dm^{-3}, such DOC decay was obtained in 240 min, while only 120 min were needed for the smaller content of 0.08 mmol dm^{-3}. However, when the corresponding MCE values were calculated, two different relative tendencies were found depending on the electrolysis time. The inset panel of Fig. 4c evidences the existence of a maximum current efficiency in all cases, which became greater and appeared at longer time as dye content increased. At the beginning of the process, the MCE values dropped with raising the organic matter, suggesting the initial generation of more amounts of products that are hardly mineralized. In contrast, after passing the maximum MCE value, the opposite tendency occurred and the higher 0.32 mmol dm^{-3} dye concentration yielded the best efficiency of 41% at 240 min. This

enhancement in efficiency can be related to the quicker oxidation of greater quantities of the remaining organics by larger amounts of •OH that cause a decay in rate of its parasitic reactions (8)-(10). This leads to a faster formation of Fe(III) complexes with the resulting products that are more rapidly photolyzed with solar radiation.

The above study evidences that the autonomous solar pre-pilot plant is able to rapidly mineralize solutions up to 0.32 mmol dm^{-3} DY4 under the synergistic action of hydroxyl radicals and sunlight in the SPEF process. This concentration (about 200 mg dm^{-3}) is the typical maximum value expected for dyeing industrial wastewaters [15,28]. Consequently, one can infer that this method can be viable for the industrial treatment of waters containing DY4.

4.4. Identification of aromatic intermediates and time course of generated carboxylic acids and released inorganic ions

Table 2 collects the eleven aromatic compounds and twenty two hydroxylated derivatives detected by LC-MS, which are originated during the initial SPEF treatment of the dye at 5.0 A. Apart from the starting DY4 with two azo bonds and four benzenic moieties (**1**), four products with one azo bond and three benzenic groups (**2**-**5**), one derivative with one azo bond and two benzenic moieties (**6**), two conjugated products with also two benzenic groups (**7** and **8**) and finally, four monobenzenic derivatives (**9**-**12)** were identified. These compounds are formed from the consecutive breaking of the two azo bonds of the dye and from the deamination, desulfonation, hydroxylation, nitration and carboxylation of the benzenic groups.

Ion-exclusion chromatograms of electrolyzed solutions exhibited the generation of nine short-linear carboxylic acids like maleic (**13**), malic (**14**), tartronic (**15**), malonic (**16**), glycolic (**17**), acetic (**18**), oxalic (**19**), formic (**20**) and oxamic (**21**). Acids **13**-**18** are expected to be produced from the oxidative cleavage of the benzenic ring of aromatic

intermediates, which are subsequently transformed into **19** and **20** [5,24,27,28]. The acid **21** should be formed from the degradation of intermediates containing a $–NH_2$ group. The products **19-21** are ultimate carboxylic acid since they are directly transformed into CO_2 [6,42].

Fig. 5 shows the evolution of the concentration of all detected acids during the SPEF treatment of 10 dm^3 of a 0.16 mmol dm^{-3} DY4 solution with 0.05 mol dm^{-3} Na_2SO_4 and 0.50 mmol dm^{-3} Fe^{2+} at pH 3.0 and 5.0 A. Acids **15** and **19** were accumulated in larger extent up to near 16-18 mg dm^{-3} in 60 min to practically disappear (< 0.2 mg dm^{-3}) for times longer than 120 min. The quick removal of these acids is due to the fast photolysis of their Fe(III) complexes via reaction (5), because at least, Fe(III)-oxalate species cannot be directly destroyed by hydroxyl radicals [5,6,42]. The rapid photolysis of the Fe(III)-complexes of acids **13**, **14**, **16**, **17** and **20** can also explain their disappearance at times lesser than 90 min. In contrast, acids **18** and **21** persisted largely up to the end of treatment, with final contents of 0.36 and 0.87 mg dm^{-3}, respectively, because their complexes with Fe(III) react very slowly with $^{\bullet}OH$ and are poorly photolyzed. A simple mass balance, for example, at 120 min reveals that all the detected acids contribute in only 0.6 mg dm^{-3} DOC, which is a value much smaller than 6.0 mg dm^{-3} DOC determined for the treated solution. This evidences that large amounts of other undetected products are accumulated and quickly mineralized by oxidation with hydroxyl radicals and/or photolysis by sunlight. The removal of such compounds along with of short-linear carboxylic acids explains the high oxidation ability of SPEF to mineralize DY4.

The mineralization of the initial N (0.64 mM, 9.0 mg dm^{-3}) contained in 0.16 mmol dm^{-3} DY4 solution in the form of NH_4^+ and NO_3^- ions was confirmed by ion chromatography. No other inorganic nitrogen ions like NO_2^- were detected by this technique. Fig. 6a highlights the much larger accumulation of NH_4^+ ion than NO_3^- ion,

as stated in reaction (7). Both ions were rapidly released attaining final N concentrations of 4.7 mg dm^{-3} related to NH_4^+ (52.2% of initial N) and 1.2 mg dm^{-3} related to NO_3^- (13.3% of initial N). Since the remaining acid **21** still contained 1.5% of the initial N, one can infer that only 67% of the initial organic N is released to the medium, while a proportion as high as 33% is lost, probably as volatile N_2 and/or N_xO_y species.

On the other hand, the release of the initial organic S as SO_4^{2-} ion was also assessed during the SPEF process of the 0.16 mmol dm^{-3} dye solution. Fig. 6b shows a rapid accumulation of SO_4^{2-} ion in the solution up to 30.7 mg dm^{-3} (97.8% of initial S) after 120 min of treatment. This corroborates the practical complete conversion of the initial S into such ion, as proposed in reaction (7).

4.5. Proposed reaction pathway for Direct Yellow 4 mineralization

Based on the above detected products, Fig. 7 presents a reaction sequence proposed for the mineralization of DY4 by the SPEF process. In this pathway, the main oxidizing agent $^{\bullet}OH$ is only considered. Although all the acids are expected to form Fe(III) complexes under the experimental conditions tested, this possibility is only stated for acids **19-21** for sake of simplicity.

The process starts with the cleavage of one azo bond of **1** to yield two aminoderivatives, the compound **2** and *p*-aminophenol, which is oxidized to its nitro product **12.** The compound **2** is degraded either to **3** via deamination or to **4** via desulfonation. Subsequent deamination of **4** leads to **5**, which is oxidized to the shorter derivatives **6** and **7**. The breaking of the azo bond of **3** followed by carboxylation or hydroxylation yields the mixture of products **8**-**10**. The compound **10** can then be either hydroxylated to **11** or desulfonated followed by nitration to produce **12**. Further cleavage of the benzenic moiety of the above aromatic intermediates yields a mixture of acids **13**-**18**, which are subsequently oxidized to **19** and **20**. The parallel degradation of aromatics

with a $–NH_2$ group generates the acid **21**. The ultimate acids **19-21** form the corresponding Fe(III) complexes. While the Fe(III)-formate species are destroyed by $^{\bullet}OH$ and photolyzed by sunlight to CO_2, the removal of Fe(III)-oxamate species under the action of these agents is much slower, giving CO_2 and NH_4^+ and NO_3^- ions [42]. In contrast, Fe(III)-oxalate is rapidly photocarboxylated under solar radiation.

5. Conclusions

The SPEF process is the more potent technology for the treatment of organic pollutants by EAOPs based on Fenton's reaction chemistry using a gas-diffusion cathode to generate H_2O_2, due to the synergistic action of generated hydroxyl radicals and solar irradiation. In this paper, it has been demonstrated that SPEF can be viable at industrial level using an autonomous solar pre-pilot plant. It contained a Pt/air-diffusion filter-press cell coupled to a solar CPCs photoreactor and a maximum average current of 5.0 A was applied by a solar photovoltaic panel, thereby making the process energetically inexpensive. The degradation of DY4 diazo dye performed with this plant showed that 0.5 mmol dm^{-3} Fe^{2+} was optimal as catalyst concentration yielding almost total mineralization. However, greater percentage of color removal was found at lower Fe^{2+} contents probably because of the smaller formation of complexes of Fe(III) with colored conjugated products that are more difficultly oxidized with $^{\bullet}OH$. The decrease in current produced less oxidizing agents giving slower decolorization, decay of substrate concentration and mineralization, although it increased the current efficiency as a result of the deceleration of the parasitic reactions of $^{\bullet}OH$. The current efficiency also grew with raising dye concentration at the end of the treatment when DOC was reduced by 96-97%. Under all the conditions tested, the substrate decay obeyed a pseudo-first-order kinetics. Eleven aromatic intermediates and twenty two hydroxylated derivatives coming from the

consecutive breaking of the two azo bonds and the deamination, desulfonation, hydroxylation, nitration and carboxylation of the benzenic groups of DY4 were detected by LC-MS. Nine short-linear carboxylic acids were quantified by ion-exclusion HPLC. The Fe(III) complexes of most acids were rapidly removed by the attack of •OH and pre-eminently photolyzed by sunlight, except those of acetic and oxamic acids that were slowly destroyed by these agents. The initial N of the dye was mainly released as NH_4^+ ion, whereas its initial S was lost as SO_4^{2-} ion.

Acknowledgements

The authors are grateful to the financial support from MICINN (Ministerio de Ciencia e Innovación, Spain) under the project CTQ2010-16164/BQU, co-financed with FEDER funds. S. Garcia-Segura thanks the grant awarded from MEC (Ministerio de Educación y Ciencia, Spain).

References

[1] C.A. Martínez-Huitle, S. Ferro, Electrochemical oxidation of organic pollutants for the wastewater treatment: direct and indirect processes, Chemical Society Review 35 (2006) 1324.

[2] C.A. Martínez-Huitle, E. Brillas, Electrochemical alternatives for drinking water disinfection, Angewandte Chemie International Edition 47 (2008) 1998.

[3] A. Anglada, A. Urtiaga, I. Ortiz, Contributions of electrochemical oxidation to wastewater treatment: Fundamentals and review of applications, Journal of Chemical Technology and Biotechnology 84 (2009) 1747.

[4] M. Panizza, G. Cerisola, Direct and mediated anodic oxidation of organic pollutants, Chemical Reviews 109 (2009) 6541.

[5] E. Brillas, I. Sirés, M.A. Oturan, Electro-Fenton process and related electrochemical technologies based on Fenton's reaction chemistry, Chemical Reviews 109 (2009) 6570.

[6] I. Sirés, E. Brillas, Remediation of water pollution caused by pharmaceutical residues based on electrochemical separation and degradation technologies: A review, Environment International 40 (2012) 212.

[7] B. Marselli, J. García-Gomez, P.A. Michaud, M.A. Rodrigo, Ch. Comninellis, Electrogeneration of hydroxyl radicals on boron-doped diamond electrodes, Journal of The Electrochemical Society 150 (2003) D79.

[8] C. Flox, J.A. Garrido, R.M. Rodríguez, F. Centellas, P.L. Cabot, C. Arias, E. Brillas, Degradation of 4,6-dinitro-o-cresol from water by anodic oxidation with a boron-doped diamond electrode, Electrochimica Acta 50 (2005) 3685.

[9] S. Ammar, R. Abdelhedi, C. Flox, C. Arias, E. Brillas, Electrochemical degradation of the dye indigo carmine at boron-doped diamond anode for wastewaters remediation, Environmental Chemistry Letters 4 (2006) 229.

[10] J. Gao, G. Zhao, M. Liu, D. Li, Mechanism of enhanced electrochemical oxidation of 2,4-dichlorophenoxyacetic acid with in situ microwave activated boron-doped diamond and platinum anodes, Journal of Physical Chemistry A 113 (2009) 10466.

[11] A.R. Khataee, M. Safarpour, M. Zarei, S. Aber, Electrochemical generation of H_2O_2 using immobilized carbon nanotubes on graphite electrode fed with air: Investigation of operational parameters, Journal of Electroanalytical Chemistry 169 (2011) 63.

[12] A. Özcan, Y. Sahin, A.S. Koparal, M.A. Oturan, Carbon sponge as a new material for the electro-Fenton process. Comparison with carbon felt cathode and application

to degradation of synthetic dye Basic Blue 3 in aqueous medium, Journal of Electroanalytical Chemistry 616 (2008) 71.

[13] K. Cruz-González, O. Torres-López, A. García-León, J.L. Guzmán-Mar, L.H. Reyes, A. Hernández-Ramírez, J.M. Peralta-Hernández, Determination of optimum operating parameters for Acid Yellow 36 decolorization by electro-Fenton process using BDD cathode, Chemical Engineering Journal 160 (2010) 199.

[14] M. Panizza, M.A. Oturan, Degradation of Alizarin Red by electro-Fenton process using a graphite-felt cathode, Electrochimica Acta 56 (2011) 7084.

[15] E.J. Ruiz, C. Arias, E. Brillas, A. Hernández-Ramírez, J.M. Peralta-Hernández, Mineralization of Acid Yellow 36 azo dye by electro-Fenton and solar photoelectro-Fenton processes with a boron-doped diamond anode, Chemosphere 82 (2011) 495.

[16] S. Garcia-Segura, J.A. Garrido, R.M. Rodríguez, P.L. Cabot, F. Centellas, C. Arias, E. Brillas, Mineralization of flumequine in acidic medium by electro-Fenton and photoelectro-Fenton processes, Water Research 46 (2012) 2067.

[17] A. Dirany, I. Sirés, N. Oturan, A. Özcan, M.A. Oturan, Electrochemical treatment of the antibiotic sulfachloropyridazine: Kinetics, reaction pathways, and toxicity evolution, Environmental & Science Technology 46 (2012) 4074.

[18] J.M. Peralta-Hernández, Y. Meas-Vong, F.J. Rodriguez, T.W. Chapman, M.I. Maldonado, L.A. Godinez, Comparison of hydrogen peroxide-based processes for treating dye-containing wastewater: Decolorization and destruction of Orange II azo dye in dilute solution, Dyes and Pigments 76 (2007) 656.

[19] A. Wang, J. Qu, H. Liu, J. Ru, Mineralization of an azo dye Acid Red 14 by photoelectro-Fenton process using an activated carbon fiber cathode, Applied Catalysis B: Environmental 84 (2008) 393.

[20] A. Dhaouadi, N. Adhoum, Degradation of paraquat herbicide by electrochemical advanced oxidation methods, Journal of Electroanalytical Chemistry 637 (2009) 33.

[21] M. Zarei, A.R. Khataee, R. Ordikhani-Seyedlar, M. Fathinia, Photoelectro-Fenton combined with photocatalytic process for degradation of an azo dye using supported TiO_2 nanoparticles and carbon nanotube cathode: Neural network modeling, Electrochimica Acta 55 (2010) 7259.

[22] A. Babuponnusami, K. Muthukumar, Advanced oxidation of phenol: A comparison between Fenton, electro-Fenton, sono-electro-Fenton and photo-electro-Fenton processes, Chemical Engineering Journal 183 (2012) 1.

[23] R. Salazar, M.S. Ureta-Zañartu, Mineralization of triadimefon fungicide in water by electro-Fenton and photoelectro-Fenton, Water Air Soil Pollution 223 (2012) 4199.

[24] C. Flox, J.A. Garrido, R.M. Rodríguez, P.L. Cabot, F. Centellas, C. Arias, E. Brillas, Mineralization of herbicide mecoprop by photoelectro-Fenton with UVA and solar light, Catalysis Today 129 (2007) 29.

[25] C. Flox, P.L. Cabot, F. Centellas, J.A. Garrido, R.M. Rodríguez, C. Arias, E. Brillas, Solar photoelectro-Fenton degradation of cresols using a flow reactor with a boron-doped diamond anode, Applied Catalysis B: Environmental 75 (2007) 17.

[26] E. Guinea, C. Arias, P.L. Cabot, J.A. Garrido, R.M. Rodríguez, F. Centellas, E. Brillas, Mineralization of salicylic acid in acidic aqueous medium by electrochemical advanced oxidation processes using platinum and boron-doped

diamond as anode and cathodically generated hydrogen peroxide, Water Research 42 (2008) 499.

[27] M. Skoumal, R.M. Rodríguez, P.L. Cabot, F. Centellas, J.A. Garrido, C. Arias, E. Brillas, Electro-Fenton, UVA photoelectro-Fenton and solar photoelectro-Fenton degradation of the drug ibuprofen in acid aqueous medium using platinum and boron-doped diamond anodes, Electrochimica Acta 54 (2009) 2077.

[28] E. Guinea, J.A. Garrido, R.M. Rodríguez, P.L. Cabot, C. Arias, F. Centellas, E. Brillas, Degradation of the fluoroquinolone enrofloxacin by electrochemical advanced oxidation processes based on hydrogen peroxide electrogeneration, Electrochimica Acta 55 (2010) 2101.

[29] S. Garcia-Segura, E.B. Cavalcanti, E. Brillas, Mineralization of the antibiotic chloramphenicol by solar photoelectro-Fenton. From stirred tank reactor to solar pre-pilot plant, Applied Catalysis B: Environmental 144 (2014) 588.

[30] A. Serra, X. Domènech, C. Arias, E. Brillas, J. Peral, Oxidation of α-methylphenylglycine under Fenton and electro-Fenton conditions in the dark and in the presence of solar light, Applied Catalysis B: Environmental 89 (2009) 12.

[31] F.C. Moreira, S. Garcia-Segura, V.J.P. Vilar, R.A.R. Boaventura, E. Brillas, Decolorization and mineralization of Sunset Yellow FCF azo dye by anodic oxidation, electro-Fenton, UVA photoelectro-Fenton and solar photoelectro-Fenton processes, Applied Catalysis B: Environmental 142–143 (2013) 877.

[32] E.J. Ruiz, A. Hernández-Ramírez, J.M. Peralta-Hernández, C. Arias, E. Brillas, Application of solar photoelectro-Fenton technology to azo dyes mineralization: Effect of current density, Fe^{2+} and dye concentration, Chemical Engineering Journal 171 (2011) 385.

[33] R. Salazar, S. Garcia-Segura, M.S. Ureta-Zañartu, E, Brillas, Degradation of disperse azo dyes from waters by solar photoelectro-Fenton, Electrochimica Acta 56 (2011) 6371.

[34] R. Salazar, E. Brillas, I. Sirés, Finding the best Fe^{2+}/Cu^{2+} combination for the solar photoelectro-Fenton treatment of simulated wastewater containing the industrial textile dye Disperse Blue 3, Applied Catalysis B: Environmental 115-116 (2012) 107.

[35] A. El-Ghenymy, S. Garcia-Segura, R.M. Rodríguez, E. Brillas, M.S. El Begrani, B.A. Abdelouahid, Optimization of the electro-Fenton and solar photoelectro-Fenton treatments of sulfanilic acid solutions using a pre-pilot flow plant by response surface methodology, Journal of Hazardous Materials 221–222 (2012) 288.

[36] A. El-Ghenymy, P.L. Cabot, F. Centellas, J.A. Garrido, R.M. Rodríguez, C. Arias, E. Brillas, Mineralization of sulfanilamide by electro-Fenton and solar photoelectro-Fenton in a pre-pilot plant with a Pt/air-diffusion cell, Chemosphere 91 (2013) 1324.

[37] E. Isarain-Chávez, R.M. Rodríguez, P.L. Cabot, F. Centellas, C. Arias, J.A. Garrido, E. Brillas, Degradation of pharmaceutical beta-blockers by electrochemical advanced oxidation processes using a flow plant with a solar compound parabolic collector, Water Research 45 (2011) 4119.

[38] S. Garcia-Segura, L.C. Almeida, N. Bocchi, E. Brillas, Solar photoelectro-Fenton degradation of the herbicide 4-chloro-2-methylphenoxyacetic acid optimized by response surface methodology, Journal of Hazardous Materials 194 (2011) 109.

[39] L.C. Almeida, S. Garcia-Segura, N. Bocchi, E. Brillas, Solar photoelectro-Fenton degradation of paracetamol using a flow plant with a Pt/air-diffusion cell coupled

with a compound parabolic collector: Process optimization by response surface methodology, Applied Catalysis B: Environmental 103 (2011) 21.

[40] S. Hammami, N. Bellakhal, N. Oturan, M.A. Oturan, M. Dachraoui, Degradation of Acid Orange 7 by electrochemically generated ˙OH radicals in acidic aqueous medium using a boron-doped diamond or platinum anode. A mechanistic study, Chemosphere 7 (2008) 678.

[41] R. Roots, S. Okada, Estimation of life times and diffusional distances of radical involved X-Ray-Induced DNA strand breaks or killing of mammalian cells, Radiation Research 64 (1975) 306.

[42] S. Garcia-Segura, E. Brillas, Mineralization of the recalcitrant oxalic and oxamic acids by electrochemical advanced oxidation processes using a boron-doped diamond anode, Water Research 45 (2011) 2975.

Figure captions

Fig. 1. Sketch of the autonomous solar pre-pilot plant used for the solar photoelectro-Fenton (SPEF) treatment of 10 dm^3 of Direct Yellow 4 (DY4) solutions. (1) Reservoir, (2) magnetic drive centrifugal pump, (3) flowmeter, (4) air pump, (5) electrochemical filter-press reactor with a Pt anode and an air-diffusion cathode of 90.2 cm^2 area, (6) solar photovoltaic panel of 50 W maximum power with the corresponding ammeter and voltmeter, (7) solar compound parabolic components (CPCs) photoreactor of 1.57 dm^3 irradiation volume and (8) heat exchangers.

Fig. 2. Effect of Fe^{2+} concentration on (a) percentage of color removal, (b) substrate decay and (c) DOC abatement for the SPEF degradation of 10 dm^3 of a 0.16 mmol dm^{-3} DY4 solution in 0.05 mol dm^{-3} Na_2SO_4 at pH 3.0 and 35 ºC using the autonomous solar pre-pilot plant at an average current of 5.0 A and liquid flow rate of 200 dm^3 h^{-1}. Fe^{2+} concentration: (□) 0.25 mmol dm^{-3}, (△) 0.50 mmol dm^{-3}, (▽) 2.0 mmol dm^{-3} and (◇) 5.0 mmol dm^{-3}. In plot (b), the inset panel shows the kinetic analysis considering a pseudo-first-order decay for the dye.

Fig. 3. Influence of current over (a) decolorization efficiency, (b) dye abatement and (c) DOC removal for the treatment of 10 dm^3 of a 0.16 mmol dm^{-3} DY4 solution in 0.05 mol dm^{-3} Na_2SO_4 with 0.50 mmol dm^{-3} Fe^{2+} at pH 3.0 and 35 ºC by SPEF in the autonomous solar pre-pilot plant at a liquid flow rate of 200 dm^3 h^{-1}. Average applied current: (○) 3.0 A and (△) 5.0 A. In plot (b), the inset panel presents the kinetic analysis assuming a pseudo-first-order reaction for DY4. In plot (c), the inset panel gives the corresponding mineralization current efficiency.

Fig. 4. Effect of dye concentration on (a) percentage of color removal, (b) dye abatement and (c) DOC removal for the SPEF treatment of 10 dm^3 of DY4 solutions in 0.05 mol

dm^{-3} Na_2SO_4 at pH 3.0 and 35 ºC using the autonomous solar pre-pilot plant at an average current of 5.0 A and liquid flow rate of 200 dm^3 h^{-1}. Initial dye content: (□) 0.08 mmol dm^{-3}, (△) 0.16 mmol dm^{-3}, (▽) 0.24 mmol dm^{-3} and (◇) 0.32 mmol dm^{-3}. The inset panels show: (b) the analysis assuming a pseudo-first-order kinetics for DY4 and (c) the mineralization current efficiency.

Fig. 5. Time course of (△) maleic (**13**), (▲) malic (**14**), (□) tartronic (**15**), (■) malonic (**16**), (▼) glycolic (**17**), (●) acetic (**18**), (○) oxalic (**19**), (◇) formic (**20**) and (▽) oxamic (**21**) acids detected during the SPEF degradation of 10 dm^3 of a 0.16 mmol dm^{-3} DY4 solution in 0.05 mol dm^{-3} Na_2SO_4 with 0.50 mmol dm^{-3} Fe^{2+} at pH 3.0 and 35 ºC using the autonomous solar pre-pilot plant at an average current of 5.0 A and liquid flow rate of 200 dm^3 h^{-1}.

Fig. 6. Evolution of inorganic ions released during the trial of Fig. 5. In plot (a), nitrogen concentration for: (○) NH_4^+ and (□) NO_3^- ions. In plot (b), (●) SO_4^{2-} concentration.

Fig. 7. Proposed reaction pathway for DY4 mineralization by SPEF.

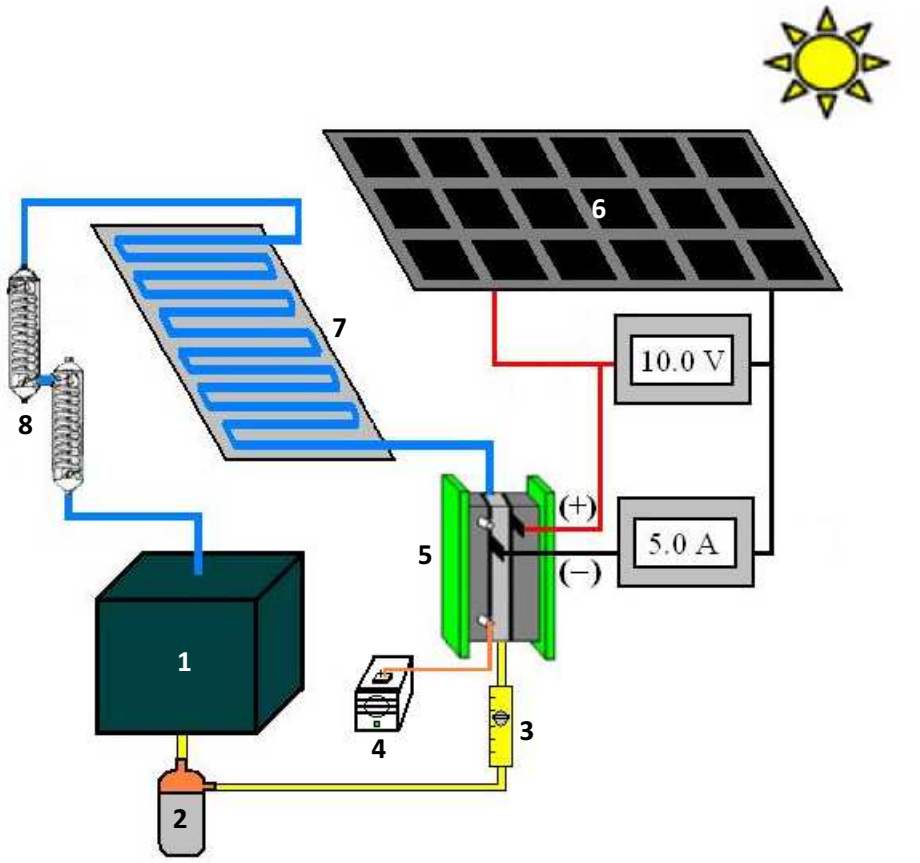

Fig. 1

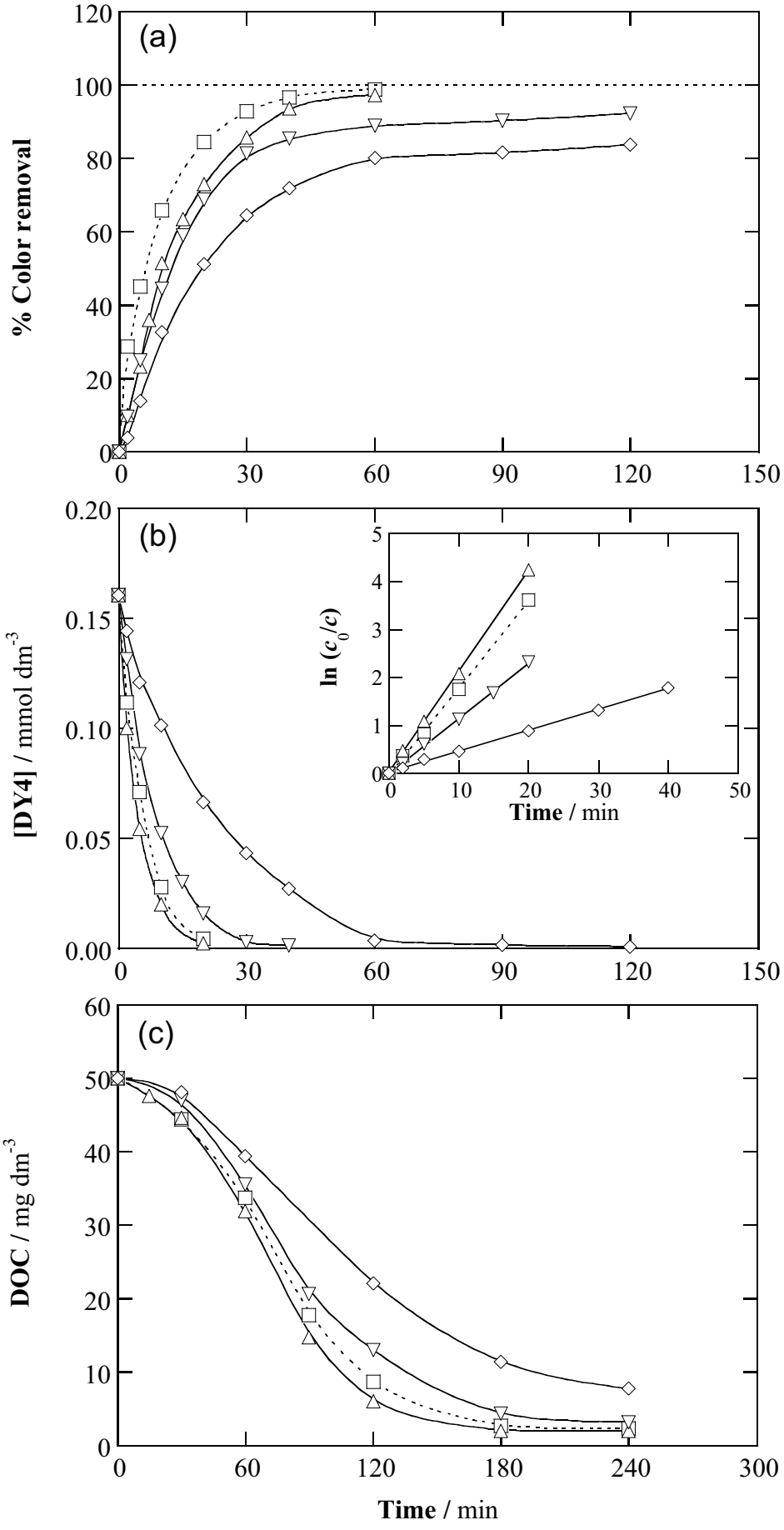
(a)
% Color removal
(b)
[DY4] / mmol dm-3
ln (c0/c)
Time / min
(c)
DOC / mg dm-3
Time / min

Fig. 2

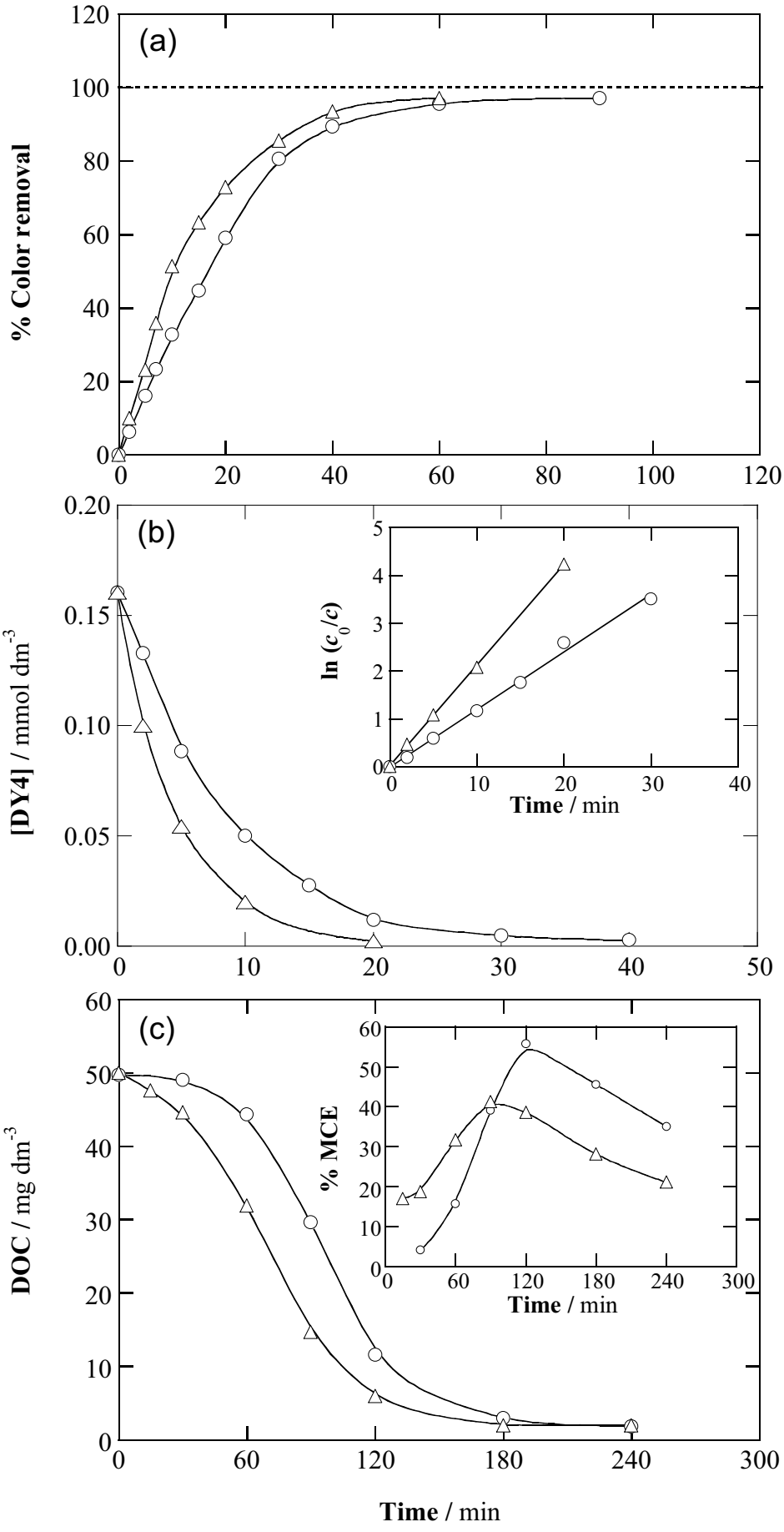
(a)
% Color removal
(b)
[DY4] / mmol dm-3
ln (c0 /c)
Time / min
(c)
DOC / mg dm-3
% MCE
Time / min
Time / min

Fig. 3

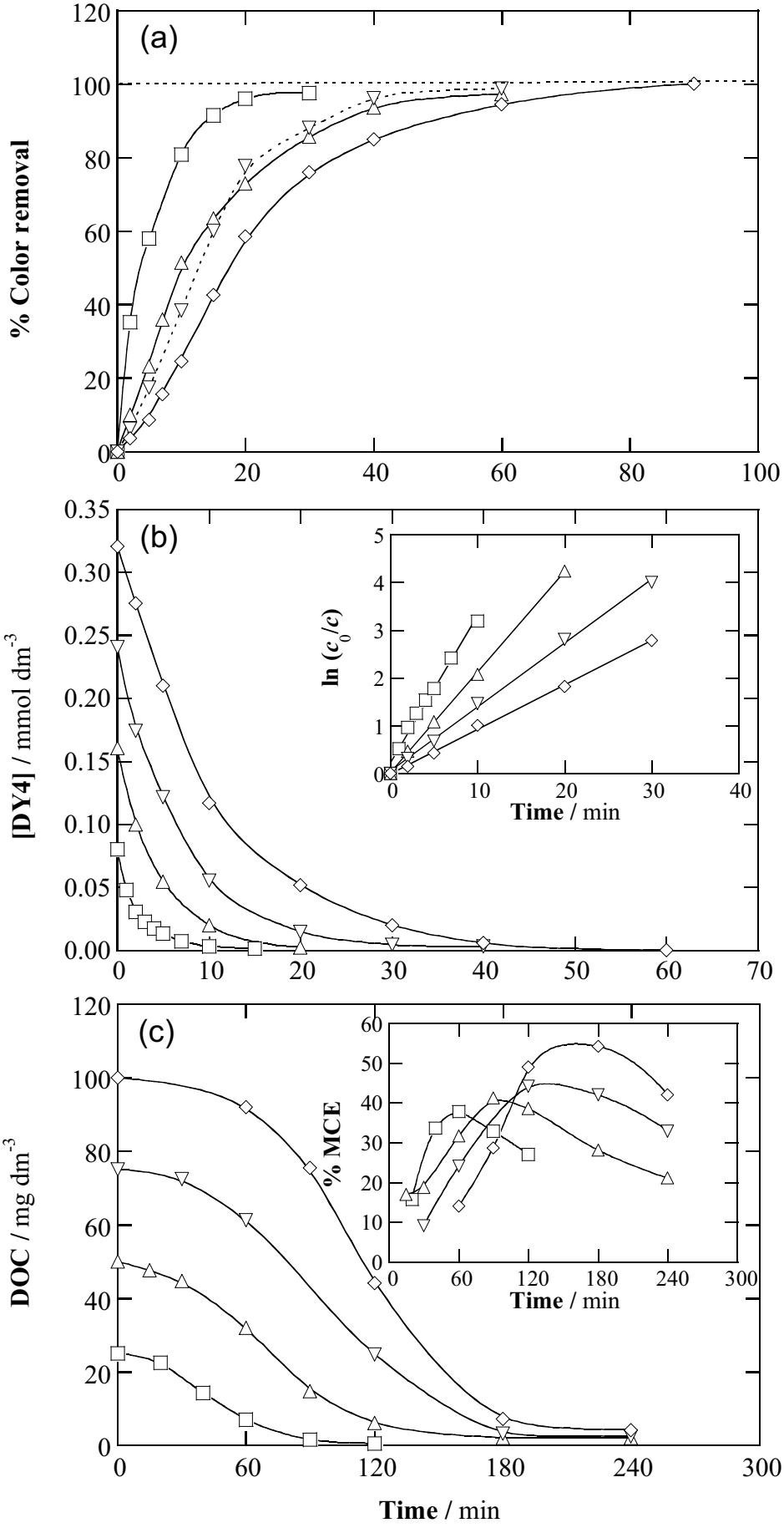
(a)
% Color removal
(b)
[DY4] / mmol dm-3
ln (c0/c)
Time / min
(c)
DOC / mg dm-3
% MCE
Time / min
Time / min

Fig. 4

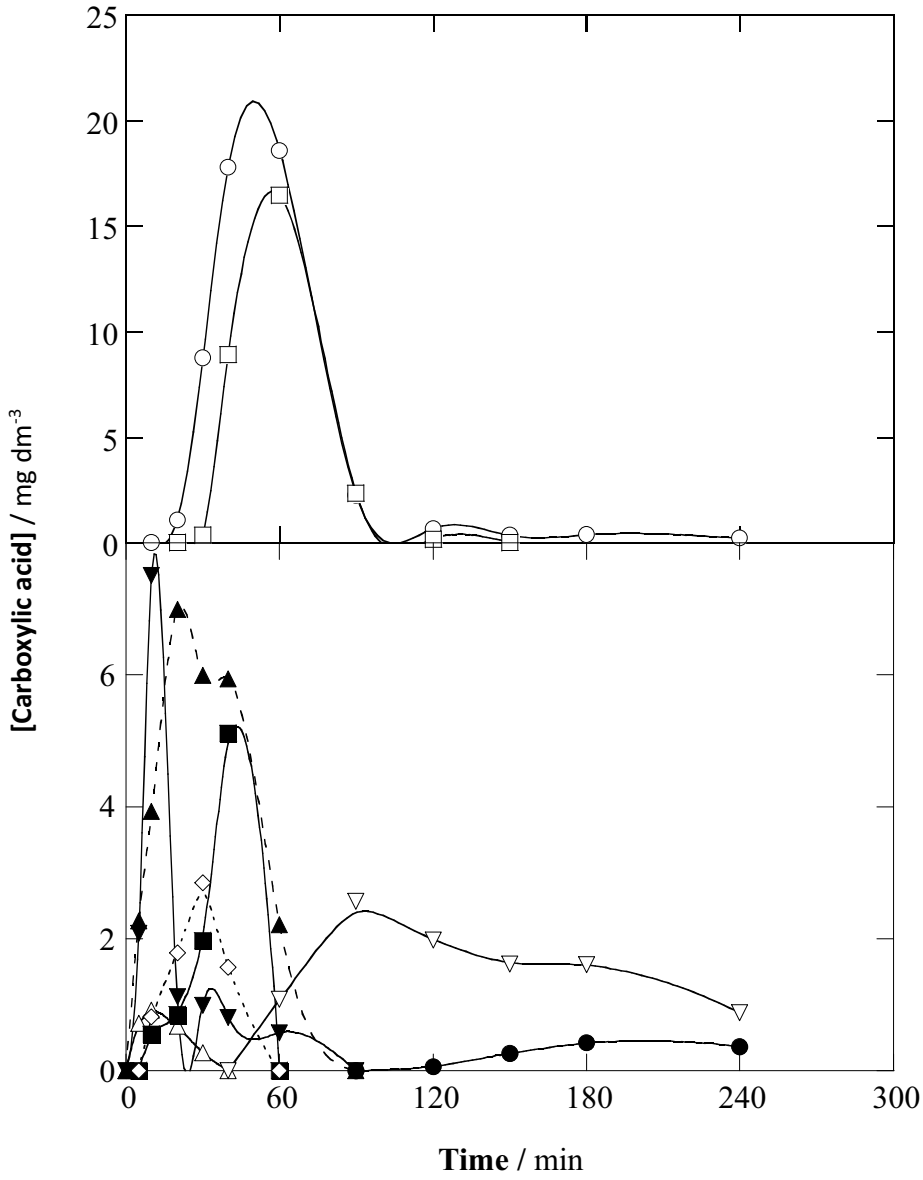
25
20
15
10
5
0
6
4
2
0
0
60
120
180
240
300
[Carboxylic acid] / mg dm-3
Time / min

Fig. 5

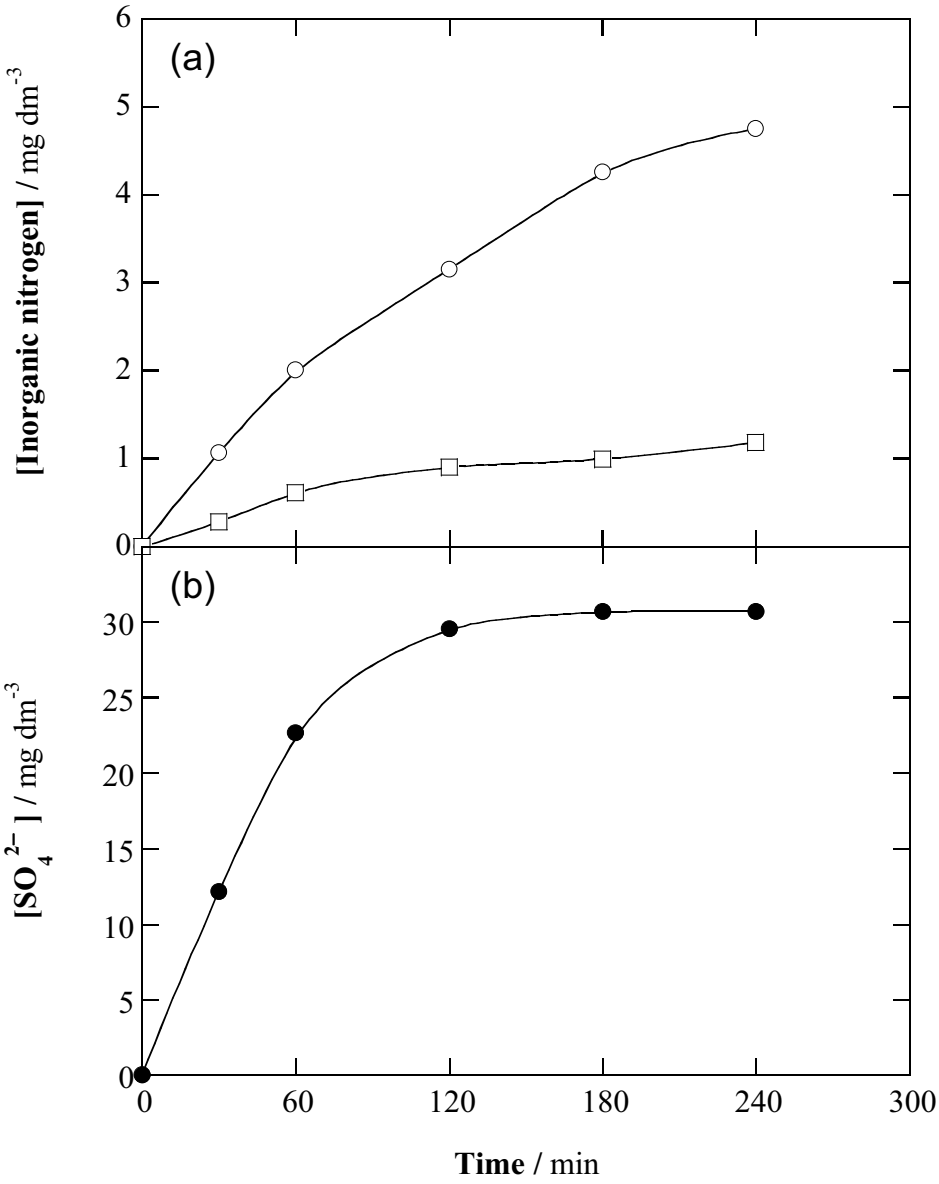
(a)
(b)
[Inorganic nitrogen] / mg dm-3
[SO4 2–] / mg dm-3
Time / min
0
60
120
180
240
300
0
1
2
3
4
5
6
0
5
10
15
20
25
30

Fig. 6

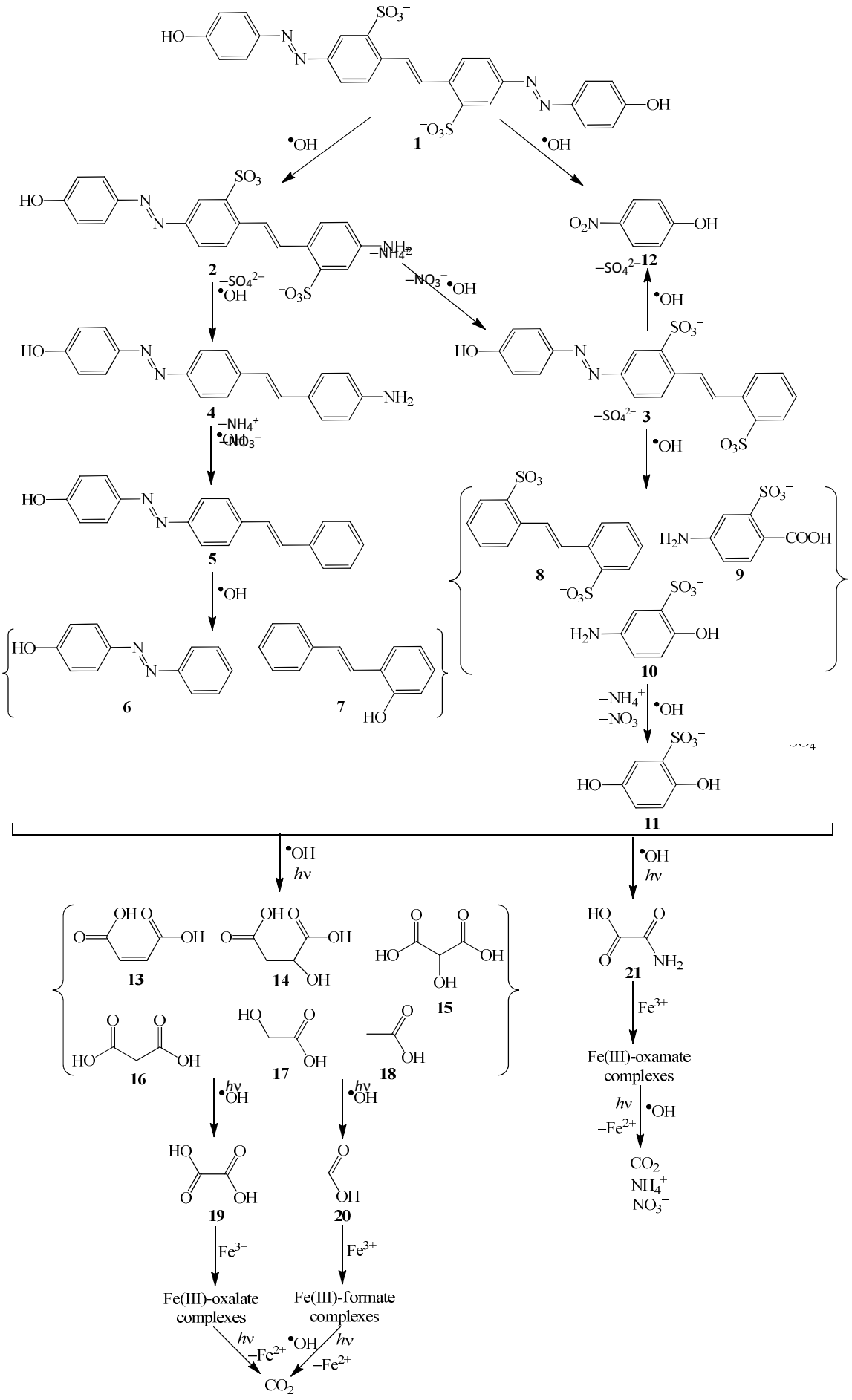

Fig. 7

Table 1.

Chemical structure and characteristics of Direct Yellow 4 (DY4) diazo dye.

Chemical structure	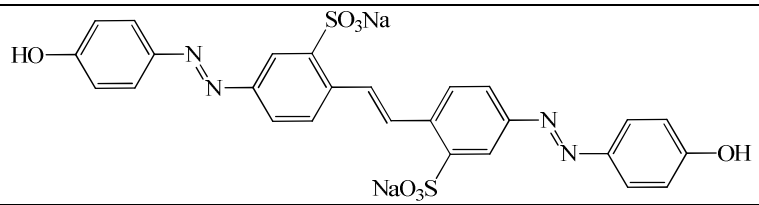
Chemical formula	$Na_2C_{26}H_{18}N_4O_8S_2$
Chemical name	Disodium 5-[2-(4-oxocyclohexa-2,5-dien-1-ylidene)hydrazinyl]-2-[(E)-2-[4-[2-(4-oxocyclohexa-2,5-dien-1-ylidene)hydrazinyl]-2-sulphonatophenyl]ethenyl]benzenesulfonate
Color index name	Direct Yellow 4
Commercial names	Brilliant Yellow, Paper Yellow CB, Fenamin Yellow, Tetrodirect Yellow B
Color index number	24890
λ_{max} (nm)	400
M (g mol^{-1})	624.55
Applied material	Cellulosa fiber, polyamide fiber, leather, paper color

Table 2.

Aromatic compounds and hydroxylated derivatives identified by LC–MS in negative mode during the SPEF treatment of 10 dm^3 of a 0.16 mmol dm^{-3} DY4 solution using an autonomous solar pre-pilot plant with a Pt/air-diffusion cell coupled to a CPCs photoreactor at average current of 5.0 A provided by a solar photovoltaic panel.

Compound	Molecular formula	Number of –OH added	*m/z*
DY4 (**1**)	Given in Table 1	-- 1 2 5 6	289[a] 297[a] 305[a] 329[a] 337[a]
2	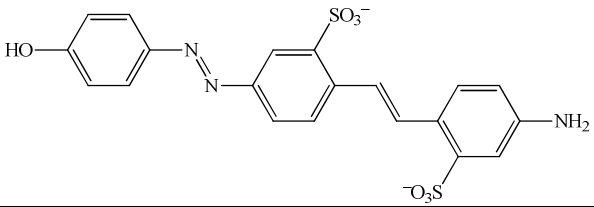	1 3 5 8 10	245[a] 261[a] 277[a] 301[a] 317[a]
3	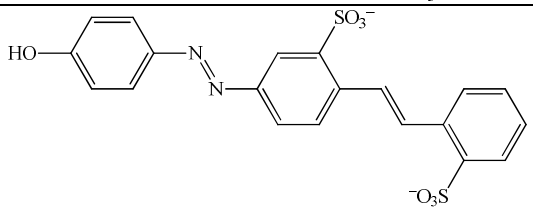	4	523[b]
4	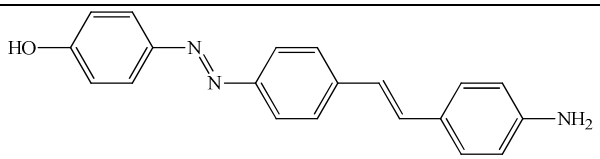	--	314[b]
5	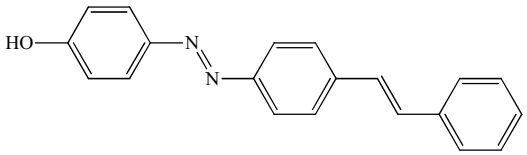	-- 1	299[b] 315[b]
6	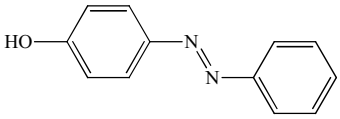	-- 1 3 4	197[b] 213[b] 245[b] 261[b]
7	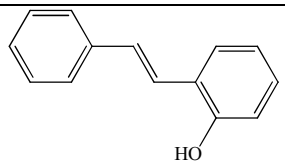	-- 1 2	195[b] 211[b] 227[b]
8	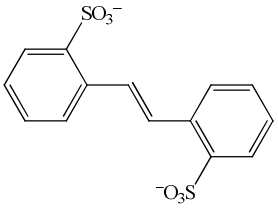	5 6 7	209[a] 217[a] 225[a]

9	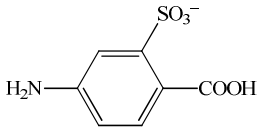	--	232[b]
10	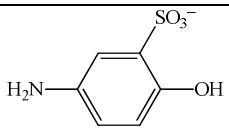	--	204[b]
11	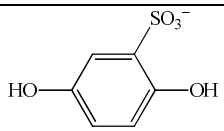	-- 1	189[b] 205[b]
12	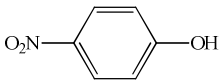	-- 2 5	139[b] 171[b] 203[b]

Negative ions with *z*: [a] 2 or [b] 1.

PAPER 8

Mineralization of phthalic acid by solar photoelectro-Fenton with a stirred boron-doped diamond/air-diffusion tank reactor: Influence of Fe^{3+} and Cu^{2+} catalysts and identification of oxidation products

Electrochimica Acta 113 (2013) 609–619

Contents lists available at ScienceDirect

Electrochimica Acta

journal homepage: www.elsevier.com/locate/electacta

Mineralization of phthalic acid by solar photoelectro-Fenton with a stirred boron-doped diamond/air-diffusion tank reactor: Influence of Fe^{3+} and Cu^{2+} catalysts and identification of oxidation products

Sergi Garcia-Segura [a], Ricardo Salazar [b,1], Enric Brillas [a,*,1]

[a] Laboratori d'Electroquímica dels Materials i del Medi Ambient, Departament de Química Física, Facultat de Química, Universitat de Barcelona, Martí i Franquès 1-11, 08028 Barcelona, Spain
[b] Departamento de Ciencias del Ambiente, Facultad de Química y Biología, Universidad de Santiago de Chile, USACh, Casilla 40, Correo 33, Santiago, Chile

ARTICLE INFO

Article history:
Received 24 July 2013
Received in revised form
14 September 2013
Accepted 16 September 2013
Available online xxx

Keywords:
Electro-Fenton
Oxidation products
Phthalic acid
Solar photoelectro-Fenton
Water treatment

ABSTRACT

Here, the substrate decay and mineralization rate for 100 cm^3 of a 2.0 mM phthalic acid solution in 0.10 M Na_2SO_4 of pH 3.0 have been studied by electro-Fenton (EF) and solar photoelectro-Fenton (SPEF). The electrochemical cell was a stirred tank reactor containing a 3 cm^2 boron-doped diamond (BDD) anode and a 3 cm^2 air-diffusion cathode that generates H_2O_2. Cu^{2+} and/or Fe^{3+} were added as catalysts with total concentration of 0.50 mM and a constant current density of 33.3 mA cm^{-2} was applied. In EF with Cu^{2+} or Fe^{3+} alone and SPEF with only Cu^{2+}, phthalic acid decayed slowly and poor mineralization was reached because the main oxidant was •OH produced at the BDD surface from water oxidation. In contrast, the substrate destruction was largely enhanced using SPEF with 0.50 mM Fe^{3+} since a high quantity of oxidant •OH was produced in the bulk induced by photo-Fenton reaction. This treatment led to an almost total mineralization by the photolysis of generated Fe(III)-carboxylate complexes. In all cases, the decay of phthalic acid obeyed a pseudo-first-order reaction. The combination of Cu^{2+} and Fe^{3+} as catalysts accelerated the mineralization process in SPEF because Cu(II)-carboxylate complexes were also removed with •OH formed from photo-Fenton reaction. The best SPEF process was found for 0.125 mM Cu^{2+} + 0.375 mM Fe^{3+}, giving rise to 99% mineralization with 40% current efficiency and 0.294 kWh g^{-1} TOC energy consumption. Eleven aromatics and six short-linear carboxylic acids were identified as oxidation products. A plausible reaction sequence for phthalic acid mineralization involving all the detected products was finally proposed.

1. Introduction

Phthalic acid and phthalate derivatives are major industrial materials used to manufacture plastic products like toys and bottles, also being widely used as plasticizers, adhesives, films, polymers, etc. However, some studies revealed that these compounds could affect the male reproductive systems producing a testicular atrophy [1] and alter the normal development of fetuses in pregnant rats [2]. In view of these adverse effects on living beings, the US Environmental Protection Agency (EPA) classified the phthalic acid and some industrial phthalates as priority pollutants [3] and so, for example, the maximum admissible content in water for a common phthalic acid derivative such as the di(2-ethylhexyl)phthalate was established in 6 μg dm^{-3}. Phthalic acid has been detected in different matrices such as landfill leachate water [4], surface water [5], sediments and even in atmospheric aerosols and rainwater [6]. Wastewaters with high concentration of phthalic acid and its derivatives are then produced, requiring effective treatments before discharge to public serve.

Several authors have reported the removal of phthalic acid and some of its esters by TiO_2 photocatalysis [7], adsorption [8], coagulation [9] and aerobic–anaerobic biodegradation [10,11]. However, less is known about the destruction of these compounds by electrochemical technologies. Only complete degradation of 531 mg dm^{-3} phthalic acid solutions was recently described by means of ultrasound assisted electrochemical oxidation on boron-doped diamond electrode after 10 h of treatment [12].

Over the last fifteen years, several electrochemical advanced oxidation processes (EAOPs) based on Fenton's reaction chemistry are being developed for water remediation [13,14]. These methods are based on the continuous supply of H_2O_2 to an acidic

* Corresponding author. Tel.: +34 934021223; fax: +34 934021231.
E-mail address: brillas@ub.edu (E. Brillas).
[1] ISE active member.

0013-4686/$ – see front matter © 2013 Elsevier Ltd. All rights reserved.
http://dx.doi.org/10.1016/j.electacta.2013.09.097

contaminated solution from the two-electron cathodic reduction of injected O_2 gas by reaction (1) [13]:

$$O_2(g) + 2H^+ + 2e^- \rightarrow H_2O_2 \quad (1)$$

Carbonaceous electrodes such as carbon nanotubes on graphite [15], carbon nanotubes-polytetrafluoroethylene (PTFE) [16,17], carbon-felt [18–22], carbon sponge [20], carbon-PTFE gas (O_2 or air) diffusion electrodes [19,23–26], graphite-felt [27] and boron-doped diamond (BDD) [28] have shown good efficiencies for H_2O_2 generation from reaction (1).

The most common EAOP is electro-Fenton (EF) in which a small catalytic amount of Fe^{2+} ion is added to the solution to react with generated H_2O_2 producing Fe^{3+} ion and hydroxyl radical (•OH) according to the classical Fenton's reaction (2) [13]:

$$Fe^{2+} + H_2O_2 \rightarrow Fe^{3+} + {}^{\bullet}OH + OH^- \quad (2)$$

•OH thus formed in the bulk is the second strongest oxidant known after fluorine. The high standard reduction potential of this radical (E°(•OH/H_2O) = 2.80 V/SHE) allows its reaction with most organics up to their mineralization to CO_2, water and inorganic ions. Reaction (2) can be propagated from the catalytic behavior of the Fe^{2+}/Fe^{3+} system, primordially involving Fe^{2+} regeneration from the reduction of Fe^{3+} at the cathode via reaction (3) [13,19,20]:

$$Fe^{3+} + e^- \rightarrow Fe^{2+} \quad (3)$$

The optimum solution pH for EF is 3.0, close to the optimum value of 2.8 for Fenton's reaction (1) [13], and its oxidation ability for organic removal in waters is closely related to the rate of reaction (3), which depends on the iron concentration and the kind of cathode used. For example, optimum concentrations of 0.1–0.2 mM Fe^{2+} or Fe^{3+} have been found using a carbon-felt cathode [18–20], whereas either 0.5–1.0 mM Fe^{2+} or a much higher content of 4.0 mM Fe^{3+} are optimal for O_2 or air-diffusion electrodes [19,24,25] due to their greater efficiency for H_2O_2 generation by reaction (1) and smaller rate for reaction (3).

The use of an undivided cell with a high O_2-overpotential anode such as BDD in EF accelerates the degradation of organics since they can also be slowly attacked by adsorbed hydroxyl radical (BDD(•OH)) formed as intermediate of the anodic water discharge [29,30]:

$$BDD + H_2O \rightarrow BDD({}^{\bullet}OH) + H^+ + e^- \quad (4)$$

The BDD anode is better than other typical electrodes like Pt and PbO_2 because it generates BDD(•OH) radicals with greater oxidation ability due to its higher O_2-overpotential [31–33], improving the destruction of aromatics and their generated carboxylic acids [13,34–36]. Moreover, the electrogenerated H_2O_2 is partly oxidized to O_2 at the anode producing the weaker oxidant hydroperoxyl radical ($HO_2^{\bullet}$) as intermediate [13].

An alternative EAOP is photoelectro-Fenton (PEF) which includes the simultaneous irradiation of the treated solution by EF either with a UV lamp or with inexpensive and renewable sunlight ($\lambda > 300$ nm), so-called solar PEF (SPEF). The catalytic action of UV light from both sources can be explained by two main processes [23–26,37–42]: (i) the photoreduction of $Fe(OH)^{2+}$, the predominant Fe^{3+} species at pH near 3, by photo-Fenton reaction (5) with Fe^{2+} regeneration and production of more •OH and (ii) the quick photolysis of Fe(III) complexes with generated carboxylic acids according to reaction (6):

$$Fe(OH)^{2+} + h\nu \rightarrow Fe^{2+} + {}^{\bullet}OH \quad (5)$$

$$Fe(OOCR)^{2+} + h\nu \rightarrow Fe^{2+} + CO_2 + R^{\bullet} \quad (6)$$

It has been found that SPEF is more potent than PEF with an artificial UVA lamp because the greater intensity of UVA and UVB of sunlight photodecomposes more rapidly the generated Fe(III)-carboxylate complexes by reaction (6). However, the role of photo-Fenton reaction (5) in the degradation process is less apparent due to the introduction of Fe^{2+} as catalyst that allows a large production of •OH in the bulk from Fenton's reaction (2).

In previous work, we have checked the synergistic action of adding small amounts of Cu^{2+} ion as co-catalyst of Fe^{2+} ion in the EF, PEF and SPEF processes of several aromatics [23,37,40]. This was attributed to: (i) the contribution of the Cu^{2+}/Cu^+ couple to •OH production and/or (ii) the formation of Cu(II)-carboxylate species that are more easily oxidized than the corresponding Fe(III) complexes. In the SPEF treatment of the dye Disperse Blue 3 by SPEF with Fe^{2+} and Cu^{2+} as catalysts [40], phthalic acid and some phthalate esters were detected as intermediates of the mineralization process, suggesting that this EAOP could be useful for the removal of these pollutants.

This paper presents a comparative study on the mineralization of a phthalic acid solution of pH 3.0 by EF and SPEF with Fe^{3+} and/or Cu^{2+} as catalysts using a stirred BDD/air-diffusion tank reactor. Small amounts of Fe^{3+} were directly added for obtaining a very slow production of •OH from Fenton's reaction (2) in EF, because of the slow Fe^{2+} regeneration at the air-diffusion cathode [19]. In this EAOP, BDD(•OH) formed from reaction (4) is expected to be the main oxidizing agent since the rate of organic pollutants with •OH is low. In this way and for the first time, the oxidant •OH formed in the SPEF process is primordially induced by photo-Fenton reaction (5) under the action of sunlight. The generation of increasing oxidizing agents in these EAOPs allowed a better interpretation of the role of Cu^{2+} alone or combined with Fe^{3+} over their performance. Our interest in Cu^{2+} is the possible future use of SPEF at industrial scale, which is economically interesting for Chile as the leading producer of copper in the world [43]. The decay kinetics for the substrate and its mineralization rate and degree were then examined as a function of catalyst content. Aromatic intermediates were detected by liquid chromatography–mass spectrometry (LC–MS) and generated short-linear carboxylic acids were quantified by HPLC. From these results, a plausible reaction pathway for phthalic acid mineralization is proposed.

2. Experimental

2.1. Chemicals

Analytical grade phthalic acid was purchased from Lancaster. Pyruvic, maleic, tartronic, succinic, acrylic and oxalic acids were of analytical grade supplied by Panreac and Avocado. Anhydrous sodium sulphate, used as background electrolyte, was of analytical grade purchased from Fluka. Hydrated Fe(III) sulfate and pentahydrated Cu(II) sulfate, used as catalysts, were of analytical grade supplied by Probus and Panreac, respectively. Organic solvents and other chemicals employed were of LC–MS, HPLC or analytical grade purchased from Teknokroma, Merck and Sigma–Aldrich. All solutions were prepared with ultrapure water obtained from a Millipore Milli-Q system with resistivity >18 MΩ cm at 25 °C. The solution pH was adjusted to 3.0 with analytical grade sulfuric acid purchased from Merck.

2.2. Electrolytic system

All the electrolytic trials were conducted in an open, undivided and cylindrical cell of 150 cm^3 capacity, with a double jacket in which external water was circulated to maintain the solution temperature at 35 °C. This temperature was chosen because it is the maximum value that can be used in the cell without significant water evaporation from the solution [44]. The anode was a

BDD thin-film electrode purchased from Adamant Technologies and synthesized by the hot filament chemical vapor deposition technique on single-crystal *p*-type Si(100) wafers. The cathode was a carbon-PTFE air-diffusion electrode supplied by E-TEK, mounted as described elsewhere [23] and fed with air pumped at 300 cm^3 min^{-1} to generate H_2O_2 from reaction (1). The area of both electrodes was 3 cm^2 and the interelectrode gap was about 1 cm. All the experiments were performed at constant current density provided by an Amel 2051 potentiostat-galvanostat. The solutions were always vigorously stirred with a magnetic bar at 800 rpm to ensure mixing and the transport of reactants toward/from the electrodes. To remove the impurity of the BDD surface and activate the air-diffusion cathode, they were previously polarized in 100 cm^3 of a 0.05 M Na_2SO_4 solution at 100 mA cm^{-2} for 60 min.

Comparative EF (in the dark) and SPEF degradations of 100 cm^3 of 2.0 mM phthalic acid solutions (corresponding to 192 mg dm^{-3} of total organic carbon (TOC)) in 0.10 M Na_2SO_4 at pH 3.0 were made at 33.3 mA cm^{-2} and 35 °C with a total Cu^{2+} + Fe^{3+} concentration of 0.50 mM. Similar electrolysis under anodic oxidation with electrogenerated H_2O_2 (AO-H_2O_2) without catalyst addition was also made. In SPEF, the solution was irradiated with direct sunlight in sunny and clear summer days in our laboratory of Barcelona, Spain (latitude: 41°21′ N, longitude: 2°10′ E). The average solar UV radiation intensity (between 300 and 400 nm) was about 31 W m^{-2}, as measured with a Kipp & Zonen CUV 5 global UV radiometer.

2.3. Apparatus and analytical procedures

The solution pH was measured with a Crison GLP 22 pH-meter. Samples withdrawn from electrolyzed solutions were neutralized at pH 7–8 to stop the degradation process and filtered with 0.45 μm PTFE filters from Whatman before analysis.

The phthalic acid decay and the evolution of generated short-linear carboxylic acids were followed by ion-exclusion HPLC using a Waters 600 LC fitted with a Bio-Rad Aminex HPX 87H, 300 mm × 7.8 mm, column at 35 °C and coupled to a Waters 996 photodiode array detector selected at λ = 210 nm. For these analyses, 20 μL aliquots were injected into the LC and 4 mM H_2SO_4 at 0.6 cm^3 min^{-1} circulated as mobile phase. The retention time was 7.0 min for oxalic acid, 7.9 min for tartronic acid, 8.2 min for maleic acid, 9.2 min for pyruvic acid, 11.7 min for succinic acid, 18.4 min for acrylic acid and 28.3 min for phthalic acid.

The mineralization of phthalic acid solutions was monitored from their TOC abatement, determined on a Shimadzu TOC-VCSN analyzer. Reproducible TOC values with an accuracy of ±1% were obtained by injecting 50 μL aliquots into the analyzer. Taking into account that the mineralization process for phthalic acid involves its conversion into CO_2 by reaction (7):

$$C_8H_6O_4 + 12H_2O \rightarrow 8CO_2 + 30H^+ + 30e^- \quad (7)$$

the mineralization current efficiency (MCE) for each trial at electrolysis time t (in h) was then estimated by Eq. (8) [25]:

$$MCE(\%) = \frac{n F V_s \Delta(TOC)_{exp}}{4.32 \times 10^7 m I t} \times 100 \quad (8)$$

where n is the number of electrons consumed per each phthalic acid molecule (30, from reaction (7)), F is the Faraday constant (96,487 C mol^{-1}), V_s is the solution volume (0.1 dm^3), $\Delta(TOC)_{exp}$ is the experimental TOC decay (in mg dm^{-3}), 4.32×10^7 is a conversion factor to homogenize units (3600 s h^{-1} × 12,000 mg mol^{-1}), m is the number of carbon atoms of phthalic acid (8 carbon atoms) and I is the applied current (0.1 A). The corresponding energy consumption per unit TOC mass removed (EC_{TOC}) was calculated as follows [38,39]:

$$EC_{TOC}(kWh\ g^{-1}TOC) = \frac{E_{cell} I t}{V_s \Delta(TOC)_{exp}} \quad (9)$$

where E_{cell} is the average potential difference of the BDD/air-diffusion cell (13.9 V).

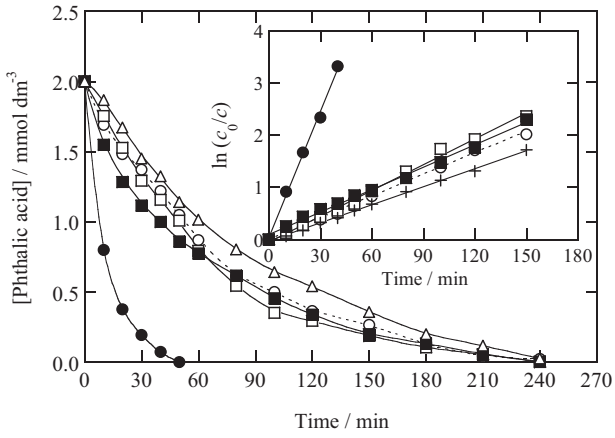

Fig. 1. Decay of phthalic acid concentration with electrolysis time for the treatment of 100 cm^3 of 2.0 mM substrate solutions in 0.10 M Na_2SO_4 at pH 3.0 and 35 °C using a stirred BDD/air-diffusion tank reactor of 3 cm^2 electrode area at 33.3 mA cm^{-2}. (△) Anodic oxidation with electrogenerated H_2O_2 (AO-H_2O_2), (○) electro-Fenton (EF) with 0.50 mM Fe^{3+}, (□) EF with 0.50 mM Cu^{2+}, (●) solar photoelectro-Fenton (SPEF) with 0.50 mM Fe^{3+} and (■) SPEF with 0.50 mM Cu^{2+}. The inset panel presents the corresponding kinetic analysis assuming that phthalic acid follows a pseudo-first-order reaction.

Aromatic derivatives produced after 10–20 min of the SPEF treatment of a 2.0 mM phthalic acid solution with 0.125 mM Cu^{2+} + 0.375 mM Fe^{3+} in a stirred BDD/air-diffusion tank reactor at 33.3 mA cm^{-2} were analyzed by LC–MS using a Shimadzu SIL-20AC LC coupled to a Shimadzu LCMS-2020 MS. The LC was fitted with a Teknokroma Mediterranea Sea C-18 3 μm, 15 mm × 0.46 mm, column at 30 °C. The MS operated in the negative and positive modes with electrospray source ionization (ESI), using an interface voltage of −4.5 and 4.5 kV, respectively, and 60 V Q-array RF voltage. The DL temperature was 250 °C and pure N_2 was used as nebulysing and dryer gas. Mass spectra were collected in the m/z range 50–420 using total ion current (TIC) acquisition and finally, they were also recorded under selected-ion monitoring (SIM) acquisition. For these analyses, 15 μL aliquots were introduced into the LC, previously filtered with a Millipore filter of 0.22 μm, and the mobile phase was a 75:25 (v/v) acetonitrile/water (5.0 mM ammonium acetate) mixture at 0.2 cm^3 min^{-1}.

3. Results and discussion

3.1. Degradation of phthalic acid by electro-Fenton and solar photoelectro-Fenton with Fe^{3+} or Cu^{2+}

Solutions with 2.0 mM phthalic acid and 0.10 mM Na_2SO_4 in the presence of either 0.50 mM Cu^{2+} or 0.50 mM Fe^{3+} were degraded by EF and SPEF at pH 3.0 and current density of 33.3 mA cm^{-2} for 240 min. It is well-known that this compound forms complexes with both Cu^{2+} [45] and Fe^{3+} [46] ions and consequently, phthalic acid along with its Cu(II) or Fe(III) complexes was oxidized in these assays. Previous blank experiments confirmed that all these species are not photolyzed under the experimental conditions tested since direct exposition of the above solutions to solar radiation did not caused any removal of the substrate.

Fig. 1 depicts the decay of phthalic acid concentration for the above trials. The solution pH remained practically unchanged

Table 1
Pseudo-first-order rate constant and square of the linear regression coefficient obtained for the phthalic acid decay in the AO-H_2O_2, EF and SPEF treatments of 100 mL of 2.0 mM compound solutions of pH 3.0 and 35 °C using a BDD/air-diffusion cell at 33.3 mA cm^{-2}.

Method	$[Cu^{2+}]$ (mM)	$[Fe^{3+}]$ (mM)	k_1 (10^{-4} s^{-1})	R^2
AO-H_2O_2	–	–	1.9	0.998
EF	0.50	–	2.7	0.993
	0.375	0.125	2.1	0.994
	0.25	0.25	1.9	0.995
	0.125	0.375	3.0	0.996
	–	0.50	2.3	0.995
SPEF	0.50	–	2.4	0.993
	0.375	0.125	3.5	0.991
	0.25	0.25	3.6	0.992
	0.125	0.375	5.9	0.986
	–	0.50	13.4	0.996

during all the electrolyses, attaining a final pH near 2.7–2.8, probably due to the formation of acidic compounds. A quite similar decay rate can be observed not only for EF and SPEF with 0.50 mM Cu^{2+} but also for EF with 0.50 mM Fe^{3+}. In all cases, phthalic acid disappeared in 240 min. Fig. 1 also shows an analogous removal rate for the comparative treatment of a 2.0 mM phthalic solution by AO-H_2O_2 without metal ions, where BDD(•OH) formed from reaction (4) is the main oxidizing agent [13]. When Cu^{2+} is added to the medium, Cu^{+} can be formed from Cu^{2+} reduction with HO_2• at the BDD surface by reaction (10) and subsequently oxidized with generated H_2O_2 to Cu^{2+} and •OH by the Fenton-like reaction (11) [37,38,47]:

$$Cu^{2+} + HO_2^{\bullet} \rightarrow Cu^{+} + H^{+} + O_2 \quad (10)$$

$$Cu^{+} + H_2O_2 \rightarrow Cu^{2+} + {}^{\bullet}OH + OH^{-} \quad (11)$$

However, our results evidence a very poor contribution of the Cu^{2+}/Cu^{+} couple to produce •OH from reactions (10)–(11) in both EF and SPEF processes with Cu^{2+}. Similarly, the Fe^{3+}/Fe^{2+} pair also yielded a little generation of •OH in EF due to the low rate of Fenton's reaction (2) as a result of the poor Fe^{3+} reduction at the air-diffusion cathode from reaction (3) [19]. In all these processes, phthalic acid and its Cu(II) or Fe(III) complexes then react primordially with BDD(•OH).

The above concentration decays were analyzed by kinetic equations related to simple reaction orders, and good linear correlations were found by using a pseudo-first-order reaction, as presented in the inset panel of Fig. 1. The apparent constant rate (k_1) and the corresponding square of the linear regression coefficient (R^2) thus obtained are summarized in Table 1. As can be seen, analogous k_1 values between 2.3×10^{-4} and 2.7×10^{-4} s^{-1} were found for EF and SPEF with Cu^{2+} and EF with Fe^{3+}, slightly higher than 1.9×10^{-4} s^{-1} obtained for AO-H_2O_2. This behavior suggests the oxidation of the electroactive species with a constant amount of hydroxyl radical, mainly BDD(•OH), in all these processes.

A different behavior can be observed in Fig. 1 when SPEF with 0.50 mM Fe^{3+} was applied. The abatement of phthalic acid was strongly enhanced respect to the other processes, completely being removed in about 50 min. This decay kinetic was also well fitted to a pseudo-first-order reaction (see the inset panel of Fig. 1) giving rise to a higher k_1 value of 1.34×10^{-3} s^{-1} (see Table 1). This enhancement can be related to the additional production of great amounts of •OH under the action of photo-Fenton reaction (5) that yield Fe^{2+} concentrations high enough to largely propagate Fenton's reaction (2). This allows concluding that in the presence of small quantities of Fe^{3+} as catalyst, the SPEF process is able to generate the oxidant •OH in the bulk primordially induced by photo-Fenton reaction (5).

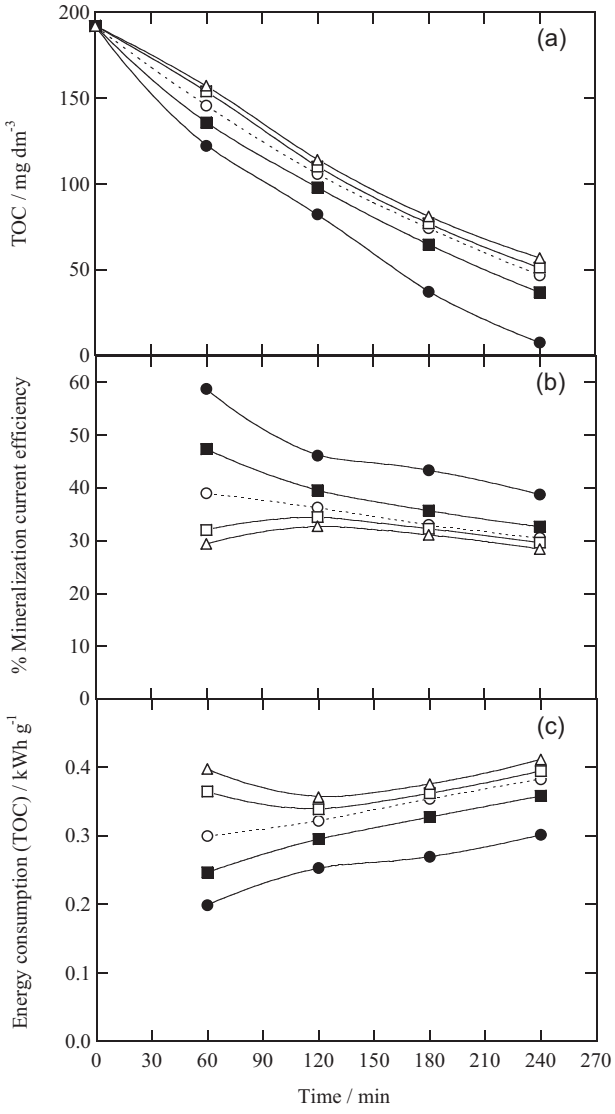

Fig. 2. (a) TOC removal and change of (b) mineralization current efficiency and (c) energy consumption per unit TOC mass for the degradation of 2.0 mM phthalic acid solutions (corresponding to 192 mg dm^{-3} TOC) under the conditions of Fig. 1. (△) AO-H_2O_2, (○) EF with 0.50 mM Fe^{3+}, (□) EF with 0.50 mM Cu^{2+}, (●) SPEF with 0.50 mM Fe^{3+} and (■) SPEF with 0.50 mM Cu^{2+}.

The positive action of sunlight using 0.50 mM Fe^{3+} was also corroborated from the TOC abatement of electrolyzed solutions. As can be seen in Fig. 2a, the EF treatments led to a continuous, but slow reduction of TOC at similar rate for both metal ions up to reach 73–75% mineralization after 240 min of electrolysis, a time in which all phthalic acid already disappeared (see Fig. 1). A similar TOC reduction of 71% was obtained for AO-H_2O_2. These findings are indicative of the formation of oxidation products like short-linear carboxylic acids that react more hardly with hydroxyl radicals than the substrate, prolonging its degradation process. A slightly quicker TOC removal up to a final value of 81% was found for SPEF with 0.50 mM Cu^{2+}, which can be associated with the parallel photolysis of some intermediates that enhances the mineralization rate of phthalic acid. In contrast, the SPEF process with 0.50 mM Fe^{3+} allowed a much more rapid TOC decay yielding an almost total mineralization (96% TOC removal) at 240 min, as expected if some Fe(III)-carboxylate complexes are quickly photodecomposed by solar radiation [13].

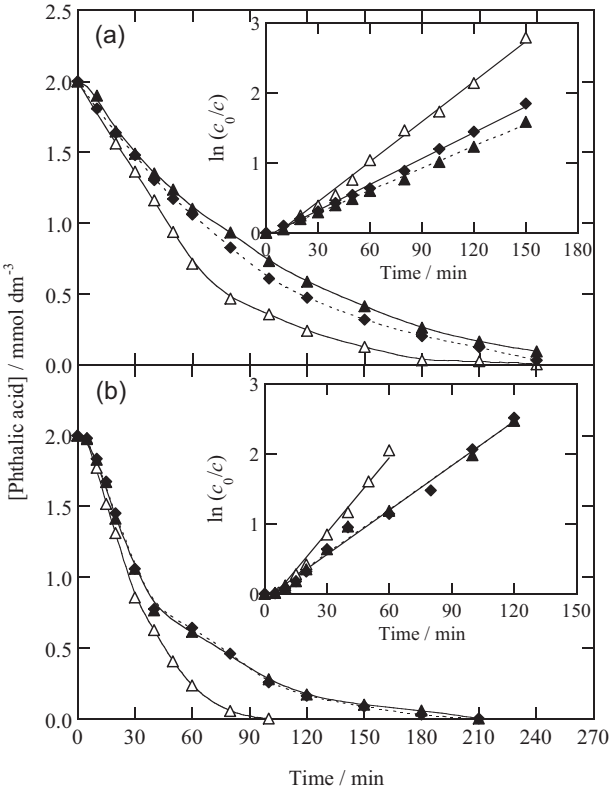

Fig. 3. Removal of phthalic acid concentration with electrolysis time determined during the degradation of 100 cm^3 of 2.0 mM substrate solutions in 0.10 M Na_2SO_4 at pH 3.0 and 35 °C by (a) EF and (b) SPEF using a stirred BDD/air-diffusion tank reactor at 33.3 mA cm^{-2}. Catalyst concentration: (♦) 0.375 mM Cu^{2+} + 0.125 mM Fe^{3+}, (▲) 0.25 mM Cu^{2+} + 0.25 mM Fe^{3+} and (△) 0.125 mM Cu^{2+} + 0.375 mM Fe^{3+}. The kinetic analysis considering a pseudo-first-order reaction for phthalic acid is shown in the inset panel.

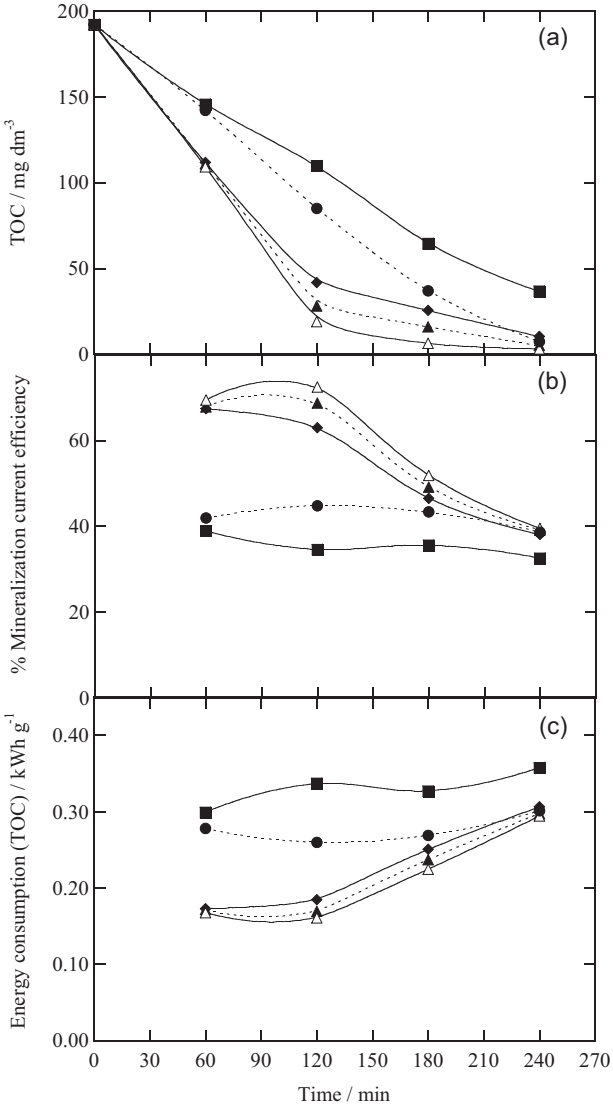

Fig. 4. (a) TOC decay and variation of (b) mineralization current efficiency and (c) energy consumption per unit TOC mass for the SPEF treatment of 100 cm^3 of 2.0 mM phthalic acid solutions at pH 3.0 and 35 °C by applying 33.3 mA cm^{-2}. Catalyst concentration: (■) 0.50 mM Cu^{2+}, (♦) 0.375 mM Cu^{2+} + 0.125 mM Fe^{3+}, (▲) 0.25 mM Cu^{2+} + 0.25 mM Fe^{3+}, (△) 0.125 mM Cu^{2+} + 0.375 mM Fe^{3+} and (●) 0.50 mM Fe^{3+}.

Note that Fig. 2a also shows a quite zero-order rate of the EF and SPEF processes respect to TOC concentration decay. This suggests a low contribution of BDD(•OH) on the whole oxidation processes, since its generation from reaction (4) is mass-transfer limited and the rate of this reaction should give a first-order rate respect to TOC removal, not experimentally observed. It can then be assumed that the low rate of •OH formation in the bulk from Fenton's reaction (2) is the step that controls the whole process, being slower than the rate of its successive reactions with organic compounds. The fact that •OH generation limits the whole oxidation rate thus explains the zero-order rate respect to TOC. The rise in the production of this radical in SPEF with 0.5 mM Fe^{3+} under the action of photo-Fenton reaction (5) causes a higher whole reaction rate, as shown in Fig. 2a, giving more rapidly products like short-chain carboxylic acids that form Fe(III) complexes which are more quickly photolyzed enhancing the mineralization degree.

The different changes in TOC in the tested EF and SPEF processes were reflected in the corresponding MCE and EC_{TOC} values, determined by Eqs. (8) and (9) and presented in Fig. 2b and c, respectively. As expected, the higher MCE of 59% was obtained at the beginning of SPEF with 0.50 mM Fe^{3+}, further dropping to 39% at 240 min. A decrease in efficiency with prolonging electrolysis time was also found for most treatments and can be accounted for by the gradual fall in organic matter with formation of hardly oxidizable products [30,36]. Similarly, the lower EC_{TOC} values were obtained for this SPEF process, although they rose from 0.198 kWh g^{-1} TOC at 60 min to 0.301 kWh g^{-1} TOC at 240 min owe to the concomitant loss in efficiency. The final energy consumption for all treatments was 55.6 kWh m^{-3}.

3.2. Combination of Fe^{3+} and Cu^{2+} to catalyze the electro-Fenton and solar photoelectro-Fenton processes of phthalic acid

To study the synergistic effect of both metal ions as catalysts on the degradation of phthalic acid by EF and SPEF, three solutions with 2.0 mM substrate in 0.10 M Na_2SO_4 containing 0.375 mM Cu^{2+} + 0.125 mM Fe^{3+}, 0.25 mM Cu^{2+} + 0.25 mM Fe^{3+} or 0.125 mM Cu^{2+} + 0.375 mM Fe^{3+} were prepared at pH 3.0 and electrolyzed in the stirred BDD/air-diffusion tank reactor at 33.3 mA cm^{-2} and 35 °C. Fig. 3a evidences that operating in the dark (EF conditions) with all the combined catalysts, phthalic acid always disappeared in 240 min following a pseudo-first-order kinetics. Nevertheless, the solution with 0.125 mM Cu^{2+} + 0.375 mM Fe^{3+} showed the fastest substrate abatement with $k_1 = 3.0 \times 10^{-4}$ s^{-1}, even slightly greater than using Cu^{2+} or Fe^{3+} alone (see Table 1). This phenomenon can be related to the interaction of both Cu^{2+}/Cu^{+} and Fe^{3+}/Fe^{2+} pairs, since Cu^{+} produced from reaction (10) can alternatively regenerate Fe^{2+} by reaction (12) [13] and propagate Fenton's reaction (2)

Table 2
Aromatic compounds detected by LC–MS during the SPEF degradation of 100 cm^3 of 2.0 mM phthalic acid with 0.125 mM Cu^{2+} + 0.375 mM Fe^{3+} at pH 3.0, 33.3 mA cm^{-2} and 35 °C using a BDD/air-diffusion tank reactor.

Compound	Name	Molecular formula	*m/z* [a]
1	Phthalic acid	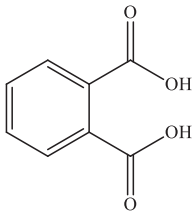	165
2	3-Hydroxyphthalic acid	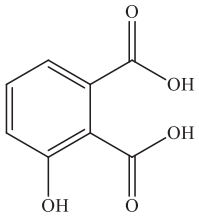	181
3	4-Hydroxyphthalic acid	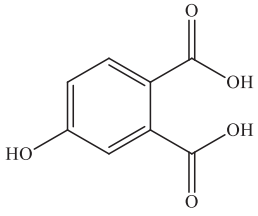	181
4	3,4-Dihydroxyphthalic acid	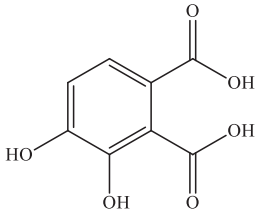	197
5	3,5-Dihydroxyphthalic acid	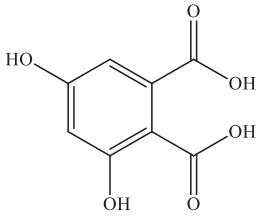	197
6	4,5-Dihydroxyphthalic acid	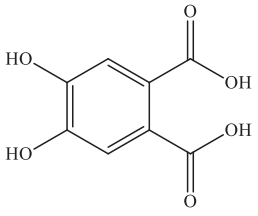	197
7	Tetrahydroxyphthalic acid	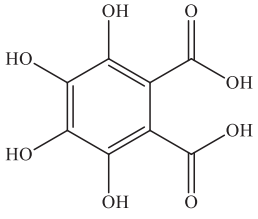	229

Table 2 (*Continued*)

Compound	Name	Molecular formula	*m/z* [a]
8	Benzoic acid	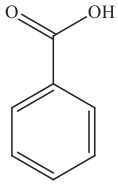	121
9	2-Hydroxybenzoic acid	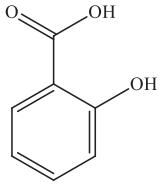	137
10	3-Hydroxybenzoic acid	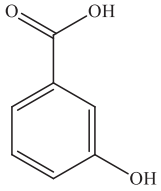	137
11	4-Hydroxybenzoic acid	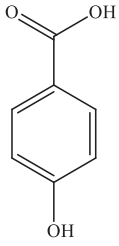	137
12	Dihydroxybenzoic acid	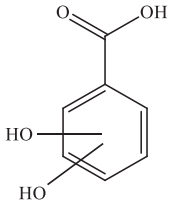	153

[a] Negative ion with $z = 1$.

in some extent generating more •OH to favor the destruction of phthalic acid.

$$Cu^{+} + Fe^{3+} \rightarrow Cu^{2+} + Fe^{2+} \quad (12)$$

Fig. 3b illustrates that the comparative SPEF processes accelerated the substrate abatement. Thus, until 0.25 mM Fe^{3+} phthalic acid disappeared in 210 min, whereas for 0.125 mM Cu^{2+} + 0.375 mM Fe^{3+} it was completely removed in 105 min. In all cases, excellent linear correlations of the concentration decays related to a pseudo-first-order reaction were found (see the inset panel in Fig. 3b). The data of Table 1 confirm that k_1 increased with increasing Fe^{3+} concentration from 0.25 mM and hence, the substrate removal was faster by using 0.50 mM Fe^{3+} alone. This behavior suggests the pre-eminent role of photo-Fenton reaction (5) to generate •OH in the bulk under the conditions tested in SPEF, which becomes more significant as Fe^{3+} concentration increases causing a faster removal of phthalic acid. Fig. 3b also shows the existence of an induction step at the beginning of all concentration decays, up to 5 min of electrolysis. This phenomenon is difficult to explain and it could be related to the slow destruction of more stable complexes of phthalic acid with both Fe^{3+} and Cu^{2+} ions. When these mixed complexes are removed, the phthalic acid abatement is rapid and obeys a pseudo-first-order kinetics.

No notable change in TOC decay was obtained for EF when treating the 2.0 mM phthalic acid solutions with combined or alone metal ions, giving about 75% mineralization after 240 min of all the electrolyses at 33.3 mA cm^{-2}. For the comparative SPEF assays, Fig. 4a evidences that all the Cu^{2+}–Fe^{3+} combinations enhance the mineralization rate compared to single metal ions. At 180 min of electrolysis, for example, TOC was reduced by 87% for 0.375 mM Cu^{2+} + 0.125 mM Fe^{3+}, 92% for 0.25 mM Cu^{2+} + 0.25 mM Fe^{3+} and up to 97% for 0.125 mM Cu^{2+} + 0.375 mM Fe^{3+}, whereas it attained 81% and only 66% decay for 0.50 mM Fe^{3+} and 0.50 mM Cu^{2+}, respectively. Besides, Fig. 4a shows that the increase in the whole oxidation rate using both ions did not followed a quite zero-order rate respect to TOC decay, as can be observed when the separated ions are utilized. This is indicative of an increase in the rate of •OH generation via photo-Fenton reaction (5) and also of the control of the whole process by the oxidation rate of several organic compounds, thus explaining that the whole reaction depends on TOC concentration. The higher mineralization obtained by rising the Fe^{3+} content from 0.125 to 0.375 mM cannot be attributed to the quicker photolysis by reaction (6) of the greater quantities of Fe(III)-carboxylate complexes that are gradually formed, since less TOC was removed only using 0.50 mM Fe^{3+}. This allows inferring that smaller Cu^{2+} contents with increasing Fe^{3+} concentrations

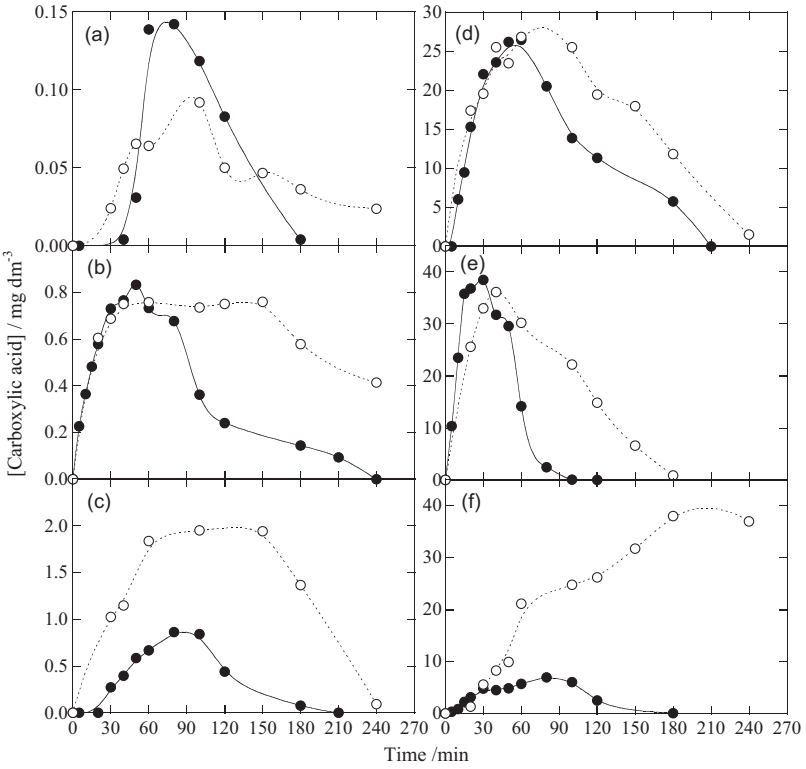

Fig. 5. Time course of the concentration of carboxylic acids detected during the (○) EF and (●) SPEF degradation of 100 cm^3 of a 2.0 mM phthalic acid solution in 0.10 M Na_2SO_4 and 0.125 mM Cu^{2+} + 0.375 mM Fe^{3+} at pH 3.0, 33.3 mA cm^{-2} and 35 °C in a stirred BDD/air-diffusion tank reactor. (a) Pyruvic (**13**), (b) maleic (**14**), (c) tartronic (**15**), (d) succinic (**16**), (e) acrylic (**17**) and (f) oxalic (**18**) acids.

improve the mineralization of phthalic acid, since competitively formed Cu(II) complexes are more rapidly destroyed with •OH in the bulk, involving, for example, the oxidation of Cu(II)-carboxylate species, as will be discussed below. These reactions could control the whole oxidation process.

The synergistic oxidation effect for all combinations of Fe^{3+} and Cu^{2+} in SPEF can then be explained by (i) the production of oxidizing •OH induced from photo-Fenton reaction (5) and (ii) the oxidation of the competitively formed Cu(II) species with this radical. The best conditions tested for phthalic acid degradation, that is, when producing the higher •OH concentration to yield the quicker removal of Cu(II) complexes formed, are found using 0.125 mM Cu^{2+} + 0.375 mM Fe^{3+}, with an almost total mineralization of 97% at 180 min and 99% at 240 min (see Fig. 4a). This treatment yielded the higher efficiencies and the lower energy consumptions per unit TOC mass of all processes tested, as illustrated in Fig. 4b and c, respectively. A maximum MCE of 72% can be observed at 120 min, which decayed to 40% at the end of the trial. The minimum EC_{TOC} of 0.160 kWh g^{-1} TOC was also found at 120 min, further increasing up to 0.294 kWh g^{-1} TOC toward the end of the electrolysis.

3.3. Identification of aromatic intermediates and time course of generated carboxylic acids

Table 2 collects the eleven aromatic intermediates detected during the SPEF treatment with 0.125 mM Cu^{2+} + 0.375 mM Fe^{3+} by LC–MS. Apart from the starting phthalic acid (**1**), two monohydroxylated (**2** and **3**) and three dihydroxylated (**4**–**6**) derivatives along with its tetrahydroxylated compound (**7**) were identified. Besides, benzoic acid (**8**) and three monohydroxylated (**9**–**11**) and one dihydroxylated (**12**) derivatives were detected as decarboxylated products, as well.

On the other hand, ion-exclusion chromatograms of electrolyzed solutions exhibited the generation of six short-linear carboxylic acids such as pyruvic (**13**), maleic (**14**), tartronic (**15**), succinic (**16**), acrylic (**17**) and oxalic (**18**). The acids **13**–**17** are expected to be formed from the oxidative cleavage of the benzenic ring of aromatic intermediates [13,23,24,37]. The oxidation of all these products yields **18**, which is the ultimate carboxylic acid since it is directly transformed into CO_2 [36].

Fig. 5a–f shows the evolution of the concentrations of acids **13**–**18**, respectively, during the most efficient SPEF process of the 2.0 mM phthalic acid solution using 0.125 mM Cu^{2+} + 0.375 mM Fe^{3+}, together the comparable results obtained by EF. As expected, all the acids were completely and rapidly removed after 240 min of SPEF, whereas they were more difficultly destroyed under EF treatment. Acids **13**–**15** were accumulated in low quantities (see Fig. 5a–c), not exceeding the 2 mg dm^{-3} during both treatments, although their disappearance in SPEF was only slightly more rapid than in EF. This suggests that the Cu(II) and Fe(III) complexes of these acids are mainly destroyed by BDD(•OH) in both cases and that in SPEF, they are additionally oxidized by •OH induced from photo-Fenton reaction (5), mainly the corresponding Cu(II) complexes, as stated above. However, the photolysis of their Fe(III) complexes by UV light of solar radiation via reaction (6) seems much less relevant. Fig. 5d and e shows a much more large accumulation of acids **16** and **17** in the solution, respectively. The acid **16** attained about 26 mg dm^{-3} at 50 min and the acid **17** reached near 37 mg dm^{-3} at 30–40 min, further being completely removed in both processes, more quickly in SPEF. This behavior is similar to that observed for acids **13**–**15**, suggesting again the destruction of the Cu(II) and Fe(III) complexes of **16** and **17** mainly by BDD(•OH) in EF and SPEF and the pre-eminent additional oxidation of their Cu(II) species by •OH induced from photo-Fenton reaction (5) in SPEF. In contrast, very different trends were found for **18** in both processes

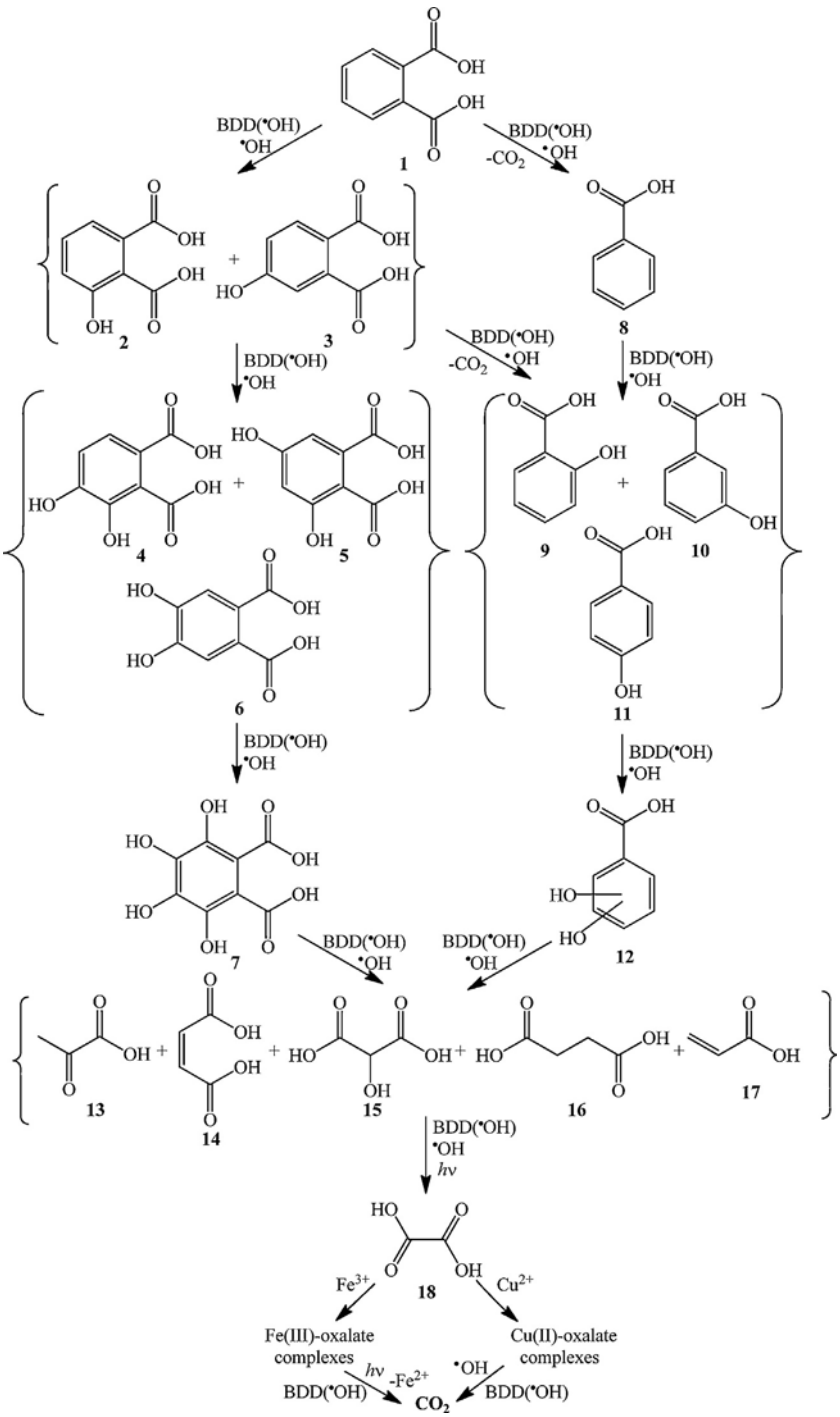

Fig. 6. Proposed reaction pathway for phthalic acid mineralization by EF and SPEF processes with Fe^{3+} and/or Cu^{2+} catalysts.

(see Fig. 5f). This acid was gradually accumulated up to a quasi-steady content of 38 mg dm^{-3} in EF indicating that Cu(II)-oxalate and Fe(III)-oxalate complexes are hardly destroyed by BDD(•OH). In SPEF, however, it was so rapidly removed that it disappeared in 180 min after reaching near 7 mg dm^{-3} as maximal. This can be related to the quick photolysis of generated Fe(III)-oxalate species by reaction (6) [36].

A simple mass balance, for example, at 180 min of electrolysis reveals that all the detected acids contribute in 16 mg dm^{-3} TOC in EF and 2.4 mg dm^{-3} TOC in SPEF, which are smaller than 75 and 6.2 mg dm^{-3} TOC determined for the electrolyzed solutions. This evidences that large amounts of other undetected products are largely accumulated in EF that are quickly mineralized by oxidation with •OH and/or photolysis by sunlight in SPEF. The fast removal of such compounds, along with the higher destruction rate of detected short-linear carboxylic acids, explain the superiority of SPEF to mineralize phthalic acid.

It is noteworthy that the Fe(III) and Cu(II) complexes of the final carboxylic acids are destroyed mainly with BDD(•OH) and also with •OH in EF. Since the former radical can only act at the BDD anode surface, its production from reaction (4) is limited by mass transfer and the destruction of such complexes should obey a first-order rate, which cannot justify the quite zero-order rate obtained for its whole reaction respect to TOC concentration decay. The quite

zero-order behavior in EF can then be explained if the whole process rate is controlled by the slow •OH generation from Fenton's reaction (2), as stated above. In contrast, the enhancement of the whole oxidation process in SPEF by the acceleration of the reaction of Cu(II)-carboxylate complexes with the greater •OH production via photo-Fenton reaction (5) can account for by the dependence of the whole rate on TOC concentration shown in Fig. 4a.

3.4. Proposed reaction pathway for phthalic acid mineralization

Fig. 6 presents a reaction sequence proposed for the mineralization of phthalic acid by the EAOPs tested taking into account all the oxidation products detected. In this pathway, two oxidizing agents, BDD(•OH) and •OH, are considered. The former is the main oxidant in EF, regardless of the presence of Cu^{2+} and/or Fe^{3+}, whereas the latter is originated in large extent in SPEF using Fe^{3+}. Although all the acids are expected to form Cu(II) and Fe(III) complexes, this possibility is only stated for acid **18** for sake of simplicity.

The process is initiated either by the hydroxylation of **1** to yield **2** and **3** or its decarboxylation to produce **8**. Consecutive oxidation of the monohydroxylated derivatives **2** and **3** gives the dihydroxylated compounds **4**–**6**, which are further degraded to the tetrahydroxylated one **7**. Parallel destruction of **8** leads to its monohydroxylated products **9**–**11**, followed by its oxidation to the dihydroxylated derivative **12**. Compounds **9**–**11** could also be formed from the decarboxylation of **2** and **3**. Further cleavage of the benzenic moiety of the above aromatic intermediates yields a mixture of acids **13**–**17**, which are subsequently oxidized to **18**. This ultimate carboxylic acid forms Cu(II)-oxalate and/or Fe(III)-oxalate complexes, which are very slowly attacked by BDD(•OH) in EF and SPEF with 0.50 mM Cu^{2+}. In contrast, in SPEF with Cu^{2+}–Fe^{3+} combination, the Cu(II)-oxalate species can also be removed by •OH, but the Fe(III)-oxalate ones are much more quickly photolyzed to CO_2 by sunlight. For the other short-linear carboxylic acids, our results using 0.125 mM Cu^{2+} + 0.375 mM Fe^{3+} suggest that the oxidation of its Cu(II) complexes with •OH predominates over the removal of its Fe(III)-complexes under the action of •OH and sunlight.

4. Conclusions

It has been demonstrated that photo-Fenton reaction (5) is able to induce the generation of •OH in concentration enough to largely accelerate phthalic acid removal in SPEF with 0.50 mM Fe^{3+} compared to EF. Almost total mineralization was achieved under these SPEF conditions due to the photolysis of generated Fe(III)-carboxylate complexes. However, the comparable EF processes with 0.50 mM Cu^{2+} or 0.50 mM Fe^{3+} led to slower substrate decay and poorer mineralization because the main oxidant is BDD(•OH). A slightly faster TOC decay was found for SPEF with 0.50 mM Cu^{2+} by the photodecomposition of several intermediates. In all cases, phthalic acid decayed following a pseudo-first-order kinetics. The combination of Cu^{2+} and Fe^{3+} as catalysts enhanced the mineralization process in SPEF as a result of the oxidation of Cu(II) complexes with •OH formed by photo-Fenton reaction (5), whereas the substrate removal was accelerated by addition of more Fe^{3+} owe to the larger production of •OH. The best SPEF degradation resulted for a 2.0 mM phthalic solution with 0.125 mM Cu^{2+} + 0.375 mM Fe^{3+} at pH 3.0 and 33.3 mA cm^{-2}, attaining 99% mineralization in 240 min with 40% current efficiency and 0.294 kWh g^{-1} TOC energy consumption. Eleven aromatic intermediates coming from the hydroxylation/decarboxylation of phthalic acid were detected by LC–MS. Six short-linear carboxylic acids formed from the cleavage of the benzenic ring of aromatic products were quantified by ion-exclusion HPLC. The Cu(II) and/or Fe(III) complexes of most of these acids were destroyed by BDD(•OH), although in SPEF their Cu(II)-carboxylate complexes were also oxidized by •OH. A different behavior was found for the ultimate acid, oxalic acid, which was quickly removed in SPEF due to the efficient photolysis of the Fe(III)-oxalate complexes.

Acknowledgements

The authors are grateful to the financial support from MICINN (Ministerio de Ciencia e Innovación, Spain) under the project CTQ2010-16164/BQU, co-financed with FEDER funds. S. Garcia-Segura thanks the grant awarded from MEC (Ministerio de Educación y Ciencia, Spain) and R. Salazar acknowledges the financial support from FONDECYT (Chile) with grant 1130391 and DICYT-USACh. The authors acknowledge to Reviewer 1 the proposal of the control of the oxidation reaction by the generation of the hydroxyl radical in the bulk and the deriving discussion in order to point out the non-coherence of authors' discussion.

References

[1] S. Oishi, K. Hiraga, Testicular atrophy induced by phthalic acid esters: Effect on testosterone and zinc concentrations, Toxicology and Applied Pharmacology 53 (1980) 35.
[2] E. Makoto, M. Emiko, H. Akira, K. Kunio, Developmental toxicity evaluation of phthalic acid, one of the metabolites of phthalic acid esters, in rats, Toxicology Letters 93 (1997) 109.
[3] United States Environmental Protection Agency (7407), Pollution Prevention and Toxics, EPA 749-F-95-016a, 1994.
[4] J.M. Bauer, R. Herrman, Estimation of the environmental contamination by phthalic acid esters leaching from household wastes, Science of the Total Environment 208 (1997) 49.
[5] L. Zhang, L. Dong, L. Ren, S. Shi, L. Zhou, T. Zhang, Y. Huang, Concentration and source identification of polycyclic aromatic hydrocarbons and phthalic acid esters in the surface water of the Yangtze River Delta, China, Journal of Environmental Sciences 24 (2012) 335.
[6] H. Fromme, T. Kuchler, T. Otto, K. Pilz, J. Muller, A. Wenzel, Occurrence of phthalates and bisphenol A and F in the environment, Water Research 36 (2002) 1429.
[7] A.V. Taborda, M.A. Brusa, M.A. Grela, Photocatalytic degradation of phthalic acid on TiO_2 nanoparticles, Applied Catalysis A: General. 208 (2001) 419.
[8] E. Ayranci, E. Bayram, Adsorption of phthalic acid and its esters onto high-area activated carbon-cloth studied by in situ UV-spectroscopy, Journal of Hazardous Materials B122 (2005) 147.
[9] Z. Zheng, H. Zhang, P.J. He, L.M. Shao, Y. Chen, L. Pang, Co-removal of phthalic acid esters with dissolved organic matter from landfill leachate by coagulation and flocculation process, Chemosphere 75 (2009) 180.
[10] C. Fang, Y. Long, D. Shen, Comparison on the removal of phthalic acid diesters in a bioreactor landfill and a conventional landfill, Bioresource Technology 100 (2009) 5664.
[11] R. Lertsirisopon, S. Soda, K. Sei, M. Ike, Abiotic degradation of four phthalic acid esters in aqueous phase under natural sunlight irradiation, Journal of Environmental Sciences 21 (2009) 285.
[12] G. Zhao, J. Gao, S. Shen, M. Liu, D. Li, M. Wu, Y. Lei, Ultrasound enhanced electrochemical oxidation of phenol and phthalic acid on boron-doped diamond electrode, Journal of Hazardous Materials 172 (2009) 1076.
[13] E. Brillas, I. Sirés, M.A. Oturan, Electro-Fenton process and related electrochemical technologies based on Fenton's reaction chemistry, Chemical Reviews 109 (2009) 6570.
[14] I. Sirés, E. Brillas, Remediation of water pollution caused by pharmaceutical residues based on electrochemical separation and degradation technologies: a review, Environment International 40 (2012) 212.
[15] A.R. Khataee, M. Safarpour, M. Zarei, S. Aber, Electrochemical generation of H_2O_2 using immobilized carbon nanotubes on graphite electrode fed with air: Investigation of operational parameters, Journal of Electroanalytical Chemistry 169 (2011) 63.
[16] M. Zarei, A.R. Khataee, R. Ordikhani-Seyedlar, M. Fathinia, Photoelectro-Fenton combined with photocatalytic process for degradation of an azo dye using supported TiO_2 nanoparticles and carbon nanotube cathode: Neural network modeling, Electrochimica Acta 55 (2010) 7259.
[17] M. Zarei, A. Niaei, D. Salari, A.R. Khataee, Application of response surface methodology for optimization of peroxi-coagulation of textile dye solution using carbon nanotube-PTFE cathode, Journal of Hazardous Materials 173 (2010) 544.
[18] N. Oturan, M.A. Oturan, Degradation of three pesticides used in viticulture by electrogenerated Fenton's reagent, Agronomy for Sustainable Development 25 (2005) 267.
[19] I. Sirés, J.A. Garrido, R.M. Rodríguez, E. Brillas, N. Oturan, M.A. Oturan, Catalytic behavior of the Fe^{3+}/Fe^{2+} system in the electro-Fenton degradation of the antimicrobial chlorophene, Applied Catalysis B: Environmental 72 (2007) 382.

[20] A. Özcan, Y. Sahin, A. Savas Koparal, M.A. Oturan, Carbon sponge as a new material for the electro-Fenton process. Comparison with carbon felt cathode and application to degradation of synthetic dye Basic Blue 3 in aqueous medium, Journal of Electroanalytical Chemistry 616 (2008) 71.
[21] A. Dirany, S. Efremova-Aaron, N. Oturan, I. Sirés, M.A. Oturan, J.-J. Aaron, Study of the toxicity of sulfamethoxazole and its degradation products in water by a bioluminescence method during application of the electro-Fenton treatment, Analytical and Bioanalytical Chemistry 400 (2011) 353.
[22] A. Dirany, I. Sirés, N. Oturan, A. Özcan, M.A. Oturan, Electrochemical treatment of the antibiotic sulfachloropyridazine: kinetics, reaction pathways, and toxicity evolution, Environmental & Science Technology 46 (2012) 4074.
[23] E. Brillas, M.A. Baños, S. Camps, C. Arias, P.L. Cabot, J.A. Garrido, R.M. Rodríguez, Catalytic effect of Fe^{2+}, Cu^{2+} and UVA light on the electrochemical degradation of nitrobenzene using an oxygen-diffusion cathode, New Journal of Chemistry 28 (2004) 314.
[24] E. Isarain-Chávez, C. Arias, P.L. Cabot, F. Centellas, R.M. Rodríguez, J.A. Garrido, E. Brillas, Mineralization of the drug beta-blocker atenolol by electro-Fenton and photoelectro-Fenton using an air-diffusion cathode for H_2O_2 electrogeneration combined with a carbon-felt cathode for Fe^{2+} regeneration, Applied Catalysis B: Environmental 96 (2010) 361.
[25] E.J. Ruiz, C. Arias, E. Brillas, A. Hernández-Ramírez, J.M. Peralta-Hernández, Mineralization of Acid Yellow 36 azo dye by electro-Fenton and solar photoelectro-Fenton processes with a boron-doped diamond anode, Chemosphere 82 (2011) 495.
[26] S. Garcia-Segura, J.A. Garrido, R.M. Rodríguez, P.L. Cabot, F. Centellas, C. Arias, E. Brillas, Mineralization of flumequine in acidic medium by electro-Fenton and photoelectro-Fenton processes, Water Research 46 (2012) 2067.
[27] M. Panizza, M.A. Oturan, Degradation of alizarin red by electro-Fenton process using a graphite-felt cathode, Electrochimica Acta 56 (2011) 7084.
[28] K. Cruz-González, O. Torres-López, A. García-León, J.L. Guzmán-Mar, L.H. Reyes, A. Hernández-Ramírez, J.M. Peralta-Hernández, Determination of optimum operating parameters for Acid Yellow 36 decolorization by electro-Fenton process using BDD cathode, Chemical Engineering Journal 160 (2010) 199.
[29] C. Flox, P.L. Cabot, F. Centellas, J.A. Garrido, R.M. Rodríguez, C. Arias, E. Brillas, Electrochemical combustion of herbicide mecoprop in aqueous medium using a flow reactor with a boron-doped diamond anode, Chemosphere 64 (2006) 892.
[30] M. Panizza, G. Cerisola, Direct and mediated anodic oxidation of organic pollutants, Chemical Reviews 109 (2009) 6541.
[31] C. Flox, C. Arias, E. Brillas, A. Savall, K. Groenen-Serrano, Electrochemical incineration of cresols: a comparative study between PbO_2 and boron-doped diamond anodes, Chemosphere 74 (2009) 1340.
[32] M. Hamza, R. Abdelhedi, E. Brillas, I. Sirés, Comparative electrochemical degradation of the triphenylmethane dye methyl violet with boron-doped diamond and Pt anodes, Journal of Electroanalytical Chemistry 627 (2009) 41.
[33] E. Brillas, S. Garcia-Segura, M. Skoumal, C. Arias, Electrochemical incineration of diclofenac in neutral aqueous medium by anodic oxidation using Pt and boron-doped diamond anodes, Chemosphere 79 (2010) 605.
[34] P. Cañizares, J. García-Gómez, J. Lobato, M.A. Rodrigo, Electrochemical oxidation of aqueous carboxylic acid wastes using diamond thin-film electrodes, Industrial & Engineering Chemical Research 42 (2003) 956.
[35] P. Cañizares, R. Paz, C. Sáez, M.A. Rodrigo, Electrochemical oxidation of alcohols and carboxylic acids with diamond anodes: a comparison with other advanced oxidation processes, Electrochimica Acta 53 (2008) 2144.
[36] S. Garcia-Segura, E. Brillas, Mineralization of the recalcitrant oxalic and oxamic acids by electrochemical advanced oxidation processes using a boron-doped diamond anode, Water Research 45 (2011) 2975.
[37] I. Sirés, J.A. Garrido, R.M. Rodríguez, P.L. Cabot, F. Centellas, C. Arias, E. Brillas, Electrochemical degradation of paracetamol from water by catalytic action of Fe^{2+}, Cu^{2+} and UVA light on electrogenerated hydrogen peroxide, Journal of the Electrochemical Society 153 (2006) D1.
[38] R. Salazar, S. Garcia-Segura, M.S. Ureta-Zañartu, E. Brillas, Degradation of disperse azo dyes from waters by solar photoelectro-Fenton, Electrochimica Acta 56 (2011) 6371.
[39] L.C. Almeida, S. Garcia-Segura, N. Bocchi, E. Brillas, Solar photoelectro-Fenton degradation of paracetamol using a flow plant with a Pt/air-diffusion cell coupled with a compound parabolic collector: Process optimization by response surface methodology, Applied Catalysis B: Environmental 103 (2011) 21.
[40] R. Salazar, E. Brillas, I. Sirés, Finding the best Fe^{2+}/Cu^{2+} combination for the solar photoelectro-Fenton treatment of simulated wastewater containing the industrial textile dye Disperse Blue 3, Applied Catalysis B: Environmental 115–116 (2012) 107.
[41] A. Babuponnusami, K. Muthukumar, Advanced oxidation of phenol: a comparison between Fenton, electro-Fenton, sono-electro-Fenton and photo-electro-Fenton processes, Chemical Engineering Journal 183 (2012) 1.
[42] R. Salazar, M.S. Ureta-Zañartu, Mineralization of triadimefon fungicide in water by electro-Fenton and photoelectro-Fenton, Water Air Soil Pollution 223 (2012) 4199.
[43] Corporación Nacional del Cobre de Chile, CODELCO, Plan de Inversiones Codelco, 2012.
[44] B. Boye, M.M. Dieng, E. Brillas, Electrochemical degradation of 2,4,5-trichlorophenoxyacetic acid in aqueous medium by peroxi-coagulation. Effect of pH and UV light, Electrochimica Acta 48 (2003) 781.
[45] S. Parthasarathy, V.S.K. Nair, Enthalpy of complex formation by calorimetry: phthalates of manganese, nickel, and copper, Thermochimica Acta 2 (1971) 69.
[46] V. Vancina, T.A. Himdan, H. Bilinski, M. Miljak, I. Kos, D. Hanzel, D. Hanzel, Thermal behavior and characterization of some novel Fe(III)-o-phthalates, Thermochimica Acta 246 (1994) 199.
[47] H. Gallard, J. De Laat, B. Legube, Comparative study of the rate of decomposition of H_2O_2 and atrazine by Fe(III)/H_2O_2, Cu(II)/H_2O_2, Fe(III)/Cu(II)/H_2O_2, Revue des Sciences de l'Eau 12 (1999) 713.

Electrochemiluminescence of luminol

During these years that I have made my PhD thesis in LEMMA, I have also been an active member of the teaching innovation group "Química a la Interfase Secundaria-Universitat" (QuISU). "Fem Química al Laboratori" (FQL) is one of the most popular activities developed by QuISU. In FQL, high school students do 4 practises in 4 h from different chemistry fields with one professor of the University of Barcelona. The last three years one biochemical practise related with the forensic science using luminol was performed in FQL.

Luminol is from far the most popular reagent used in CL. The emission of a characteristic fluorescent light of λ_{max} = 425 nm when a solution of luminol and hydrogen peroxide in alkaline medium is sprayed on dried blood stains has been widely utilized by forensic scientists for more than 40 years. Luminol is oxidized at pH 8−12 in the presence of H_2O_2 and a suitable catalyst such the hemo group. The most important fact that could be noticed is that the Fe^{2+} from the hemo group catalyses the oxidation of luminol when reacts with H_2O_2, thereby showing certain similitudes with the Fenton's reaction (10).

Based on the hypothesis that the generation of hydroxyl radicals would be the main responsible of the CL reaction due to the luminol oxidation, we decided to test if the radicals electrogenerated on the BDD surface could be able to generate ECL. The results showed a novel characteristic property of BDD not previously described, the light emission in a wide potential range of 0.5-5.0V vs Ag|AgCl, KCl(sat.) by an ECL reaction with luminol, which has not been observed for other anodes.

The linear sweep voltammetry study of the system explained the electrochemical behaviour of luminol, H_2O_2 and their mixture in an alkaline pH media. The onset potentials evidenced that $^{\bullet}OH$ was not generated under these pH conditions where superoxide ion radical ($O_2^{\bullet-}$) was formed instead. Also the results allowed us to conclude that $O_2^{\bullet-}$ generation was enhanced when hydroperoxyl radical ($HO_2^{\bullet}$) was formed as the predominant species at pH 12.0, coming from the oxidation of added H_2O_2. The light emission measurements also evidenced the enhancement effect of H_2O_2 addition. Thus, the maximum light emission of 1.65 μW cm^{-2} without H_2O_2 increased up to 104 μW cm^{-2} (63 times higher) in 0.05 M of H_2O_2. An inhibition of light emission with increasing H_2O_2 concentration was also observed and ascribed to the higher rise in rate of parasitic reactions that consume the radical species.

Additionally the use of specific scavengers and quenchers of $^{\bullet}OH$ and $O_2^{\bullet-}$ such as DMSO and *p*-benzoquinone, respectively, allowed ascertaining which radical was the responsible of the ECL reaction. The insignificant influence of DMSO and the high effect of *p*-benzoquinone on light emission corroborated that the large enhancement of ECL of luminol in presence of H_2O_2 on BDD was related with $O_2^{\bullet-}$ electrogeneration. These results allowed us to propose a double via for the ECL of luminol in alkaline medium related with the direct charge transfer and the indirect electrochemical oxidation by $O_2^{\bullet-}$.

The ECL process showed a strongly relationship with the electrogeneration of physisorbed $O_2^{\bullet-}$ anion radicals at the BDD surface. This finding can contribute to a better characterization of the properties of conductive-diamond electrodes, the understanding of the oxidation mechanisms of organics by ROS and the development of BDD sensors for biomolecules. Furthermore, the corroboration of the no generation of $^{\bullet}OH$ radicals at pH over 12.0 explains the lower oxidation ability of these anodes in alkaline media than in neutral and acidic pH.

PAPER 9

Unprecedented electrochemiluminescence of luminol on a boron-doped diamond thin-film anode. Enhancement by electrogenerated superoxide radical anion

THE JOURNAL OF PHYSICAL CHEMISTRY C

Article

pubs.acs.org/JPCC

Unprecedented Electrochemiluminescence of Luminol on a Boron-Doped Diamond Thin-Film Anode. Enhancement by Electrogenerated Superoxide Radical Anion

Sergi Garcia-Segura, Francesc Centellas,* and Enric Brillas

Laboratori d'Electroquímica dels Materials i del Medi Ambient, Departament de Química Física, Facultat de Química, Universitat de Barcelona, Martí i Franquès 1-11, 08028 Barcelona, Spain

ABSTRACT: Electrochemiluminescence (ECL) of 0.01 M luminol in NaOH medium of pH 12.0 on a boron-doped diamond (BDD) thin-film anode was studied in the absence and presence of H_2O_2. Here we show a new characteristic property of BDD allowing light emission in a wide potential range of 0.5−5.0 V vs Ag|AgCl, KCl(sat.), a behavior not observed for other anodes. Maximum ECL intensity was found at 2.2−2.8 V without H_2O_2, which became 63 times more intense after adding 0.05 M H_2O_2. The strong enhancement of ECL in the presence of H_2O_2 is attributed to the larger production of emitter 3-aminophthalate dianion, formed by selective nucleophilic attack of superoxide radical anion ($O_2^{\bullet-}$) to the radical electrogenerated from one-electron oxidation of the monoanionic form of luminol. Linear sweep voltammetry showed that $^{\bullet}OH$ was not generated from OH^- oxidation, whereas $O_2^{\bullet-}$ can be produced from HO_2^- oxidation. The performance of $O_2^{\bullet-}$ in ECL was confirmed by *p*-benzoquinone quenching.

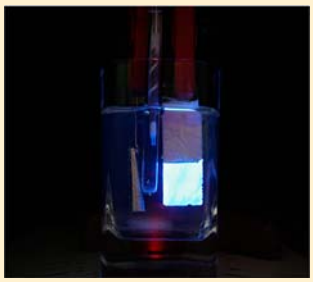

1. INTRODUCTION

Luminol (5-amino-2,3-dihydro-1,4-phthalazinedione) is the most popular reagent used in chemiluminescence (CL). The emission of characteristic fluorescent light of λ_{max} = 425 nm when a solution of luminol and hydrogen peroxide in alkaline medium is sprayed on dried blood stains has been widely utilized by forensic scientists for more than 40 years.[1] It is known that luminol is oxidized at pH 8−12 in the presence of a mild−strong oxidant such as H_2O_2 and a suitable catalyst such as a metal ion. This oxidation is caused via charge-transfer reactions between reactive oxygen species (ROS) and the excited form of the 3-aminophthalate dianion. CL is emitted when this dianion decays to the ground state.[2]

Recently, electrogenerated CL or electrochemiluminescence (ECL) has received considerable interest in analytical chemistry due to its high sensitivity, low background, wide dynamic range, and simple formats.[3] Several authors have reported the ECL of luminol in alkaline medium, but in the absence of H_2O_2, on anodes of Au,[3,4] Pt,[5] carbonaceous materials,[5−7] and indium tin oxide.[8,9] In these works, ECL is conventionally initiated by cyclic voltammetry and linear sweep voltammetry, yielding light emission at defined low potential ranges only. ECL processes are usually explained by similar pathways to the CL ones involving direct anodic oxidation of luminol and electrogenerated ROS as oxidant to obtain the emitter 3-aminophthalate dianion, but disregarding the potential positive action of added H_2O_2.

Boron-doped diamond (BDD) thin-film electrodes are the most potent anodes known for anodic oxidation. This is due to their technological features, such as an inert surface with low adsorption properties, remarkable corrosion stability, and a wide potential window in acidic medium.[10−12] Compared with conventional anodes such as Pt, the BDD anode has higher O_2-overvoltage, generating more amount of $^{\bullet}OH$ from water oxidation, resulting in a quicker destruction of a large variety of organics. However, less known are the ECL properties of organics on a BDD anode. As far as we know, light emission of the Ru-tris(2,2′)bipyridyl dication promoted by oxidation of coreactants such as ascorbic acid[13] and tripropylamine[14] using BDD has only been described in the literature. Thus, the aim of the present work is to study the ECL of luminol on BDD in a NaOH solution of pH 12.0 in order to clarify the characteristics of this process and the mechanism of the oxidation of luminol in the absence and presence of H_2O_2.

2. EXPERIMENTAL SECTION

2.1. Chemicals. Luminol was of HPLC grade, purchased from AppliChem, and used as received. DMSO (>99.9%) and *p*-benzoquinone (>99%) were of analytical grade, supplied by Sigma-Aldrich. Sodium hydroxide (98−100%) and hydrogen peroxide (33% w/v) were of analytical grade from Acros and Panreac, respectively. All solutions were prepared with high-purity water obtained from a Millipore Milli-Q system with resistivity >18 MΩ cm at 25 °C. To adjust the solution pH at 12.0, increasing amounts of NaOH with increasing H_2O_2 concentration were needed to be added due to the conversion of H_2O_2 into HO_2^-. The H_2O_2 concentration was determined by standard permanganometric titration before luminol addition.

2.2. Electrodes. All BDD thin-film electrodes were 1 μm thick, and 1300 ppm of boron content was supplied by

Received: June 5, 2012
Published: July 2, 2012

Adamant Technologies (La-Chaux-de-Fonds, Switzerland). They were synthesized by the hot filament chemical vapor deposition technique on single-crystal *p*-type Si(100) wafers with resistivity of 0.1 Ω cm. Prior to use, the impurities of the BDD surfaces were removed by polarizing each electrode in 0.05 M Na_2SO_4 at 100 mA cm^{-2} for 60 min. The Pt electrodes were of 99.99% purity, supplied by SEMPSA (Barcelona, Spain), and were cleaned by heating in a flame before use.

2.3. Voltammetric Experiments. Linear sweep voltammetry was conducted in a three-electrode cylindrical cell using an Ecochemie Autolab PGSTAT100 potentiostat-galvanostat controlled by Autolab Nova 1.5 software. The working electrode was a 0.50 cm^2 BDD thin-film electrode, the counter electrode was a Pt wire, and the reference electrode was an Ag|AgCl, KCl (sat.) electrode ($E°$ = 0.197 V vs SHE). All voltammograms were recorded at a scan rate of 5 mV s^{-1}, at room temperature (25 °C), and under stirring with a magnetic bar at 700 rpm.

2.4. ECL Measurements. A three-electrode glass (Pyrex) tank reactor with flat walls operating in potentiostatic mode and controlled by an Amel 2053 potentiostat-galvanostat was used. The anode was a 3 cm^2 BDD thin-film electrode, the cathode was a 5 cm^2 Pt sheet, and the reference electrode was an Ag|AgCl, KCl (sat.) electrode. All electrolyses were performed at room temperature (25 °C) and under magnetic stirring at 700 rpm. The relative ECL intensity emitted by the BDD anode was determined with a Thorlabs S110 Optical Power Meter Console system, coupled with a 1 cm^2 S120A sensor head. For this, the electroactive face of the BDD anode was placed parallel to one flat wall of the cell, at a distance of about 0.5 cm, and the sensor head was then located on the external wall in front of the center of the BDD. The Pt cathode was placed behind the BDD anode at a distance of ca. 2 cm. The positions of both electrodes and the sensor head remained unchanged during comparative ECL measurements.

In the electrochemical trials, the cells were filled with 125−150 mL of NaOH solutions of pH 12.0. The solution pH was measured on a Crison GLP 22 pH-meter. The luminol concentration was always 0.01 M. Comparative ECL experiments were made without H_2O_2 and with H_2O_2 concentrations up to 5.0 M. In each of these trials, an increasing anode potential between 0.0 and 5.0 vs Ag|AgCl was applied, holding each selected potential value steady for 10 s. No significant change in ECL intensity was found by repeating the measurements in a consecutive potential run.

3. RESULTS AND DISCUSSION

Linear sweep voltammetry was first used to ascertain the electrochemical behavior of luminol and H_2O_2 on a 0.50 cm^2 BDD anode in NaOH solutions at pH 12.0. In this background electrolyte, OH^- was oxidized at the electrode instead of H_2O, which takes place up to pH 9.[3,4,15] Voltammograms were recorded as explained in the Experimental Section. The solution was vigorously stirred with a magnetic bar at 700 rpm to ensure the transport of reactants toward the electrodes at a continuous rate. Curve *a* of Figure 1 shows an onset potential of 0.81 V vs Ag|AgCl (1.01 V vs SHE) for OH^- oxidation, whereupon the corresponding current density (*j*) increased progressively when increasing BDD potential. A similar voltammogram for 0.25 M NaOH with 0.5 M Na_2SO_4 on BDD has been reported by Martínez-Huitle and coworkers.[16] The overall electrode reaction for this process is

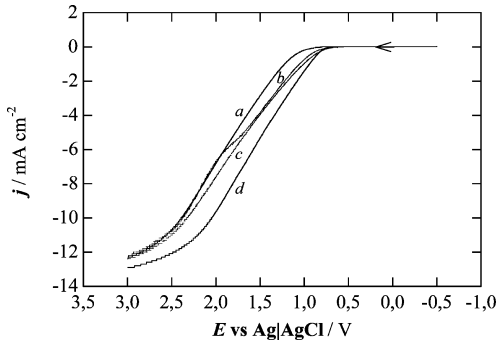

Figure 1. Linear sweep voltammograms for the oxidation of NaOH solutions of pH 12.0 on a 0.50 cm^2 BDD thin-film electrode. The three-electrode cylindrical cell contained a Pt wire as cathode and an Ag|AgCl, KCl(sat.) reference electrode. Voltammograms were recorded at a scan rate of 5 mV s^{-1}, at 25 °C, and under magnetic stirring at 700 rpm. (*a*) Background electrolyte. After addition of (*b*) 0.01 M luminol, (*c*) 0.01 M luminol and 0.05 M H_2O_2, and (*d*) 0.10 M H_2O_2.

given by eq 1 with standard reduction potential $E°$ = 0.40 V vs SHE:

$$4OH^- \rightarrow O_2(g) + 2H_2O + 4e^- \quad (1)$$

Taking into consideration that $E°(^{\bullet}OH/OH^-)$ = 1.77 V vs SHE[17] is a value much more positive than the onset potential found for OH^- oxidation at BDD and $E°$ for reaction 1, one can conclude that OH^- oxidation does not form $^{\bullet}OH$ at pH 12.0. A similar conclusion has been made by Enache and coworkers.[15] This behavior differs from the ability of BDD to produce large amounts of $^{\bullet}OH$ from H_2O oxidation in acidic and neutral aqueous solutions in order to mineralize organic pollutants.[10−12]

Curve *b* of Figure 1 for 0.01 M luminol in the same alkaline solution depicts a lower onset potential of 0.56 V vs Ag|AgCl with a clear oxidation wave up to about 2 V vs Ag|AgCl, indicating that luminol undergoes direct anodic oxidation through electron-transfer reactions on BDD. When 0.05 M H_2O_2 was added in the medium (curve *c* of Figure 1), luminol oxidation was slightly enhanced. Since pK_a = 11.67 for H_2O_2,[18] its conjugated base, the hydroperoxide ion (HO_2^-) is the predominant electroactive species in alkaline solution, and therefore, the enhancement of luminol oxidation should be related to its reaction with generated species from HO_2^- oxidation. This was confirmed by recording the *j*−*E* plot for a 0.10 M H_2O_2 solution (curve *d* of Figure 1), which showed an onset potential of 0.70 V vs Ag|AgCl and an easier oxidation than that of luminol and OH^-. Evidences on the generation of superoxide radical anion ($O_2^{\bullet -}$) from HO_2^- oxidation will be discussed below. Thereby, the reaction mechanism proposed for the electrodic oxidation of HO_2^- at pH 12.0 can be written as follows:[3,19,20]

$$HO_2^- \rightarrow HO_2^{\bullet} + e^- \quad (2)$$

$$HO_2^{\bullet} \leftrightarrows O_2^{\bullet -} + H^+ \quad (3)$$

$$O_2^{\bullet -} \rightarrow O_2 + e^- \quad (4)$$

where the initially electrogenerated hydroperoxyl radical ($HO_2^{\bullet}$) with pK_a = 4.88 is completely converted into $O_2^{\bullet -}$, which is subsequently oxidized to O_2 ($E°(O_2/O_2^{\bullet -})$ = −0.33 V vs SHE). Consequently, one can suppose that, in H_2O_2

dx.doi.org/10.1021/jp305493g | J. Phys. Chem. C 2012, 116, 15500−15504

solutions at pH = 12.0, $O_2^{\bullet-}$ is the species that enhances luminol oxidation on BDD (curve *c* of Figure 1). Only under these conditions in linear sweep voltammetry did the BDD surface emit the characteristic light of luminol of λ_{max} = 425 nm.

The ECL intensity produced by the potentiostatic oxidation of 0.01 M luminol in stirred NaOH solutions at pH 12.0 in the absence and presence of H_2O_2 was measured. For this purpose, a three-electrode cell with flat walls equipped with a 3 cm^2 BDD anode and a 5 cm^2 sheet cathode was used following the procedure described in the Experimental Section. Weak light emission was observed for a luminol solution without H_2O_2, which became much more intense by adding H_2O_2. Constant ECL intensity was determined for all selected potentials when the reactants were transported to the BDD anode at constant rate by magnetic stirring at 700 rpm.

Figure 2a highlights that ECL started at a BDD potential of about 0.5 V vs Ag|AgCl and attained a maximum intensity of

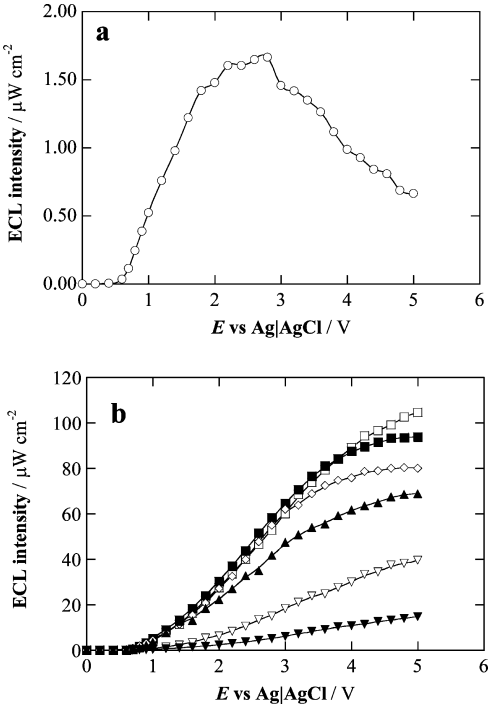

Figure 2. Variation of ECL intensity with potential applied to a 3 cm^2 BDD thin-film anode. The three-electrode cell with flat walls contained a 5 cm^2 Pt sheet as cathode and an Ag|AgCl, KCl(sat.) reference electrode. Solutions of 0.01 M luminol in NaOH at pH 12.0, at 25 °C, and under magnetic stirring at 700 rpm were oxidized. (a) Without H_2O_2. (b) H_2O_2 concentration: (□) 0.05 M, (■) 0.10 M, (◇) 0.50 M, (▲) 1.0 M, (▽) 2.5 M, and (▼) 5.0 M.

1.65 μW cm^{-2} between 2.2 and 2.8 V vs Ag|AgCl. The increase in ECL intensity from 0.5 to 2.2 V vs Ag|AgCl can be ascribed to the concomitant increase in rate of electron-transfer reactions that convert luminol into the emitter 3-amino-phthalate dianion. The gradual inhibition of ECL from 2.8 to 5.0 V vs Ag|AgCl shown in Figure 2a suggests a larger acceleration of other oxidation reactions of luminol at high BDD potentials decreasing the proportion of 3-aminophthalate dianion produced. It is worth noting that the continuous ECL emitted by luminol at potentials from 0.5 to 5.0 V vs Ag|AgCl is a characteristic property of BDD, since other anodes only show this phenomenon at defined intervals of potential, usually <1 V vs Ag|AgCl.[3−9]

Addition of H_2O_2 to the luminol solution caused a large enhancement of ECL, which reached maximum intensities for 0.05 M H_2O_2. Figure 2b shows that a solution with 0.01 M luminol and 0.05 M H_2O_2 yielded increasing light emission in the BDD potential range from 0.5 to 5.0 V vs Ag|AgCl, which can be accounted for by the action of the progressive larger production of $O_2^{\bullet-}$ from reactions 2 and 3. The maximum ECL intensity reached at the highest BDD potential was 104 μW cm^{-2}, i.e. 63 times higher than the 1.65 μW cm^{-2} found as the maximum for luminol without H_2O_2 under comparable conditions (Figure 2a). However, Figure 2b also shows that the presence of greater H_2O_2 concentrations caused a gradual loss in ECL intensity. Thus, for 5.0 M H_2O_2 only 15 μW cm^{-2} was obtained as maximal at 5.0 V vs Ag|AgCl. The progressive fall in light emission for H_2O_2 concentrations >0.05 M can be related to the loss of generated $O_2^{\bullet-}$ by enhancement of its parasitic reactions, e.g. reaction 5[21] with second-order rate constant $k = 9.7 \times 10^7$ M^{-1} s^{-1}:

$$O_2^{\bullet-} + HO_2^{\bullet} \rightarrow HO_2^{-} + O_2 \qquad (5)$$

Photographs of Figure 3 illustrate the light emitted by BDD from oxidation of 0.01 M luminol at pH 12.0 in the cylindrical

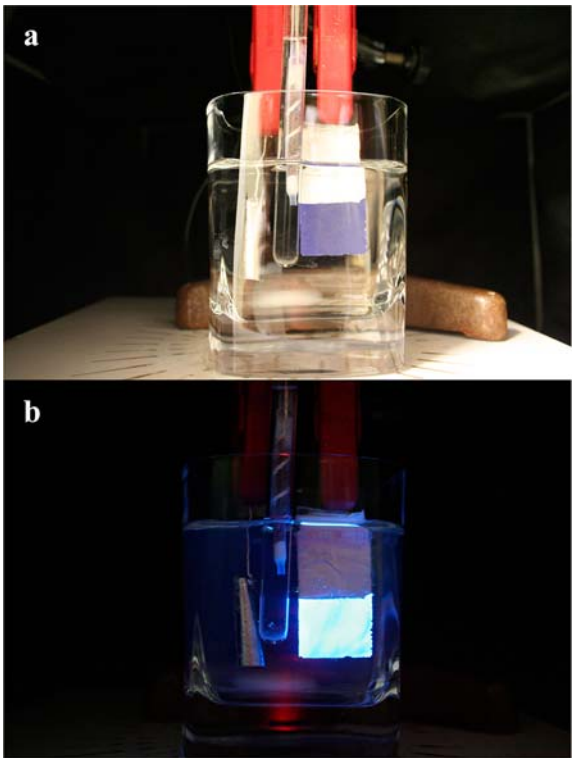

Figure 3. Photographs of the ECL emitted by a 3 cm^2 BDD thin-film anode during luminol oxidation. The three-electrode cylindrical cell contained a 5 cm^2 Pt sheet as cathode and an Ag|AgCl, KCl(sat.) reference electrode. (a) Solution of 0.01 M luminol in NaOH of pH 12.0 oxidized at *E* = 2.5 V vs Ag|AgCl and 25 °C under magnetic stirring at 700 rpm. (b) Solution with 0.10 M H_2O_2.

cell. As can be seen in Figure 3a, a uniform blue color over the 3 cm^2 anode surface is achieved when the higher ECL intensity is obtained in the absence of H_2O_2 at 2.5 V vs Ag|AgCl. A much more intense ECL can be observed in Figure 3b by applying the same potential after addition of 0.10 M H_2O_2. Note that BDD not only emitted a much more brilliant blue color, but also the solution was illuminated by light reflection on the cell glass.

dx.doi.org/10.1021/jp305493g | J. Phys. Chem. C 2012, 116, 15500−15504

The role of ROS generated from OH^- and HO_2^- oxidation on the ECL process of luminol was analyzed from the influence of radical scavengers such as DMSO and *p*-benzoquinone on light emission. DMSO is a well-known scavenger of $^{\bullet}OH$ and was chosen due to the second-order rate constant for its reaction with this radical ($k = 5.4 \times 10^9$ M^{-1} s^{-1})[22] being greater than that of luminol with $^{\bullet}OH$ ($k = 4.8 \times 10^9$ M^{-1} s^{-1}).[23] On the other hand, the action of *p*-benzoquinone was checked since it is a specific quencher[24] of $O_2^{\bullet-}$ via fast electron transfer reaction with $k = 9.6 \times 10^8$ M^{-1} s^{-1}.[25]

Figure 4a evidences the existence of 9.5% reduction for the ECL intensity of luminol with 0.10 M H_2O_2 when 0.01 M

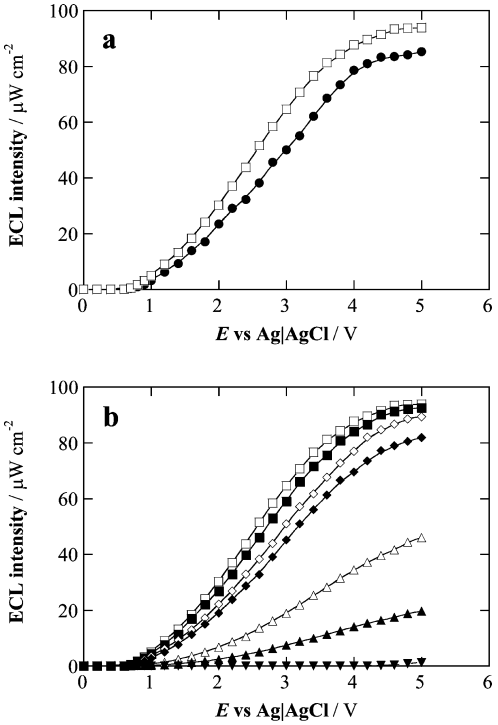

Figure 4. Effect of radical scavengers on ECL intensity vs potential applied to a 3 cm^2 BDD thin-film anode. The same three-electrode cell as in Figure 2 was used. (a and b) (□) 0.01 M luminol with 0.10 M H_2O_2 in NaOH of pH 12.0 at 25 °C under stirring at 700 rpm. (a) (●) With 0.01 M DMSO. (b) *p*-Benzoquinone concentration: (■) 10^{-5} M, (◇) 10^{-4} M, (◆) 10^{-3} M, (Δ) 2.5×10^{-3} M, (▲) 5.0×10^{-3} M, and (▼) 0.01 M.

DMSO was also present in solution. This little effect on light emission can be explained by the competence of the anodic oxidation of DMSO by electron transfer, thereby confirming $^{\bullet}OH$ is not produced during OH^- and HO_2^- oxidation, as suggested above from results of linear sweep voltammetry. In contrast, Figure 4b shows a dramatic decay of ECL intensity from the same luminol solution by increasing *p*-benzoquinone concentration up to 0.01 M. The inhibition was already significant for 10^{-3} M *p*-benzoquinone, while at 0.01 M a maximum intensity as low as 1.2 μW cm^{-2} at 5.0 V vs Ag|AgCl was determined. These findings corroborate that the large enhancement of ECL of luminol in the presence of H_2O_2 on BDD is due to the participation of $O_2^{\bullet-}$ formed from HO_2^- oxidation.

From the above results, a reaction mechanism for the ECL of luminol on BDD in alkaline solution is proposed in Scheme 1. Since $pK_{a1} = 6.7$ and $pK_{a2} = 15.1$ for luminol,[1] its monoanionic

Scheme 1. Reaction Mechanism Proposed for the ECL of Luminol in Alkaline Medium on a BDD Thin-Film Anode in (I) the Absence and (II) Presence of H_2O_2

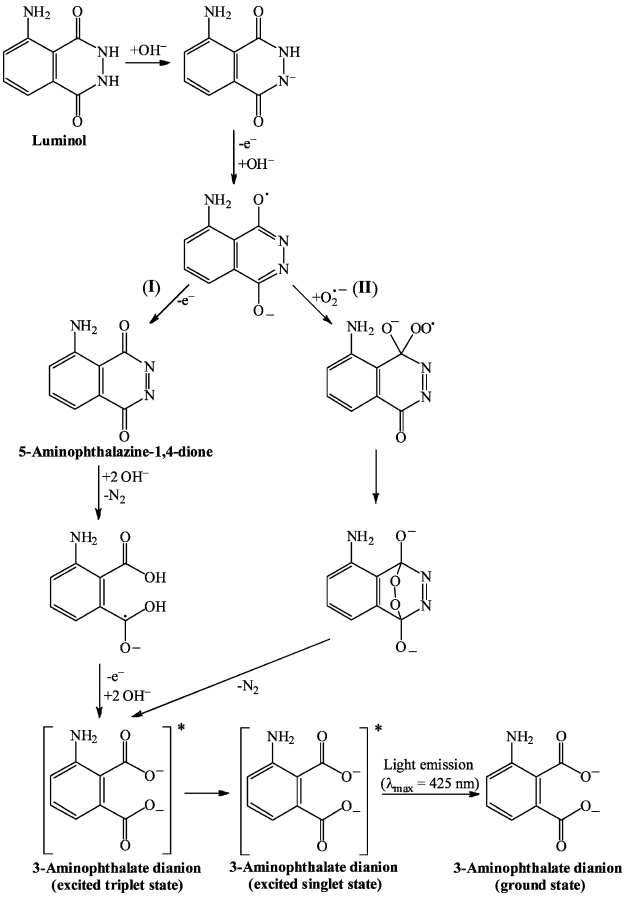

form is the prevalent species at pH = 12.0. The mechanism is then initiated by the one-electron oxidation of this monoanionic form with deprotonation to obtain a phthalazinequinone radical that follows pathway I in the absence of H_2O_2 or mainly pathway II in the presence of H_2O_2. Direct oxidation of the monoanionic form of luminol with $O_2^{\bullet-}$ via electron transfer can be discarded due to its small second-order rate constant ($k = 1 \times 10^4$ M^{-1} s^{-1}).[26] In pathway I, the phthalazinequinone radical undergoes a one-electron oxidation to 5-aminophthalazine-1,4-dione. This species is subsequently transformed into 3-aminophthalate dianion in the excited triplet state via nucleophilic attack of OH^- followed by denitrogenation, one-electron oxidation of the radical anion formed, and finally deprotonation.[5] 3-Aminophthalate dianion is also generated in pathway II via nucleophilic attack of $O_2^{\bullet-}$ on the less poorly charged carbonyl group of phthalazinequinone radical, followed by cyclic addition of oxygen from the added superoxide to the other carbonyl carbon forming a cyclic-antiaromatic endoperoxide and loss of N_2.[1] The 3-aminophthalate dianion in the excited triplet state formed in pathways I and II then undergoes a slow spin-flip process to an excited single state, which in turn falls to the ground state with light emission.[1] The weak intensity obtained in pathway I can account for the disappearance of intermediates by alternative oxidation reactions, as evidenced by the ECL decay found at BDD potentials >2.8 V vs Ag|AgCl (Figure 2a). In contrast, the selective nucleophilic attack of $O_2^{\bullet-}$ on the phthalazinequinone radical can justify a larger formation of the 3-aminophthalate

dx.doi.org/10.1021/jp305493g | J. Phys. Chem. C 2012, 116, 15500−15504

dianion in the excited triplet state giving rise to the strong enhancement of ECL.

When the polarity of the electrodes in the potentiostatic experiments was reversed and the Pt sheet acted as anode, no ECL at potentials up to 5.0 V vs Ag|AgCl was observed. This behavior could seem surprising because similar electron-transfer and chemical reactions for luminol could be postulated, in principle, for both Pt and BDD anodes. However, BDD differs from other anodes by its ability of adsorbing very weakly ROS and organics.[10−12] This suggests that luminol is able to continuously emit ECL at BDD potentials from 0.5 to 5.0 V vs Ag|AgCl due to chemical reactions of intermediates taking place in the vicinity of the BDD surface, whereas such reactions are not produced when reactants remain adsorbed on the Pt surface.

4. CONCLUSIONS

In summary, it has been found that luminol in alkaline medium of pH 12.0 emits ECL when it is oxidized on a BDD thin-film surface at potentials higher than 0.5 V vs Ag|AgCl, reaching maximum intensity at about 2.5 V vs Ag|AgCl. The formation of the emitter 3-aminophthalate dianion can be accounted for by direct electron-transfer reactions of luminol and its oxidation products, combined with chemical reactions involving the nucleophilic attack of OH^- and loss of N_2, without participation of $^{\bullet}OH$. In the presence of H_2O_2, $O_2^{\bullet-}$ is also produced from direct oxidation of HO_2^- on BDD. This radical anion is able to react very rapidly with the initially electrogenerated radical from the monoanionic form of luminol, leading to a much greater generation of the emitter, strongly enhancing the ECL process. The oxidant role of $O_2^{\bullet-}$ was confirmed by the dramatic inhibition of light emission after addition of the scavenger *p*-benzoquinone. This behavior is characteristic of luminol on BDD, since it is not observed for conventional anodes such as Pt. It can then be associated with the reactions of intermediates with OH^- and/or $O_2^{\bullet-}$ near the BDD vicinity due to the low adsorption of these species on the anode surface. These findings can contribute to a better properties characterization of the conductive-diamond electrodes, the understanding of the oxidation mechanisms of organics by ROS, and the development of BDD sensors for biomolecules.[27−29]

AUTHOR INFORMATION

Corresponding Author

*E-mail: facentellas@ub.edu.

Notes

The authors declare no competing financial interest.

ACKNOWLEDGMENTS

We acknowledge financial support from MICINN (Ministerio de Ciencia e Innovación, Spain) through Project CTQ 2010-16164/BQU, cofinanced with FEDER funds. The grant awarded to S.G.-S. by MEC (Ministerio de Educación y Ciencia, Spain) is also acknowledged.

REFERENCES

(1) Barni, F.; Lewis, S. W.; Berti, A.; Miskelly, G. M.; Lago, G. *Talanta* **2007**, *72*, 896−913.
(2) Barnett, N. W.; Francis, P. S. In *Encyclopedia of Analytical Science*; Worsfold, P., Townshend, A., Poole, C., Eds.; Elsevier Academic Press: London, 2005; pp 506−511.
(3) Wang, W.; Cui, H.; Deng, Z.-X.; Dong, Y.-P.; Guo, J.-Z. *J. Electroanal. Chem.* **2008**, *612*, 277−287.
(4) Cui, H.; Zhang, Z. F.; Zou, G. Z.; Lin, X. Q. *J. Electroanal. Chem.* **2004**, *566*, 305−313.
(5) Wróblewska, A.; Reshetnyak, O. V.; Koval'chuk, E. P.; Pasichnyuk, R. I.; Błazejowski, J. *J. Electroanal. Chem.* **2005**, *580*, 41−49.
(6) Janiak, D. S.; Kofinas, J. P. *Anal. Bioanal. Chem.* **2007**, *389*, 399−404.
(7) Lin, Y.; Chen, J. H.; Chen, G. N. *Electrochim. Acta* **2008**, *53*, 2396−2401.
(8) Guo, W. Y.; Li, J. J.; Chu, H. H.; Yan, J. L.; Tu, Y. F. *J. Lumin.* **2010**, *130*, 2022−2025.
(9) Chen, M.; Wei, X. H.; Tu, Y. F. *Talanta* **2011**, *85*, 1304−1309.
(10) Martínez-Huitle, C..A.; Ferro, S. *Chem. Soc. Rev.* **2006**, *35*, 1324−1340.
(11) Martínez-Huitle, C..A.; Brillas, E. *Angew. Chem., Int. Ed.* **2008**, *47*, 1998−2005.
(12) Panizza, M.; Cerisola, G. *Chem. Rev.* **2009**, *109*, 6541−6569.
(13) Honda, K.; Yamaguchi, Y.; Yamanaka, Y.; Yoshimatsu, M.; Fukuda, Y.; Fujishima, A. *Electrochim. Acta* **2005**, *51*, 588−597.
(14) Yang, Y.; Oh, J.-W.; Kim, Y.-R.; Terashima, C.; Fujishima, A.; Kim, J. S.; Kim, H. *Chem. Commun.* **2010**, *46*, 5793−5795.
(15) Enache, T. A.; Chiorcea-Paquim, A.-M.; Fatibello-Filho, O.; Oliveira-Brett, A. M. *Electrochem. Commun.* **2009**, *11*, 1342−1345.
(16) Martínez-Huitle, C. A.; Ferro, S.; Reyna, S.; Cerro-López, M.; De Battisti, A.; Quiroz, M. A. *J. Braz. Chem. Soc.* **2008**, *19*, 150−156.
(17) Koppenol, W. H.; Liebman, J. F. *J. Phys. Chem.* **1984**, *88*, 99−101.
(18) Brillas, E.; Maestro, A.; Moratalla, M.; Casado, J. *J. Appl. Electrochem.* **1997**, *27*, 83−92.
(19) Chan, P. C.; Bielski, B. H. J. *J. Biol. Chem.* **1974**, *249*, 1317−1319.
(20) Wood, P. M. *Biochem. J.* **1988**, *253*, 287−289.
(21) Bielski, B. H. J.; Cabelli, D. E.; Arudi, R. L.; Ross, A. B. *J. Phys. Chem. Ref. Data* **1985**, *14*, 1041−1100.
(22) Bardouki, H.; Barcellos da Rosa, M.; Mihalopoulos, N.; Palm, W.; Zetzsch, C. *Atmos. Environ.* **2002**, *36*, 4627−4634.
(23) Schiller, J.; Arnhold, J.; Schwinn, J.; Sprinz, H.; Brede, O.; Arnold, K. *Free Radical Res.* **1999**, *30*, 45−57.
(24) Stylidi, M.; Kondarides, D. I.; Verykios, X. E. *Appl. Catal. B: Environ.* **2004**, *47*, 189−201.
(25) Bandara, J.; Kiwi, J. *New J. Chem.* **1999**, *23*, 717−724.
(26) Nosaka, Y.; Yamashita, Y.; Fukuyama, H. *J. Phys. Chem. B* **1997**, *101*, 5822−5827.
(27) Guinea, E.; Centellas, F.; Brillas, E.; Cañizares, P.; Sáez, C.; Rodrigo, M. A. *Appl. Catal. B: Environ.* **2009**, *89*, 645−650.
(28) Patel, B. A. In *Synthetic Diamond Films: Preparation, Electrochemistry, Characterization, and Applications*; Brillas, E., Martínez-Huitle, C. A., Eds.; John Wiley & Sons, Inc.: Hoboken, NJ, 2011; pp 513−550.
(29) Yang, N.; Nebel, C. E. In *Synthetic Diamond Films: Preparation, Electrochemistry, Characterization, and Applications*; Brillas, E., Martínez-Huitle, C. A., Eds.; John Wiley & Sons, Inc.: Hoboken, NJ, 2011; pp 551−619.

Removal of residual persistant organic pollutants in a real secondary effluent by anodic oxidation with BDD anodes

The work developed during my pre-doctoral stay in the AWMC of Australia consisted of the application of the AO with BDD to remove pollutants from a real matrix of wastewater. This work allowed deepening on the EAOPs processes in order to assess their viability. The removal of 29 POPs (see **Table 13**) including pharmaceuticals and herbicides in real concentration of 100 μg L^{-1} was studied for a real secondary effluent from a sewage treatment plant. Experiments with 10 L of this complex pollutant matrix were conducted in a pre-pilot flow plant containing a divided electrochemical filter-press reactor separated by a cation exchange membrane with a BDD anode and a stainless steel cathode of 40.8 cm^2 of electroactive area and a constant liquid flow rate of 162 mL min^{-1}. The assays were made during 24 or 48 h. In order to evaluate the mineralization and the reduction of oxidisable matter, the change in DOC and COD was monitored. The LC-MS/MS analysis after samples extraction with pre-concentration with solid phase extraction (SPE) carridges allowed following the pollutants decay during the process. The influence of experimental variables such as applied density current and pH was checked. The evolution of Cl^- ion present in the real wastewater was determined by measuring the contents of Cl^-, ClO_3^-, ClO_4^-, free Cl_2, and organohalogenated compounds generated during the treatment.

As can be seen in **Fig. 14,** pollutants **1-20** were completely removed in 24 h under all the conditions tested. Nevertheless, working at pH 3.0 and 800 mA almost all them disappeared. The last pollutants hardly degraded due to their recalcitrant character were mainly herbicides. This recalcitrant character favours the quicker competitive destruction of other compounds with oxidizing BDD($^\bullet$OH) formed at the anode from reaction (9).

Furthermore, **Fig. 15** highlights that operating at pH 3.0 and applying 800 mA it is possible to reach the same removal than applying 400 mA, but only in 2 h of treatment. This can be ascribed to the larger generation of BDD($^\bullet$OH) at greater current that accelerates the destruction of pollutants.

Table 13. *Persistent organic pollutants treated in the secondary effluent complex water matrix.*

Number	***Name***	***Type and Usage***
1	Sulfadiazone	Sulfonamide antibiotic
2	Diazonin	Organophosphate insecticide
3	Trimethoprim	Bacteriostatic antibiotic
4	Ranitidine hydrochloride	Pharmaceutical for gastric diseases
5	Norfloxacin	Fluoroquinolone antibiotic
6	Lincomycin	Lincosamide antibiotic
7	Gemfibrozil	Lipid regulating agent
8	Acetominophen	Analgesic and anti-inflammatory
9	Tramadol hydrochloride	Opioid analgesic
10	Metoprolol	β-blocker
11	Diclofenac	Non-steroidal anti-inflammatory and analgesic
12	Carbamazepine	Anticonvulsive
13	Caffeine	Metabolic stimulant
14	Enrofloxacin	Fluoroquinolone antibiotic
15	Venlafaxine hydrochloride	Anti-depressive
16	Citalopram	Anti-depressive
17	Roxithromycin	Macrolide antibiotic
18	Sertraline hydrochloride	Anti-depressive
19	Diuron	Herbicide
20	Hydrochlorothiazide	Thiazide diuretic
21	Ibuprophen	Non-steroidal anti-inflammatory and antipyretic
22	Metalochlor	Aniline derivative herbicide
23	Ditriazoate	Radiocontrast
24	Phenytoin	Antiepileptic
25	Iopromide	Contrast for intravascular use
26	Atrazine	Herbicide
27	DEET	Insect repellent
28	2,4-D	Herbicide
29	Trichlopyr	Herbicide

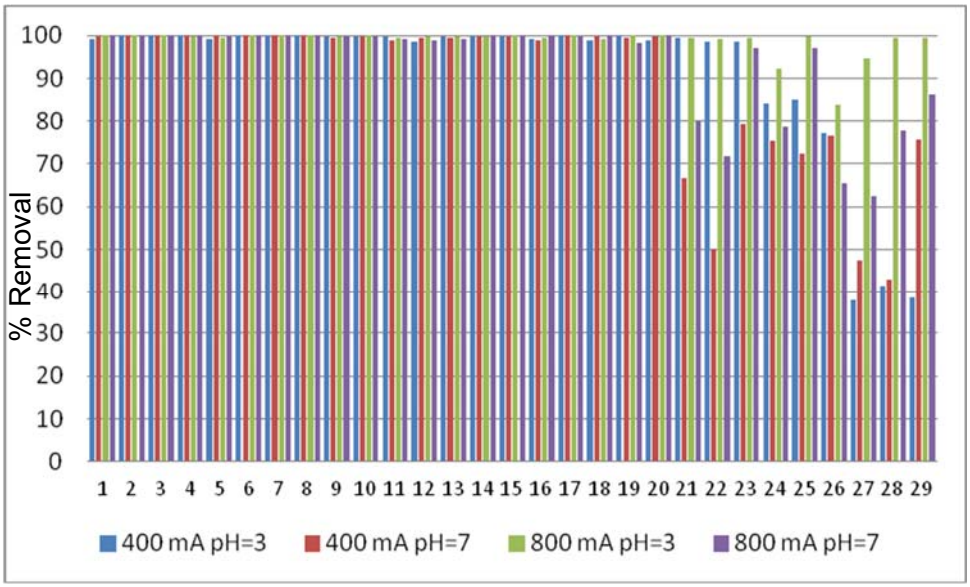

Figure 14. *Percentage of pollutant removal listed on Table 13 in a real wastewater matrix after 24 h of AO treatment with BDD in a pre-pilot flow plant of 10 L.*

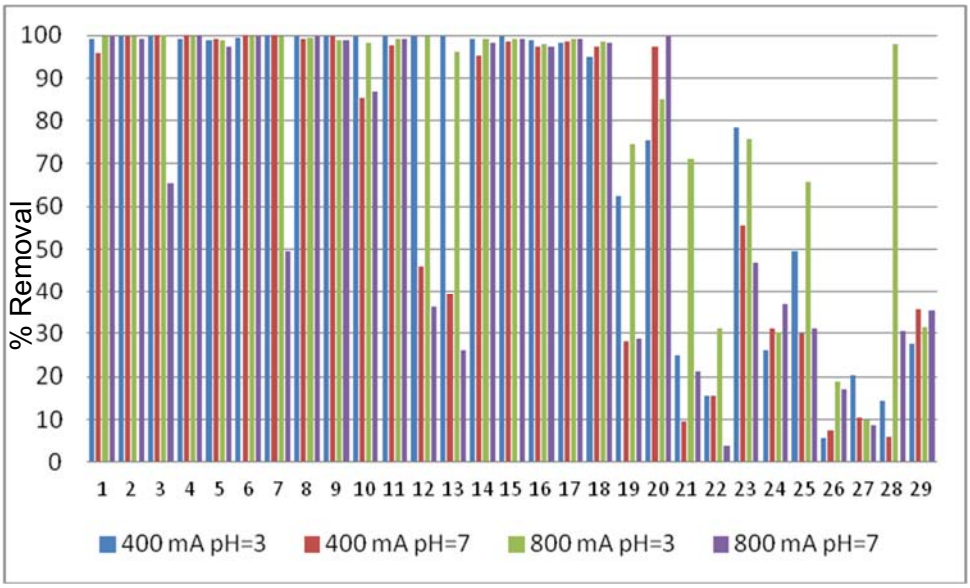

Figure 15. *Percentage of pollutants removal in a pre-pilot flow plant of 10 L after 2h of AO with BDD.*

The COD and DOC evolution depicted in **Fig. 16a** and **b**, respectively, also showed higher effectiveness for organic matter removal at the higher current of 800 mA instead of applying 400 mA. The pH of the reaction medium was also important for the destruction of organics, and so, the removal of COD and DOC was strongly enhanced at pH 3 in front of neutral pH. Note that the main DOC content was due to the presence of recalcitrant natural organic matter (NOM) contained in the real water sample, which is

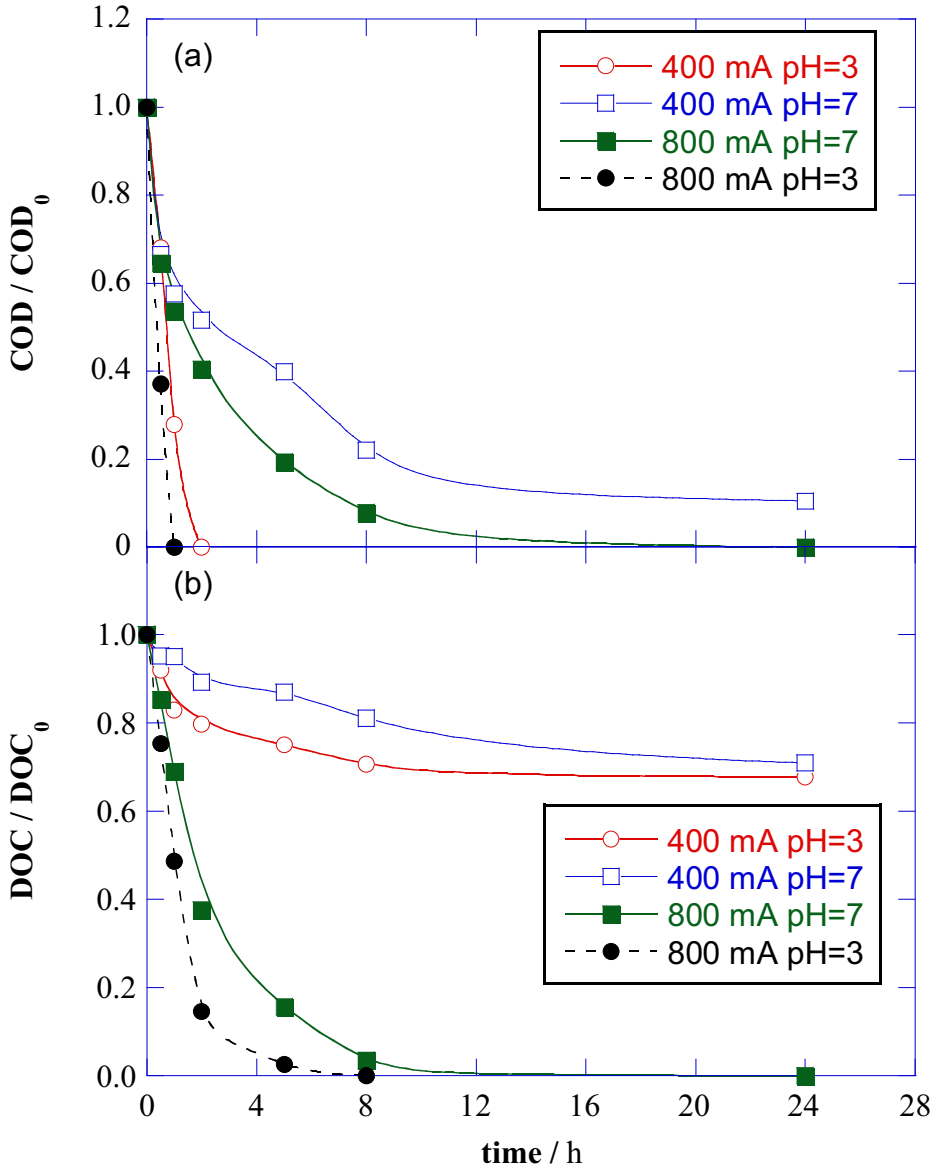

Figure 16. *(a) Chemical oxygen demand and (b) dissolved organic carbon decay during the AO treatment with BDD of a real water matrix of 29 persistent organic pollutants in a secondary effluent from a sewage water treatment plant.*

also completely removed during the treatment. Results of **Fig. 16** then demonstrate that the AO process with BDD is able to destroy the POPs, their by-products (sometimes even worse than the POPs) and even the NOM.

A content of 305.5 mg L^{-1} of Cl^- ion in the secondary effluent was determined. In fact, the presence of Cl^- and other inert inorganic ions in solutions are the responsible of the water conductivity and enable direct treatment without adding any salt as supporting electrolyte. It is well known that the oxidation of Cl^- ion at the BDD anode yields Cl_2, and ClO^-/HClO depending on pH, which can attack the organic matter generating organochlorinated compounds that are even more toxic and hazardous than the treated pollutants. Besides, these chlorinated species con also evolve to other ions like chlorate (ClO_3^-) or perchlorate (ClO_4^-) that are considered noxious. For all these reasons, the knowledge of the evolution of chloride ion and chlorinated species is of great interest to evaluate the viability of AO with BDD for POPs remediation.

As expected, **Fig. 17a** highlights that the Cl^- concentration underwent a slow, but progressive, decay during the treatment. A continuous generation and accumulation of ClO_3^- and ClO_4^- ions can be observed in **Figs. 17 band c**, respectively. At higher current more amount of ClO_4^- was produced due to the quicker oxidation of ClO_3^-. ClO_4^- ion was always accumulated in larger extent at pH 7.0. The AOX measurements allowed evaluating the organochlorates generated during the treatments (see **Fig. 18**), which showed a low accumulation (< 20 μM), considerably under the limits by law.

The ClO^- ion and chloroamines generation were also determined in order to perform a complete mass balance. The final results after 24 h of treatment are summarized in **Table 14**, were the concentrations of all species are expressed as mg L^{-1} of Cl. The sum of all the determined species disagree with the initial concentration of Cl^- ion due to the loss of Cl_2 gas. From the chlorine mass balance, one can conclude that the method is viable due to the lower concentration of chlorine species generated and accumulated in the different media, always lower than the recommended concentrations by law. Furthermore the generation of ClO^- and chloramines stimulate water disinfection processes.

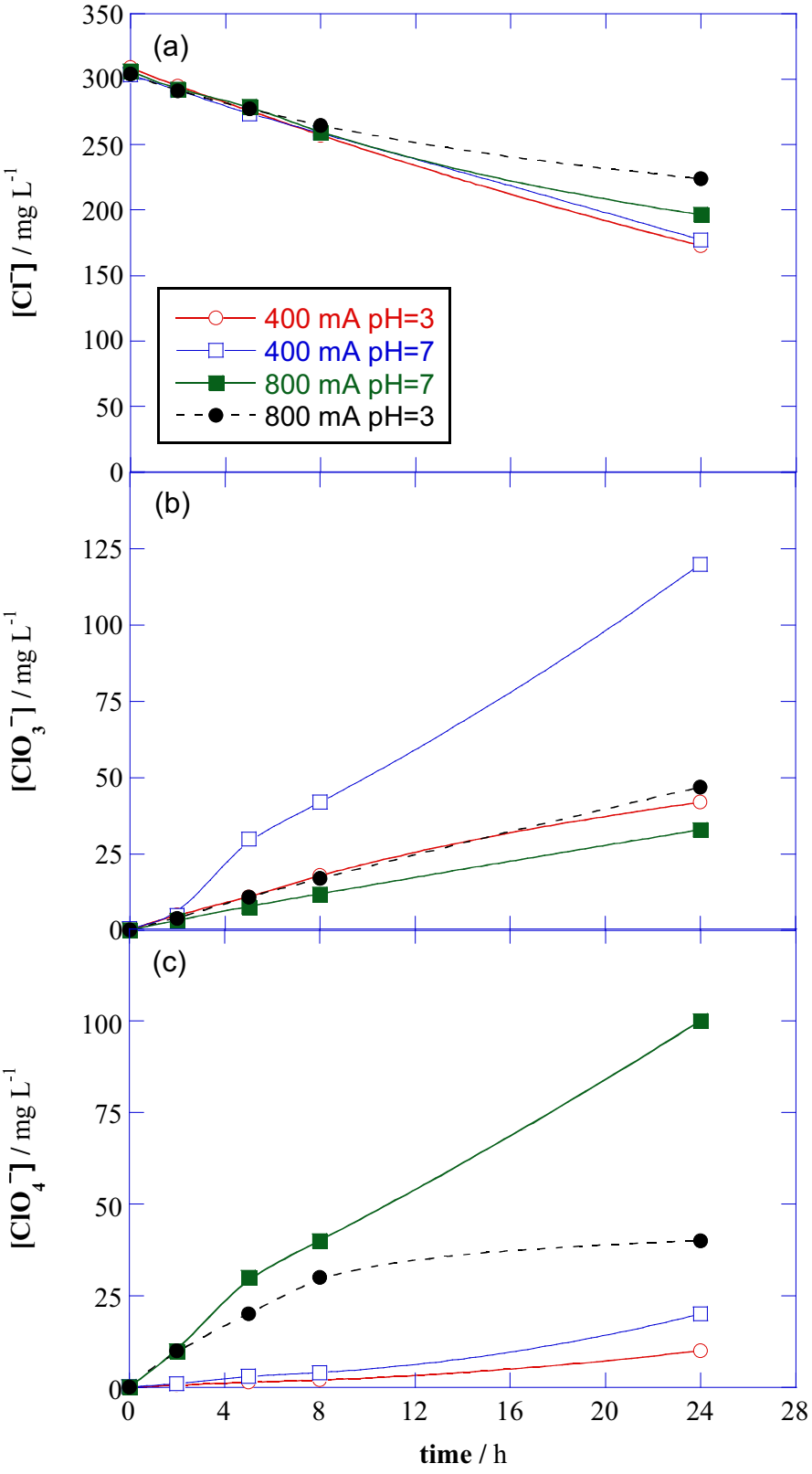

Figure 17. *Change of concentration of (a) Cl^-, (b) ClO_3^- and (c) ClO_4^- ions during the AO treatment with BDD of 29 POPs in a pre-pilot flow plant of 10 L using a divided electrochemical filter-press cell.*

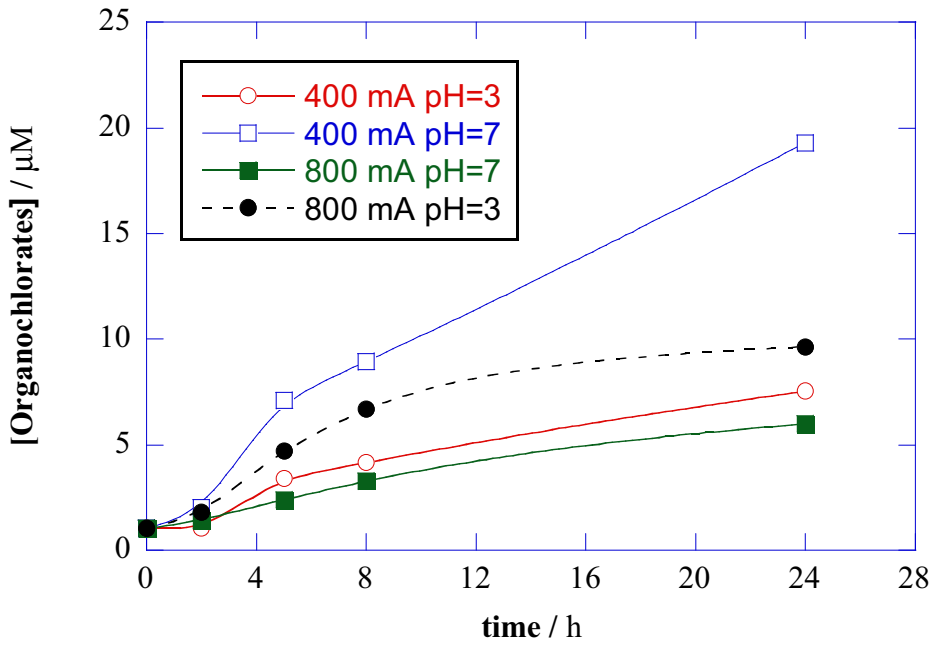

Figure 18. *Generated organochlorinated species during the same treatments of Fig. 17.*

Table 14. *Concentration of chlorinated species accumulated after 24 h of AO with BDD at 800 mA expressed as mg L^{-1} of Cl. Initial Cl^- concentration in the secondary effluent of 305.5 mg L^{-1}.*

	Cl^-	ClO^-	ClO_3^-	ClO_4^-	Chloramines	Total	Initial-total
400 mA pH= 3	172.0	11.71	17.71	3.53	68.0	273.09	32.40
400 mA pH= 7	171.0	17.24	50.60	7.07	56.8	302.71	2.79
800 mA pH= 7	196.0	0.21	13.92	35.35	2.2	247.44	57.82
800 mA pH= 3	224.0	0.20	19.82	14.14	6.3	264.44	41.06

The main conclusion of this work developed is that it has been demonstrated the effectiveness of AO with BDD to decontaminate a real complex matrix of pollutants at real concentration in secundary effluents from sewage treatment plants. The study has shown not only the complete removal of the organic matter associated to these pollutants and NOM, but also their viability by the quantification of the low amounts of chlorinated species generated during the treatment.

RESUMEN

El principal objetivo de esta tesis ha sido el estudio de la aplicabilidad de metodologías electroquímicas de oxidación avanzada al tratamiento de aguas contaminadas con contaminantes orgánicos persistentes. En este sentido, los resultados de la investigación se presentan agrupados en cuatro bloques referente al tratamiento de fármacos, colorantes azoicos, un efluente real contaminado con 29 POPs en concentración real (trabajo desarrollado durante mi estancia pre-doctoral en el AWMC de la UQ de Australia) y, finalmente, el estudio de ECL sobre ánodo de BDD como método de estudio de la electrogeneración de radicales fisisorbidos.

El tratamiento de aguas sintéticas contaminadas con los fármacos antibacterianos FLU y CHL mediante los EAOPs conocidos como AO, EF, PEF y SPEF puso de manifiesto la gran eficiencia de estos procesos de descontaminación. La comparación entre los cuatro procesos evidenció una más rápida eliminación del contaminante de partida en el orden AO -Pt < AO -BDD < EF < PEF < SPEF. La utilización de un ánodo de BDD en lugar de uno de Pt tanto en AO como en los EAOPs basados en la reacción de Fenton favoreció los procesos degradativos de forma apreciable. Al comparar los procesos de AO se pudo comprobar que mientras que con el ánodo Pt el fármaco no se mineralizaba, con el BDD alcanzaba un 78% de eliminación del DOC en 6 h. Estos resultados suponen una prueba fehaciente de la mayor reactividad de los radicales BDD(•OH) frente a los de Pt(•OH). Por otro lado, los análisis de HPLC permitieron constatar que si bien el ánodo de Pt es incapaz de mineralizar, sí que favorece los procesos de conversión del contaminante de partida disminuyendo su concentración en disolución, aunque más lentamente que el ánodo de BDD.

La mayor eficiencia de los EAOPs basados en la reacción de Fenton se relaciona con la doble vía de generación de radicales, los BDD(•OH) fisisorbidos en el ánodo que son los generados en AO y los •OH en el seno de la disolución generados mediante la reacción de Fenton. Los radicales •OH generados en el seno de la disolución presentan una mayor reactividad debido a que no están controlados por el transporte de materia hacia/desde los electrodos, eliminando los compuestos aromáticos en tiempos muy cortos. El proceso de EF presenta, sin embargo, cierta limitación al alcanzar un porcentaje de mineralización en el que se mantiene prácticamente estacionario que fue de un 77% para la FLU y de 81% para el CHL. Este comportamiento se debe a la formación de complejos de hierro (III) con algunos ácidos carboxílicos generados como intermedios finales, por ejemplo el ácido oxálico, que son aún más recalcitrantes que el ácido libre. Afortunadamente,

muchos de estos complejos son rápidamente fotodegradados por la luz UVA en el proceso PEF, donde se alcanzan mineralizaciones prácticamente completas en 360 min y 270 min de tratamiento para la FLU y el CHL, respectivamente. Cuando se utilizó radiación solar como fuente gratuita de radiación en lugar de la lámpara UVA, se obtuvieron mineralizaciones completas para el CHL en tan solo 90 min de tratamiento. Este hecho pone de manifiesto la influencia de la intensidad de radiación en la cinética de fotólisis de los complejos, donde la radiación UV de la luz solar de 30 W m^{-2} es hasta seis veces superior a la de 5 W m^{-2} emitida por la lámpara.

Se estudiaron diferentes variables como parámetros de control de los procesos EAOPs, tales como la concentración inicial de contaminante, la densidad de corriente aplicada y la concentración del catalizador de Fenton o sea el Fe^{2+}. La influencia de la concentración inicial de contaminante se evaluó tratando disoluciones de CHL con contenidos de 10 a 100 mg L^{-1} de DOC iniciales por SPEF, donde las disoluciones tratadas se mineralizaron totalmente a tiempos similares independientemente de su concentración inicial. Estos resultados indican que un aumento de la concentración inicial incrementa la eficiencia del proceso con diferencias que van del 12% al 100% de la MCE, que se justifica por la inhibición de las reacciones parásitas con el aumento de la concentración del DOC. Los análisis de HPLC para la degradación de CHL permitieron la determinación de k_1, que sorprendentemente resultó ser mayor para menores concentraciones iniciales de CHL. Este hecho experimental se explica por la corta vida de los radicales hidroxilos generados, de 4×10^{-9} s, que deben ser continuamente generados y presentan una concentración constante en el medio que queda englobada dentro de la constante cinética k_1, cuyo valor depende de cada condición experimental. Con el aumento de la DOC en solución disminuye la acumulación de radicales y en consecuencia decrece el valor de k_1.

Un parámetro de control electroquímico indiscutible es la *j*. La influencia de esta variable en el tratamiento de ambos antibióticos era similar. El incremento de *j* produjo un aumento gradual pero no proporcional de la velocidad de mineralización, alcanzándose mayores porcentajes de eliminación a menores tiempos de tratamiento. En contrapartida, el incremento de *j* causó un descenso de la MCE debido al enaltecimiento de las reacciones parasitas. La pérdida de eficiencia es la causa directa por la que la velocidad de degradación no aumenta proporcional con *j*. A partir de estos resultados se puede concluir que una mayor *j* no siempre mejora las condiciones de tratamiento, puesto que disminuye la MCE y además aumenta el consumo energético.

La concentración inicial de Fe^{2+} es un parámetro que ha sido ampliamente estudiado en nuestro grupo, donde se había determinado que un valor de 0,05 mM era óptima en una amplia mayoría de casos. Se observó que mayores concentraciones inhibían los procesos degradativos ya que el aumento de concentración de Fe^{2+} en disolución favorecía a su vez el aumento de la reacción de oxidación del catalizador a Fe^{3+} con el radical $^{\bullet}OH$, inhibiendo consecuentemente la reacción de Fenton y consumiendo radicales perdiendo así capacidad oxidativa del sistema. Sin embargo, la FLU es una excepción pues se determinó que la concentración óptima de Fe^{2+} de 2,0 mM. Ello se debe a que el Fe^{2+} juega un doble papel, el ya conocido de catalizador y como agente complejante de la FLU. La formación del complejo anaranjado de Fe^{2+} con FLU aumenta la solubilidad del contaminante e inhibe la reacción de Fenton al "capturar" el catalizador por la formación del complejo.

Los análisis de LC-MS, de HPLC de fase inversa y de exclusión iónica y la cromatografía iónica permitieron la identificación y cuantificación de diferentes intermedios de mineralización de los contaminantes. Al contener los antibióticos en sus estructuras moleculares N y F (en el caso de la FLU) o Cl (en el caso de CHL) el proceso de mineralización conlleva la generación de iones inorgánicos como NO_3^-, NH_4^+, Cl^- y F^- tal y como se detectó y cuantificó por cromatografía iónica. En ambos casos, se liberó y acumuló en el medio rápidamente el ion Cl^-, el cual fue posteriormente oxidado a Cl_2. Por otro lado, el N contenido tanto en la FLU como en el CHL se mantuvo invariable en disolución y fue principalmente transformado y acumulado en forma de ion NO_3^- y ácido oxámico, aunque también se detectaron pequeñas concentraciones de ion NH_4^+.

Los análisis de muestras de disoluciones de CHL tratadas por EAOPS analizadas por LC-MS, permitieron la identificación de diferentes intermedios aromáticos de degradación y de sus derivados hidroxilados. Los análisis de HPLC por exclusión iónica detectaron ácidos carboxílicos de cadena corta procedentes de la rotura y apertura de los anillos aromáticos de la FLU y del CHL. A partir de todos los intermedios detectados para la FLU y el CHL se propusieron las correspondientes secuencias de reacción para su mineralización por los distintos procesos ensayados.

Cabe destacar que en los tratamientos de la FLU y del CHL se detectaron como intermedios de degradación los ácidos oxálico y oxámico, ambos acumulados en gran concentración. El DOC correspondiente a la suma de ambos intermedios suponía en

ambos casos la práctica totalidad del DOC en disolución en los tiempos finales de las electrólisis. Este hecho puso de manifiesto el alto carácter recalcitrante de estos compuestos y su relevancia e influencia en la eficiencia de los EAOPs, por lo que se realizó un estudio más profundo sobre ellos.

Se realizaron ensayos de fotólisis de los ácidos oxálico y oxámico en ausencia y en presencia de iones hierro (II) y (III). Los análisis de las cinéticas de degradación de ambos compuestos demostraron que los complejos de los ácidos con el Fe(III) son las especies fotoactivas, conduciendo a una rápida mineralización de las disoluciones, tal y como se había observado en PEF. Se consideró así que el proceso de oxidación por fotólisis es debido a una reacción de transferencia de carga del ligando al metal. Por otro lado, los ensayos con EAOPs demostraron que la oxidación del acido oxálico libre es mucho más rápida que la de sus complejos con Fe(II) y Fe(III). Sin embargo, ocurre todo lo contrario en el caso del ácido oxámico. Este comportamiento fue corroborado a través del análisis por voltamperometría cíclica. También se pudo comprobar que la curvas de de descensos del DOC correspondientes al tratamiento con celdas de BDD/SS y de BDD/ADE ambos en presencia de Fe^{2+} eran superponibles. Estos resultados indican que la oxidación de estos ácidos está solamente relacionada con el ánodo de BDD y los radicales BDD($^{\bullet}$OH) y no con los $^{\bullet}$OH generados en las condiciones electro-Fenton (BDD/ADE en presencia de Fe^{2+}). El tratamiento de AO en presencia de Fe^{2+} e irradiación con luz UVA permitió alcanzar en ambos casos una mineralización completa en menores tiempos de tratamiento. El tratamiento de mezclas de oxálico-oxámico por los diferentes tratamientos evidenció cambios en las constantes k_1 de cada compuesto en función de la relación de concentración oxálico/oxámico, debido no sólo a que las reacciones de oxidación son competitivas sino a que también lo son la formación de sus complejos con los iones hierro.

Los prometedores resultados obtenidos en el tratamiento de disoluciones con CHL por SPEF desembocó en el escalado del proceso a una planta pre-piloto de 10 L conteniendo una celda filtro prensa de Pt/ADE acoplada a un CPC como fotorreactor solar. Para el tratamiento de 10 L aplicando 100 mA cm^{-2} se obtuvieron eliminaciones del 89% de DOC en 180 min con un coste energético total de 0,347 kWh g^{-1} DOC (30,8 kWh m^{-3}) y un coste estimado de 4,35 € m^{-3}.

Dentro del estudio del tratamiento de aguas contaminadas con fármacos mediante EAOPs, se consideró el tratamiento de un agua real contaminada con FLU. En este

estudio se demostró que tanto los tratamientos EF como PEF eran capaces de eliminar la NOM del efluente real así como el contaminante FLU con la misma eficiencia y prácticamente velocidad en que era eliminado en el tratamiento del agua sintética.

El tratamiento de aguas sintéticas contaminadas con los colorantes azoicos AO7, AR151, DB71 y DY4 mediante SPEC, AO, EF, PEF, PA-EF y SPEF puso de manifiesto la viabilidad de los mismos en el tratamiento de estos contaminantes.

El proceso de decoloración se estudió en profundidad dado el elevado interés industrial como principal objetivo en el tratamiento de este tipo de aguas. Se consideró la decoloración de tres colorantes con una estructura similar e idénticos grupos funcionales (-OH, $-SO_3^-$) pero con número creciente de enlaces azo. Estos colorantes fueron el monoazo AO7, el diazo RA151 y el triazo DB71. La decoloración mediante EF demostró ser mucho más rápida (entre 30-60 min) que por AO donde se requiere más de 6 h. También se comprobó que otros cátodos diferentes del ADE como el grafito propiciaban procesos de reducción del enlace azo aumentando la velocidad de decoloración debido a una vía alternativa de degradación del compuesto. Es por ello que se aconseja utilizar el ADE o trabajar en celdas separadas para estudiar exclusivamente el proceso de oxidación. Para el estudio comparativo se introdujo un parámetro experimental denominado velocidad de decoloración inicial (δ_0), se define como la pendiente de la curva del porcentaje de de eliminación de color con el tiempo al inicio del proceso (20-25% de decoloración) donde el responsable del color es primordialmente el colorante de partida debido a la baja concentración de intermedios coloreados en ese estadio La representación de este parámetro versus la concentración de enlaces azoicos totales en disolución evidenció que la velocidad de decoloración estaba estrechamente ligada con el número de enlaces azo por molécula. La disminución de la velocidad de decoloración se justificó por la mayor estabilización de los sistemas π conjugados que hace que se precise de una mayor energía de activación para el ataque electrofilico de los radicales hidroxilo. El incremento de la *j* se traduce en un aumento de la δ_0 hasta un valor máximo, relacionado con el enaltecimiento de las reacciones parásitas como ya se comentó anteriormente. El aumento de la velocidad de decoloración con *j* era menor al aumentar el número de enlaces azo por molécula. Este hecho empírico se puede relacionar nuevamente con la estabilización de los sistemas π. Los valores determinados de k_1 y k_{dec} son diferentes entre sí aún cuando muestran las mismas tendencias, por lo que se puede concluir que la consideración de que la k_{dec} describe la cinética de decoloración del compuesto es errónea.

La diferencia entre ambas constantes se debe a la generación de intermedios de oxidación del colorante que presentan unos valores de $\lambda_{máx}$ de absorción similares o cercanas a las del contaminante de partida. Este hecho es fácilmente constatable en los espectros de absorción de UV-vis registrados en los que se aprecia un desplazamiento del valor de $\lambda_{máx}$ y de un ensanchamiento de la banda con el tiempo de tratamiento.

El estudio del comportamiento de los ácidos oxálico y oxámico propició el desarrollo de un método derivado que denominamos PA-EF. Esta técnica consiste en aplicar el tratamiento de EF hasta la máxima acumulación de los ácidos carboxílicos, parar la electrólisis y posteriormente irradiar la disolución con luz UVA para fotolizar los complejos de Fe(III)-carboxilato generados y acumulados en el medio. El resultado obtenido en el tratamiento de disoluciones de DY4 demostró que se podía alcanzar mineralizaciones completas por esta técnica en tiempos de tratamiento similares a los utilizados en PEF pero con un consumo de energía apreciablemente menor.

Se realizó el escalado del proceso PEF a una planta pre-piloto de 10 L para tratar las disoluciones contaminadas mediante SPEF, obteniéndose mineralizaciones prácticamente completas en 240 min. Como diferencia sustancial respecto al escalado anteriormente realizado en el tratamiento de CHL, se utilizó como fuente renovable de energía para el funcionamiento de la planta la proporcionada por una placa fotovoltaica acoplada al sistema, con lo que el consumo energético se redujo en su totalidad.

Se estudiaron los efectos de variables clave sobre el tratamiento de colorantes como son la concentración inicial de substrato y del catalizador Fe^{2+} o de *j*, encontrándose comportamientos similares a los de los fármacos. Los análisis de HPLC y de LC-MS permitieron identificar diferentes compuestos aromáticos y sus hidroxilados, ácidos carboxílicos e iones inorgánicos generados en el tratamiento de DY4 por SPEF, permitiendo proponer su secuencia de reacción. Además, los análisis de iones realizados junto con las medidas de TN permitieron comprobar que durante el tratamiento de los colorantes azoicos el N inicial se pierde primordialmente en forma de especies volátiles de N, como N_2 o NOx, y que el remanente en disolución (~20-40%) está en forma de NH_4^+ y NO_3^- en cantidades similares.

En colaboración con el CPT de la UB se sintetizaron y caracterizaron fotoánodos de TiO_2 que se aplicaron al tratamiento de colorantes por SPEC. Los resultados experimentales evidenciaron que aguas contaminadas con bajas concentraciones del colorante AO7 (15

mg L^{-1}) pueden ser completamente decoloradas en 180 min de tratamiento. Se estudió la influencia de *j* en el tratamiento por SPEC hasta 2 mA cm^{-2}. Se observó que la aplicación de una corriente anodica tan baja como 0,25 mA cm^{-2} incrementaba notablemente la decoloración en comparación con el proceso SPC (sin corriente). Se determinó que la *j* óptima para el tratamiento SPEF era de 1 mA cm^{-2}. El pH demostró afectar de forma directa el proceso de degradación del colorante AO7 ya que los espectros registrados tras el tratamiento indicaban la formación de intermedios diferentes. Además, sólo a pH 7,0 se alcanzó la decoloración completa, por lo que se consideró como el pH óptimo. Los análisis de HPLC por exclusión iónica de las disoluciones de AO7 tratadas por SPEC pusieron de manifiesto que el 86% del DOC remanente al final del proceso correspondía a ácidos carboxílicos de cadena corta y bajas concentraciones de ácido ftálico que provenían de la rotura de los anillos aromáticos del colorante.

Dado que el ácido ftálico es un intermedio comúnmente identificado en el tratamiento de colorantes y otros contaminantes con anillos naftalénicos en su estructura, se estudió este intermedio para clarificar de forma más completa su mecanismo de degradación. En este estudio se evaluó la actividad de los iones de Cu(II) y de Fe(III) como catalizadores de la reacción de Fenton y de sus mezclas como co-catalizadores. Se pudo comprobar que las mezclas de ambos catalizadores permitían obtener mineralizaciones más rápidas ya que los complejos de los ácidos carboxílicos con Cu(II) se degradaban por la acción del radical $^{\bullet}OH$, cosa que no tiene lugar con los complejos que se forman competitivamente con Fe(III). Se propuso como composición óptima de catalizador la mezcla de 0,125 mM de Cu^{2+} y 0,375 mM of Fe^{3+}. Los análisis por cromatografía de HPLC y de LC-MS permitieron detectar 11 derivados aromáticos y seis ácidos carboxílicos de cadena corta, a partir de los cuales se planteó una secuencia de degradación que puede ser aplicable siempre que aparezca el ácido ftálico o sus derivados como intermedios de reacción.

Durante la estancia pre-doctoral realizada en el AWMC de la UQ en Australia se descontaminó un efluente secundario de una depuradora municipal que contenía una mezcla compleja de 29 POPs en concentraciones de 100 μg L^{-1} por AO en una planta pre-piloto de 10 L con una celda tipo filtro prensa de dos compartimentos. Se encontró que todos los contaminantes eran completamente eliminados a pH 3,0 y 20 mA cm^{-2} tras 24 h de tratamiento, excepto para el fármaco fenitoína y los herbicidas DEET y atrazina que fueron eliminados en un 90%. Los análisis de COD y DOC demostraron que la NOM

presente en el agua tratada también se mineralizaba completamente. Asimismo, se llevó a cabo un profundo estudio sobre la evolución de los 305 mg L^{-1} de ion cloruro presentes en el efluente secundario. Después de 24 h de AO, este ión generó ClO_3^- (13,92 mg L^{-1} de Cl), ClO_4^- (35,35 mg L^{-1} de Cl) y concentraciones muy bajas de organoclorados (5 μM). El contenido de ion Cl^- remanente fue de 196 mg L^{-1}. El estudio de la evolución del Cl^- demostró la posibilidad de eliminar los POPs de aguas reales con una baja producción de organoclorados durante el tratamiento.

La investigación sobre la ECL con ánodos de BDD permitió aportar evidencias que demuestran que los radicales $^{\bullet}OH$ no son generados en condiciones de pH muy básicas (12,0), donde se electrogenera en su lugar el anión radical superóxido $O_2^{\bullet-}$. La oxidación directa de luminol en ánodos de BDD emitía luminiscencia en un rango definido de potencial, pero tras la adición de H_2O_2 se observó la emisión de luz en un amplio rango de potenciales (de 0.5 a 5.0 V vs Ag|AgCl, KCl(sat.)). Se demostró que la presencia del anión hidroperóxido HO_2^- propiciaba la electrogeneración de $O_2^{\bullet-}$ que resultó ser, tal y como probó la utilización de *scavengers* específicos, el responsable directo del incremento de emisión de luz en ECL con una intensidad hasta 63 veces superior en presencia de H_2O_2 que en su ausencia. Los resultados obtenidos abren la puerta al desarrollo de nuevos biosensores de BDD, a la mejor comprensión de los mecanismos de oxidación de compuestos orgánicos por ROS y a la caracterización de ánodos de BDD.

CONCLUSIONS

This work has led to the following conclusions:

1. Acidic aqueous solutions of 62 mg L^{-1} of flumequine can be completely mineralized by PEF in 360 min using a stirred BDD/ADE tank reactor. Solutions with 245 mg L^{-1} chloramphenicol were completely mineralized by SPEF in 90 min in the 100 mL tank reactor and in 180 min when the process was scaled-up to a 10 L pre-pilot flow plant, with an energy cost of 0.347 kWh g^{-1} DOC corresponding to 0.141 € kWh^{-1}.

2. In the flumequine treatment by EF and PEF, the Fe^{2+} ion played a double role, since it formed an orange complex with the drug enhancing its solubility and acted as catalyst of the Fenton's reaction.

3. The decay kinetics for both antibiotics always followed a pseudo-first-order reaction with increasing rate constant as the current rose. Similar drug abatement for EF and PEF at each current tested was found. This evidenced that the complex of Fe(II) with flumequine was not directly photolyzed by UVA irradiation, that chloramphenicol was not photodegradable and that the photo-Fenton reaction (17) participates very poorly to generate $^{\bullet}OH$.

4. The increase in drug concentration enhanced the efficiency of the mineralization process due to the inhibition of parasitic reactions, but decreasing the pseudo-first order rate constant because the $^{\bullet}OH$ generation was affected by the concentration of other compounds in solution.

5. The degradation of flumequine and chloramphenicol involved the formation of short-linear aliphatic carboxylic acids due to the rupture of the aromatic ring. Oxalic and oxamic acids are the ultimate and more recalcitrant compounds generated.

6. The improvement of the DOC removal in the PEF process was related to the UVA irradiation, mainly due to the rapid photodecarboxylation of some Fe(III)-carboxylate complexes such as formed by oxalic and oxamic acids.

7. The F of flumequine was lost as F^- ion, whereas the Cl of chloramphenicol was released as Cl^- ion to be further oxidised to Cl_2. In both cases, the fate of the initial N was NO_3^- ion and oxamic acid, although NH_4^+ ion was also produced in lesser extent.

8. The treatment of flumequine in real wastewater led to similar degradation degree to that of synthetic solution. The NOM influenced poorly the mineralization process and it

was removed under the main oxidation action of $^{\bullet}OH$. The PEF treatment could then be applicable to the treatment of flumequine in real wastewater.

9. The treatment of 2.08 mM of oxalic and oxamic acids showed that they were efficiently removed by AO with BDD in the presence of Fe^{2+} and simultaneously irradiated with UVA light due to the high photoactivity of their Fe(III) complexes and their oxidation by BDD($^{\bullet}OH$). Fe(III)-maleate complexes were not photodecomposed, but they were quickly destroyed with $^{\bullet}OH$.

10. Fe(III)-oxamato complexes presented a lower photoactivity than Fe(III)-oxalato ones. The photodegradation of Fe(III)- oxamate complexes favoured the release of NH_4^+ ion. Also, it was well proven that these Fe(III) complexes were not attacked with $^{\bullet}OH$ in the bulk generated by Fenton's reaction, although they were slowly mineralized by BDD($^{\bullet}OH$) and also by direct charge transfer at the BDD anode.

11. Voltammetric analysis showed that Fe(III)-oxamato complexes were oxidized more quickly with BDD($^{\bullet}OH$) than the free acid, whereas the opposite trend happened for oxalic acid which was easily removed than its Fe(III) complexes.

12. The DOC content in solution was directly related with the oxalic or oxamic acid concentration at each time, indicating an insignificant formation of by-products.

13. The treatment of oxalic and oxamic acids mixtures evidenced that both acids were independently oxidized by AO with BDD. However, remarkable influences of their concentration ratio on their degradation rate were found in the presence of Fe^{2+} and when the solutions were simultaneously irradiated with UVA light. The effect was associated with the different distribution of iron complexes in solution.

14. The increase in Fe^{2+} concentration inhibited the oxidation process of oxamic acid because of the enhancement of the oxidation of Fe^{2+} to Fe^{3+} The loss of oxidation power was also observed in the distribution of NH_4^+, NO_3^- and NOx since greater amounts of Fe^{2+} ion caused a lower accumulation of NO_3^- ion.

15. The decolorization process of azo dyes by EF showed a marked influence of the number of azo bonds per molecule, dropping the initial decoloration rate with increasing the number of azo bonds. This phenomenon was explained by the generation of more stable conjugated π systems when the number of azo bonds per molecule increased.

16. The decolorization rate was limited by the slower parallel destruction of colored conjugated by-products that are formed in larger extent in diazo and triazo dyes than in monoazo ones.

17. The initial decoloration rate increased with rising *j* due to the greater generation of $^{\bullet}OH$ that accelerated the solution color removal. HPLC analysis confirmed the complete removal of azo dyes by EF which disappeared in shorter times at higher applied current density and lower number of azo dyes per molecule.

18. The pseudo-first-order rate constants for azo dyes removal and their respective initial decoloration rate showed the same trends. Consequently, the initial decoloration rate is a simple and suitable parameter to analyze the azo dyes decolorization process. Although the pseudo-first-order kinetics determined by the absorbance decay showed the same trends than the rate constants found by HPLC, their values were very different as a result of the formation of colored by-products during decolorization.

19. The PEF and PA-EF processes of DY4 solutions yielded almost total mineralization in 4 h. The PA-EF method was always more economic than PEF and at higher *j* even less expensive than EF.

20. The major part of N of the azo bonds was lost as *N*-products volatiles such as N_2 and NO_x. The remaining N in solution was mainly present as NH_4^+ ion.

21. The scale-up to an autonomous 10 L pre-pilot flow plant demonstrated the viability of SPEF to mineralize azo dyes in short times and treat polluted effluents without energy consumption. The cost of the process only corresponded to the initial investment.

22. The degradation of a real secondary effluent of a wastewater treatment plant, polluted with a complex pollutant matrix in an pre-pilot flow plant with a divided reactor by AO with BDD, evidenced the viability to mineralize and remove completely all the pollutants apart from phenitoin, atrazine and DEET, which were only removed up to 80-90 % in 24 h.

23. Low amounts of chlorate and perchlorate ions as well as of organochlorinated species were formed during the AO treatment with BDD of the polluted secondary effluent as a result of the oxidation of its content of 305 mg L^{-1} of chloride ion. These promising results allow us to consider this method as a viable treatment for POPs removal under real conditions.

24. The study of the electrochemiluminiscence of luminol demonstrated the electrogeneration of physisorbed radicalary species at the BDD anode. Voltammetric analyses and the use of specific quenchers and scavengers proved the generation of radical anion superoxide $O_2^{\bullet -}$ and the inhibition of $^{\bullet}OH$ generation at alkaline pH.

25. The findings on the electrochemiluminiscence of luminol can contribute to develop better techniques to characterize the conductive-diamond electrodes properties, to improve the understanding of the oxidation mechanisms of organics by ROS and the design of new BDD sensors for biomolecules.

REFERENCES

Akpan, U.G., Hameed, B.H., 2009. *Parameters affecting the photocatalytic degradation of dyes using TiO_2-based photocatalysts: A review*. J. Hazard. Mater. 170, 520-529.

Almeida, L.C., Garcia-Segura, S., Bocchi, N., Brillas, E., 2011. *Solar photoelectro-Fenton degradation of paracetamol using a flow-plant with a Pt/air-diffusion cell coupled with a compound parabolic collector: Process optimization by response Surface methodology*. Appl. Catal. B: Environ. 103, 21-30.

Almeida, L.C., Garcia-Segura, S., Arias, C., Bocchi, N., Brillas, E., 2012. *Electrochemical mineralization of the azo dye Acid Red 29 (Chromotrope 2R) by photoelectro-Fenton process*. Chemosphere 89, 751-758.

Andreozzi, R., Caprio, V., Insola, A., Marotta, R., 1999. *Advanced oxidation processes (AOP) for water purification and recovery*. Catal. Today 53, 51-59.

Andreozzi, R., Marotta, R., Nicklas, P., 2003. *Pharmaceuticals in STP effluents and their solar photodegradation in aquatic environmen*t. Chemosphere 50, 1319-1330.

Anotai, J., Singhadech, S., Su, C.C., Lu, M.C., 2011. *Comparison of o-toluidine degradation by Fenton, electro-Fenton and photoelectro-Fenton processes*. J. Hazard. Mater. 196, 395-401.

Aquino, J.M., Pereira, G.F., Rocha-Filho, R.C., Bocchi, N., Biaggio, S., 2011. *Electrochemical degradation of a real textile effluent using boron-doped diamond or β-PbO_2 as anode*. J. Hazard. Mater. 192, 1275-1282.

Aquino, J.M., Rodrigo, M.A., Rocha-Filho, R.C., Sáez, C., Cañizares, P., 2012. *Influence of the supporting electrolyte on the electrolyses of dyes with conductive-diamond anodes.* Chem. Eng. J. 184, 221-227.

Ayranci, E., Bayram, E., 2005. *Adsorption of phthalic acid and its esters onto high-area activated carbon-cloth studied by in situ UV-spectroscopy*. J. Hazard. Mater. B122, 147-153.

Bagastyo, A.Y., Batstone, D.J., Kristiana, I., Gernjak, W., Joll, C., Radjenovic, J., 2012. *Electrochemical oxidation of reverse osmosis concentrate on boron-doped diamond anodes at circumneutral and acidic pH*. Water Res. 46, 6104-6112.

Bagastyo, A.Y., Batstone, D.J., Rabaey, K., Radjenovic, J., 2013. *Electrochemical oxidation of electrodialysed reverse osmosis concentrate on Ti/Pt–IrO_2, Ti/SnO_2–Sb and boron-doped diamond electrodes*. Water Res. 47, 242-250.

Barni, F., Lewis, S.W., Berti, A., Miskelly, G.M., Lago, G., 2007. *Forensic application of the luminol reaction as a presumptive test for latent blood detection*. Talanta 72, 896-913.

Bauer, J.M., Herrman, R., 1997. *Estimation of the environmental contamination by phthalic acid esters leaching from household wastes*. Sci. Total Environ. 208, 49-57.

Bellagamba, R., Michaud, P.A., Comninellis, Ch., Vatistas, N., 2002. *Electro-combustion of polyacrylates with boron-doped diamond anodes*. Electrochem. Commun. 4, 171-176.

Borràs, N., Arias, C., Oliver, R., Brillas, E., 2013. *Anodic oxidation, electro-Fenton and photoelectro-Fenton degradation of cyanazine using a boron-doped diamond anode and an oxygen-diffusion cathode*. J. Electroanal. Chem. 689, 158-167.

Boye, B., Dieng, M.M., Brillas, E., 2003. *Electrochemical degradation of 2,4,5-trichlorophenoxyacetic acid in aqueous medium by peroxi-coagulation. Effect of pH and UV light*. Electrochim. Acta 48, 781-790.

Boye, B., Brillas, E., Marselli, B., Michaud, P.A., Comninellis, CH., Farnia, G., Sandonà, G., 2006. *Electrochemical incineration of chloromethylphenoxy herbicides in acid medium by anodic oxidation with boron-doped diamond electrode*. Electrochim. Acta 51, 2872-2880.

Brillas, E., Baños, M.A., Garrido, J.A., 2003. *Mineralization of herbicide 3,6-dichloro-2-methoxybenzoic acid in aqueous medium by anodic oxidation, electro-Fenton and photoelectro-Fenton*. Electrochim Acta 48, 1697-1705.

Brillas, E., Sirés, I., Oturan, M.A., 2009. *Electro-Fenton process and related electrochemical technologies based on Fenton's reaction chemistry*. Chem. Rev. 109, 6570-6631.

Brillas, E., Garcia-Segura, S., Skoumal, M., Arias, C., 2010. *Electrochemical incineration of diclofenac in neutral aqueous médium by anodic oxidation using Pt and boron-doped diamond anodes*. Chemosphere 79, 605-612.

Burridge, L., Weis, J.S., Cabello, F., Pizarro, J., Bostick, K., 2010. *Chemical use in salmon aquaculture: a review of current practices and possible environmental effects*. Aquaculture 306, 7-23.

Cavalcanti, E.B., Garcia-Segura, S., Centellas, F., Brillas, E., 2013. *Electrochemical incineration of omeprazole in neutral aqueous médium using a platinum or boron-doped diamond anode: Degradation kinetics and oxidation products*. Water Res. 47, 1803-1815.

Cañizares, P., García-Gómez, J., Lobato, J., Rodrigo, M.A., 2003. *Electrochemical oxidation of aqueous carboxylic acid wastes using diamond thin-film electrodes*. Ind. Eng. Chem. Res. 42, 956-962.

Cañizares, P., Sáez, C., Lobato, J., Rodrigo, M.A., 2004. *Electrochemical treatment of 2,4-dinitrophenol aqueous wastes using boron-doped diamond anodes*. Electrochim. Acta 49, 4641-4650.

Cañizares, P., Arcís, M., Sáez, C., Rodrigo, M.A., 2007. *Electrochemical synthesis of ferrate using boron doped diamond anodes*. Electrochem. Commun. 9, 2286-2290.

Chan, Y.J., Chong, M.F., Law, C.L., Hassell, D.G., 2009. *A review on anaerobic–aerobic treatment of industrial and municipal wastewater*. Chem. Eng. J.155, 1-18.

Chatzitakis, A., Berberidou, C., Paspaltsis, I., Kyriakou, G., Sklaviadis, T., Poulios, I., 2008. *Photocatalytic degradation and drug activity reduction of chloramphenicol*. Water Res. 42, 386-394.

Chung, F.H., 1974. *Quantitative interpretation of X-ray diffraction patterns of mixtures. I. Matrix-flushing method for quantitative multicomponent analysis*. J. Appl. Crist. 7, 519-525.

Comninellis, Ch., 1994. *Electrocatalysis in the electrochemical conversion/combustion of organic pollutants for waste water treatment*. Electrochim. Acta 39, 1857-1862.

Crane, M., Watts, C., Boucard, T., 2006. *Chronic aquatic environmental risks from exposure to human pharmaceuticals*. Sci. Total Environ. 367, 23-41.

Cruz-González, K., Torres-López, O., García-León, A., Guzmán-Mar, J.L., Reyes, L.H., Hernández-Ramírez, A., Peralta-Hernández, J.M., 2010. *Determination of optimum operating parameters for Acid Yellow 36 decolorization by electro-Fenton process using BDD cathode*. Chem. Eng. J. 160, 199-206.

Cui, H.; Zhang, Z. F.; Zou, G. Z.; Lin, X. Q. J., 2004. *Potential-dependent electrochemiluminescence of luminol in alkaline solution at a goldelectrode.* J. Electroanal. Chem. 556, 305−313.

Daghrir, R., Drogui, P., Robert, D., 2012. *Photoelectrocatalytic technologies for environmental applications*. J. Photochem. Photobiol. A: Chem. 238, 41-52.

Devlin, R.H., Nagahama, Y., 2002. *Sex determination and sex differentiation in fish: an overview of genetic, physiological, and environmental influences*. Aquaculture 208, 191-364.

Dionysiou, D.D., Suidan, M.T., Baudin, I., Laîné, J.M., 2004. *Effect of hydrogen peroxide on the destruction of organic contaminants-synergism and inhibition in a continuous-mode photocatalytic reactor*. Appl. Catal. B: Environ. 50, 259-269.

Dodeigne, C., Thunus, L., Lejeune, R., 2000. *Chemiluminescence as diagnostic tool. A review*. Talanta 51, 415-439.

Donose, B.C., Sukumar, S., Pidou, M., Poussade, Y., Keller, J., Gernjak, W., 2013. *Effect of pH on the ageing of reverse osmosis membranes upon exposure to hypochlorite*. Desalination 309, 97-105.

Dosta, S., Cano, I.G., Miguel, J.R., Guilemany, J.M., 2008. *Production and characterization of metastable ZrO_2-Al_2O_3 coatings bbtained by APS + quench*. J. Therm. Spray Technol. 17, 360-364.

Duo, I., Fujishima, A., Comninellis, Ch., 2003. *Electron transfer kinetics on composite diamond (sp^3)-graphite (sp^2) electrodes*. Electrochem. Commun. 5, 695-700.

Ebrahim, S., 1994. *Cleaning and regeneration of membranes in desalination and wastewater applications: State-of-the-art*. Desalination 96, 225-238.

El-Ghenymy, A., Arias, C., Cabot, P.L., Centellas, F., Garrido, J.A., Rodríguez, R.M., Brillas, E., 2012a. *Electrochemical incineration of sulfanilic acid at boron-doped diamond anode*. Chemosphere 87, 1126-1133.

El-Ghenymy, A., Garcia-Segura, S., Rodríguez, R.M., Brillas, E., El Begrani, M.S., Abdelouahid, B.A., 2012b. *Optimization of the electro-Fenton and solar photoelectro-Fenton treatments of sulfanilic acid solutions using a pre-pilot flow plant by response surface methodology*. J. Hazard. Mater. 221-222, 288-297.

El-Ghenymy, A., Garrido, J.A., Rodríguez, R.M., Cabot, P.L., Centellas, F., Arias, C., Brillas, E., 2013a. *Degradation of sulphanilamide in acidic medium by anodic oxidation with a boron-doped diamond anode*. J. Electroanal. Chem. 689, 149-157.

El-Ghenymy, A., Oturan, N., Oturan, M.A., Garrido, J.A., Cabot, P.L., Centellas, F., Rodríguez, R.M., Brillas, E., 2013b. *Comparative electro-Fenton and UVA photoelectro-Fenton degradation of the antibiotic sulfanilamide using a stirred BDD/air-diffusion tank reactor*. Chem. Eng. J. 234, 115-123.

Elmorsi, T.M., Riyad, Y.M., Mohamed, Z.H., Abd El Bary, H.M.H., 2010. *Decolorization of Mordant red 73 azo dye in water using H_2O_2/UV and photo-Fenton treatment*. J. Hazard. Mater.174, 352-358.

Ersahin, M.E., Ozgun, H., Dereli, R.K., Ozturk, I., Roest, K., van Lier, J.B., 2012. *A review on dynamic membrane filtration: Materials, applications and future perspectives*. Bioresour. Technol. 122, 196-206.

Essawy, A.A., El-Hag Ali, A., Abdel-Mottaleb, M.S.A., 2008. *Application of novel copolymer-TiO_2 membranes for some textile dyes adsorptive removal from aqueous solution and photocatalytic decolorization*. J. Hazard. Mater. 157, 547-552.

Fang, C., Long, Y., Shen, D., 2009. *Comparison on the removal of phthalic acid diestersin a bioreactor landfill and a conventional landfill*, Bioresource Technol. 100, 5664-5670.

Faust, B.C., Zepp, R.G., 1993. *Photochemistry of aqueous iron(III)-polucarboxylate complexes: roles in the chemistry of atmospheric and Surface waters*. Environ. Sci. Technol. 27, 2517-2522.

Feng, L., van Hullebusch, E.D., Rodrigo, M.A., Esposito, G., Oturan, M.A., 2013. *Removal of residual anti-inflammatory and analgesic pharmaceuticals from aqueous systems by electrochemical advanced oxidation processes*. Chem. Eng. J. 228, 944-964.

Fenton, H.J.H., 1894. *Oxidation of tartaric acid in the presence of iron*. J. Chem. Soc. 65, 899-910.

Flox, C., Ammar, S., Arias, C., Brillas, E., Vargas-Zavala, A., Abdelhedi, R., 2006 *Electro-Fenton and photoelectro-Fenton degradation of indigo carmine in acidic aqueous médium*. Appl. Catal. B: Environ. 67, 93-104.

Flox, C., Arias, C., Brillas, E., Savall, A., Groenen-Serrano, K., 2009. *Electrochemical incineration of cresols: A comparative study between PbO_2 and boron-doped diamond anodes*. Chemosphere 74, 1340-1347.

Forgacs, E., Cserháti, T., Oros, G., 2004. *Removal of synthetic dyes from wastewaters: a review*. Environ. Int. 30, 953-971.

Freese, S.D., Nozaic, D., Pryor, M.J., Trollip, D.L., Smith, R.A., 1999. *Comparison of ozone and hydrogen peroxide/ozone for the treatment of eutrophic water*. Water Sci. Technol. 39, 325-328.

Fromme, H. Kuchler, T. Otto, T. Pilz, K. Muller, J. Wenzel, A., 2002. *Occurrence of phtha-lates and bisphenol A and F in the environment*. Water Res.36, 1429-1438.

Fujishima, A., Zhang, X., Tryk, D.A., 2008. *TiO_2 photocatalysis and related surface phenomena*. Surf. Sci. Rep. 63, 515-582.

Garcia-Segura, S., Brillas, E., 2011. *Mineralization of the recalcitrant oxalic and oxamic acids by electrochemical advanced oxidation processes using a boron-doped diamond anode*. Water Res. 45, 2975-2984.

Garcia-Segura, S., Centellas, F., Arias, C., Garrido, J.A., Rodríguez, R.M., Cabot, P.L., Brillas, E., 2011. *Comparative decolorization of monoazo, diazo and triazo dyes by electro-Fenton process*. Electrochim. Acta 58, 303-311.

Garcia-Segura, S., Cavalcanti, E.B., Brillas, E., 2014. *Mineralization of the antibiotic chloroamphenicol by solar photoelectro-Fenton. From stirred tank reactor to solar pre-pilot plant*. Appl. Catal. B: Environ. 144, 588-598.

Gardon, M., Dosta, S., Guilemany, J.M., Kourasi, M., Mellor, B., Wills, R., 2013. *Improved, high conductivity titanium sub-oxide coated electrodes obtained by Atmospheric Plasma Spray*. J. Power Sources 238, 430-434.

Gernjak, W., Krutzler, T., Glaser, A., Malato, S., Caceres, J., Bauer, R., Fernández-Alba, A.R., 2003. *Photo-Fenton treatment of water containing natural phenolic pollutants*. Chemosphere 50, 71-78.

Guinea, E., Centellas, F., Garrido, J.A., Rodríguez, R.M., Arias, C., Cabot, P.L., Brillas, E., 2009. *Solar photoassisted anodic oxidation of carboxylic acids in presence of Fe^{3+} using a boron-doped diamond electrode*. Appl. Catal. B: Environ. 89, 459-468.

Guinea, E., Garrido, J.A., Rodríguez, R.M., Cabot, P.L., Arias, C., Centellas, F., Brillas, E., 2010. *Degradation of the fluoroquinolone enrofloxacin by electrochemical advanced oxidation processes based on hydrogen peroxide electrogeneration*. Electrochim. Acta 55, 2101-2115.

Guo, W.Y., Li, J.J., Chu, H.H., Yan, J.L., Tu, Y.F.J., 2010. *Studies on the electrochemiluminescent behavior of luminol on indium tin oxide (ITO) glass.* J. Lumin. 130, 2022-2025.

Hammami, S., Bellakhal, N., Oturan, N., Oturan, M.A., Dachraoui, M., 2008. *Degradation of Acid Orange 7 by electrochemically generated $^{\bullet}OH$ radicals in acidic aqueous médium using a boron-doped diamon or platinum anode. A mechanistic study*. Chemosphere 73, 678-684.

Hamza, M., Abdelhedi, R., Brillas, E., Sirés, I., 2009. *Comparative electrochemical degradation of the triphenylmethane dye Methyl Violet with boron-doped diamon and Pt anodes*. J. Electroanal. Chem. 627, 41-50.

Homem, V., Santos, L., 2011. *Degradation and removal methods of antibiotics from aqueous matrices- a review*. J. Environ. Manage. 92, 2304-2347.

Iniesta, J., González-García, J., Expósito, E., Montiel, V., Aldaz, A., 2001. *Influence of chloride ion on electrochemical degradation of phenol in alkaline medium using bismuth doped and pure PbO_2 anodes*. Water Res. 35, 3291-3300.

Isarain-Chávez, E., Arias, C., Cabot, P.L., Centellas, F., Rodríguez, R.M., Garrido, J.A., Brillas, E., 2010. *Mineralization of the drug β-blocker atenolol by electro-Fenton and photoelectro-Fenton using an air-diffusion cathode for H_2O_2 electrogeneration combined with a carbon-felt cathode for Fe^{2+} regeneration*. Appl. Catal. B: Environ. 96, 361-369.

Isarain-Chávez, E., Cabot, P.L., Centellas, F., Rodríguez, R.M., Arias, C., Garrido, J. A., Brillas, E., 2011. *Electro-Fenton and photoelectro-Fenton degradations of the drug beta-blocker propranolol using a Pt anode: Identification and evolution of oxidation products*. J. Hazard. Mater. 185, 1228-1235.

Ivancev-Tumbas, I., Dalmacija, B., Tamas, Z., Karlovic, E., 1999. *The effect of different drinking water treatment processes on the rate of chloroform formation in the reactions of natural organic matter with hypochlorite*. Water Res. 33, 3715-3722.

Juang, R.-S., Lin, S.-H., Hsueh, P.-Y., 2010. *Removal of binary azo dyes from water by UV-irradiated degradation in TiO_2 suspensions*. J. Hazard. Mater. 182, 820-826.

Julien, F., Güeroux, B., Mazet, M., 1994. *Comparison de l'elimination de molecules organiques par coagulation-floculation et par adsorption sur flocs d'hydroxyde metallique preformes*. Water Res. 28, 2567-2574.

Kapalka, A., Fóti, G., Comninellis, Ch., 2008. *Kinetic modelling of the electrochemical mineralization of organic pollutants for wastewater treatment*. J. Appl. Electrochem. 38, 7-16.

Karthikeyan, K.G., Meyer, M.T., 2006. *Occurrence of antibiotics in wastewater treatment facilities in Wisconsin, USA*. Sci. Total Environ. 361, 196-207.

Khataee, A.R., Zarei, M., Asl, S.K., 2010. *Photocatalytic treatment of a dye solution using immobilized TiO_2 nanoparticles combined with photoelectro-Fenton process: optimization of operational parameters*. J. Electroanal. Chem. 648, 143-150.

Klamerth, N., Malato, S., Maldonado, M.I., Agüera, A., Fernández- Alba, A.R., 2011. *Modified photo-Fenton for degradation of emerging contaminants in municipal wastewater effluents*. Catal. Today 161, 241-246.

Klavarioti, M., Mantzavinos, D., Kassinos, D., 2009. *Removal of residual pharmaceuticals from aqueous systems by advanced oxidation processes*. Environ. Int. 35, 402-417.

Knight, A.W., 1999. *A review of recent trends in analytical applications of electrogenerated chemiluminescence*. Trends Anal. Chem. 18, 47-62.

Kümmerer, K., 2009. *The presence of pharmaceuticals in the environment due to human use – present knowledge and future challenges*. J. Environ. Manage. 90, 2354-2366.

Lin, Y., Chen, J.H., Chen, G.N., 2008. *Electrochemiluminescent behavior of luminol on the glassy carbon electrode modified with CoTPP/MWNT composite film.* Electrochim. Acta 53, 2396−2401.

Makoto, E., Emiko, M., Akira, H., Kunio, K., 1997. *Developmental toxicity evaluation ofphthalic acid, one of the metabolites of phthalic acid esters, in rats*. Toxicol. Lett. 93, 109-115.

Marselli, B., García-Gómez, J., Michaud, P.A., Rodrigo, M.A., Comninellis, Ch., 2003. *Electrogeneration of hydroxyl radicals on boron-doped diamond electrodes*. J. Electrochem. Soc. 150, D79-D83.

Martínez-Huitle, C.A., Ferro, S., De Battisti, A., 2004a. *Electrochemical incineration of oxalic acid: role of electrode material*. Electrochim. Acta 49, 4027-4034.

Martínez-Huitle, C.A., Quiroz, M.A., Comninellis, Ch., Ferro, S., Battisti, A., 2004b. *Electrochemical incineration of chloranilic acid using Ti/IrO_2, Pb/PbO_2 and Si/BDD electrodes*. Electrochim. Acta 50, 949-956.

Martínez-Huitle, C.A., Brillas, E. 2009. *Decontamination of wastewaters containing syntheticorganic dyes by electrochemical methods. A general review*. Appl Catal. B: Environ. 87, 105-145.

Martínez-Huitle, C.A., Viera dos Santos, E., Medeiros de Araújo, D., Panizza, M., 2012. *Applicability of diamond electrode/anode to the electrochemical treatment of a real textile effluent*. J. Electroanal. Chem. 674, 103-107.

Martins, A.O., Canalli, V.M., Azevedo, C.M.N., Pires, M., 2006. *Degradation of pararosaniline (C.I. Basic Red 9 monohydrochloride) dye by ozonation and sonolysis*. Dyes Pigments 68, 227-234.

Migliore, L., Civitareale, C., Brambilla, G., Di Delupis, G.D., 1997. *Toxicity of several important agricultural antibiotics to Artemia*. Water Res. 37, 1801-1806.

Migliorini, F.L., Braga, N.A., Alves, S.A., Lanza, M.R.V., Baldan, M.R., Ferreira, N.G., 2011. *Anodic oxidation of wastewater containing the Reactive Orange 16 dye using heavily boron-doped diamond electrodes.* J. Hazard. Mater. 192, 1683-1689.

Miranda-García, N., Suárez, S., Sánchez, B., Coronado, J.M., Malato, S., Maldonado, M.I., 2011. *Photocatalytic degradation of emerging contaminants in municipal*

wastewater treatment plant effluents using immobilized TiO_2 in a solar pilot plant. Appl. Catal. B: Environ. 103, 294-301.

Moreira, F.C., Garcia-Segura, S., Vilar, V.J.P., Boaventura, R.A.R., Brillas, E., 2013. *Decolorization and mineralization of Sunset Yellow FCF azo dye by anodic oxidation, electro-Fenton, UVA photoelectro-Fenton and solar photoelectro-Fenton processes*. Appl. Catal. B: Environ. 142–143, 877-890.

Muñoz, I., Martínez-Bueno, M.J., Agüera, A., Fernández-Alba, A.R., 2010. *Environmental and human health risk assessment of organic micro-pollutants occurring in a Spanish marine fish farm*. Environ. Pollut. 158, 1809-1816.

Naviner, M., Gordon, L., Giraud, E., Denis, M., Mangion, C., Le Bris, H., Ganière, J.P., 2011. *Antimicrobial resistance of Aeromonas spp. Isolated from the growth pond to the comercial product in a rainbow trout farm following a flumequine treatment*. Aquaculture 315, 236-241.

Newcombe, G., Morrison, J., Hepplewhite, C., Knappe, D.R.U., 2002. *Simultaneous adsorption of MIB and NOM onto activated carbon: II. Competitive effects.* Carbon 40, 2147-2156.

Nieto, J., Freer, J., Contreras, D., Candal, R.J., Sileo, E.E., Mansilla, H.D., 2008. *Photocatalyzed degradation of flumequine by doped TiO_2 and simulated solar light.* J. Hazard. Mater. 155, 45-50.

O'Melia, C.R., 1998. *Coagulation and sedimentation in lakes, reservoirs and water treatment plants.* Water Sci. Technol. 37, 129-135.

Oh, K.H., Tuovinen, O.H., 1991. *Detection and identification of substituted phenols as intermediates of concurrent bacterial degradation of the phenoxy herbicides MCPP and 2,4-D*. Microbiol. Lett. 79, 141-146.

Oishi, S., Hiraga, K., 1980. *Testicular atrophy induced by phthalic acid esters: Effect ontestosterone and zinc concentrations.* Toxicol. Appl. Pharm. 53, 35-41.

Oturan, M.A., Edelahi, M.C., Oturan, N., El Kacemi, K., Aaron, J.J., 2010. *Kinetics of oxidative degradation/mineralization pathways of the phenylurea herbicides diuron, monuron and fenuron in water during application of the electro-Fenton process.* Appl. Catal. B: Environ. 97, 82-89.

Özcan, A., Oturan, M.A., Nihal, O., Sahin, Y., 2009. *Removal of Acid Orange 7 from water by electrochemically generated Fenton's reagent*. J. Hazard. Mater.163, 1213-1220.

Özcan, A., Sahin, Y., Koparal, S., Oturan, M.A., 2008. *Propham mineralization in aqueous medium by anodic oxidation using boron-doped diamond anode: Influence of experimental parameters on degradation kinetics and mineralization efficiency*. Water Res. 42, 2889-2898.

Panizza, M, Michaud, P.A., Cerisola, G., Comninellis, Ch., 2001. *Electrochemical treatment of wastewaters containing organic pollutants on boron-doped diamond electrodes: Prediction of specific energy consumption and required electrode área.* Electrochem. Commun. 3, 336-339.

Panizza, M., Cerisola, G., 2009. *Direct and mediated anodic oxidation of organic pollutants*. Chem. Rev. 109, 6541-6569.

Panizza, M., Oturan, M.A., 2011. *Degradation of alizarin red by electro-Fenton process using a graphite-felt cathode.* Electrochim. Acta 56, 7084-7087.

Pera-Titus, M, García-Molina, V., Baños, M.A., Giménez, J., Esplugas, S., 2004. *Degradation of chlorophenols by means of advanced oxidation processes: a general review*. Appl. Catal. B: Environ. 47, 219-256.

Pignatello, J.J., 1992. *Dark and photoassisted Fe^{3+}-catalyzed degradation of chlorophenoxy herbicides by hydrogen peroxide*. Environ. Sci. Technol. 26, 944-951.

Pomati, F., Orlandi, C., Clerici, M., Luciani, F., Zuccato, E., 2008. *Effects and interactions in an environmentally relevant mixture of pharmaceuticals*. Toxicol. Sci. 102, 129-137.

Pouliquen, H., Delépée, R., Larhantec-Verdier, M., Morvan, M.L., Le Bris, H., 2007. *Comparative hydrolysis and photolysis of four antibacterial agents (oxytetracycline oxolinic acid, flumequine and florfenicol) in deionised water, freshwater and seawater under abiotic conditions*. Aquaculture 262, 23-28.

Radjenovic, J., Bagastyo, A., Rozendal, R.A., Mu, Y., Keller, J., Rabaey, K., 2011. *Electrochemical oxidation of trace organic contaminants in reverse osmosis concentrate using RuO_2/IrO_2-coated titanium anodes.* Water Res. 45, 1579-1586.

Ramírez, C., Saldaña, A., Hernández, B., Acero, R., Guerra, R., Garcia-Segura, S., Brillas, E., Peralta-Hernández, J.M., 2013. *Electrochemical oxidation of methyl orange azo dye at pilot flow plant using BDD technology*. J. Ind. Eng. Chem. 19, 571-579.

Robinson, T., McMullan, G., Marchant, R., Nigam, P., 2001. *Remediation of dyes in textile effluent: a critical review on current treatment technologies with a proposed alternative*. Bioresour. Technol. 77, 241-255.

Rocha, J.H.B., Soares-Gomes, M.M., Fernandes, N.S., Ribeiro da Silva, D., Martínez-Huitle, C.A., 2012. *Application of electrochemical oxidation as alternative treatment of produced water generated by Brazilian petrochemical industry*. Fuel Proces. Technol. 96, 80-87.

Rodríguez, M., Sarria, V., Esplugas, S., Pulgarín, C., 2002. *Photo-Fenton treatment of a biorecalcitrant wastewater generated in textile activities: biodegradability of the photo-treated solution*. J. Photochem. Photobiol. A: Chem 151, 129-135.

Rodrigues-Silva, C., Maniero, M.G., Rath, S., Guimarães, J.R., 2013. *Degradation of flumequine by the Fenton and photo-Fenton processes: Evaluation of residual antimicrobial activity*. Sci. Total Environ. 445-446, 337-346.

Root, R., Okada, S., 1975. *Estimation of life times and diffusion distances of radicals involved in X-Ray-induced DNA strand breaks or killing of mammalian cells*. Radiat. Res. 64, 2975-2984.

Ruiz, E.J., Arias, C., Brillas, E., Hernández-Ramírez, A., Peralta-Hernández, J.M., 2011. *Mineralization of Acid Yellow 36 azo dye by electro-Fenton and solar photoelectro-Fenton processes with a boron-doped diamond anode*. Chemosphere 82, 495-501.

Salazar, R., Garcia-Segura, S., Ureta-Zañartu, M.S., Brillas, E., 2011. *Degradation of disperse azo dyes from wastewaters by solar photoelectro-Fenton*. Electrochim. Acta 56, 6371-6379.

Salazar, R., Sirés, I., Brillas, E., 2012. *Finding the best Fe^{2+}/Cu^{2+} combination for the solar photoelectro-Fenton treatment of simulated wastewater containing the industrial textile dye Disperse Blue 3.* Appl. Catal. B: Environ. 115-116, 107-116.

Sales, A.S., Costa de Araújo, C.K, Viera de Melo, J., Peralta-Hernández, J.M., Ribeiro da Silva, D., Martínez-Huitle, C.A., 2013. *Decontamination of a real textile industrial effluent by strong oxidant species electrogenerated on diamond electrode: viability and disadvantages of this electrochemical technology*. Appl. Catal. B: Environ. 130-131, 112-120.

Sánchez, A., Llanos, J., Sáez, C., Cañizares, P., Rodrigo, M.A., 2013. *On the applications of peroxodiphosphate produced by BDD-electrolyses*. Chem. Eng. J. 233, 8-13.

Scialdone, O., Galia, A., Guarisco, C., Randazzo, S., Filardo, G., 2008. *Electrochemical incineration of oxalic acid at boron-doped diamond anodes: role of operative parameters*. Electrochim. Acta 53, 2095-2108.

Scialdone, O., Randazzo, S., Galia, A., Filardo, G., 2009. *Electrochemical oxidation of organics at metal oxide electrodes: The incineration of oxalic acid at IrO_2–Ta_2O_5 (DSA-O_2) anode*. Electrochim. Acta 54, 1210-1217.

Serra, A., Domènech, X., Arias, C., Brillas, E., Peral, J., 2009. *Oxidation of α-methylphenylglycine under Fenton and electro-Fenton conditions in the dark and in the presence of solar light*. Appl. Catal. B: Environ. 89, 12-21.

Serrano, K., Michaud. P.A., Comninellis, Ch, Savall, A., 2002. *Electrochemical preparation of peroxodisulfuric acid using boron doped diamond thin film electrodes*. Electrochim. Acta 48, 431-436.

Shan, A.Y., Ghazi, T.M.I., Rashid, S.A., 2010. *Immobilisation of titanium dioxide onto supporting materials in heterogeneous photocatalysis: A review*. Appl. Catal. A: Gen. 389, 1-8.

Sharma, K.P., Sharma, S., Sharma, S., Singh, P.K., Kumar, S., Grover, R., Sharma, P.K., 2007. *A comparative study on characterization of textile wastewaters (untreated and treated) toxicity by chemical and biological tests*. Chemosphere 69, 48-54.

Shende, R.V., Mahajani, V.V., 2002. *Wet oxidative regeneration of activated carbon loaded with reactive dye*. Waste Manage. 22, 73-83.

Šima, J., Makáňová, J. 1997. *Photochemistry of iron (III) complexes*. Coord. Chem. Rev. 160, 161-189.

Sirés, I., Arias, C., Cabot, P.L., Centellas, F., Rodrígues, R.M., Garrido, J.A., Brillas, E., 2004. *Paracetamol mineralization by advanced electrochemical oxidation processes for wastewater treatment*. Environ. Chem. 1, 26-28.

Sirés, I., Cabot, P.L., Centellas, F., Garrido, J.A., Rodrígues, R.M., Arias, C., Brillas, E., 2006. *Electrochemical degradation of clofibric acid in water by anodic oxidation: Comparative study with platinum and boron-doped diamond electrodes.* Electrochim. Acta 52, 75-85.

Sirés, I., Brillas, E., Cerisola, G., Panizza, M., 2008. *Comparative depollution of mecoprop aqueous solutions by electrochemical incineration using BDD and PbO_2 as high oxidation power anodes*. J. Electroanal. Chem. 613, 151-159.

Sirés, I., Brillas, E., 2012. *Remediation of water pollution caused by pharmaceutical residues based on electrochemical separation and degradation technologies: A review*. Environ. Int. 40, 212-229.

Skoumal, M., Cabot, P.L., Centellas, F., Arias, C., Rodríguez, R.M., Garrido, J.A., Brillas, E., 2006. *Mineralization of paracetamol by ozonation caralyzed with Fe^{2+}, Cu^{2+} and UVA light*. Appl. Catal. B: Environ 66, 228-240.

Skoumal, M., Rodríguez, R.M., Cabot, P.L., Centellas, F., Garrido, J.A., Arias, C., Brillas, E., 2009. *Electro-Fenton, UVA photoelectro-Fenton and solar photoelectro-Fenton degradation of the drug ibuprofen in acid aqueous medium using platinum and boron-doped diamond anodes*. Electrochim. Acta 54, 2077-2085.

Smith, R.M., Martell., A.E., 1997. *Critical stability constants. Volume 3: Organic ligands*. Ed. Plenum Press, New York.

Soon, A.N., Hameed, B.H., 2011. *Heterogeneous catalytic treatment of synthetic dyes in aqueous media using Fenton and photo-assisted Fenton process*. Desalination 269, 1-16.

Suling, V., Wohlers, J., Reinhard, M., Thiemann, W., 2002. *Photooxidation by Utraviolet Irradiation and Treatment with Ionized Air of Selected Antibiotics*. Vom Wasser 98, 145–158.

Sun, Y., Pignatello, J.J., 1993. *Photochemical reactions involved in the total mineralization of 2,4-D by $Fe^{3+}/H_2O_2/UV$*. Environ. Sci. Technol. 27, 304-310.

Taborda, A.V., Brusa, M.A., Grela, M.A., 2001. *Photocatalytic degradation of phthalic acidon TiO_2 nanoparticles*. Appl. Catal. A: Gen. 208, 419-426.

Tamtam, F., Mercier, F., Le Bot, B., Eurin, J., Dinh, Q.T., Clément, M., Chevreuil, M., 2008. *Ocurrence and fate of antibiotics in the Seine River in various hydrological conditions*. Sci. Total Environ. 393, 84-95.

Tokumura, M., Znad, H.T., Kawase, Y., 2008. *Decolorization of dark brown colored coffee effluent by solar photo-Fenton reaction: Effect of solar light dose on decolorization kinetics*. Water Res. 42, 4665-4673.

Triebskor, R., Casper, H., Heyda, A., Eikemper. R., Köhler, H.R., Sgwaiger, J., 2004. *Toxic effects of the non-steroidal anti-inflammatory drug diclofenac. Part II: Cytological effects in liver, kidney, gills and intestine of rainbow trout (Oncorhynchus mykiss)*. Aquat. Toxicol. 68, 151-166.

Turhan, K., Turgut, Z., 2009. *Decolorization of direct dye in textile wastewater by ozonization in a semi-batch bubble column reactor.* Desalination 242, 256-263.

Ulson de Souza, S.M.A.G., Forgiarini, E., Ulson de Souza, A.A., 2007. *Toxicity of textile dyes and their degradation by the enzime horseradish peroxidase (HRP)*. J. Hazard. Mater. 147, 1073-1078.

Umbuzeiro, G.A., Freeman, H.S., Warren, S.H., Oliveira, D.P., Terão, Y., Watanabe, T., Claxton, L.D., 2005. *The contribution of azo dyes to the mutagenic activity of the Cristais river*. Chemosphere 60, 55-64.

UNESCO, 2012. Managing Water Report under Uncertainty and Risk. THE UNITED NATIONS WORLD WATER DEVELOPMENT REPORT 4. Web: http://unesdoc.unesco.org/images/0021/002156/215644e.pdf#page=812

United States Environmental Protection Agency (7407), 1994. Pollution Prevention and Toxics, EPA 749-F-95-016a.

USGS – United States Geological Survey. Web: http://ga.water.usgs.gov/edu/earthwherewater.html

Vaid, R., Linton, R.H., Morgan, M.T., 2010. *Comparison of inactivation of Listeria monocytogenes within a biofilm matrix using chlorine dioxide gas, aqueous chlorine dioxide and sodium hypochlorite treatments*. Food Mricrobiol. 27, 979-984.

Valero, D., Ortiz, J.M., Expósito, E., Montiel, V., Aldaz, A., 2008. *Electrocoagulation of a synthetic textile effluent powered by photovoltaic energy without batteries: Direct connection behaviour*. Sol. Ener. Mat. Sol. C. 92, 291-297.

Velazquez-Peña, S., Sáez, C., Cañizares, P., Linares-Hernández. I., Martínez-Miranda, V., Barrera-Díaz, C., Rodrigo, M.A., 2013. *Production of oxidants via electrolysis of carbonate solutions with conductive-diamond anodes*. Chem. Eng. J. 230, 272-278.

Wang, A., Qu, J., Liu, H., Ru, J., 2008a. *Mineralization of an azo dye acid red 14 by photoelectro-Fenton process using an activated carbón fiber cathode*. Appl. Catal. B: Environ. 84, 393-399.

Wang, W., Cui, H., Deng, Z.X., Dong, Y.P., Guo, J.Z., 2008b. *A general E-E/C mechanism for the counter-peak in luminol electrochemiluminescence.* J. Electroanal. Chem. 612, 277-287.

Wang, P., He, Y.L., Huang, C.H., 2010. *Oxidation of fluoroquinolone antibiotics and structurally related amines by chlorine dioxide: Reaction kinetics, product and pathway evaluation.* Water Res. 44, 5989-5998.

Wang, J., Sun, W., Xu, C., Liu, W., 2012. *Ozone degradation of chloramphenicol: Efficacy, products and toxicity.* Int. J. Environ. Technol. Manage. 15, 180–192.

Welcher, F.J. (Ed.). *Standard Methods of Chemical Analysis, vol.2, Part B*, 6th ed., R.E. Krieger Publishers Co., Huntington, New York, 1975, p. 1827.

Wróblewska, A., Reshetnyak, O.V., Koval'chuk, E.P., Pasichnyuk, R.I., Błazejowski, J.J., 2005. *Origin and features of the electrochemiluminescence of luminol – Experimental and theoretical investigations.* J. Electroanal. Chem. 580, 41−49.

Xu, Y., Luo, F., Pal, A., Gin, K.Y.-H., Reinhard, M., 2011. *Occurrence of emerging organic contaminants in a tropical urban catchment in Singapore.* Chemosphere 83, 963–969.

Yeh, S.L., Kuo, C.M., Ting, Y.Y., Chang, C.F., 2003. *Androgens stimulate sex change in protogynous grouper, Epinephelus coioides: spawning performance in sex-changed males*. Comp. Biochem. Phys. C. 135, 375-382.

Zarei, M., Khataee, A.R., Ordijhani-Sevedlar, R., Fathinia, M., 2010. *Photoelectro-Fenton combined with photoatalytic process for degradation of an azo dye using supported TiO_2 nanoparticles and carbón nanotube cathode: neural network modeling*. Electrochim. Acta 55, 7250-7265.

Zhang, L., Dong, L., Ren, L., Shi, S., Zhou, L., Zhang, T., Huang, Y., 2012. *Concentration and source identification of polycyclic aromatic hydrocarbons and phthalic acid esters in the surface water of the Yangtze River Delta*, J. Environ. Sci. 24, 335-342.

Zhang, L., Ma, J., Li, X., Wang. S., 2009. *Enhanced removal of organic by permanganate peroxidation using tannic acid as a model compound – Role of in situ formed manganese dioxide*. J. Environ. Sci. 21, 872-876.

Zheng, Z., Zhang, H., He, P.J., Shao, L.M., Chen, Y., Pang, L., 2009. *Co-removal of phthalic acid esters with dissolved organic matter from landfill leachate by coagulationand flocculation process*. Chemosphere 75, 180-186.

Zhou, L.-J., Ying, G.-G., Liu, S., Zhao, J.-L., Yang,, B. Chen, Z.-F., Lai, H.-J., 2013. *Occurrence and fate of eleven classes of antibiotics in two typical wastewater treatment plants in South China.* Sci. Total. Environ. 452–453, 365–376.